

THE DESIGN OF STRUCTURES FOR STRENGTH

by

PHAM LAM, B.E. (Hons.), M.Eng. Sc., M.I.E. Aust.

Submitted in fulfilment of the requirements

for the degree of

Doctor of Philosophy in the

Faculty of Engineering

UNIVERSITY OF TASMANIA

AUSTRALIA

~~May, 1974~~

1975

ARCHIVES

Record Copy

I hereby declare that, except as stated herein, this thesis contains no material which has been accepted for the award of any other degree or diploma in any University, and that, to the best of my knowledge or belief, this thesis contains no copy or paraphrase of material previously published or written by any other person, except when due reference is made in the text of the thesis.

Pham Lam.

ACKNOWLEDGEMENTS

The work described in this thesis was carried out under the supervision of Dr. M.S. Gregory whose continued guidance and stimulus is deeply appreciated. The author has benefited greatly from his association with the engineers of Gutteridge, Haskins, and Davey, Consulting Engineers, Hobart, and the Hydro-Electric Commission of Tasmania. The author also wishes to thank the following persons:

- Prof. A.R. Oliver, Dr. F. Van Der Woude, and the Staff of the Civil and Mechanical Engineering Department, University of Tasmania, for reviewing various parts of the thesis.

- Mr. A. Christian and Mr. B. Stiberc of the Civil Engineering Laboratory, University of Tasmania, for their assistance with the experimental work.

- Maunsell and Partners and the Department of Main Roads (N.S.W.) for providing information on the Gladesville Bridge.

- The Hydro-Electric Commission of Tasmania for providing the model and related calculations on the Gordon Arch Dam.

Thanks are also due to Mrs. G. Stabb for typing this thesis and the papers associated with this work.

The support of the University of Tasmania in the form of a Post-graduate Research Scholarship is gratefully acknowledged.

CONTENTS

	Page
PREFACE	(viii)
CHAPTER I - PRINCIPLES OF DESIGN OF STRUCTURES FOR STRENGTH	
1.1 Introduction	1
1.2 The problem of design	1
1.3 The load factor	2
1.4 Basic principles of design	4
1.5 Discussions on the basic principles	8
1.6 The statically admissible state design	11
1.7 Techniques of obtaining statically admissible states	12
1.8 Concluding remarks.	13
CHAPTER II - THE STRENGTH OF BOLTED JOINTS UNDER ECCENTRIC LOADING	
2.1 Introduction	14
2.2 Review of previous research	14
2.3 Behaviour of a joint with a single bolt	15
2.4 Behaviour of bolted joints under eccentric loading	17
2.5 Analysis of bolted joints under eccentric loading	17
2.6 Application of limit principles to the design of a bolted joint	21
2.7 Limitations on the application of the method	23
2.8 Concluding remarks.	27
CHAPTER III - THE USE OF THRUST LINES IN THE DESIGN OF FRAMES	
3.1 Introduction	28
3.2 Practical minimum mass design of frames by guessing points of inflexion	28

	Page
3.2.1 Representation of forces in frames by thrust lines	29
3.2.2 Minimum mass design by guessing points of inflexion	33
Single-bay portal frame	33
Two-bay portal frame	35
Two-storey frame	38
3.3 The use of thrust line in the analysis of space frames	38
3.3.1 Simple space frames under horizontal loads	39
3.3.2 The free-standing staircase	44
3.3.3 The arch-ribbed dome	44
3.4 Concluding remarks.	50

CHAPTER IV - THE STRENGTH OF ORTHOTROPIC SLABS

4.1 Introduction	51
4.2 Lower bound approach	51
4.2.1 Basic conditions	51
4.2.2 Difficulties with the lower bound approach	52
4.2.3 Existing lower bound solutions	54
4.3 Outline of the approximate method	55
4.4 Collapse load for slabs with various boundary conditions	56
4.5 Comparison with upper bound solutions	59
4.6 Comparison with lower bound solutions	63
4.6.1 Slabs supported on four sides	63
4.6.2 Slabs supported on three sides	64
4.7 Concluding remarks.	67

CHAPTER V - LOAD-CARRYING CAPACITY OF STRUCTURES WITH NO

TENSILE STRENGTH

5.1 Introduction	69
5.2 Strength of a section	70
5.3 Strength of masonry walls	74

	Page
5.4 Strength of Gladesville Arch Bridge	79
5.4.1 General description of the arch and the actual design method	79
5.4.2 Strength of the voussoir section	80
5.4.3 Strength of a single arch rib under point load	80
5.4.4 Strength of the arch bridge under live load over half span	91
5.4.5 Strength of a single arch rib under lateral load	91
5.5 Concluding remarks.	100
 CHAPTER VI - SOME ASPECTS OF DESIGN OF ARCH DAMS FOR STRENGTH	
6.1 Introduction	101
6.2 State of arch dam design	101
6.3 Preliminary design of arch dams with string models	104
6.4 The load-carrying capacity of arch dams	114
6.4.1 Review of existing literature	115
6.4.2 Inclined arch method	119
6.4.3 'Tumbler' method	122
6.5 Concluding remarks.	125
 CHAPTER VII - DEFLEXION, BUCKLING, AND STRENGTH	
7.1 Introduction	126
7.2 Deflexion	126
7.3 Buckling	127
7.3.1 Euler and Non-Euler buckling	129
7.3.2 Relevance of Euler-type analysis in the prediction of strength of structures	132
7.4 Concluding remarks.	134.

	Page
CHAPTER VIII - PRACTICAL DESIGN CONSIDERATION	
8.1 Introduction	136
8.2 Fatigue and brittle fracture of steel	136
8.2.1 Design against brittle fracture	137
8.2.2 Design against fatigue	138
8.3 Creep and shrinkage of concrete	140
8.3.1 Effects of creep and shrinkage on structural behaviour	141
8.3.2 Design to avoid creep and shrinkage effects	142
8.3.3 Design to allow for creep and shrinkage effects	143
8.4 Detailed design for Ductility	144
8.4.1 Concrete detailing	144
8.4.2 Steel detailing	145
8.5 Concluding remarks.	148
APPENDIX A1 - TEST OF ARCHES AND RELATED CALCULATIONS	
Introduction	150
General description of test set-up and experimental procedures	150
Experimental results, related calculations, and discussions	153
Steel Arches	153
Arches under single point load at quarter span	153
Arches under single point load at the crown	155
Effect of strain-hardening	155
Reinforced concrete Arches	162
Arches under single point load at quarter span	162
Arches under four symmetrical point loads	169
Plain concrete Arches	169
Arches under single point load at one third span	169
Arches under four symmetrical point loads	169
Conclusion	173

	Page
APPENDIX A2 - YIELD LINE PATTERNS OF SLABS AND THE ROOF ANALOGY	
Introduction	176
General description of test set-up and experimental procedures	176
Observed collapse behaviour	176
The roof analogy	177
Comparison of yield line pattern and roof analogies	177
APPENDIX A3 - TEST OF A SHELL AND RELATED CALCULATIONS	
Introduction	182
General description of test set-up and experimental procedures	182
Observed behaviour	182
Calculations	185
Approximate elastic-plastic analysis of cylindrical shell under radial loads	188
Conclusions	192
APPENDIX B1 - DYNAMIC RELAXATION TREATMENT OF DEFLEXIONS IN ELASTIC-PLASTIC FRAMED STRUCTURES	
Summary	194
Introduction	194
Formulation of the method	194
Examples	196
Conclusions	196
APPENDIX B2 - DYNAMIC RELAXATION TREATMENT OF ELASTIC STABILITY PROBLEMS IN OVERBRACED FRAMES	
Summary	200
Introduction	200

	Page
Formulation of the problem	200
Effects of crookedness and prestrain	203
Summary of results of calculations	203
Conclusions	204
APPENDIX B3 - DYNAMIC RELAXATION TREATMENT OF STRUCTURES	
WITH NO TENSILE STRENGTH	
Summary	212
Introduction	212
Formulation of the method	213
Prestressed wooden block beam	214
Voussoir Arch	215
Conclusions.	215
REFERENCES	227

PREFACE

There is still an obvious need for better understanding of structural action and simpler methods of design of engineering structures. The increased use of the computer, in recent years, has facilitated the design and the checking of certain standard structural components and assemblies. However, computers are only tools; the preliminary design of the structure and the final checking (of computer solutions) must still be performed manually. There are also problems, such as detailed designs and particular one-off structures that computers cannot handle efficiently. These are problems that I have been confronted with in the three years of design work with Gutteridge, Haskins, and Davey, Consulting Engineers, Hobart, Tasmania. I have designed a number of industrial plants, school and office buildings, and also sewage and water treatment works. After having performed the tasks of preliminary design and final checking using the conventional elastic methods, it appears to me that the basic ideas of the plastic limit theory, particularly the lower bound theorem, may be better suited for the purposes. I have, therefore, spent a period of full-time experimental and theoretical research, exploring the power and the limitation of the plastic limit principles with a view to their use in the design of a wide range of civil engineering structures.

* * *

This thesis is written, for the appraisal of the professional engineers and research workers, to present a point of view on structural design. It is hoped that the view and the methods of solution presented here will achieve, in a small but important way, the above objectives, namely better understanding of structural action, leading to simpler preliminary design processes, and quicker methods of checking and assessing

the strength of existing designs and structures. Although the basic principles are well known, the view presented herein has not been previously sufficiently developed in this particular direction.

I have learnt the idea of design based on picturing a statically admissible state from "Theory of Limit Design" by Van den Broek. The larger part of the thesis, however, is based on the principles developed by Baker, Horne, and Heyman in "The Steel Skeleton, Vol. II". The later work has served both as a standard reference and a source of inspiration.

* * *

* The thesis is composed of a series of studies in the design of structures based on the "statically admissible state" techniques. A wide range of problems with increasing difficulty is chosen to demonstrate the power of the lower bound design technique.

niques are further developed in subsequent chapters. The simple but practical problem of bolted joints under eccentric loading (Chapter II) is used as an example of how limit principles, derived from the plastic analysis of steel frames, are made to work or can be made to work in a given easily definable situation. The limit analysis is supported by a series of tests of bolted joints under eccentric loading.

The concept of thrust line, well known in the theory of arches, is extended in Chapter III to multi bay-storey frames and space frames. This extension, although simple, provides a direct way of picturing the structural action of many frames, which cannot be obtained in any other way. I have also, with some satisfaction, combined the thrust-line concept and the older method of design of frames by guessing points of inflexion to produce a simple minimum mass design method.

A simple way of picturing the structural action of slabs is

presented in Chapter IV. The proposed method is only approximate; however, it gives a fairly good estimate of the load-carrying capacity of any orthotropic slab within a practical range of dimensions. All the above problems have their origins in my practical design work.

My interest in "funicular" structures arose from the reading of Heyman's work. I have applied these ideas to the assessment of the strength and safety of one of Australia's most important and beautiful bridges, the Gladesville Arch Bridge. The approach used herein in this investigation is very similar to Heyman's approach to stone and masonry structures. My contribution is the establishing of the load factors for the bridge under three different loading conditions with allowance being made for the effects of deflexion and the danger of the crushing of the concrete. The work has been done as far as possible from published data; however, the Department of Main Roads, (New South Wales) and Maunsell and Partners (London and Melbourne) supplied some preliminary design drawings.

The work on arch dams (Chapter VI) is another attempt at establishing statically admissible states as the basis of design of these structures of great interest and importance. Any attempt to visualize the structural behaviour of an arch dam in a simple manner is of value to the designer, especially if he has a difficult site, whether the difficulty arises from geological considerations, or merely from the lack of symmetry. An experimental method of directly obtaining a shape for the dam under a given loading condition is proposed. Other statically admissible states are then used to estimate the load-carrying capacity of arch dams. The latter work also gives an indication of how the dam may act structurally in transmitting the force to the abutments (which, in practice, also have to be analysed and designed.) I have

received generous assistance from the Hydro-Electric Commission of Tasmania, which has provided a model for the 420 ft high Gordon Arch Dam, related design calculations, and valuable advice on various aspects of arch dam design.

Chapters VII and VIII give attention to some additional considerations relevant to the proposed method of design of structures based on statically admissible states. Buckling and deflexion are discussed in Chapter VII because they do put a limit on the strength of structures. These limits arise in various ways which should be understood, if possible. The view on Non-Euler Buckling, presented herein, is known to be controversial, and is intended to be so. It is submitted for appraisal.

A summary of some practical aspects of design is presented in Chapter VIII, gathered from my own experience (in the design office and in the field) and from existing literature. ~~This material is included~~

The intention is to indicate the type of troubles which may limit strength. Although most of the material presented in this chapter is well-known, the material is included to emphasize the importance of practical considerations, which have often been overlooked in theoretical studies, although, of course, designers and builders are well aware of the problems.

The thesis is supported by experimental work consisting of laboratory loading tests on various structural models. Attention has not been focussed completely on the load-carrying capacity. Instead, much work has been done to ascertain the statical (load transmission) action and the geometrical (deformation) behaviour of the tested structures, at working load and later as failure begins to take place, and, where possible, as failure occurs. This experimental work, reported in Appendices A1, A2, and A3, consisted of tests of twenty steel, reinforced concrete, and

plain concrete arches, three reinforced concrete slabs, and a shell. They form the background from which various ideas presented in the thesis have arisen.

The numerical works, reported in Appendices B1, B2, and B3, form an addendum to the thesis and present some new extension of the method of dynamic relaxation to non-linear problems. They are included because they are used in various chapters to substantiate other simple limit calculations.

* * *

The design method proposed in this thesis is, for historical reasons, referred to as "limit design", and the principles of plastic theory are called "limit principles". Otherwise, the terminology follows the standard usage in literature, such as the standard set of terms recommended by the American Society of Civil Engineers (to whom, however, "limit design" means any limit, and the term loses its meaning through loss of connection with its history).

Metric units are adopted generally throughout the thesis, except where existing structures or data are analysed. Imperial units have been retained in these situations for ease of reference.

CHAPTER I

PRINCIPLES OF DESIGN OF STRUCTURES FOR STRENGTH

1.1 INTRODUCTION

The thesis has one single theme, namely "statically admissible state" design and is composed of a series of design studies based on various techniques of constructing statically admissible states. To set the stage for further discussion, the basic elements of the plastic limit theory are first reviewed in this chapter. Emphasis is then placed on "statically admissible state" design. Various techniques of obtaining statically admissible states are outlined and briefly discussed. More thorough applications of the techniques are presented in subsequent chapters.

designer usually does not have a clear picture of what the final design will be. The shapes and dimensions of the structure are first roughly determined by its functional or aesthetic requirements. A structural design is then carried out. The task is to proportion and detail the members so that a safe, economical, and suitable structure is produced on drawings and specifications. A suitable construction method must also be considered, to enable the structure to be built. The three phases of work are interconnected. Difficulties in structural design often can be avoided by altering the design concept; actual construction practice determines how refined the design must be.

The structural design may be separated into three activities:

- (i) the determination of the loads to be supported by the structure,
- (ii) the selection of suitable materials, and (iii) the application of a design theory to proportion and detail the members of the structure, for the given loads, with the given materials.

This thesis is concerned only with the design of structures for which strength is the prime design criterion. The structure is to be

designed so that it will not collapse at a certain level and combination of loading, which, of course, must be above the working loads. The design is thus based on the concept of a 'load factor', i.e. the ratio of the load at collapse to working load. This concept is examined in the next section.

1.3 THE LOAD FACTOR

The load factor λ is defined in most literature as the ratio of the predicted collapse load to the normal working load (Ref 1.1). This simple definition has many implications which the designer must beware of.

(i) Of all possible states of loading, only one particular combination is considered at a time.

(ii) The loads in any particular combination are not allowed to vary independently, but are imagined to be slowly increased in proportion until collapse is reached.

(iii) Most of limit design literature is concerned only with static loadings. In the absence of guidance, designers usually convert dynamic loads into equivalent static loads. This approach may or may not be valid depending on the nature of the particular problem in hand. It is further mentioned that the thesis is concerned only with static loads.

(ii) There is no connection between the collapse calculation based on a load factor and the real state of overloading (Ref 1.2). The load factor is only a device to proportion the structure with some margin of safety.

(iii) Since the load factor reflects the margin of safety, it should be chosen with due reference to various uncertainties such as the inaccurate assessment of the loads, variations in the strength of materials, imperfection in fabrication, and so on.

The idea of a single load factor as presented above is rather limited since:

- (i) Some loads can be estimated more accurately than others.
- (ii) Some loads can possibly be increased beyond the estimated values while others cannot.

The concept of a partial load factor is then introduced to overcome the above restrictions. Various load factors are chosen for different classes of loading to account for their different characteristics. The magnitudes of the partial load factors are also varied according to the loading combination being considered.

The choice of a load factor (or partial load factors) involves considerable judgement. The values chosen in the design codes are usually "arranged so that the same margin of safety is achieved as for conventional designs which experience has shown to be satisfactory",

(Ref 1.3). With the advance of probabilistic design, the load factors have been given new meanings related to the reliability of the design. Load factors are related to the expected loadings and therefore can be assessed using statistical methods. The subject of probabilistic design is well outside the scope of the thesis and a lengthy discussion is not intended. As far as the thesis is concerned, a load factor (or a set of load factors) must be established by whatever means before the design can proceed. At present the load factors are established at best semi-probabilistic, usually empirical. It should also be noted that the load factors do not have any relation to real overloading states. Certain overloading states must be examined separately as required by the Codes of Practice, such as in bridge design. The assessment of safety with regard to failure must be made according to the physical conditions involved, and its relations to the design of the structure. For example, wilful destruction is an overloading which cannot be allowed for; similarly the safety of a structure also depends on the condition of the supports, and this cannot be ignored.

1.4 BASIC PRINCIPLES OF DESIGN

(a) The breakdown of the problem.

The designer usually starts by dividing his structure into elements. Each element is required to carry part of the loads in a particular manner, and it is designed accordingly. The breakdown of structure into elements is made based on: (i) a prior conception of how the loads can be carried, (ii) some understanding of the statics of the elements and (iii) certain simplifications as to what structural actions are unimportant and can be neglected.

The breakdown of a structure into elements may occur at many levels. For example, a building is usually designed as a series of plane frames; this is an arbitrary way of deciding how the loads can be carried. The actions of members which connect the frames are neglected. A plane frame is further divided into beam and column elements, where the beams carry the loads mainly by bending action and the columns carry theirs by both bending and axial actions.

A successful breakdown is not easy to make for complicated structures. Usually the design is first made at some drastic level of simplification and other effects are then introduced as corrections.

(b) Basic Conditions

Once the structure has been divided into elements and the major forces acting between the elements have been decided, three basic conditions require examination:

(i) The Geometrical Conditions which ensure the compatibility of deformation or movements of the elements.

(ii) The Equilibrium Conditions of the structure under external loads, reactions, and the internal forces between the elements.

(iii) The Load-deformation characteristics of the elements.

In relation to strength, these conditions take special forms. The deformations that are of interest are only those deformations that could

cause collapse; movements must occur at sufficient regions to make collapse possible. This condition is difficult to put, because a structure even at collapse is still intact in some sense. For framed structures which carry their loads mainly by bending moment, a 'plastic hinge' is considered as a kind of discontinuity with arbitrary rotation. The requirement is that ^{sufficient} ~~different~~ hinges form to allow the structure or part of it to move as a mechanism which is compatible with the remaining constraints. This condition is generally termed the "mechanism condition".

The equilibrium conditions are often written with reference to the undeformed state of the structure. This implies that the deformations, even at collapse, are small and do not markedly change the equilibrium equations written without them. However, deformation may not be neglected for certain classes of elements such as the column element, if collapse condition is affected by deformation. The equations of equilibrium must include the changing geometrical terms in these cases.

In a design for strength, only the limiting load-deformation characteristic is considered. The main features, that the load deformation relations must have, are that a definite collapse load must be reached and that the collapse load stays constant as deformation increases. This condition is generally known as the "yield condition"; it is characterized by the idealized load-deformation curve of Fig 1.1. Figure 1.1 results from an assumption of an elastic-perfectly plastic behaviour of the material. In most calculations, the curve is approximated to two straight lines as shown partly dotted.

When there are several forces causing collapse, the interaction of the forces must be considered. The plot of all the combinations of the forces that could cause collapse is known as a "yield surface". The localized deformations at the yielded zones associated with the forces are fixed in ratio and direction, i.e. they must be geometrically permissible along the chosen collapse mode. This condition is generally known as the "normality rule". (Ref 1.5)

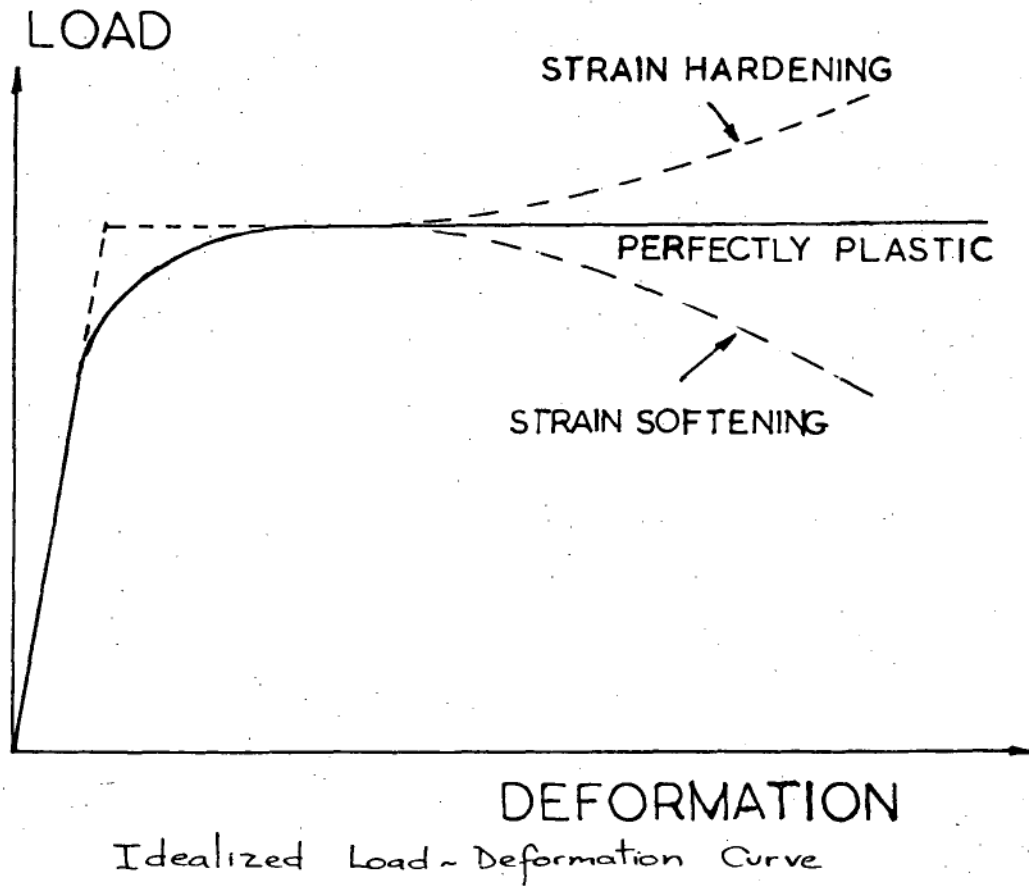
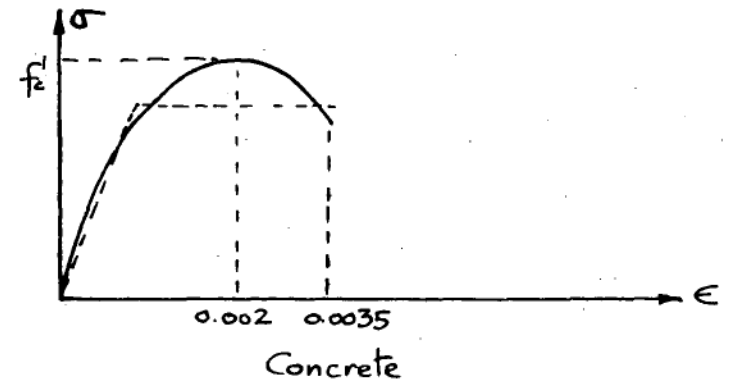
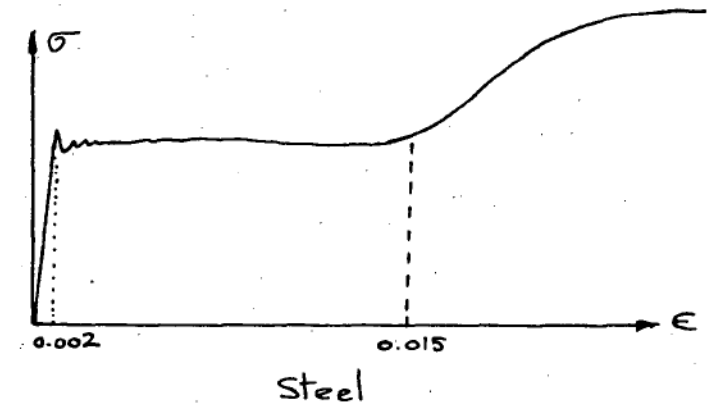
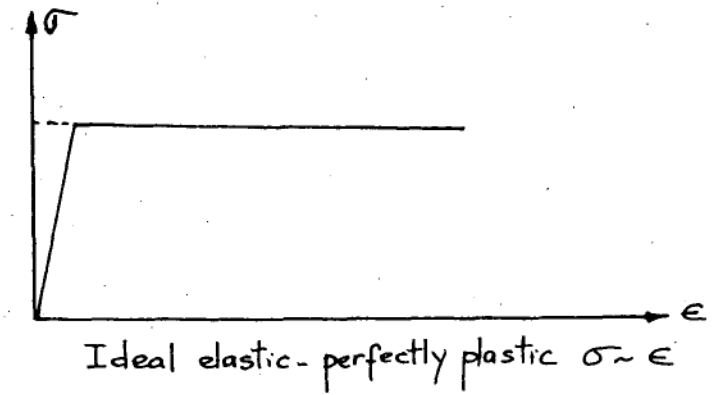


Figure 1.1

$\sigma \sim \epsilon$ CURVES



The preceding presentation of basic relations emphasizes the importance of the decision as to what are the vital internal forces. This decision requires an understanding of the manner in which the structure carried its loads.

(c) Fundamental Theorems

The simple concept of load factor based upon proportional loading is used here to state the fundamental theorems.

The uniqueness theorem states that if all three basic conditions of mechanism, equilibrium, and yield are satisfied, then the load factor has a definite unique value λ_c , which is the collapse load factor of the structure.

The upper bound theorem states that for any assumed mechanism of collapse which satisfies the yield condition, the load factor λ is always greater than or at best equal to the collapse load factor λ_c . The theorem is also known as 'unsafe' or 'kinematic' theorem.

The lower bound theorem states that for any statically admissible state which balances the applied load and is everywhere satisfying the yield condition, the associated load factor λ is always less than or at best equal to the collapse load factor λ_c . The theorem is also known as 'safe' or 'static' theorem.

The formal proofs for these theorems can be found in the standard texts (Ref 1.1, 1.4, 1.13, 1.14, 1.15). It is noted that the theorems were intuitively understood and used by engineers long before they were formally stated. Coulomb made good use of the upper bound theorem in solving the problems of strength of a prism, of soil thrusting against a retaining wall, and of the failure of masonry arches (Ref 1.6). Rankine's solution of the limiting equilibrium problem of soil mass, or the old method of designing frames by guessing points of inflexion, can be considered as applications of the lower bound theorem.

1.5 DISCUSSIONS ON THE BASIC PRINCIPLES

The implications of the basic principles as presented above to the actual design of a structure are now examined.

(i) Load redistribution and sharing

The prime requirement for strength design is the ability of the structure to adjust itself to carry the applied load if at all possible, within the limits assumed in the design. Load redistribution is a statical concept based upon the 'flatness' of the load-deformation curve (Fig 1.1). Once certain regions of the structure reach their ultimate load-carrying capacity, they are capable of holding this load with further deformation, therefore allowing the other regions to take up the extra load if possible.

The suitability of a structure to be designed by this method depends on how closely the load-deformation relation for its members can approximate the ideal curve of Figure 1.1, which represents the elastic-perfectly plastic behaviour. Structural steel is normally ductile and its properties

can be approximated fairly well to this curve. Strain hardening will occur eventually for mild structural steel but its neglect is intuitively 'safe' in a general sense. For most commonly used sections in flexure, strain hardening has a more important role in preventing local instability, and in maintaining the 'plateau' of the moment-curvature curve. Its presence allows the force redistribution process to occur more completely. moment redistribution should be allowed in the design since unlimited load redistribution can no longer be assumed. Dry friction may also be represented by the characteristics of Figure 1.1, therefore the plastic theory is also applicable to structures whose load carrying capacity is derived from frictional forces.

Detailed design is another important consideration. It is useless to provide ductility for the members when ductility is absent in the joints, where the forces are likely to be the highest. Joints should be designed

not only to have sufficient strength but also to possess adequate rotational capacity so that full load redistribution can be achieved. The problem will be further discussed in Chapter VIII.

(ii) Use of fundamental theorems

The upper bound theorem implies that if a failure path exists, then the structure will not stand up. It is mainly an analysis tool; the load computed on the basis of an assumed mechanism will always be greater or at best equal to the true collapse load. Its usefulness lies in the relative ease of picturing the collapse mode, and of calculating a collapse load from this. If a wrong mode of collapse is pictured, an incorrect result is obtained. The ability to perform the calculation from a pictured collapse mode depends on a knowledge of the main actions at sufficient points in the structure from geometrical and statical considerations. The use of upper bound theorem requires some prior knowledge of the structure; some minimisation techniques are also used to obtain the lowest possible collapse load.

The lower bound theorem, on the other hand, is a powerful design tool, since its use, as will be described herein, does not require any prior knowledge of the structural members. The theorem reflects the ability of the structure to adjust itself to carry the loads if at all possible. The main problem is to construct a "statically admissible state"; the yield condition can be met by "covering" the structure with adequate strength. This aspect is perhaps the most important contribution of the plastic limit theory; it allows a design to be made by equilibrium considerations alone. The designer selects a suitable pathway for the forces and provides the members with sufficient strength to carry those forces.

The collapse mode is often easier to picture than a statically admissible state; therefore the upper bound theorem is, in many cases, easier to use than the lower bound theorem. Practically, one finds that the upper bound calculation is often very close to the actual collapse load

if a nearly correct mode of collapse is pictured. For difficult problems where an 'exact' calculation of the ultimate load is not possible, the two theorems enable the collapse load to be bracketed closely enough for practical engineering purposes.

The words "lower bound" and "upper bound" are meaningful only in a mathematical sense. For complicated structures, the mathematical model used in the analysis involves drastic simplification of the actual structure. The actual collapse load (experimentally obtained from models for example) can even be higher than the upper bound solution. One classic example is the failure of a slab with restrained edges; the yield line solution (upper bound) is usually conservative; the slab has some reserve of strength due to membrane effects which have been neglected in the analysis.

(iii) Limiting factors. Two kinds of limiting factors must be considered in the application of the fundamental theorems to the design of structures. Firstly, the basic assumptions of the method must be met. The proofs of theorems (Ref 1.4), in particular the lower bound theorem, require ductility in the members and the structure. Local and overall instability of the members and structure must be prevented. Construction materials do not always behave in a ductile manner. For steel structures, the effects of brittle fracture, fatigue, and residual stress must be prevented. For concrete structures, the effects of shrinkage, creep, and temperature must be allowed for. Secondly, there are serviceability limit states which must be considered since a plastic design is based solely on the limit state of collapse. There are the limit states of deflexion, local damage, vibration, durability, and fire resistance. The criteria governing these serviceability limit states vary with the kind of structures and service conditions, and may well become the governing design criteria. Proper attention to the detailed design, however, can often help to alleviate some of these problems.

1.6 THE STATICALLY ADMISSIBLE STATE DESIGN

Design based on statically admissible state is the central theme of this thesis. The approach is valid only if strength is the prime design criterion. The design process consists of picturing a way the structure can carry its loads, then providing adequate strength in the structure so that the loads can be carried that way. Care of course must be taken to ensure that the designed strength can actually be realized, i.e. the level of load redistribution assumed in the design is acceptable geometrically.

The concept of statically admissible state is now further examined.

Firstly, the statically admissible state is constructed at some level of approximation. The question of statically admissible state is relevant only after a prior decision has been made regarding those aspects of structural actions that are important for a particular structure. A design based on the statically admissible state is only safe if the main action that causes collapse is included in the calculations.

Secondly, for statically indeterminate structures there are many possible statically admissible states. The more statically indeterminate the structure is, the more ways it can find to carry its loads, or, what is more important, the more pathways the designer has at his disposal to provide the total load carrying capacity.

Thirdly, the statically admissible state of a highly indeterminate structure can be made to be statically determinate. This is an important aspect since it allows a simple way of constructing the statically admissible state. The picturing of collapse mode can be used here, since the collapse state is often statically determinate. If a wrong mode is pictured, the equilibrium calculations will suggest an alternative. In this connection the two techniques, of constructing statically admissible state and of picturing collapse mode, complement each other. Problems may arise when partial collapse occurs, as this may leave part of the structure statically indeterminate.

Fourthly, the statically admissible state must satisfy the statical boundary conditions for the design to be safe. For example, a statically admissible state for a fixed-base portal frame cannot be used to design a pinned-base portal frame. However, some minor geometrical changes such as the settlement of supports do not invalidate the basis of the design as long as the change does not materially affect the statical equilibrium of the system.

1.7 TECHNIQUES OF OBTAINING STATICALLY ADMISSIBLE STATES

The statically admissible state can only be obtained if the basic statical concept of load carrying and distribution throughout the structure is understood. Once the understanding of the way the structure carries its load is achieved, simplification is possible and will still give adequate design. Some of the techniques of obtaining the statically admissible state are described below.

(i) Slicing Technique. This technique divides a complex structure into simpler parts, whose structural actions are better understood. The design of a building as a series of plane frames can be considered as an application of the technique. Heyman (Ref 1.16) used the slicing technique in assessing the strength of stone domes and vaults. The early method of designing an arch dam as a series of arches is another application. The interacting effects between various slices are neglected, and therefore the technique is only successful if such neglects are justifiable. The slicing technique is used in Chapter VI to estimate the load-carrying capacity of arch dams.

(ii) Replacing a complex structure by overlapping simpler structural elements. The division of a slab into two series of beams or the division of an arch dam into two series of arches and cantilevers are applications of this technique. The replacement is valid only if the interaction effects between various structural actions are negligible. This technique is used in Chapter IV to estimate the strength of slabs and in Chapter VI to estimate the strength of arch dams.

(iii) Algebraic technique. This technique is useful in two or three dimensional problems, such as slabs or shells, where the structural actions are too difficult to picture but the differential equations representing the equilibrium state are readily available. Algebraic expressions are specified for all structural actions, such that the equilibrium equations are satisfied everywhere and the yield conditions are nowhere violated. The technique is used most often in deriving lower bound solutions for slabs. Further discussions will be found in Chapter IV.

(iv) Thrust Lines and Surfaces. This is perhaps the most satisfying way of picturing the statically admissible state. The idea, originated in the design of masonry arches, can be extended to handle frames and similar structures. The use of the thrust line concept is particularly useful in space frames where structural actions are numerous and difficult to picture. The thrust surface is an extension of the thrust line into three dimensions. A membrane is the inverted picture of a thrust surface under acting loads. Heyman mentioned the concept of a thrust surface in the assessment of dome strength (Ref 1.17). The uses of thrust lines in the design of plane and space frames are explored in Chapter III; a three dimensional thrust surface is constructed experimentally for an arch dam in Chapter VI.

1.7 CONCLUDING REMARKS

The basic principles of the plastic limit theory have been presented together with discussions on the aims, assumptions, and limitations of the method. The limit design method of picturing statically admissible states is chosen for further development. Various techniques of obtaining statically admissible states are outlined, and they will be further developed in subsequent chapters for particular structures or members.

CHAPTER II

THE STRENGTH OF BOLTED JOINTS UNDER ECCENTRIC LOADING

2.1 INTRODUCTION

The problem of beam bending and the concept of the plastic hinge have been used too often (to the exclusion of almost everything else) to demonstrate limit design ideas. The concept of 'statically admissible state' design pursued in the thesis is much more fundamental and is capable of much wider applications. The problem of bolted joints under eccentric loading, therefore, has been selected to demonstrate the basic design approach used in the thesis.

The problem of bolted joints under eccentric loading is in itself an interesting one.

relationship of the joint is not linear. These objections led the American Institute of Steel Construction (Ref. 2.1) to adopt the empirical approach of "effective eccentricity" to provide a less conservative and more realistic allowable load; this is the currently accepted method of design.

This chapter does not contain any original contribution. The plastic design of bolted joints under eccentric loading and its various limitations are presented together with extra supporting experimental works. The emphasis, however, is not on the method itself but on the limit design thinking behind the method.

2.2 REVIEW OF PREVIOUS RESEARCH

A full bibliography on bolted and riveted joints has been prepared by the American Society of Civil Engineers (Ref. 2.2). This section is only concerned with the ultimate strength approach to the problem.

For friction-grip joints, there is little published guidance for the designer of eccentrically loaded joints. For bearing joints, Abolitz (Ref. 2.3) has used an ultimate strength approach with the basic assumption

that each bolt would exert its maximum resistance at collapse. This is not fully justified due to the lack of ductility of individual bolts.

Kulak (Ref. 2.4) has used the "load-deformation response of the individual bolt" to predict the ultimate strength of the joint. ~~Kulak has~~

Kulak and Crawford's method is applicable only to bearing joints in which there is no lack of fit. Since both statics and geometry of deformation are used in Kulak and Crawford's solution, the "statically admissible state" philosophy is not used, although the results are, of course, statically admissible.

The behaviour of a double lapped joint with a single bolt is used as the basis for the treatment which follows and is described briefly here. Three test specimens were assembled as shown in Fig. 2.1(a). Each specimen consists of two identical joints. The test bolt was tightened according to the standard turn-of-nut procedure (Ref. 2.7). The assemblies were loaded in tension in a testing machine. Movement of the joint was measured from the gauge points set on the plates. Due to material discrepancies, manufacturing tolerances, etc., the ultimate load of the specimens was reached when only one joint had failed.

Fig. 2.1 shows a complete graph, of load against movement, for a specimen tested to failure. There are three distinct phases of behaviour.

(i) The Friction Grip Region OA: very small movement, measured across the joint, is recorded and the load is carried mainly by friction. Examination of the plate, after failure, indicates that the grip is provided mainly by a small region around the nut.

(ii) The Slippage Region AB: the joint begins to slip. It is still capable of resisting the severe load as before. A slight increase in load is noted as slipping progresses.

(iii) The Shearing Region BC: the bolt is actually being sheared when all the clearance around the hole has been taken up. The behaviour is non-linear and there is little ductility in the bolt itself.

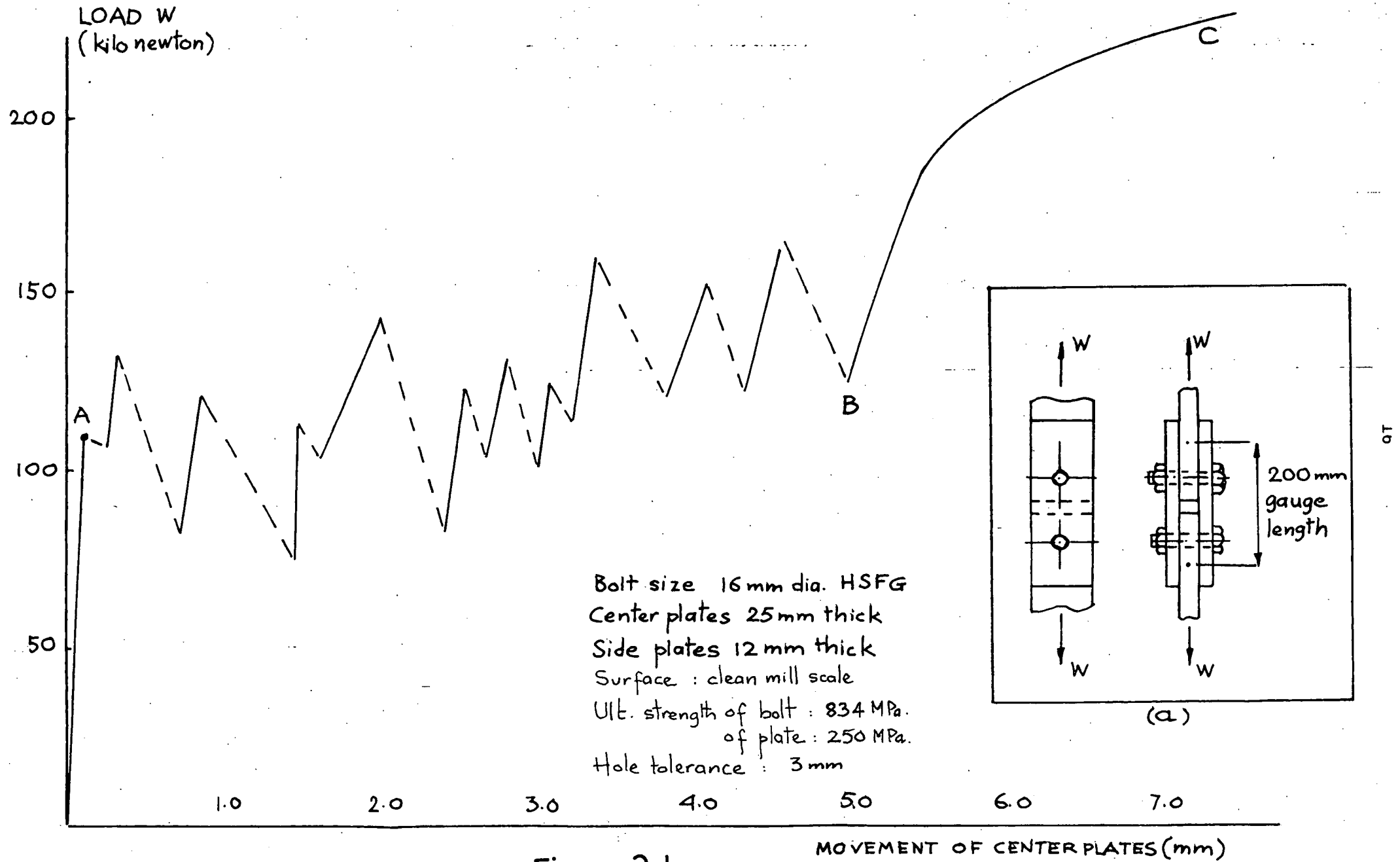


Figure 2.1

The friction-grip strength is only achieved if the bolt is high-strength friction-grip type, and is tightened according to a proper procedure such as the turn-of-nut method. (Ref. 2.7). Otherwise, the friction-grip strength is considerably reduced but the rest of the joint behaviour remains the same. The load-movement curve for the joint in the shearing region is affected by the type of materials and the thickness of the connecting plates, although the ultimate strength of the joint is not very much affected by these parameters. (Ref. 2.9).

2.4 BEHAVIOUR OF BOLTED JOINTS UNDER ECCENTRIC LOADING

Fig. 2.2 shows the general arrangement for the tests. Fifteen specimens, which included seven different bolt groupings with varying eccentricities and bolt sizes were tested. The specimens were designed so that the test bolts were the critical components. Two joints were tested simultaneously. Measurements were made of the movement of one plate relative to the other. A typical load-movement graph is shown in Fig. 2.3.

The behaviour follows closely that of a joint with a single bolt. There is a friction-grip region, a slippage region, and a shearing region. It is significant that not all the bolts have attained their full strength when the joint fails. Examination of the bolts, after collapse, indicates that all bolts deform substantially, although some have more deformation than others. ^{from the load-movement graph of Fig. 2.1} It follows that there is a certain amount of load redistribution, but it is incomplete when failure occurs.

2.5 ANALYSIS OF BOLTED JOINTS UNDER ECCENTRIC LOADING

The bolted joint of Fig. 2.4 is subjected to an eccentric force P acting at a distance e from the centroid of the joint. (Ref. 2.5). Rotation is presumed to take place about some point A , whose position is as yet unknown. Bolt 1, distance r_1 from A , has coordinates (x_1, y_1)

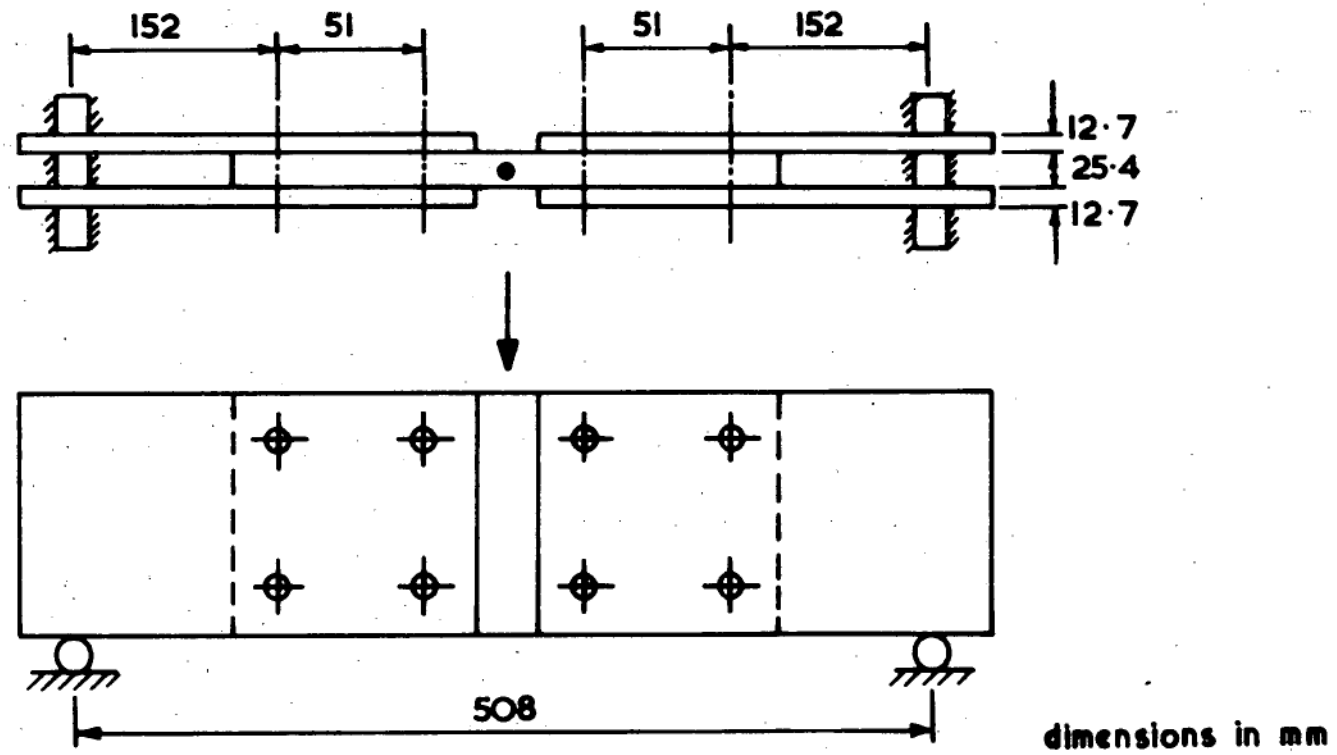


Figure 2.2

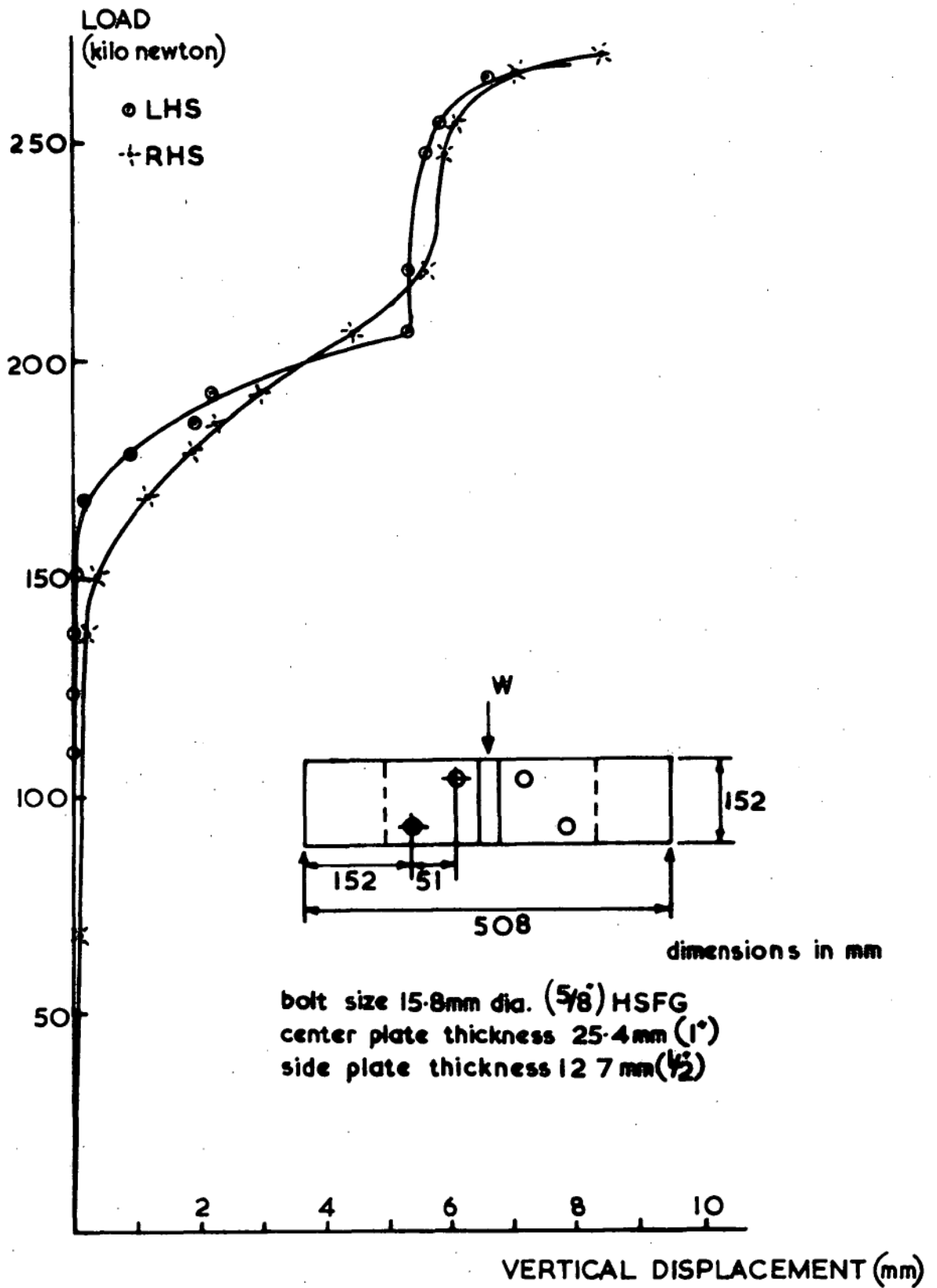


Figure 2.3

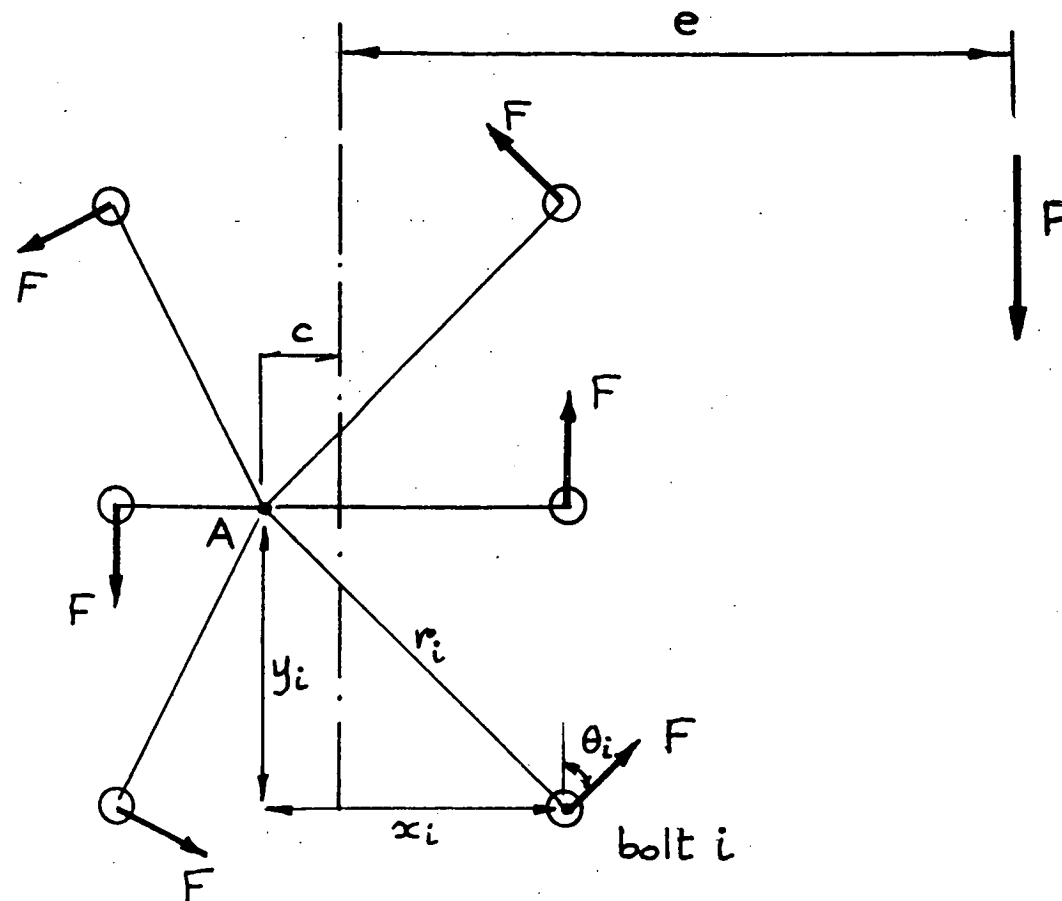


Figure 2.4

measured from A. All bolts are, at this stage, considered to carry equal forces F acting in the direction normal to the line joining A to the bolt. The equations of equilibrium are

$$(i) \text{ Vertical equilibrium: } \sum F \cos \theta_i = P \quad \dots (2.1)$$

$$(ii) \text{ Horizontal equilibrium: } \sum F \sin \theta_i = 0 \quad \dots (2.2)$$

$$(iii) \text{ Sum of moments about A: } \sum F \cdot r_i = P(e+c) \quad \dots (2.3)$$

where θ_i, c are defined in Fig. 2.4.

These equations may be easily solved graphically by trial and error, for most joints having simple layouts of the bolts, to give a position for the centre of rotation A, and the magnitude of the bolt force F .

2.6 APPLICATION OF LIMIT PRINCIPLES TO THE DESIGN OF A BOLTED JOINT

Before a bolted joint can be designed using limit principles, it must be clearly defined what constitutes 'failure'. If no movement of the joint can be tolerated, then from the load-movement graph of Fig. 2.3, 'failure' starts at the beginning of slippage. This type of joint is generally known as friction-grip joint. On the other hand, if movement can be tolerated, then the joint can take up much higher load before failure occurs. This type of joint is generally known as bearing joint. It is noted that movement of the joint can be beneficial; it allows some load redistribution, not only in the joint itself, but also in the frame of which it is a part. Both types of joints described above can be designed using limit principles.

(i) Friction grip joints

The load is carried by friction, and failure is considered to occur at slippage. From the shape of the load-movement graph (Fig. 2.1) for this region, there is little doubt that limit principles are applicable. Fig. 2.5 shows a summary of the results of test and calculation based on the strength of a single bolt joint. It is seen that good agreement is obtained.

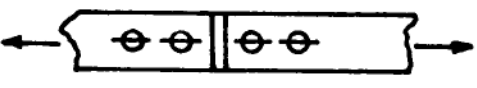
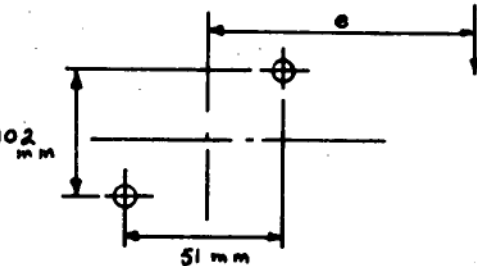
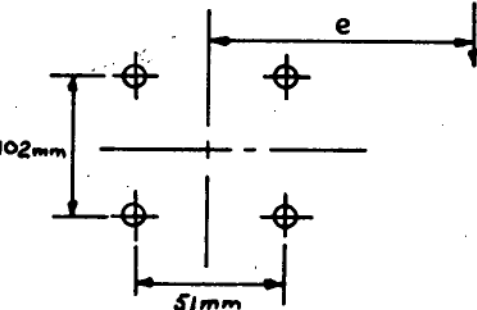
BOLT GROUP	BOLT SIZE AND TYPE	ECCEN-TRICITY (mm)	TEST SLIP LOAD (kN)	CALCULATED SLIP LOAD (kN)
	19.05 mm diam ($\frac{3}{4}$ ") HSFG	0	302 306 346	294
	15.8 mm diam ($\frac{5}{8}$ ") HSFG	152	26.7	26.7
	15.8 mm diam ($\frac{5}{8}$ ") HSFG	127	66.7	65.8

Figure 2.5

FRICTION GRIP TEST

Friction grip strengths of single bolt joints are:

147 kN for 19.05 mm HSFG bolt (average of three)

44.5 kN for 15.8 mm HSFG bolt

(ii) Bearing joints

The designer may be prepared in some cases to define failure as occurring when the ultimate load-carrying capacity of the joint is reached, i.e. some slippage is allowed. From the characteristic load-movement graph of Fig. 2.1 for this region, it is seen that there is little ductility in the bolt itself. One cannot assume, in this case, that all the bolts will reach their full strength. If limit principles of design are used, one has to designate a bolt strength at some level which all the bolts can reach on the average.

Fig. 2.6 shows a summary of the results of tests and calculations. It can be said that on the average all bolts reach about 80% of their ultimate strength. To support this conclusion results of Kulak's test (Ref. 2.4) and American Institute of Steel Construction test on rivets (Ref. 2.6) are analysed in Fig. 2.7.

2.7 LIMITATIONS ON THE APPLICATION OF THE METHOD

Limit principles can be used in the design of eccentrically loaded bolted joints without any reservation if the joint is of the high strength friction-grip type, and failure is considered to occur at slippage. It should be noted that slip resistance is affected by the condition of the surface of the connecting plates and the shape of the holes (Ref. 2.8); proper allowances must be made in the design accordingly.

If the joint is of the bearing type, certain limitations are necessary. It is obvious that the amount of load redistribution before failure in a bearing joint depends on (i) the shape and fit of the joint, and (ii) the rigidity of the connecting plates. The conclusion reached in the previous section is based on existing experimental data in which the joints are compact and the connecting plate is rather rigid. If these requirements are not met, then the above figures may be misleading. A simple way of testing the compactness of the joint is to plot eccentricity

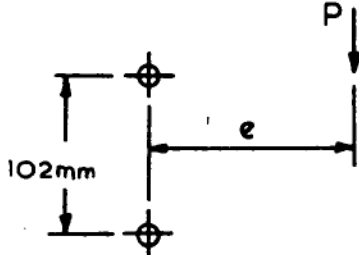
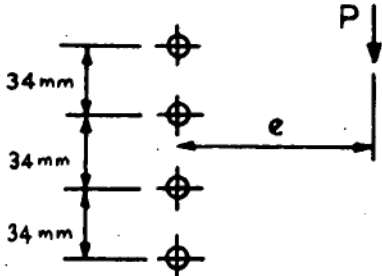
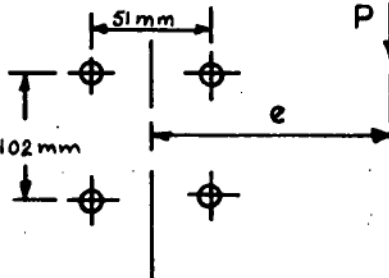
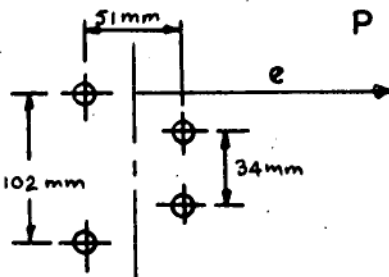
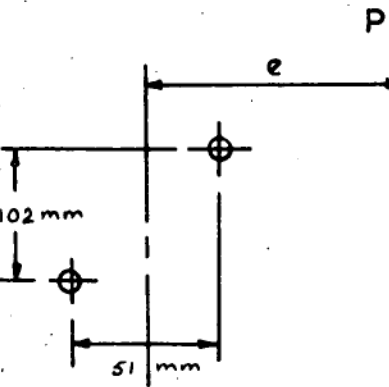
BOLT GROUP	BOLT SIZE & TYPE	EC-CENTRICITY e , in mm	TEST ULT LOAD in kN	POSITION OF CENTER e , in mm	CALCU- LATED ULT LOAD *	F/F_u
	6.35 mm dia ($\frac{1}{4}$ ") H.S. bolt $F_u =$ 38 ± 2 kN	152.4	20.7	16.9	0.632F	0.856
	as above	152.4	23.6 22.7	5.8	0.871F	0.707 0.681
	as above	177.8	36.5 40.5	46.9 21.5	1.205F	0.791 0.878
	as above	177.8	36.2	29.9	0.978F	0.968
	15.8 mm dia ($\frac{5}{8}$ ") HSFG $F_u =$ 289 kN	152.4	147.9 153.0		0.6F	0.853 0.882

Figure 2-6

BEARING TEST

* Calculations were done assuming each bolt carried the same force F at collapse.

KULAK'S TEST

(Bolts are ASTM A325 $\frac{3}{4}$ in diam. — for details of joints see Ref.2.4)

Ultimate strength of individual bolt $F_u = 329 \pm 10$ kN.

Specimen Number	Eccentricity e, in mm.	Test ultimate load, in kN	Position of center c, in mm.	Calculated Ultimate Load (% F) *	F/F _u
B1	203	500.4	18.2	1.836F	0.828
B2	254	511.5	20.0	1.768F	0.879
B3	305	422.6	12.5	1.489F	0.862
B4	330	558.2	28.8	1.996F	0.849
B5	381	491.5	24.3	1.747F	0.855
B6	305	587.1	25.4	2.119F	0.842
B7	381	471.5	20.3	1.717F	0.834
B8	381	591.6	22.4	2.199F	0.817

A I S C TEST

(Rivets are $\frac{3}{4}$ in diam. — for details of joints see Ref.2.6)

Ultimate strength of individual rivet $F_u = 267$ kN

Specimen Number	Eccentricity e, in mm.	Test ultimate load, in kN	Position of center c, in mm.	Calculated Ultimate Load *	F/F _u
TP1	63	480	46.5	2.041F	0.88
TP2	89	358	25.0	1.624F	0.82
TP3	165	222	3.82	0.910F	0.92
TP4	63	1223	245.9	5.371F	0.85
TP5	114	978	118.9	4.407F	0.83
TP6	165	805	72.1	3.506F	0.86
TP7	89	493	34.1	1.855F	0.99
TP8	165	267	21.8	1.124F	0.89
TP9	89	1263	75.6	5.480F	0.86
TP10	165	787	42.6	3.603F	0.81

* Calculations were done assuming each bolt carried the same force F at collapse.

Figure 2.7

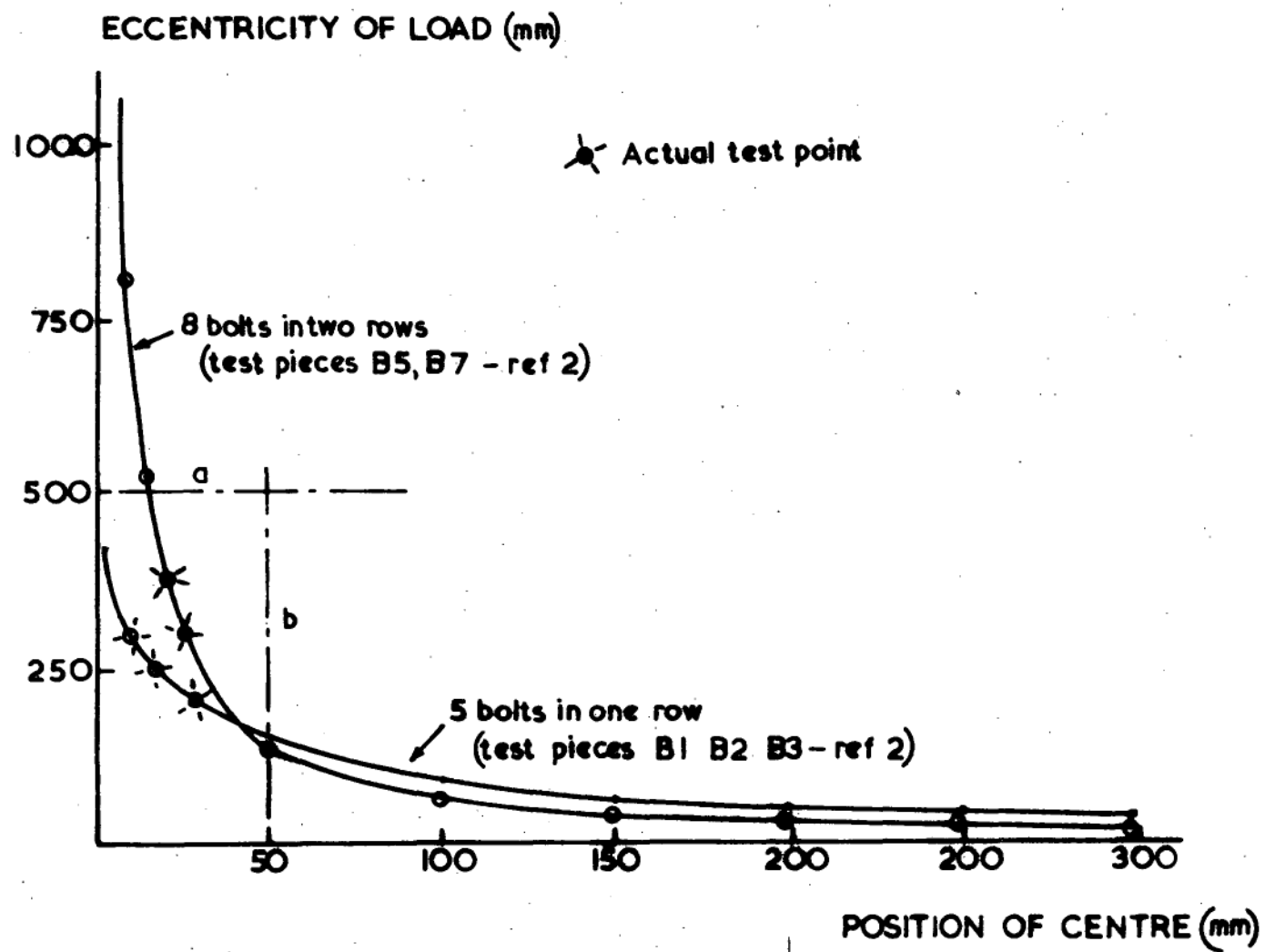


Figure 2.8

against the position of the centre. In Fig. 2.8 it is seen that most tested joints fall in the region a b. Another criterion, which is rather obvious, is that the amount of load redistribution occurs more fully if the bolt lever arms 'r' are more nearly 'equal'. If the two above criteria are observed, then the limit design method will give a good indication of the joint strength.

2.8 CONCLUDING REMARKS

The design method presented above is a good example of how the limit principles, derived from the plastic analysis of steel frames, are made to work or can be made to work in a different situation. A simple statically admissible state is chosen, from which the strength of the joint is estimated. For friction grip joints it is a lower bound method. For bearing joints it is not a lower bound method due to the lack of ductility of the individual bolts. An empirical factor has been introduced by assigning the average strength of the bolts to some value less than their actual strength. The complexities of the joint (lack of fit, local yielding of plate, non-linear behaviour of the bolt) and the need for a simple method of design makes the introduction of such an empirical factor unavoidable. What is needed is further experimental data so that definite limitations can be placed on the size and layout of joints, and thus render this approach acceptable for use in the design office.

Since the strength of the whole connection must necessarily include the strength of the connecting members, the established solution, strictly speaking, are only partial lower bound solution. A complete lower bound solution can only be established if the strengths of the connecting members are also assessed.

CHAPTER III

THE USE OF THRUST LINES IN THE DESIGN OF FRAMES

3.1 INTRODUCTION

In this chapter, the use of the limit design method of picturing the statically admissible state is further explored, in a simple well-known context, that of the design of frames. One of the most satisfying ways of picturing the statically admissible state for a frame is to draw its thrust lines. The idea, which originated in the design of masonry arches, is extended here to cover multi-bay, multi-storey frames and some classes of space frames.

Once the thrust lines are drawn, moments, shears, and thrusts can be estimated. The moment-shear-thrust diagrams are then 'covered' with strength, i.e. the members are proportioned so that the yield condition is satisfied everywhere. A safe design results, based on the lower bound theorem of plastic limit analysis.

This chapter consists of two parts. In the first part, a practical minimum mass design method is proposed combining the older and well-tried method of design of plane frames by guessing points of inflexion and the lower bound theorem of plastic limit analysis. In the second part, the use of thrust lines in the analysis of space frames is explored. Three cases are considered: (i) simple space frames under horizontal loads, (ii) free-standing staircases, and (iii) arch-ribbed domes. Experimental results are used to check the calculations.

3.2 PRACTICAL MINIMUM MASS DESIGN OF FRAMES BY GUESSING POINTS OF INFLEXION

A simple way of obtaining a statically admissible state for a frame is to guess enough points of inflexion so that the thrust line can be drawn. If a linear relation is used between the mass /length of a beam and its plastic moment, as depicted by Baker in Reference 3.1, then a practical

approximate minimum mass design can be achieved by moving the points of inflexion until a more favorable moment distribution results. The method need not be pressed so far that an absolute minimum mass solution is achieved. The designer, with a table of available beam sizes, can soon reach a satisfactory solution which is sufficiently close to minimum mass.

Many plane frames or structures containing plane frames are designed and built. Often much time is spent in proportioning them, whether by elastic design (which is very tedious) or by the quicker known method of plastic design. It is a matter of some satisfaction to the author to have combined the very old method of guessing points of inflexion with the power of the lower bound theorem of plastic design to produce a simple and rapid method of direct design.

3.2.1 REPRESENTATION OF FORCES IN FRAMES BY THRUST LINES

The basic properties of the thrust line hold whether the frame is elastic or plastic; namely its component in the direction of the member is the axial force, the component normal to the member is the shear force, and the product of the normal distance from any point on the member and the magnitude of the thrust is the bending moment at the point. The idea is quite often used in the analysis of arches. The extension to plane frames containing several bays or several storeys appears complicated but is in fact simple. The seemingly complex force diagrams can be drawn quite readily with practice and need little explanation, so little is given.

Fig. 3.1(b) shows the thrust line for the loaded portal frame of Fig. 3.1(a). The thrust line is drawn by guessing two points of inflexion on the beam and one on one of the columns. The fourth point of inflexion is given by equilibrium considerations as indicated by the force diagram, Fig. 3.1(c). The resultant bending moment diagram is given in Fig. 3.1(d).

Similarly, Fig. 3.2(b) shows the diagram of the thrust lines for the

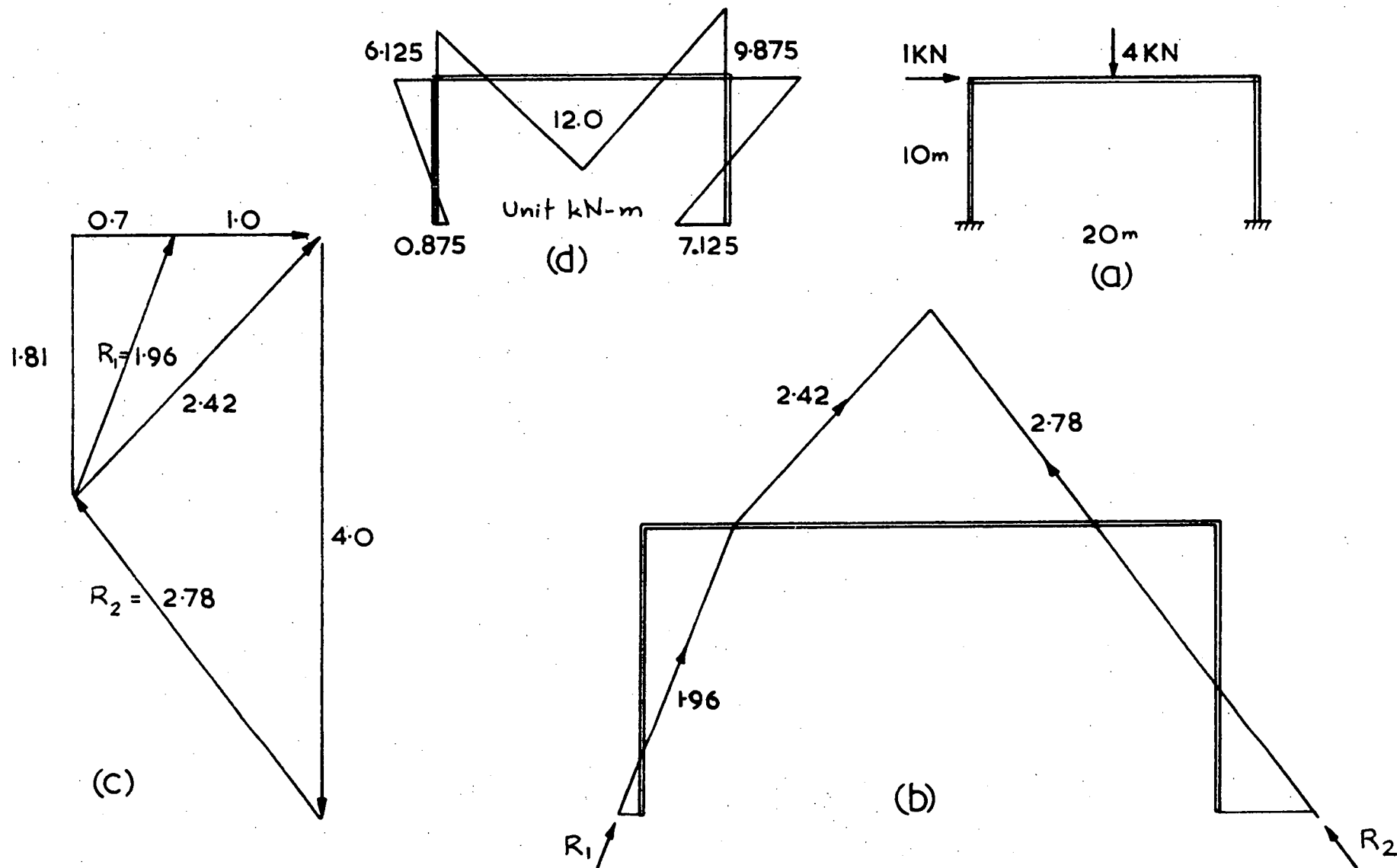


Figure 3.1

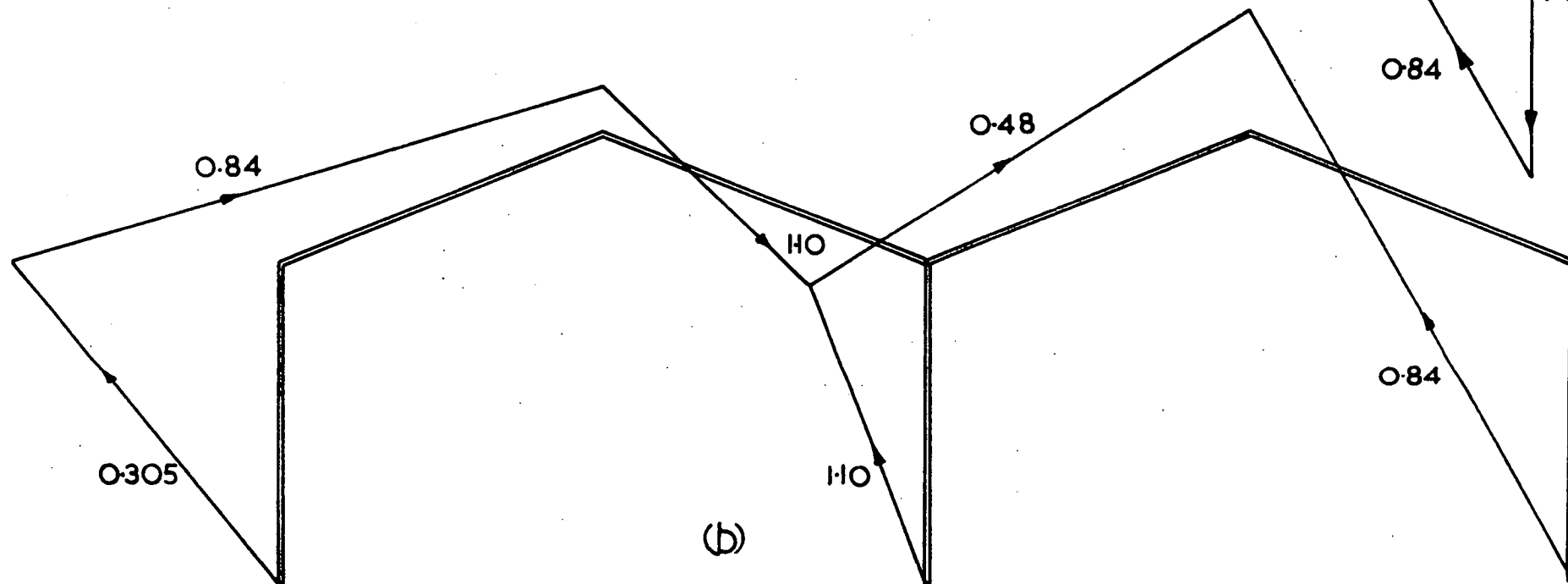
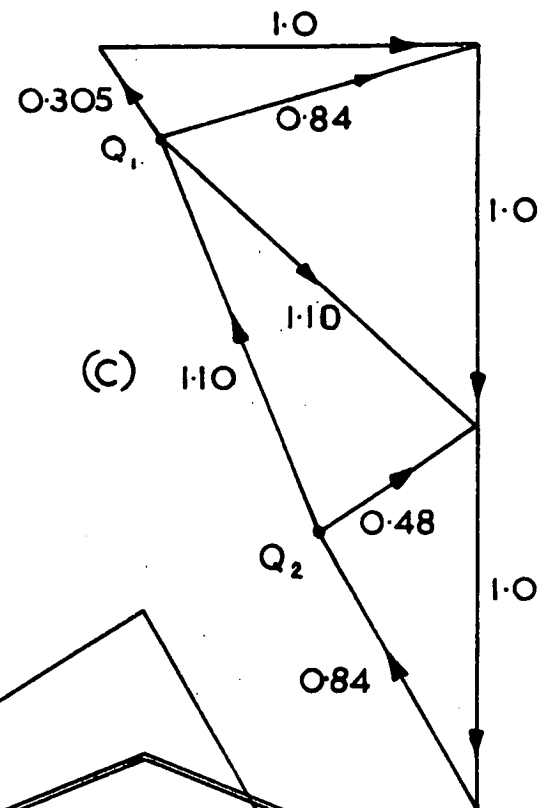
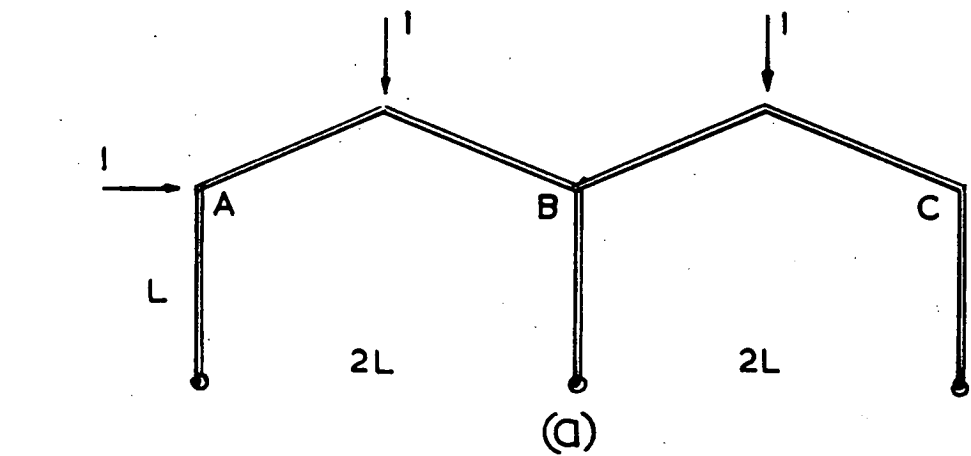
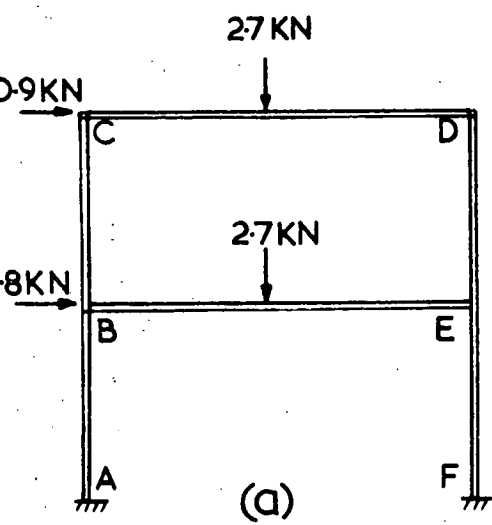
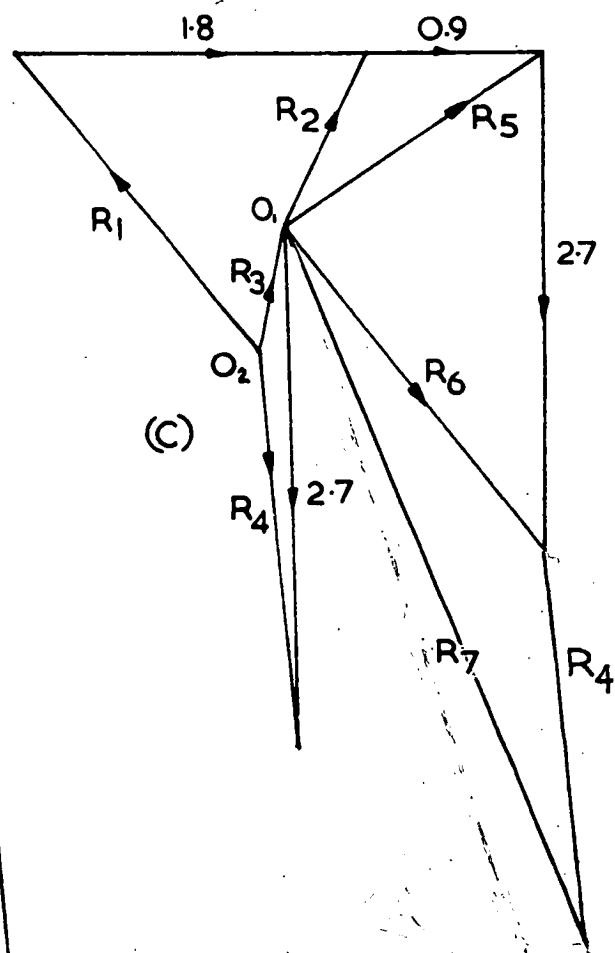


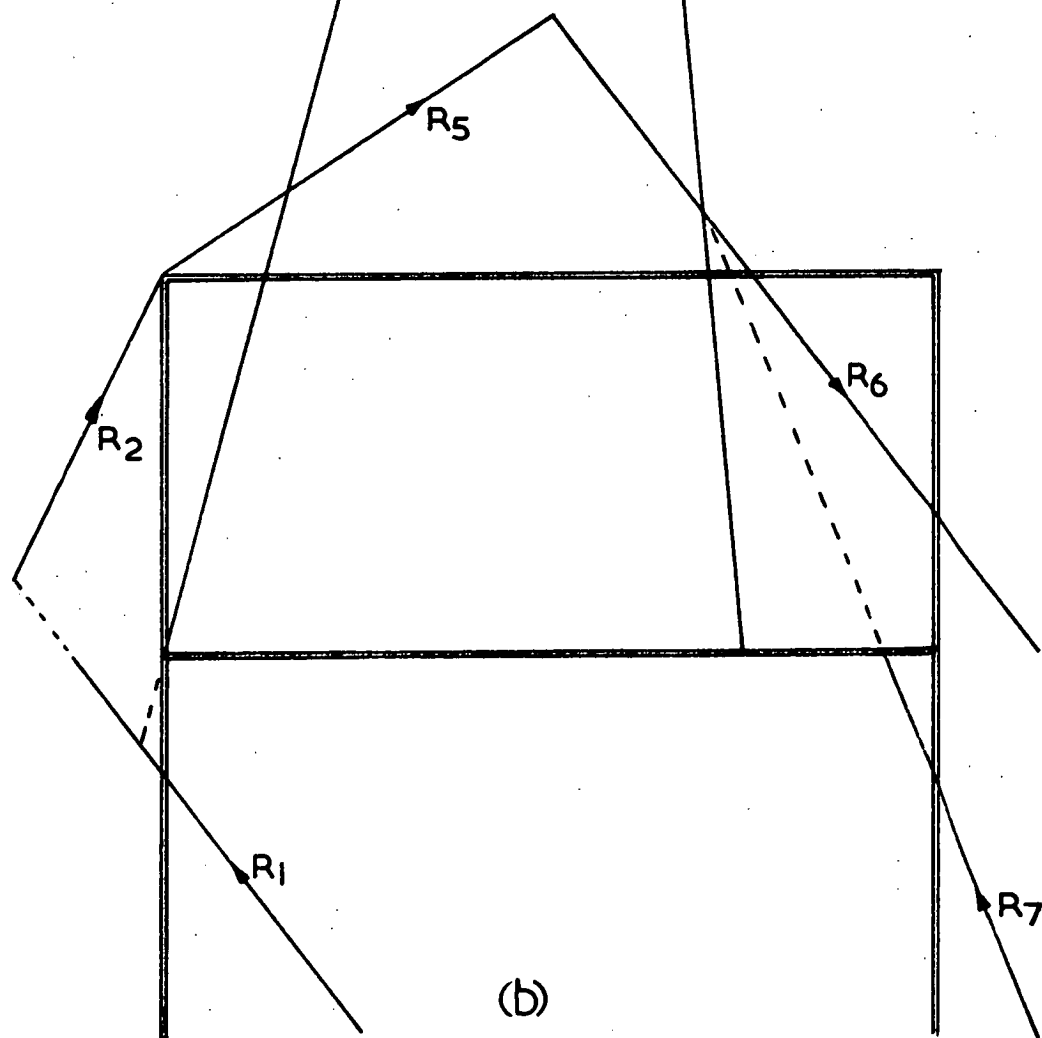
Figure 3.2



(a)



(c)



(b)

Figure 3.3

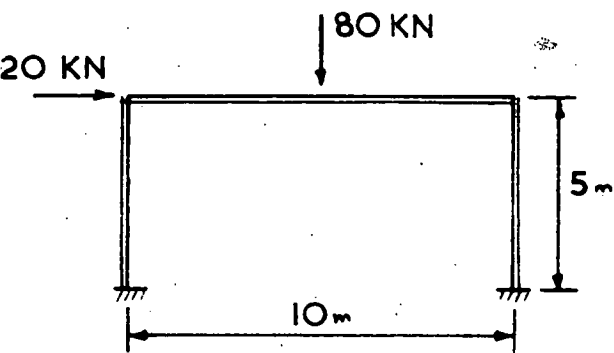
two-bay pitched roof frame of Fig. 3.2(a). The three thrust lines for the three members that meet at joint B also meet, but elsewhere, to satisfy statical equilibrium. Fig. 3.3(b) shows a suitable statically admissible state for a two-storey frame with both vertical and horizontal loadings, Fig. 3.3(a). Note that the three thrust lines for the three members with the common joint E meet, while those for joint B do not meet, but are in equilibrium with the external horizontal load as shown on the force diagram, Fig. 3.3(c). The diagrams of Fig. 3.2 and 3.3 may appear a little complex, as graphical constructions often do. They are, with a little practice, very easy to draw, and their drawing gives an insight into frame behaviour which is obtainable in no other simple way.

3.2.2 MINIMUM MASS DESIGN BY GUESSING POINTS OF INFLEXION

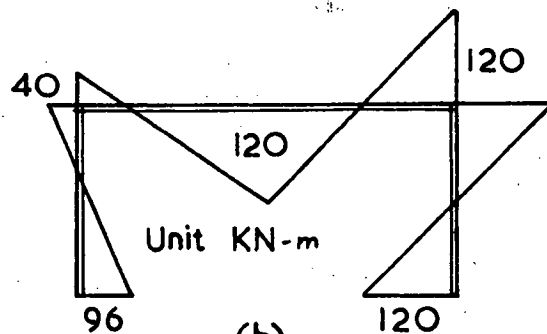
Figs. 3.1, 3.2 and 3.3 are pictures of plausible equilibrium states, upon which designs can be based by drawing the resultant bending moment diagrams and shear force diagrams and "covering" the members with strength. The designs are then safe. It is obvious that the resulting bending moment diagram should be made to correspond to a collapse mechanism so that all three basic conditions of equilibrium, mechanism, and yield are met. This is done by matching the maximum bending moments with the plastic moments of the sections at a sufficient number of points on the frame. To obtain a minimum weight design it is only necessary to shift the points of inflexion to obtain a more favourable distribution of moments. The following examples illustrate the method. In these examples, the loads have been multiplied by a design load factor λ , and since the mechanism condition is always observed, λ is also the actual collapse load factor for the frame. Some of the examples are taken from Reference 3.2.

Single-bay portal frame

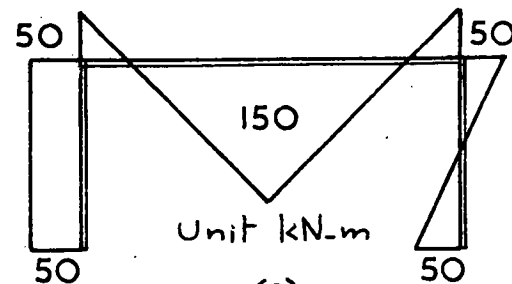
Consider the frame of Fig. 3.4(a). A plausible equilibrium state is obtained by guessing two points of inflexion on the beam at $1/8$ and $1/4$



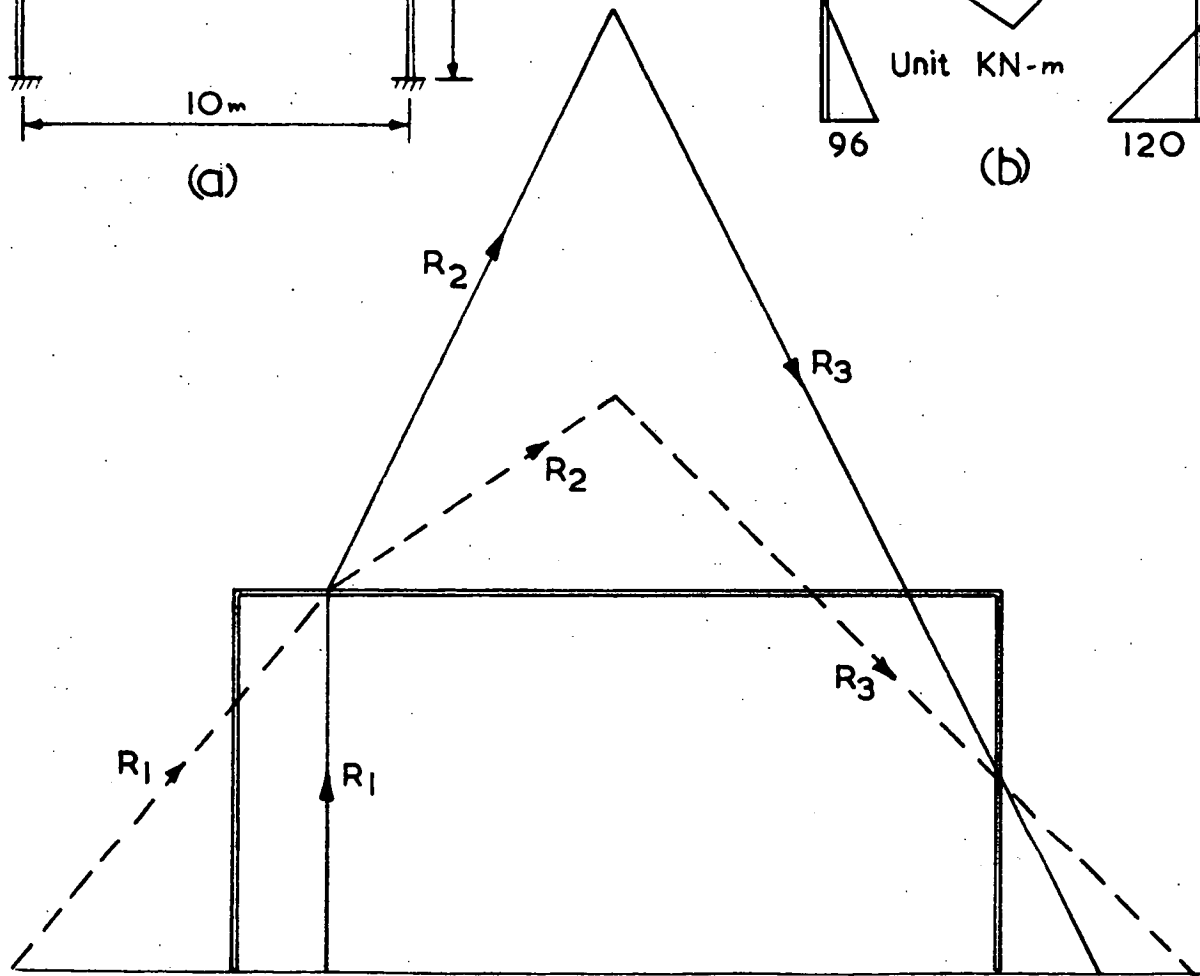
(a)



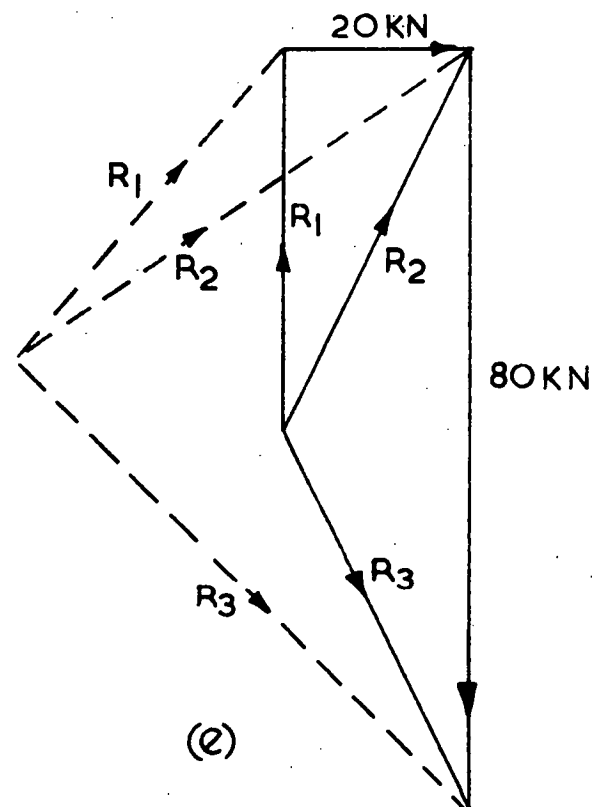
(b)



(c)



(d)



(e)

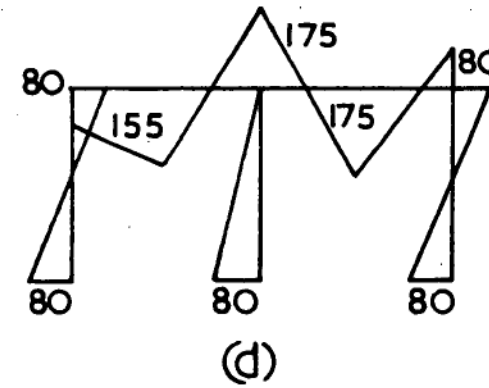
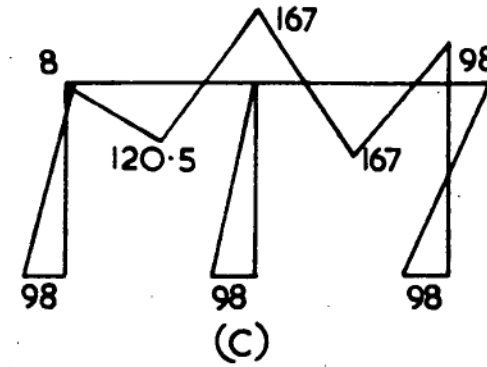
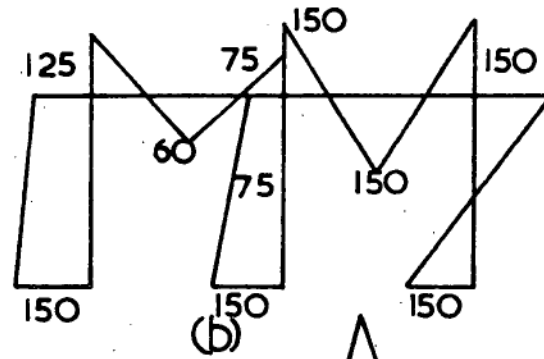
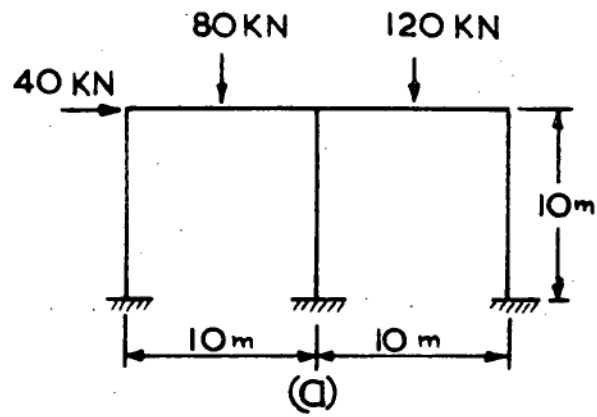
Figure 3·4

span from each end. The thrust line, shown dotted in Fig. 3.4(d), indicates that the frame requires a plastic moment of 120 kN-m for both beam and column. The nearest universal section, available in Australia (Ref. 3.3), is a 250 UB, 37 kg/m, with plastic section modulus $Z_p = 485 \times 10^3 \text{ mm}^3$. The mass of the designed frame is $20 \times 37 = 740 \text{ kg}$. To reduce the mass of the frame, it is desirable that more moment should be put in the beam and less in the columns. This is done by shifting the $1/4$ span point of inflexion to $1/8$. This gives the solid thrust line of Fig. 3.4(d) and the resultant bending moment diagram Fig. 3.4(c). The design becomes: column: 200 UB, 25 kg/m, $Z_p = 260 \times 10^3 \text{ mm}^3$, beam: 310 UB, 40 kg/m, $Z_p = 625 \times 10^3 \text{ mm}^3$. The mass of the frame is then $(10 \times 40) + (19 \times 25) = 650 \text{ kg}$. Any further shift will not give a lower mass design, and the above design is accepted as satisfactory.

Two-bay portal frame

Consider the two-bay portal frame of Fig. 3.5(a) with the loading as shown. This frame is first designed with the condition that all members are of equal cross section, of uniform M_p . Thus from among various possible statically admissible states that state which has all the bending moment distributed rather evenly must be selected. This is done by trial and error. One of the more favourable bending moment distributions is represented by the dotted thrust line of Fig. 3.5(e); the resultant bending moment diagram is drawn in Fig. 3.5(b). To "cover" this bending moment diagram with bending strength, the section 310 UB, 40 kg/m, $Z_p = 625 \times 10^3 \text{ mm}^3$, is selected. This gives the mass of the frame as $5 \times 10 \times 40 = 2000 \text{ kg}$.

Alternatively, if we are prepared to use two sizes of ^{section} beam, one for the two beams and the other for the three stanchions, the minimum mass design proceeds as follows. More moment should be placed on the beams and less on the columns. The solid thrust lines of Fig. 3.5(c) give the bending moment diagram of Fig. 3.5(c). This results in the design



B.M.D Unit kN-m.

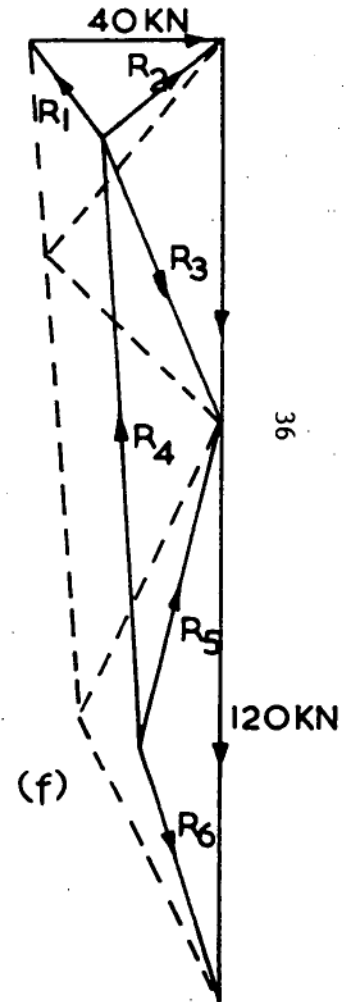
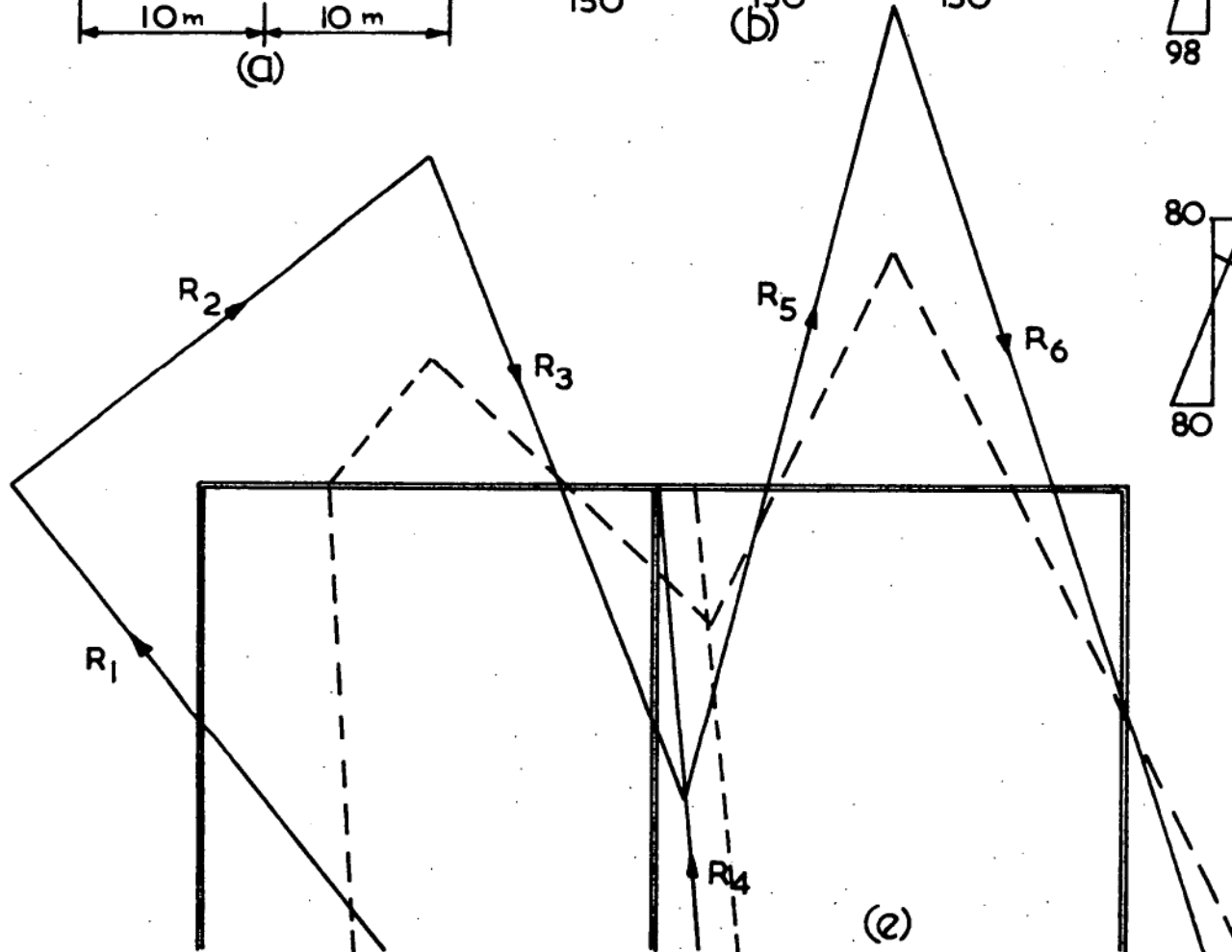


Figure 3.5

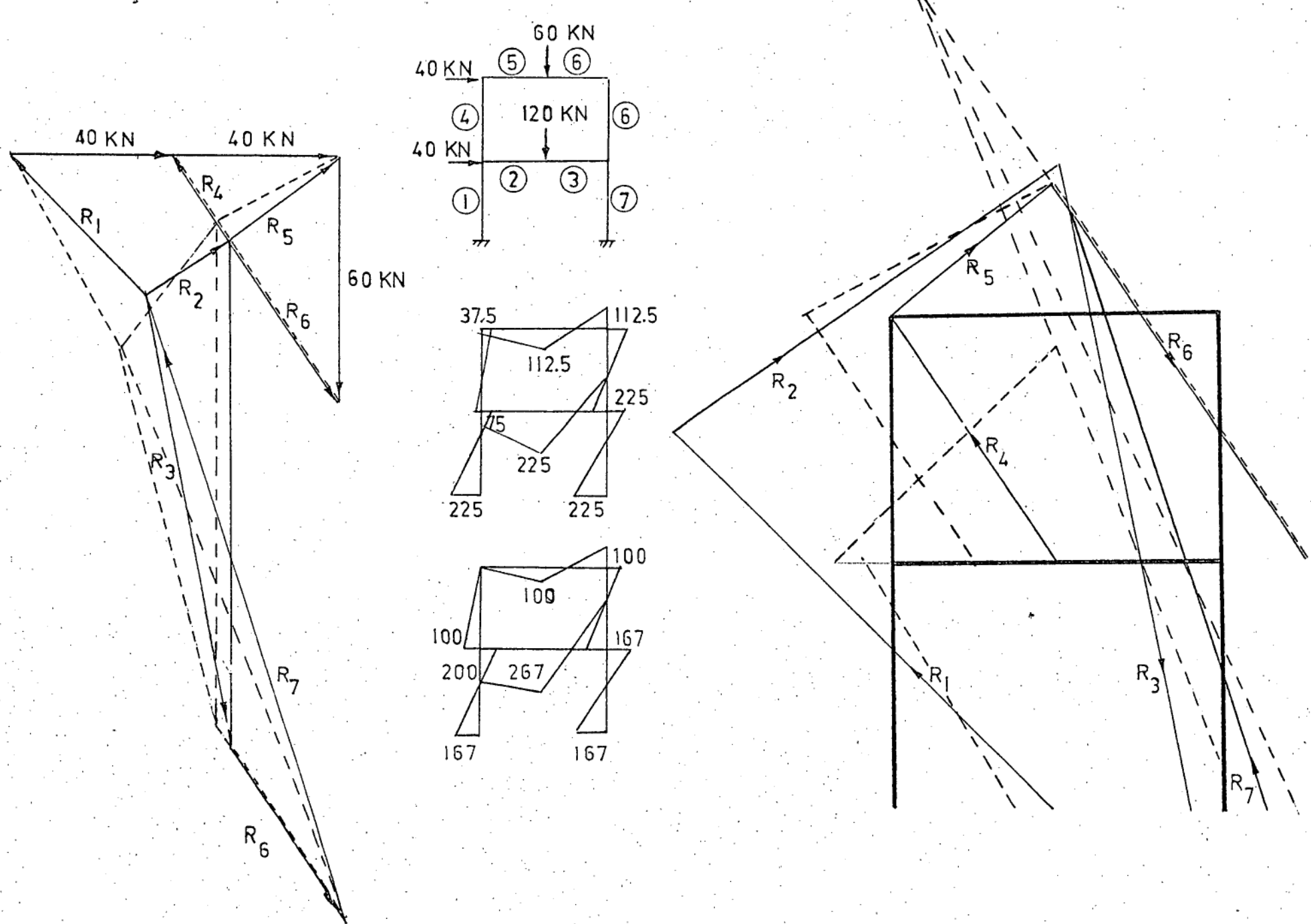


FIGURE 3.6

columns: 250 UB, 31 kg/m, $Z_p = 396 \times 10^3 \text{ mm}^3$; beams 310 UB, 46 kg/m, $Z_p = 723 \times 10^3 \text{ mm}^3$. The mass of the frame is then $(30 \times 31) + (20 \times 46) = 1850 \text{ kg}$. This is a practical minimum mass. The "true" minimum mass solution is given by Fig. 3.5(d), (if a linear weight function is used), but will not result in a lighter frame due to the limited availability of sections.

Two-storey frame

The two-storey frame of Fig. 3.6(a) is to be designed for the loading shown. The frame is first designed so that each storey has uniform section members. This condition requires an even moment distribution for each storey, such as that given in Fig. 3.6(b). The design is then top storey: 250 UB, 37 kg/m, bottom storey: 410 UB, 54 kg/m. The mass of the frame is then $(37 \times 25) + (54 \times 25) = 2280 \text{ kg}$.

The frame is now re-designed for minimum mass. This is done by reducing the moments in the top storey, increasing the moments in the bottom storey beam and reducing those in the bottom columns. The modified thrust line of Fig. 3.6(d) gives the bending moments of Fig. 3.6(c). The design becomes: top storey beam and stanchion: 250 UB, 31 kg/m; bottom storey beam: 410 UB, 54 kg/m; bottom storey stanchions: 360 UB, 45 kg/m. The mass of the frame is reduced to $(31 \times 25) + (45 \times 15) + (54 \times 10) = 1990 \text{ kg}$.

3.3 THE USE OF THRUST LINES IN THE ANALYSIS OF SPACE FRAMES

Most of the research work in plastic limit analysis applying to space frames has been concerned with either transversely loaded grids or with beams which are curved in plane. For space frames, the number of possible collapse modes is large, and the reliability of designs based on an assumed collapse mode depends very much on how closely the assumed mode approximates the actual collapse mode.

In this section, the use of thrust lines to picture statically admissible state is explored for various frames and loading conditions. The basic properties of the space thrust line are similar to those of the plane thrust line. Since the line is now in space there are two shear components, two bending moment components, and one torsion component to be considered, in addition to the axial force.

3.3.1 Simple space frames under horizontal loads

The load-carrying capacity of the simple portal type space frame of Fig. 3.7(a) is examined for horizontal loads in two different directions. All the horizontal members of the frame form a truss-like structure, which will not deform substantially under horizontal load. The collapse mode of the frame involves the formation of hinges on the columns only. The column section is circular so that the plastic moment is the same about any cross-sectional axis. ~~The torsional resistance of the column is neglected~~

The test frames were made from 3mm diameter welding rod, the column length is 210 mm. The torsional strength of the column is therefore negligible compared with its flexural strength. Fig. 3.7(a) shows a plausible thrust line pattern for the indicated horizontal loading. Torsional strength has been neglected in this construction of the thrust line, therefore the thrust line is in the same plane with the column. It is part of the lower limit design philosophy that a minor source of strength can be neglected.

thrusts are in equilibrium with the applied force H . Since the frame has rigid bases, it can be shown that the maximum resistance of each column is $F = 2M_p/h$, where M_p is the plastic moment of the section and h is the height of the columns.

For the case of Fig. 3.7(a), the center of rotation is found to be at A; for the case of Fig. 3.8(a), the center is found to be at a distance $0.355L$ from the side. Fig. 3.9 shows the measured load against deflexion graphs and the results of calculations. The calculated values are less than the actual collapse loads due to the omission of torsional strength

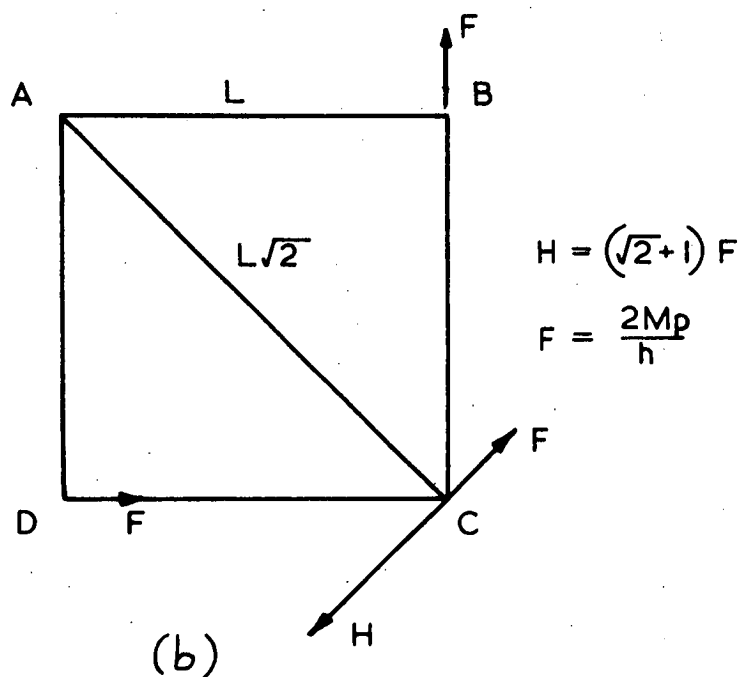
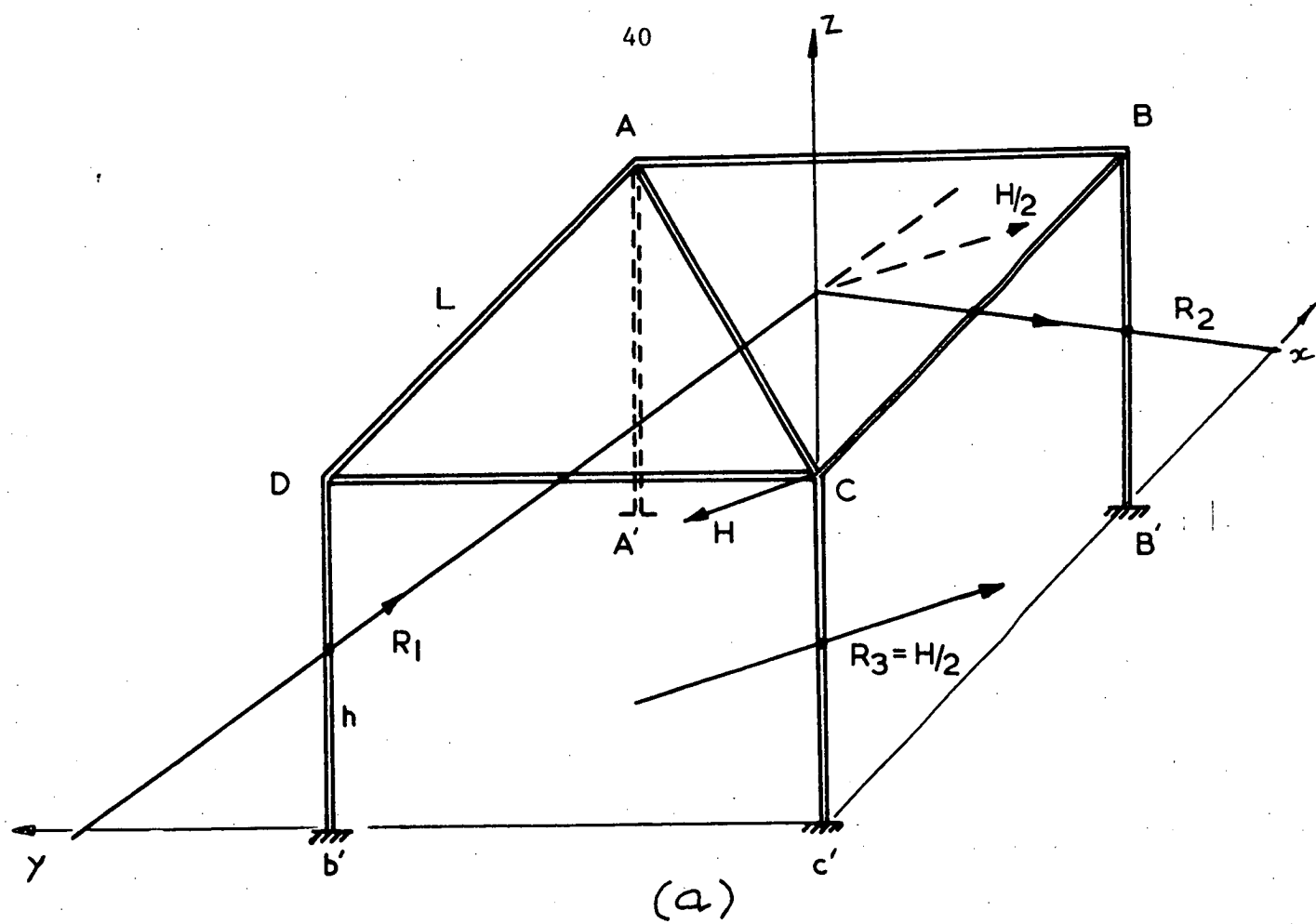
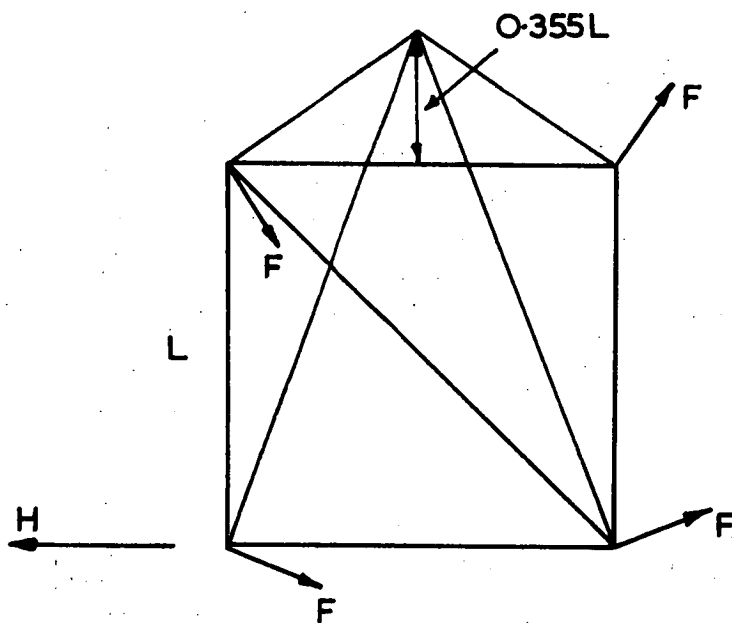
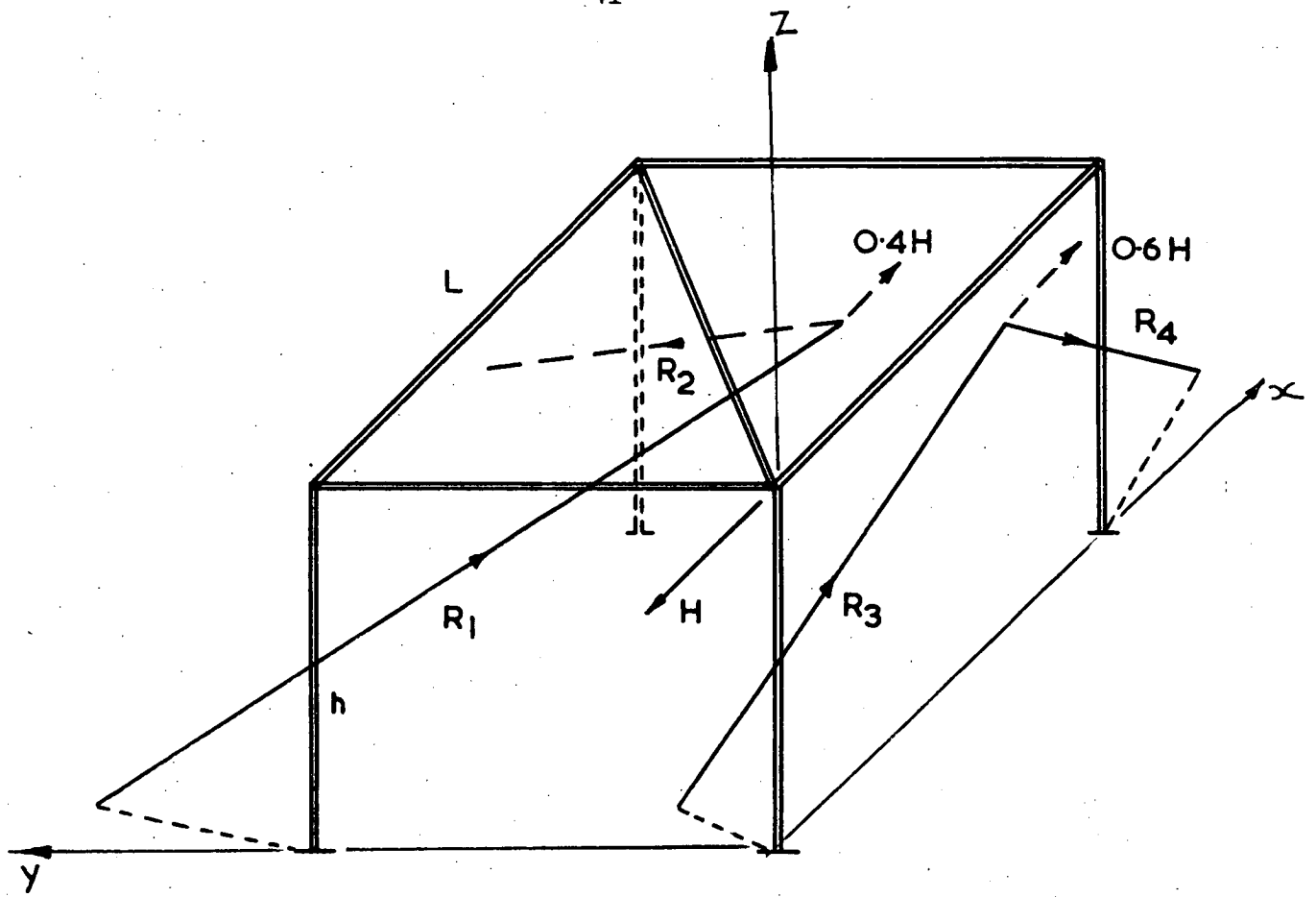


Figure 3.7



$$H = 3.03F$$

$$F = \frac{2Mp}{h}$$

Figure 3.8

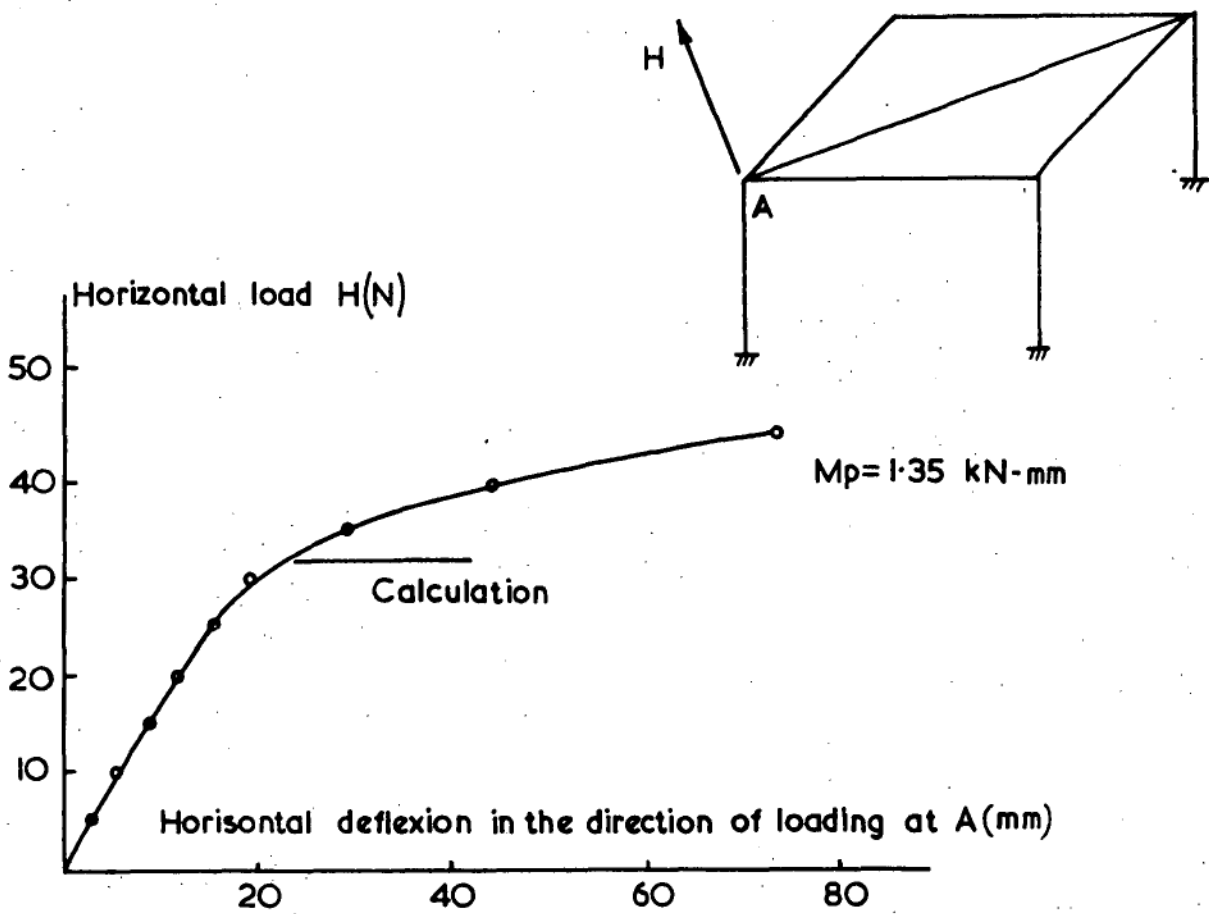
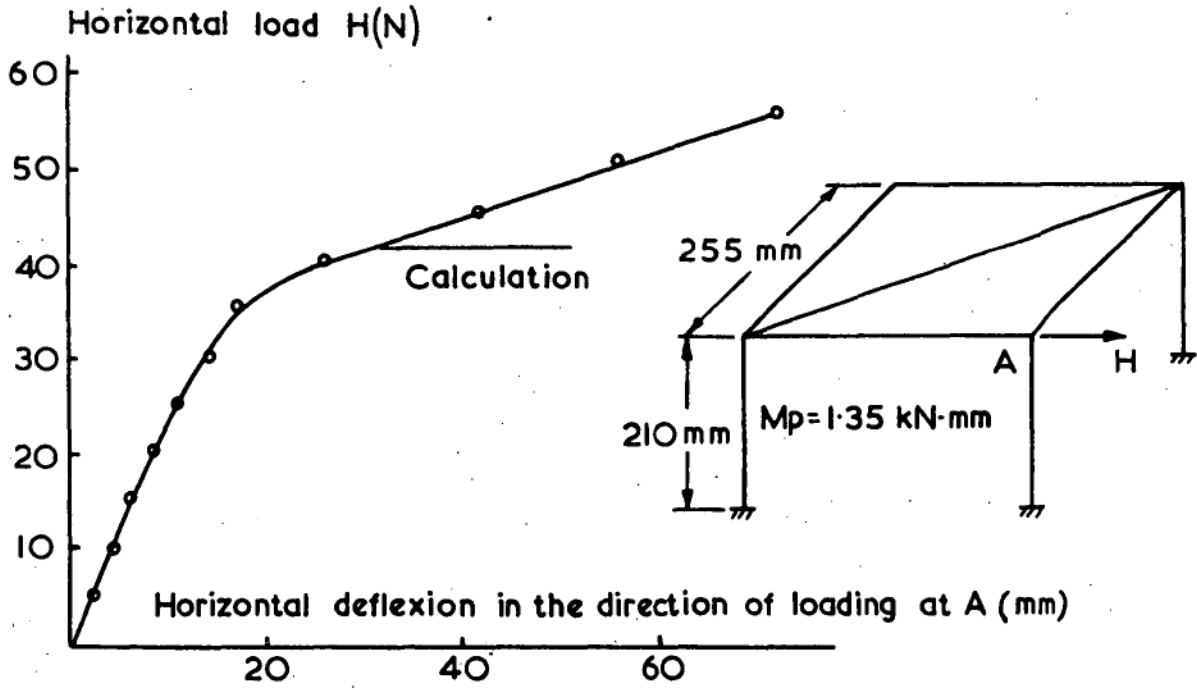


Figure 3.9

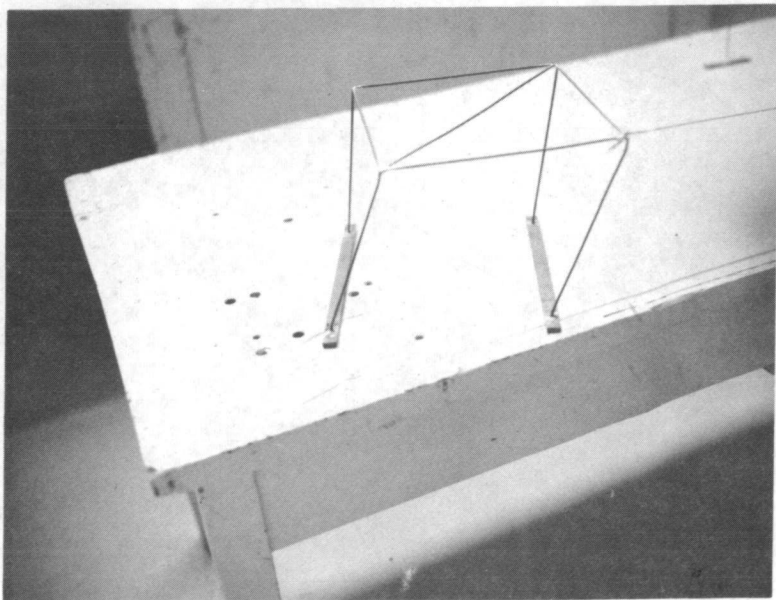
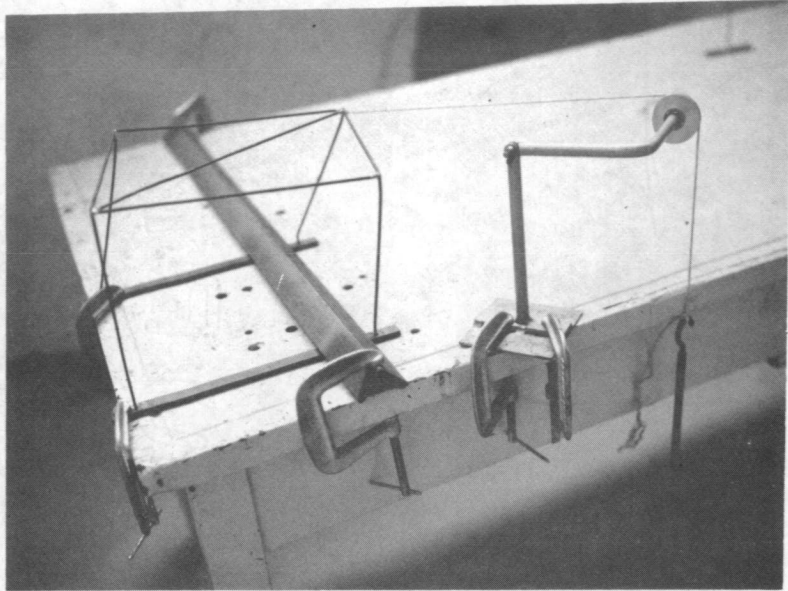


FIGURE 3.10

The collapse of space frames under horizontal loads.

in the calculations. Fig. 3.10 shows the actual collapse pictures of the frames; it can be seen that the assumptions of a rigid platform and of a center of rotation are experimentally justified.

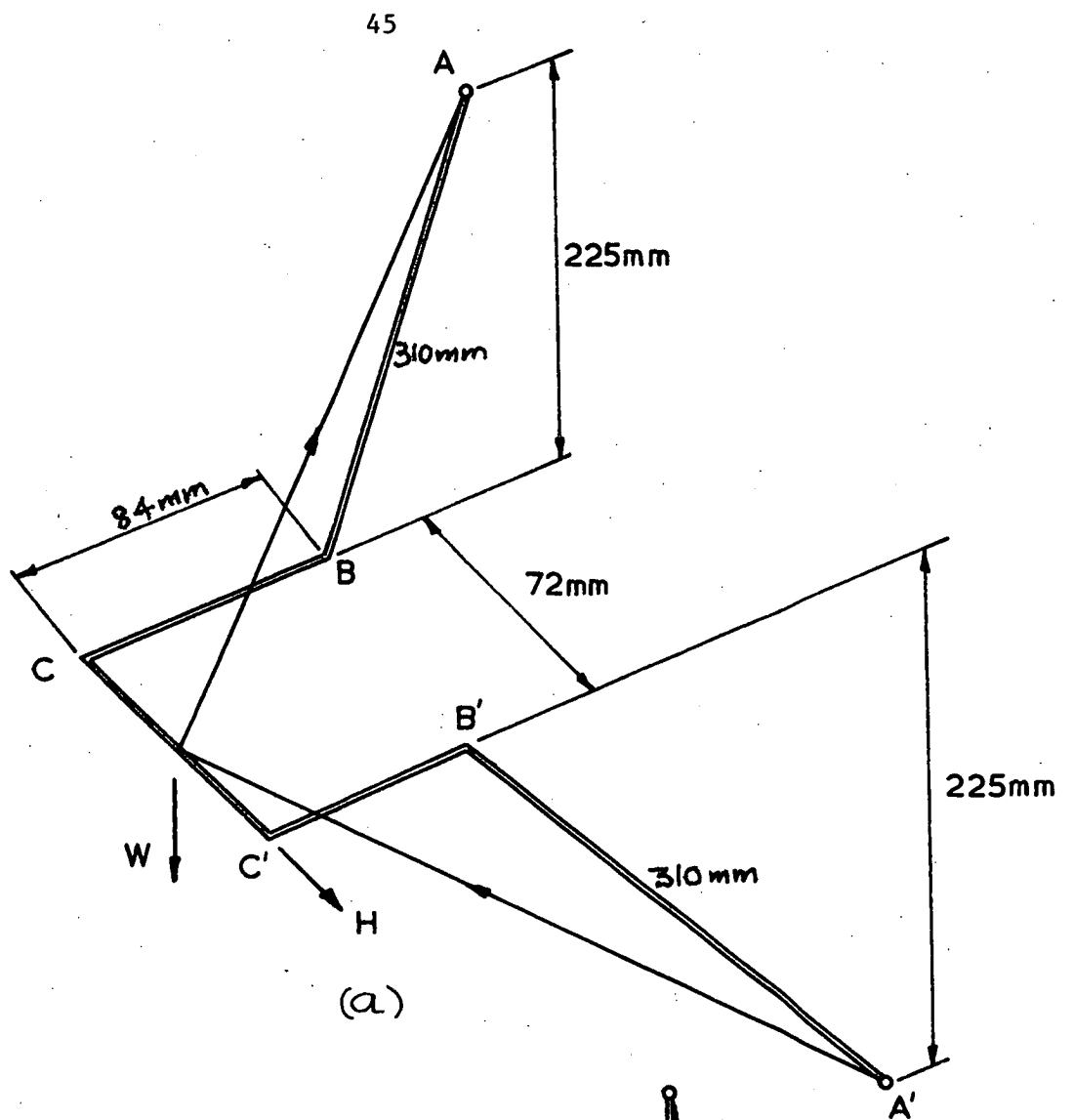
3.3.2 The free-standing staircase

The free-standing staircase of Fig. 3.11(a) is analysed for a concentrated vertical load W as shown. For ease of analysis, the end of the stair is assumed to be pinned. The stair is restrained from horizontal sway. The thrust line indicates that there is a horizontal force component H . The value of H can be estimated from the thrust line position and the value of W .

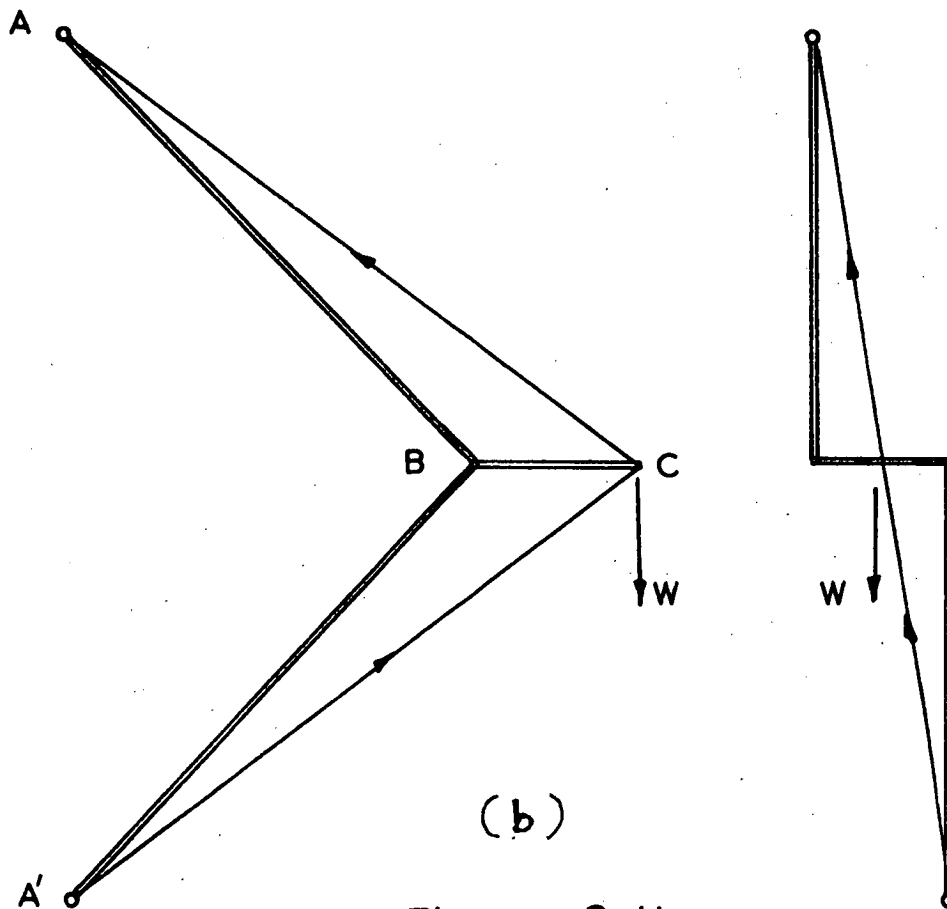
From the thrust line of Fig. 3.11(b), the three components of the thrust are $F_x = 0.67W$, $F_y = 0.08W$, $F_z = 0.50W$; the magnitude of the thrust F is $0.834W$. The maximum moments occur at the joints B and B' , and their magnitudes are given by $M_{\max} = F \cdot a$, where a is the normal distance from the thrust line to joints B or B' . Calculations were performed with the values of a measured from the undeformed and deformed frame. Fig. 3.12 shows the results of measurement and calculation on a small model staircase, made of circular rods. The calculation is not a complete analysis, but only a statical check via thrust line. The purpose is to demonstrate the use of thrust line in picturing the statics of this particular frame.

pinned arch-ribbed dome under a vertical load placed on one of the ribs. (see Fig. 3.14).

For the arches 2-2', 3-3' and 4-4', which carry no external loads, the thrust lines are straight lines which go through the pins at crown and supports. The maximum moments occur at the centers of the ribs. Due to symmetry, the thrusts in the arches 2-2', 3-3', 4-4', and in the rib 0-1' can be resolved into a vertical force and a horizontal force at the crown 0 in the plane of the arch 1-1'. These forces must be in equilibrium with



(a)



(b)

Figure 3·11

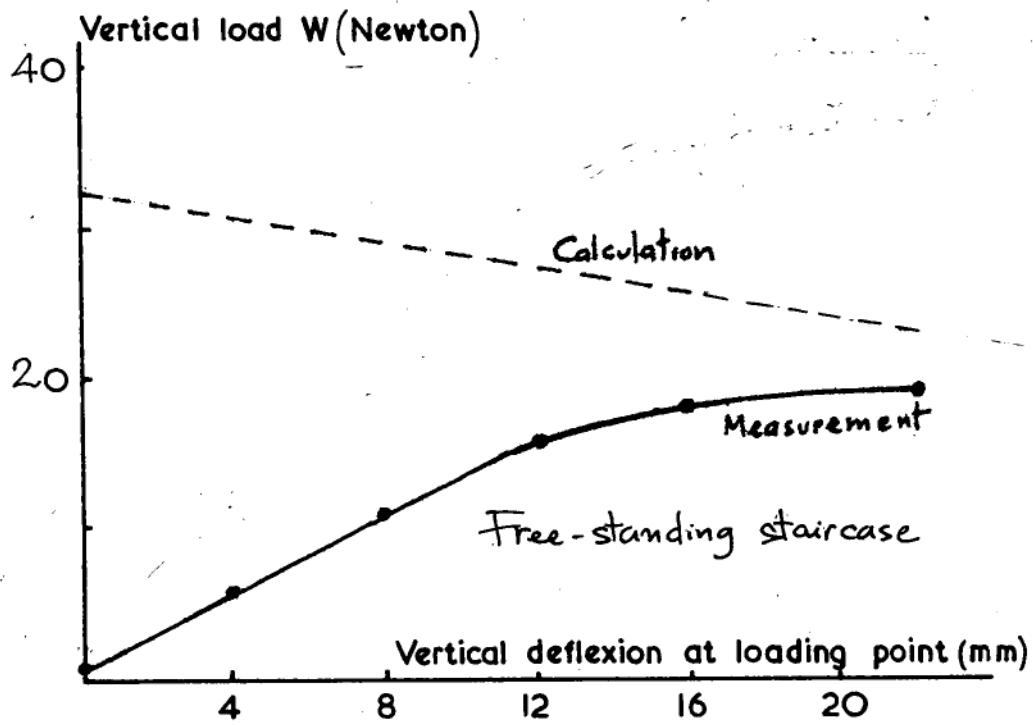


Figure 3.12

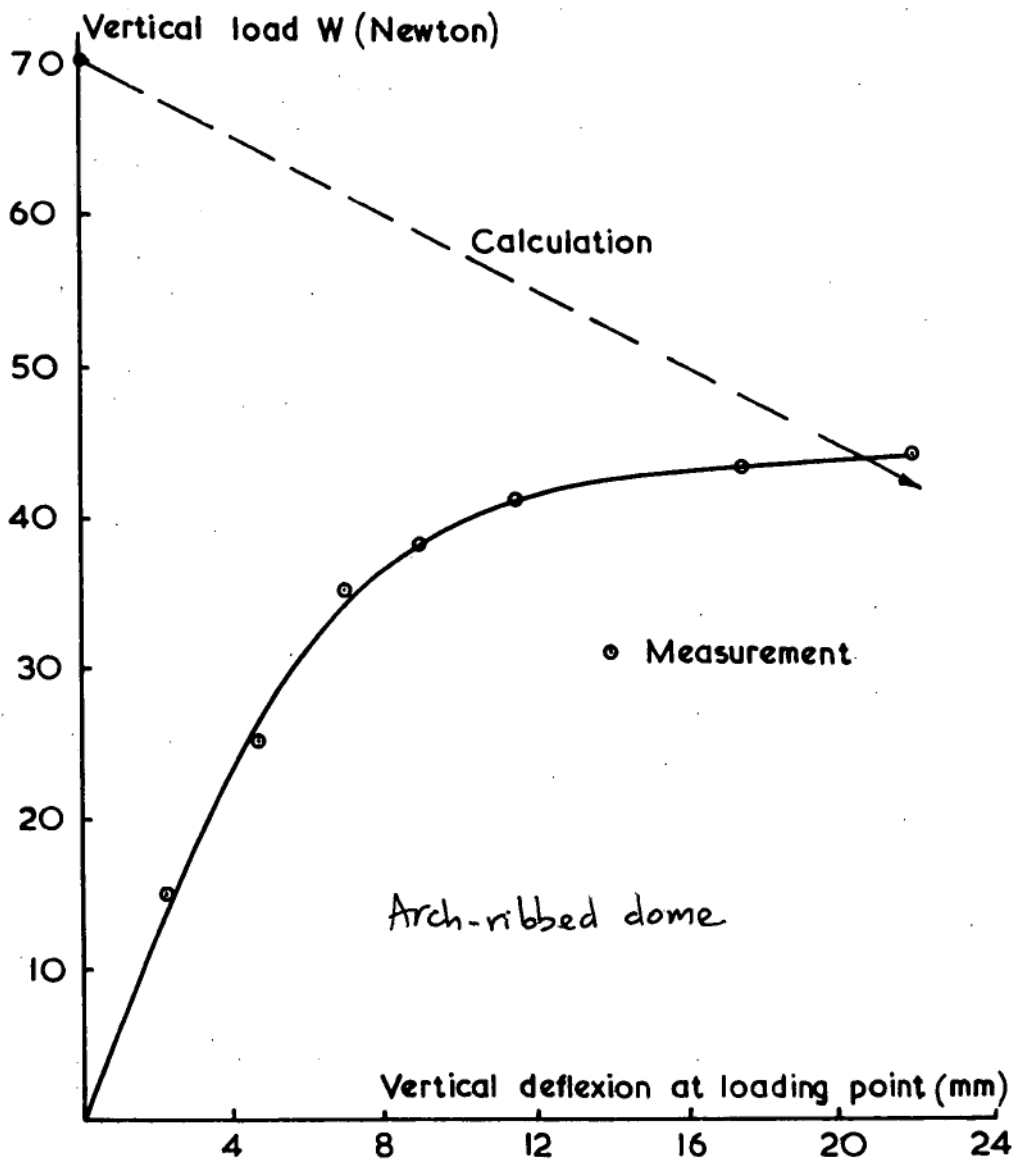


Figure 3.16

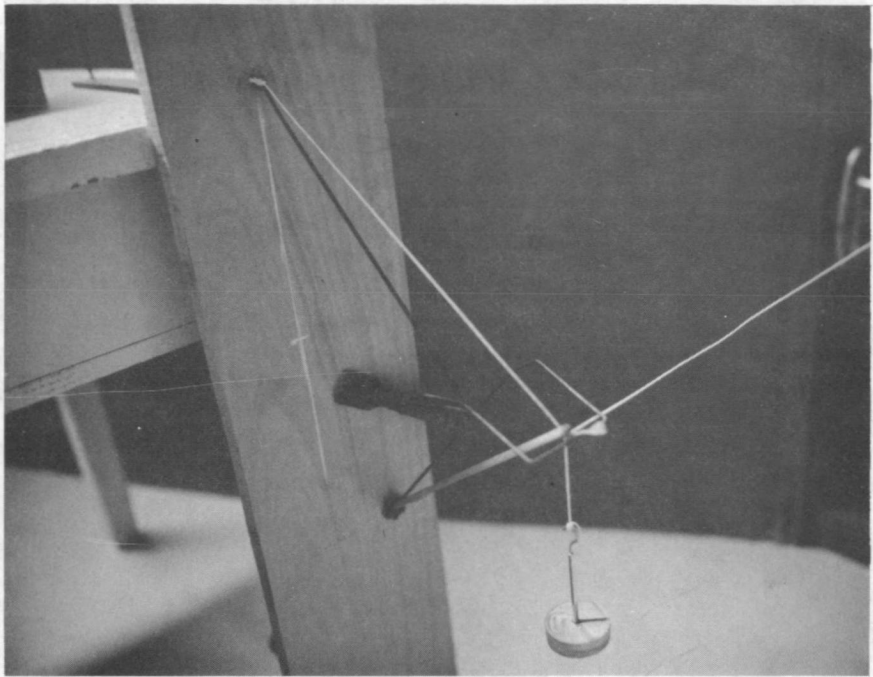


FIGURE 3.13

Model of the thrust line for the free standing staircase.

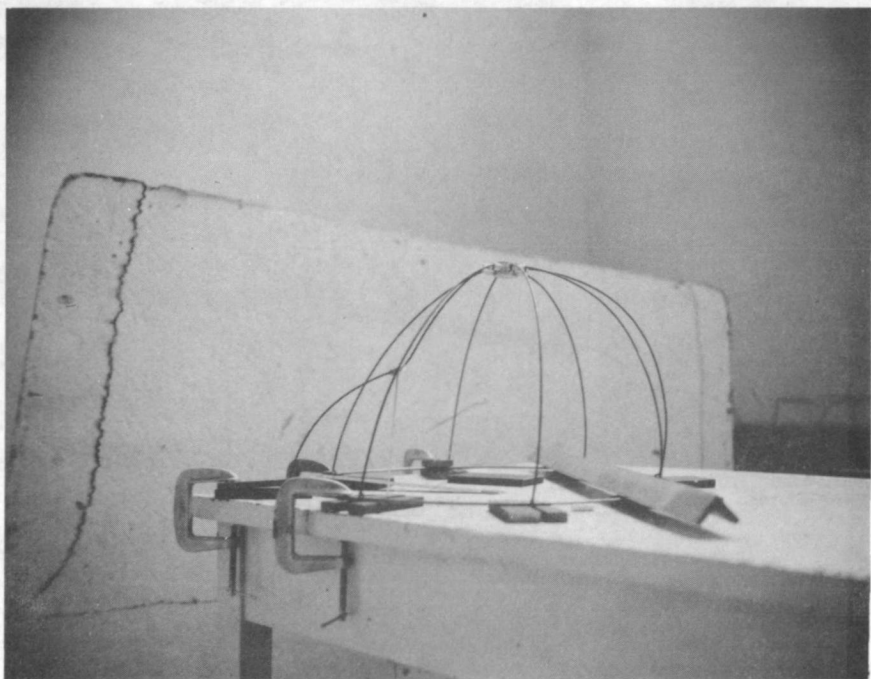


FIGURE 3.17

The collapse of an arch ribbed dome.

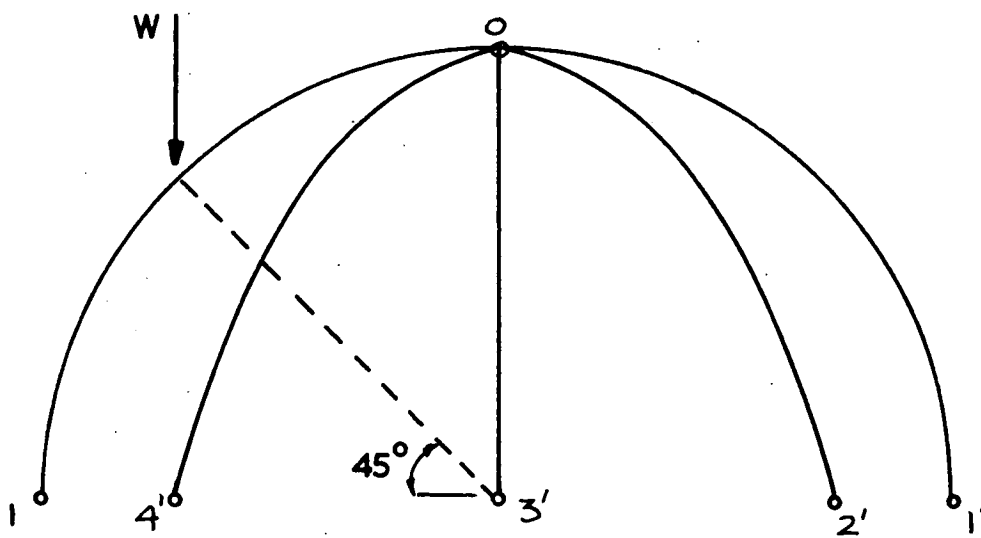
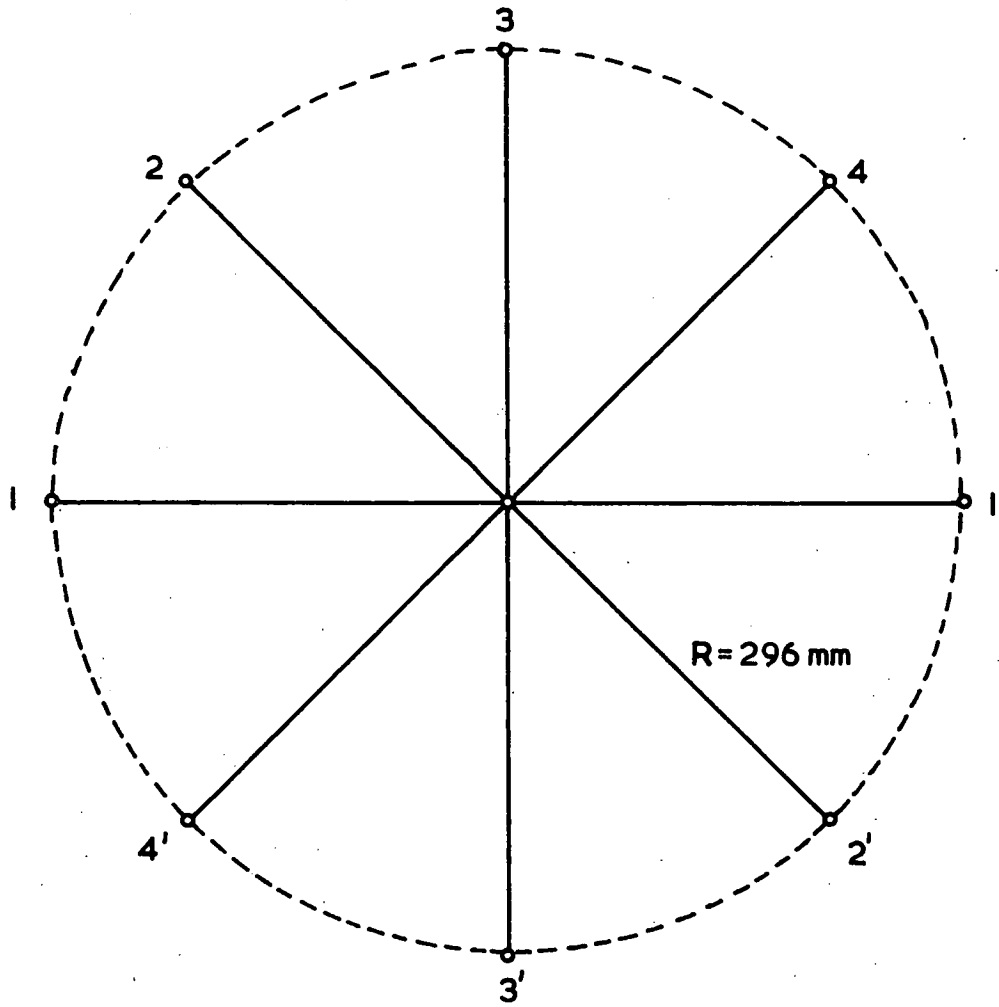
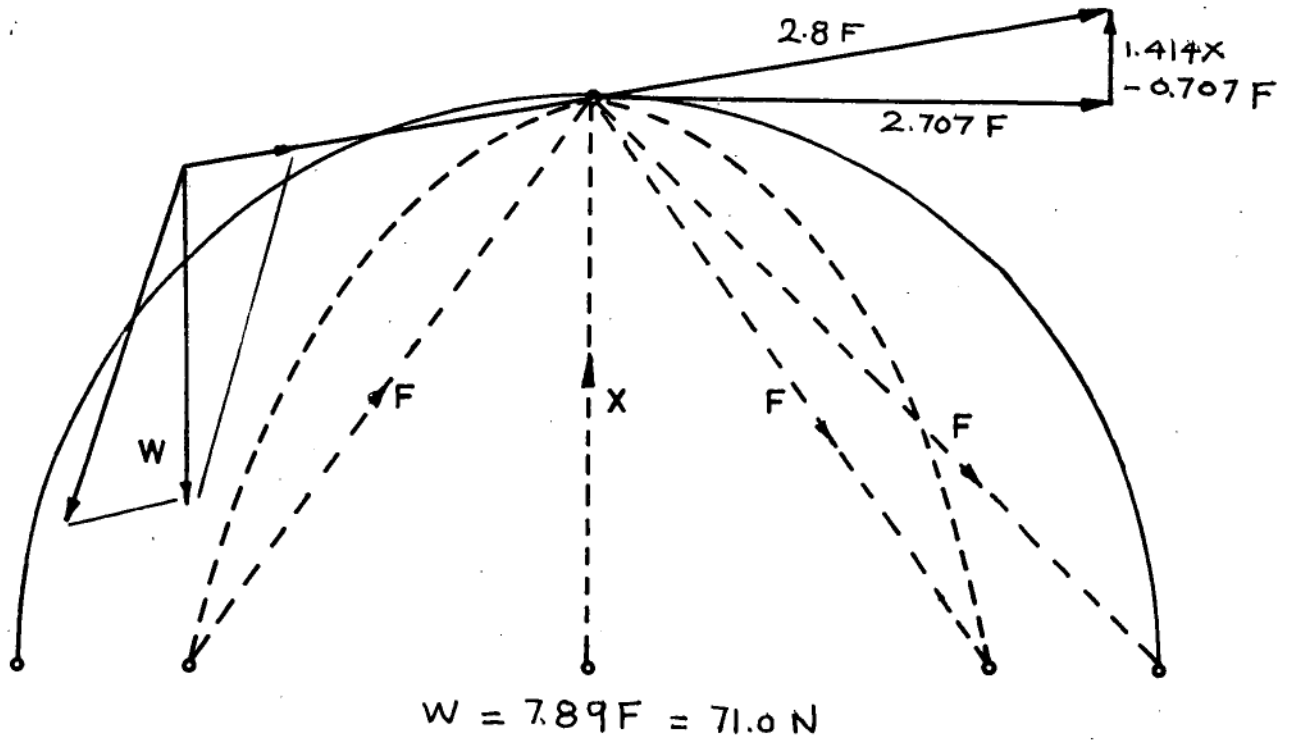
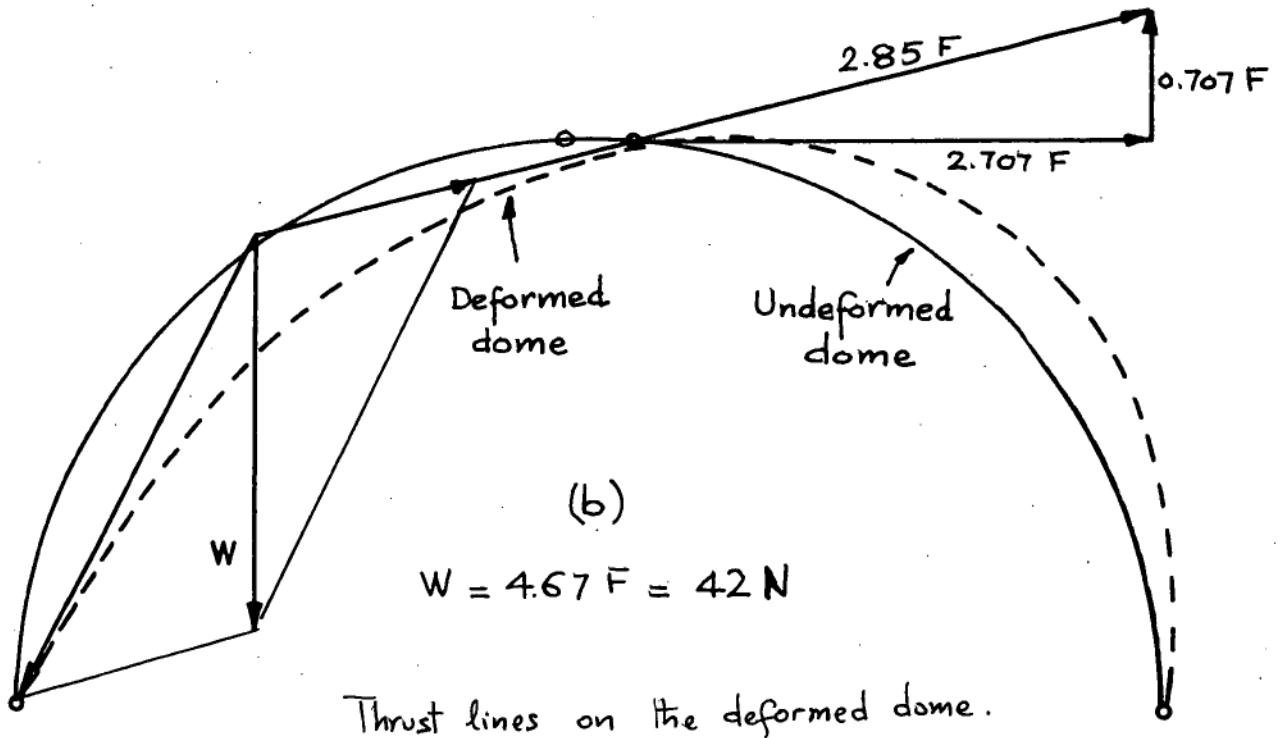


Figure 3-14



Thrust lines on undeformed dome.

(a)



Thrust lines on the deformed dome.

Figure 3.15

the external load W and the reaction at support 1. Figure 3.15(a) shows the constructions of the thrust lines on the undeformed dome.

A semi-circular arch-ribbed dome, consisting of eight ribs made from $1/8''$ diameter rod, was tested under a single vertical load at midspan of one of the ribs. It was found experimentally that hinges formed at midrib in all ribs except 3-0-3'. The maximum thrust that each rib can take was 9.0 Newton. This data was derived theoretically and checked experimentally.

Calculation was made based on the observed collapse mode: ribs 2-2', 3-3', 1-1' were failing while rib 4-4' remained elastic. If F is the force in the failing ribs (9.0 Newton previously established) and X is the force in the elastic rib, then the value of X can be determined from the knowledge that a full plastic moment value (1.35 kN mm) occurs at the loading point. The problem is best solved by graphical trial and error method. From the calculated value of X , the collapse load can be determined.

Figure 3.15(a) shows the equilibrium condition of the undeformed dome. The ultimate load is estimated at 71.0 N. This value is well above the measured collapse load 45.0N. The measured vertical deflexion at the leading point at near collapse is about 22 mm. It is thought therefore that the deformation may have a large effect on the final collapse load. To obtain a statical check via thrust line for the dome, the deformed shape of the dome was traced and calculations similar to those done on the undeformed shape were performed. Figure 3.15(b) shows the equilibrium condition of the deformed dome; the ultimate load is estimated at 42.0 N. Figure 3.16 compares the measurements and calculations, while Figure 3.17 shows the collapsed dome.

CHAPTER IV

THE STRENGTH OF ORTHOTROPIC SLABS

4.1 INTRODUCTION

In this chapter, the strength of rectangular orthotropic slabs under uniformly distributed load is examined. Unlike frames whose structural actions can be pictured by thrust lines, there is no similar way of picturing the structural actions of slabs. The standard lower bound solutions, giving moment fields and collapse loads in terms of closed-form expressions, are available only for a few cases.

The aim of this chapter is to find a simple way of picturing the structural actions of slabs. The proposed approach is to replace the slab by an assembly of simpler structural components. The solutions for the slabs obtained in this way are very simple both in form and in derivation. The solutions are not strictly lower bound solutions since the interaction effects between various structural components have been neglected. However, by comparing the proposed approximate solutions with yield line solutions, existing and newly-derived lower bound solutions, it is found that the proposed method gives a fairly accurate estimate of the strength of the rectangular orthotropic slabs.

4.2 LOWER BOUND APPROACH

4.2.1 Basic Conditions

A lower bound solution for slabs requires the specification of the moment fields such that (i) the equilibrium condition is satisfied everywhere, including the boundary conditions and (ii) the yield condition is nowhere violated.

* The idea was introduced by the author in a discussion on a paper by Ragan (Ref 4.15). The discussion is published in Journl.of Struct. Div. ST2, ASCE, Feb, 1974.

The equilibrium equations for the slab are:

$$\left. \begin{aligned} \frac{\partial M_x}{\partial x} - \frac{\partial M_{xy}}{\partial y} &= Q_x \\ \frac{\partial M_y}{\partial y} - \frac{\partial M_{xy}}{\partial x} &= Q_y \\ \frac{\partial Q_x}{\partial x} + \frac{\partial Q_y}{\partial y} &= -p \end{aligned} \right\} \dots\dots\dots (1a)$$

in which M_x and M_y are bending moments per unit lengths in x and y direction respectively, M_{xy} is the twisting moment per unit length, Q_x and Q_y are the shears per unit length, and p is the collapse load per unit area of the slab. Figure 4.1 shows the sign convention for shear, moment, and twist in a slab. Other general notations are also included in the same figure.

Equations (1a) are usually reduced to a single second order equation by eliminating the shear force terms (Ref 4.1).

$$\frac{\partial^2 M_x}{\partial x^2} + \frac{\partial^2 M_y}{\partial y^2} - 2 \frac{\partial^2 M_{xy}}{\partial x \partial y} = -p \dots\dots\dots (1b)$$

The yield condition for an orthotropically reinforced concrete slab with equal positive and negative yield moments is as follows:

$$\left. \begin{aligned} \text{For positive yield} \quad M_{xy}^2 &\leq (M - M_x)(\mu M - M_y) \\ \text{For negative yield} \quad M_{xy}^2 &\leq (M + M_x)(\mu M + M_y) \end{aligned} \right\} \dots\dots\dots (2)$$

where M and μM are yield moments in x and y directions, μ is the coefficient of orthotropy. The yield criterion has been derived theoretically by various authors (Ref 4.2, 4.3) and experimentally checked by others (Ref 4.4).

4.2.2 Difficulties with the lower bound approach

The main difficulty with the lower bound approach lies in the

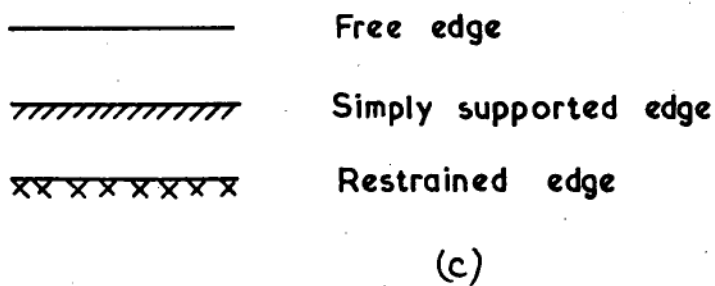
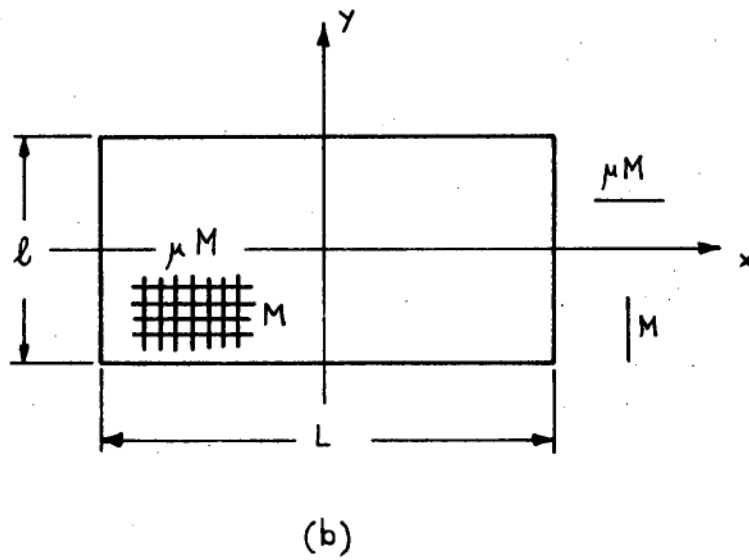
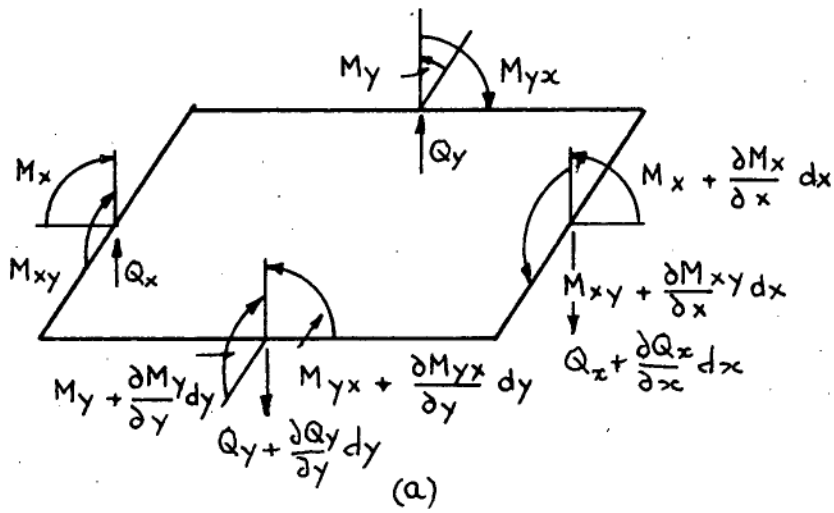


Figure 4.1

specifications of the moment fields M_x , M_y and M_{xy} such that (1b) and (2) are satisfied everywhere. The moment fields at any point, following a Mohr's circle, must be tested in every direction, against the normal yield moments M_n , which are governed by a different Mohr's circle, applying to the reinforcement, ($M_n = M \cos^2 \theta + \mu M \sin^2 \theta$). Kemp (Ref 4.5) pointed out that the success of any prescribed moment fields depends on whether the yield moment is reached at the corners; the specification of the twisting moment field is particularly important in this aspect.

The use of the differential equation (1b) requires careful consideration of the boundary conditions. The rigorous definition of statically admissible field as proposed by Fox (Ref 4.6) must be followed. For example, the conditions (1b) and (2) alone are not adequate to ensure a lower bound solution for a slab with a free edge; the condition of no shear along the free edge must also be observed.

4.2.3 Existing lower bound solutions

As the result of the difficulties encountered, few lower bound solutions exist. Hillerborg (Ref 4.7) developed the strip method, in which the torsional moment capacity is neglected and the load at any point on the slab is carried to the nearest support by bending in the plane perpendicular to the support. The method attempts to directly design a slab with variable reinforcement. Wood (Ref 4.8) has shown that the method can be modified to give an exact solution. Kemp (Ref 4.5) proposed a closed form lower bound solution for slabs uniformly loaded and simply supported on four sides. Holmes and Steel (Ref, 4.9) used numerical method to obtain lower bound solutions for isotropically reinforced slabs restrained on the shorter sides. Ragan (Ref 4.15) gave lower bound solutions for slabs restrained on the shorter sides and slabs restrained on all sides.

Due to the difficulties with the strict lower bound approach and the scarcity of existing lower bound solutions, the following approximate method is proposed.

4.3 OUTLINE OF THE APPROXIMATE METHOD

The proposed method is based on the basic hypothesis that the applied load can be carried independently by the moment capacity in two directions and the torsional moment capacity of the slab. Accordingly, the slab is subdivided into three parts: (i) a series of strips in x-direction, (ii) a series of strips in y-direction, and (iii) a number of plates which can carry only twisting moments.

Under these restrictions the yield conditions become:

$$\begin{aligned} \text{For the strips in the x-direction} \quad M_x &\leq M ; \\ \text{For the strips in the y-direction} \quad M_y &\leq \mu M ; \quad \dots\dots\dots (3) \\ \text{For the twisted plates} \quad M_{xy} &\leq \sqrt{\mu} M \quad (M_x = M_y = 0) . \end{aligned}$$

In equation(3), M and μM are yield moment in x and y directions respectively, and μ is the coefficient of orthotropy.

It is seen that the yield conditions as stated in (3) are not identical to the exact yield conditions of (2). The interaction effects between various structural actions have been neglected. To determine how serious the effect of this is upon the solutions, comparison will be made between the ensuing solutions, the yield line solutions, and other existing and newly derived lower bound solutions.

If the above conditions are accepted, a solution can be obtained very simply as follows. The general forms of the moment values are

$$M_x = K_1 p_1 L^2 ; \quad M_y = K_2 p_2 L^2 ; \quad M_{xy} = K_3 p_3 L^2 \quad \dots\dots\dots (4)$$

where $p = p_1 + p_2 + p_3$ is the collapse load of the slab; K_1 , K_2 and K_3 are constants whose values depend on the boundary conditions.

The solution of equation (3) and (4) gives the collapse load in the following form

$$C = \frac{pL^2}{M} = a_1 \mu + a_2 \sqrt{\mu} p + a_3 p^2 \quad \dots\dots\dots (5)$$

where a_1 , a_2 , and a_3 are constants whose values depend on boundary conditions, and $p = t/L$.

In equation (5) the first and third terms are the contributions of the moment capacity in x and y directions and the second term is the torsional moment capacity contribution to the total load carried by the slab. Several examples, making use of the above solution, are discussed in the following section.

4.4 COLLAPSE LOADS FOR SLABS WITH VARIOUS BOUNDARY CONDITIONS

A slab supported on four sides is replaced by three simpler structural components: strips in the x-direction, strips in the y-direction, and a number of plates which can only carry twisting moments, Fig 4.2(a). The twisted plates are obtained by making two cuts along the line of symmetry and by replacing the loading and its reactions to two equivalent couples acting at the four corners of each quarter of the slab. The average value of the twisting moment due to a uniform load p_3 is then $M_{xy} = 1/8 p_3 lL$.

For a slab simply supported on four sides, Fig 4.2(a)

$$\begin{aligned}
 M_x &= \frac{1}{8} p_1 L^2 \leq M & p_1 &\leq 8M/L^2 \\
 M_y &= \frac{1}{8} p_2 l^2 \leq \mu M & p_2 &\leq 8\mu M/l^2 \\
 M_{xy} &= \frac{1}{8} p_3 lL \leq \sqrt{\mu} M & p_3 &\leq 8\sqrt{\mu} M/lL \\
 p &= p_1 + p_2 + p_3 \leq 8(p^2 + \sqrt{\mu} p + \mu) \frac{M}{l^2} \\
 C = \frac{pl^2}{M} &= 8(\mu + \sqrt{\mu} p + p^2) \dots\dots\dots (6)
 \end{aligned}$$

Similarly, for slabs restrained on four sides, Fig 4.2(b),

$$C = 16(\mu + \sqrt{\mu} p/2 + p^2) \dots\dots\dots (7)$$

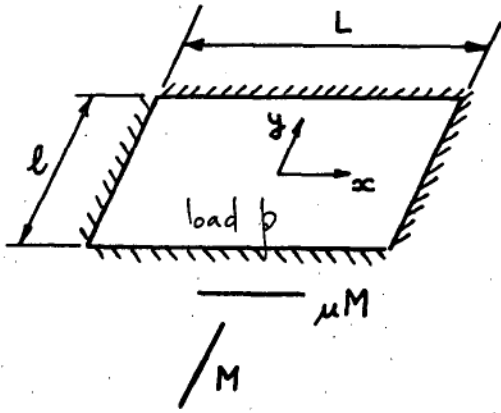
For slabs restrained on two shorter edges, Fig 4.2(c),

$$C = 8(\mu + \sqrt{\mu} p + 2p^2) \dots\dots\dots (8)$$

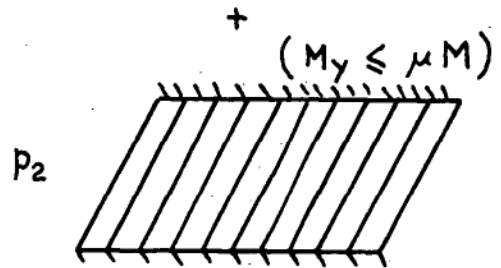
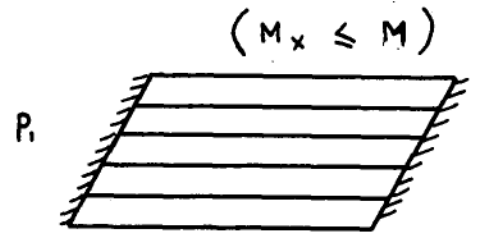
For slabs restrained on one short edge, Fig 4.2(d),

$$C = 8(\mu + \sqrt{\mu} p + 1.457 p^2) \dots\dots\dots (9)$$

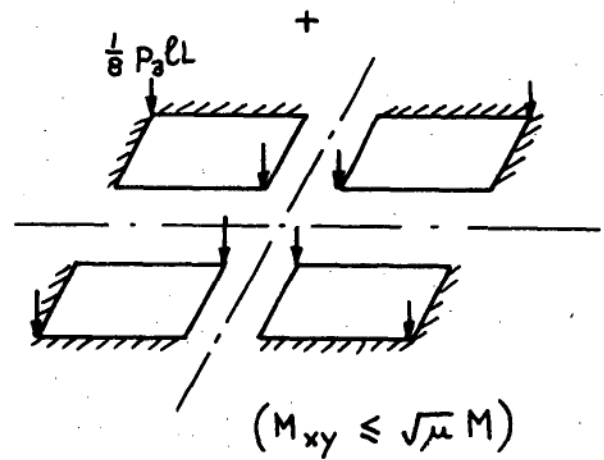
Slabs supported on four sides



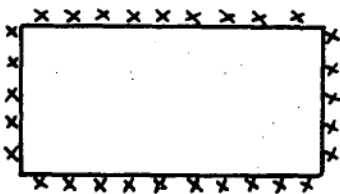
=



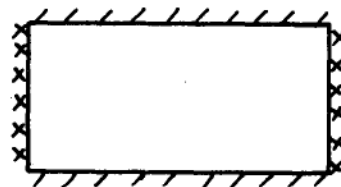
P_3



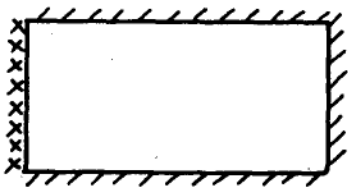
(a)



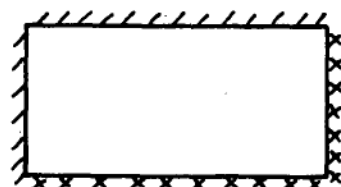
(b)



(c)



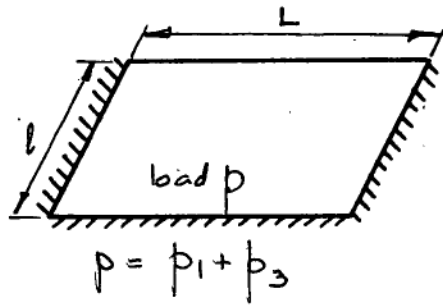
(d)



(e)

Figure 4.2

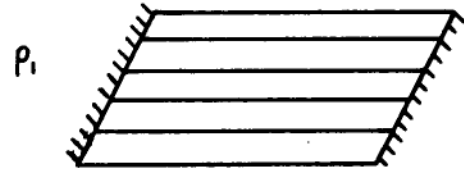
Slabs supported on three sides



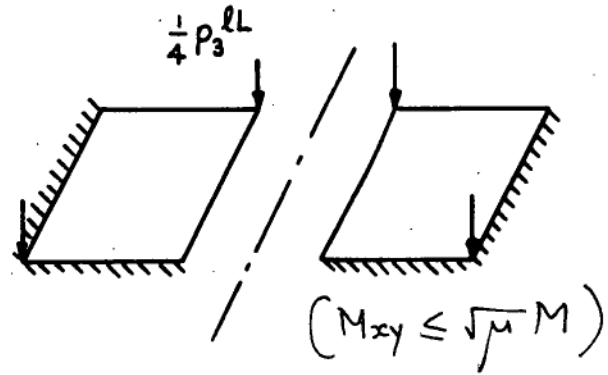
p_3

=

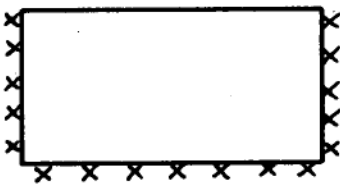
$(M_x \leq M)$



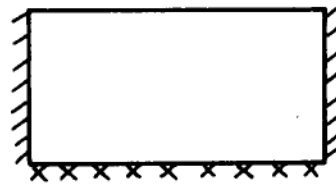
+



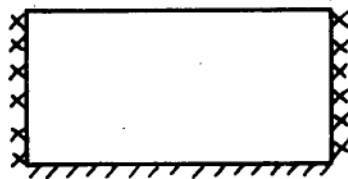
(a)



(b)



(c)



(d)

Figure 4.3

For slabs restrained on two adjacent edges, Fig 4.2(e),

$$C = 8(1.457\mu + \sqrt{\mu}p + 1.457p^2) \quad \dots\dots\dots (10)$$

Similarly, a slab supported on three sides can be replaced by two components: strips between the opposite supporting sides, and a number of twisted plates. The twisted plates are obtained, in this case, by making one cut along the line of symmetry and replacing the loading and its reactions to two equivalent couples acting at the four corners of each half of the slab, Fig 4.3(a). The average twisting moment due to a uniform load p_3 is then $M_{xy} = 1/4 p_3 lL$.

For slabs with three sides simply supported, Fig 4.3(a),

$$C = 8(p^2 + p\sqrt{\mu}/2) \quad \dots\dots\dots (11)$$

For slabs with three sides restrained, Fig 4.3(b),

$$C = 16p^2 + 4p\sqrt{\mu} + 2\mu \quad \dots\dots\dots (12)$$

For slabs with two short edges simply supported and one long edge restrained, Fig 4.3(c),

$$C = 8p^2 + 4p\sqrt{\mu} + 2\mu \quad \dots\dots\dots (13)$$

For slabs with two short edges restrained and one long edge simply supported, Fig 4.3(d),

$$C = 16p^2 + 4p\sqrt{\mu} \quad \dots\dots\dots (14)$$

4.5 COMPARISON WITH UPPER BOUND SOLUTIONS

Figure 4.4 shows a summary of the upper bound solutions, obtained from yield line theory (Ref 4.10, 4.11), and the corresponding approximate solutions, obtained from the proposed approximate method. According to Wood (Ref 4.14), the upper bound solutions can be reduced by up to 8%, depending on the boundary conditions, to account for the corner effects.

EDGE CONDITIONS	$C = p^2/M$	
	UPPER BOUND (YIELD LINE)	PROPOSED METHOD
four edges simply supported	$\frac{24\mu}{\left\{\sqrt{3+p^2/\mu} - p/\sqrt{\mu}\right\}^2}$	$8(\mu + \sqrt{\mu}p + p^2)$
four edges restrained	$\frac{48\mu}{\left\{\sqrt{3+p^2/\mu} - p/\sqrt{\mu}\right\}^2}$	$16(\mu + \sqrt{\mu}p/2 + p^2)$
two long edges simply supported and two short edges restrained	$\frac{24\mu}{\left\{\sqrt{3+2p^2/\mu} - p\sqrt{2}/\sqrt{\mu}\right\}^2}$	$8(\mu + p\sqrt{\mu} + 2p^2)$
one short edge restrained and other edges simply supported	$\frac{24\mu}{\left\{\sqrt{3+1.457p^2/\mu} - 1.207p/\sqrt{\mu}\right\}^2}$	$8(\mu + p\sqrt{\mu} + 1.457p^2)$
two adjacent edges restrained and other two edges simply supported	$\frac{34.97\mu}{\left\{\sqrt{3+p^2/\mu} - p/\sqrt{\mu}\right\}^2}$	$8(1.457\mu + p\sqrt{\mu} + 1.457p^2)$
three edges simply supported and one long edge free	$\frac{24\mu}{\left\{\sqrt{4+9\mu/p^2} - 2\right\}^2} \quad \frac{\mu}{p^2} > 2$ $\frac{24\mu}{\left\{\sqrt{3+\mu/4p^2} - \sqrt{\mu}/2p\right\}^2} \quad \frac{\mu}{p^2} \leq 2$	$8(p^2 + p\sqrt{\mu}/2)$
three edges restrained and one long edge free	$\frac{6\mu(4\beta_1+1)}{3-4\beta_1} \quad \text{or} \quad \frac{12\mu}{\beta_2^2}$ <p>where</p> $\beta_1 = p^2\{\sqrt{4+6\mu/p^2} - 2\}/2\mu$ $\beta_2 = \mu\{\sqrt{1+12p^2/\mu} - 1\}/4p^2$	$(16p^2 + 4\sqrt{\mu}p + 2\mu)$
two short edges simply supported, one long edge restrained, and the other free	$\frac{6\mu(4\beta_1+1)}{3-4\beta_1} \quad \text{or} \quad \frac{12\mu}{\beta_2^2}$ <p>where</p> $\beta_1 = p^2\{\sqrt{4+12\mu/p^2} - 2\}/4\mu$ $\beta_2 = \mu\{\sqrt{1+6p^2/\mu} - 1\}/2p^2$	$(8p^2 + 4\sqrt{\mu}p + 2\mu)$
two short edges restrained, one long edge simply supported, and one long edge free	$\frac{24\mu\beta_1}{3-4\beta_1} \quad \text{or} \quad \frac{6\mu}{\beta_2^2}$ <p>where</p> $\beta_1 = 2p^2\{\sqrt{4+9\mu/2p^2} - 2\}/3\mu$ $\beta_2 = \mu\{\sqrt{1+24p^2/\mu} - 1\}/8p^2$	$(16p^2 + 4\sqrt{\mu}p)$

Figure 4.4

$$C = pl^2/M$$

ρ	three edges simply supported and one long edge free		three edges restrained and one long edge free	
	$\mu = 1$	$\mu = 1/4$	$\mu = 1$	$\mu = 1/4$
1	13.86 * 12.00 † (13.41)°	10.45 10.00 (4.34)	26.58 22.00 (17.25)	20.05 18.50 (7.75)
$3/4$	9.35 7.50 (19.82)	6.47 6.00 (7.20)	17.94 14.00 (21.98)	12.40 11.00 (11.31)
$2/3$	8.04 6.22 (22.63)	5.35 4.89 (8.70)	15.50 11.78 (24.01)	10.27 8.94 (12.93)
$1/2$	5.44 4.00 (26.45)	3.46 3.00 (13.41)	11.02 8.00 (27.40)	6.65 5.50 (17.25)

U B reduced by 2%

U B reduced by 6%

$$C = pl^2/M$$

ρ	two short edges simply supported, one long edge restrained, other free		two short edges restrained, one long edge simply supported, other free	
	$\mu = 1$	$\mu = 1/4$	$\mu = 1$	$\mu = 1/4$
1	17.01 * 14.00 † (17.71)°	11.52 10.50 (8.85)	23.04 20.00 (13.19)	18.83 18.00 (4.42)
$3/4$	12.05 9.50 (21.15)	7.40 6.50 (12.13)	14.79 12.00 (18.89)	11.33 10.50 (7.35)
$2/3$	10.53 8.22 (21.92)	6.24 5.39 (13.63)	12.48 9.78 (21.64)	9.26 8.44 (8.82)
$1/2$	7.82 6.00 (23.23)	4.25 3.50 (17.71)	8.51 6.00 (29.47)	5.76 5.00 (13.19)

U B reduced by 4%

U B reduced by 4%

* Upper bound value (Yield Line Theory)

† Approximate Lower bound value

° Percentage of difference

Figure 4.6

$$C = pl^2/M$$

p	four edges restrained		two short edges restrained two long edges simply supported	
	$\mu = 1$	$\mu = 4$	$\mu = 1$	$\mu = 4$
1	44.16 * 40.00 † (9.42)	104.08 96.00 (7.76)	34.11 32.00 (6.19)	68.05 64.00 (5.95)
3/4	34.13 31.00 (9.18)	90.49 85.00 (6.06)	24.47 23.00 (6.01)	56.15 53.00 (5.62)
2/3	31.22 28.44 (8.90)	86.32 81.78 (5.26)	21.75 20.44 (6.00)	52.60 49.78 (5.37)
1/2	26.02 24.00 (7.76)	78.51 76.00 (3.19)	17.01 16.00 (5.95)	46.08 44.00 (4.51)

U B reduced by 8%

U B reduced by 4%

$$C = pl^2/M$$

p	one short edge restrained others simply supported		two adjacent edges restrained others simply supported	
	$\mu = 1$	$\mu = 4$	$\mu = 1$	$\mu = 4$
1	28.77 * 27.66 † (3.87) °	62.12 59.66 (3.96)	33.57 31.31 (6.73)	79.12 74.28 (6.12)
3/4	21.37 20.56 (3.80)	52.58 50.56 (3.85)	25.95 24.21 (6.69)	68.79 65.18 (5.25)
2/3	19.26 18.51 (3.85)	49.70 47.85 (3.73)	23.74 22.17 (6.60)	65.62 62.47 (4.80)
1/2	15.53 14.91 (3.96)	44.35 42.91 (3.25)	19.78 18.57 (6.12)	59.68 57.54 (3.59)

U B reduced by 2%

U B reduced by 4%

* Upper bound value (Yield Line Theory)

† Approximate lower bound value

° Percentage of difference

Figure 4.5

Figure 4.5 and Figure 4.6 compare the upper and approximate values.

The following points may be noted:

(i) From Figure 4.4 it is seen that the proposed formulae are simpler both in form and in derivation. Yield line solutions, although simple in principle, involve a considerable amount of algebraic manipulation. The proposed method on the other hand, is very simple algebraically; the only complication is the estimate of the load that can be carried by twisting action alone.

(ii) Figure 4.5 compares the approximate and upper bound values of $C = \frac{pl^2}{M}$, for slabs supported on all four sides. All values are in agreement to within 10%. The case of slabs with four sides simply supported has been found by Kemp (Ref 4.5) to give even better agreement (within 2%).

(iii) Figure 4.6 compares the approximate and upper bound values for slabs supported on three sides. The agreement is poorer in these cases, variation ranging from 4% to 30%. The proposed method did not allow any load to be carried in the direction normal to the free edge, while obviously some load must be carried in this way. The argument is justified by observing that the agreements between the approximate and upper bound solutions are better for cases where $\mu = 1/4$ than that for $\mu = 1$.

4.6 COMPARISON WITH LOWER BOUND SOLUTIONS

A strict lower bound solution to the collapse load is obtained by specifying the moment fields M_x , M_y , and M_{xy} such that (i) the statical boundary conditions, (ii) the equilibrium condition as given by Equation 1(b), and (iii) the yield condition as given by Equation 2, are satisfied. Existing and newly derived lower bound solutions are now compared with the approximate solutions obtained in 4.4.

4.6.1 Slabs supported on four sides

For slabs simply supported on four sides, Kemp (Ref 4.5) proposed the

following moment fields:

$$\begin{aligned} M_x &= M (1 - 4x^2/L^2) \\ M_y &= \mu M (1 - 4y^2/l^2) \\ M_{xy} &= 4\sqrt{\mu} M (x/L)(y/l) \end{aligned} \quad \dots\dots\dots (15)$$

The above fields give the same collapse load as the approximate method, i.e.

$$C = pl^2/M = 8(\mu + \sqrt{\mu}p + p^2)$$

For slabs restrained on the shorter sides, Ragan (4.15) proposed the following moment fields

$$\begin{aligned} M_x &= M \left[(1 - 8x^2/L^2) + (4\lambda/p)(x^4/L^4)(1 - 4x^2/L^2) \right] \\ M_y &= \mu M (1 - 4y^2/l^2) \\ M_{xy} &= \lambda M (x/L)(y/l)(1 - 4x^2/L^2)(1 + 12x^2/L^2) \end{aligned} \quad \dots\dots\dots (16)$$

The collapse load is given by

$$C = pl^2/M = 8\mu + 2\lambda p + 16p^2$$

with $\lambda = 4\sqrt{\mu}^3\sqrt{p}$

Ragan obtained the value of λ 's by using a curve fitting process.

The proposed approximate solution is equivalent to Ragan's solution with

$$\lambda = 4\sqrt{\mu}.$$

4.6.2 Slabs supported on three sides.

For slabs with a free edge, there is no existing lower bound solution, and the following solutions are proposed. It may be noted that one extra condition is required here, besides 1(b) and 2, namely there is no reaction along the free edge, i.e.

$$\left[\frac{\partial M_y}{\partial y} - 2 \frac{\partial M_{xy}}{\partial x} \right] = 0 \quad \dots\dots\dots (17)$$

along free edge

(a) Slabs simply supported on three sides.

A simple solution can be obtained from the following fields.

$$\begin{aligned} M_x &= M(1 - 4x^2/L^2) \\ M_y &= 0 \quad \dots\dots\dots (18) \\ M_{xy} &= 2\sqrt{\mu} M(x/L)(y/l) \end{aligned}$$

The above fields satisfy (1b), (2), and (15) and give the same collapse load as the approximate method, i.e.

$$C = pl^2/M = 8p^2 + 4\sqrt{\mu} p$$

An improved solution is obtained by allowing some load to be taken flexurally in the y direction; the moment fields for these conditions are

$$\begin{aligned} M_x &= M(1 - 4x^2/L^2) \\ M_y &= k\mu M(y/l)^2(1 - y/l) \quad \dots\dots\dots (19) \\ M_{xy} &= 2\sqrt{\mu} M(x/L)(y/l) + \frac{3}{2} k(\mu/p) M(x/L)(y/l)(1 - y/l) \end{aligned}$$

The collapse load is

$$C = pl^2/M = 8p^2 + 4\sqrt{\mu} p + k\mu \quad \dots\dots\dots (20)$$

in which k is a parameter to be determined so that the yield condition is satisfied everywhere.

The value of k is found numerically by drawing the Mohr's circles for a number of points on the slab and checking the yield conditions accordingly. The value of k is given in Figure 4.7 for various values of p and μ .

(b) Slabs restrained on one long side.

The moment fields are

$$\begin{aligned} M_x &= M(1 - 4x^2/L^2) \\ M_y &= -\mu M(y/l)^2 + k\sqrt{\mu} p M(y/l)^2(1 - y/l) \quad \dots\dots\dots (21) \\ M_{xy} &= \frac{3}{2} k\sqrt{\mu} M(x/L)(y/l)(1 - y/l) \end{aligned}$$

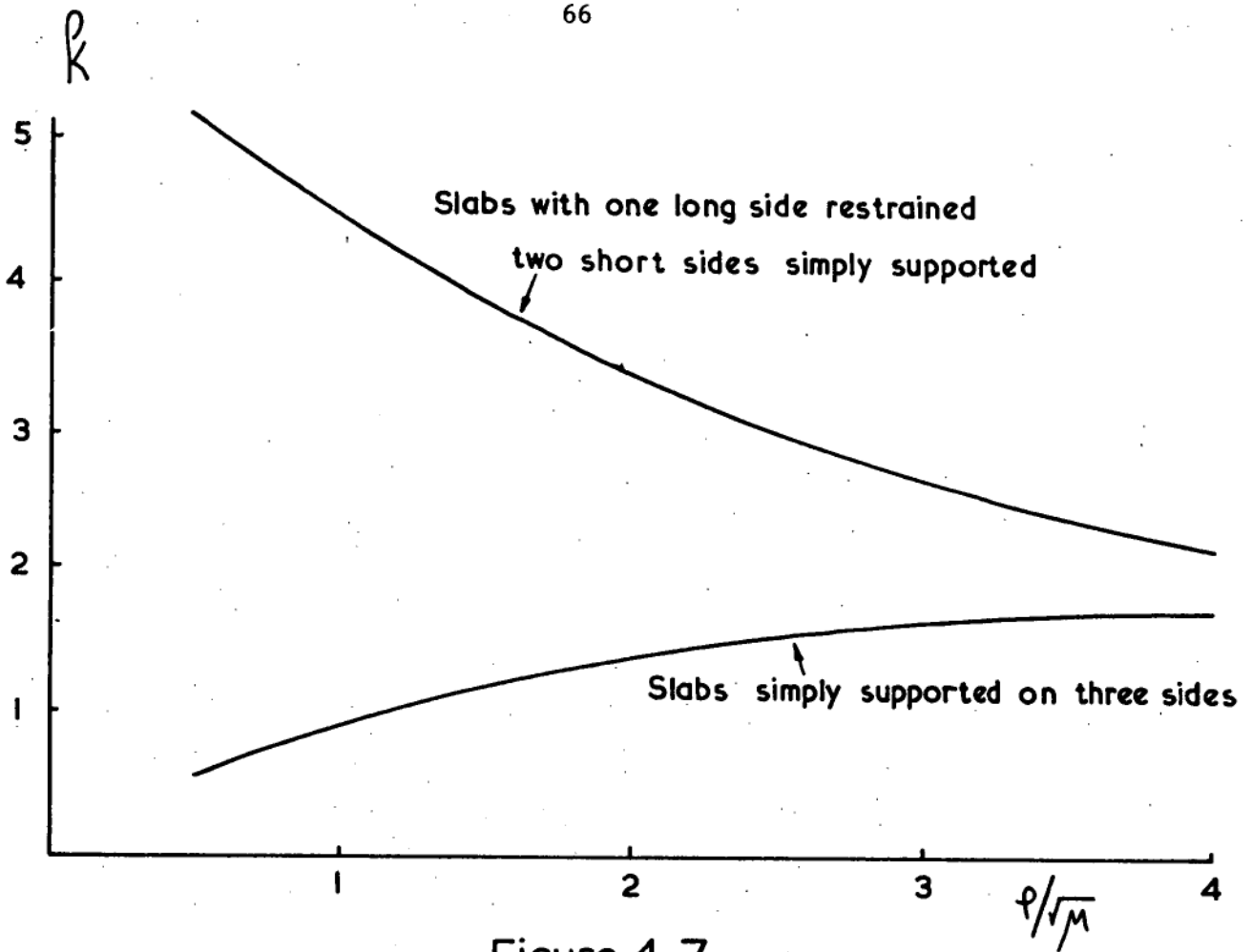


Figure 4.7

p	Slabs with three simply supported sides		Slabs with one long side restrained two short sides simply supported	
	$\mu = 1/4$	$\mu = 1$	$\mu = 1/4$	$\mu = 1$
2	36.42 [*] 36.00 ^o	41.33 40.00	34.6 36.5	40.00 42.00
1	10.33 10.00	12.92 12.00	10.20 10.50	14.44 14.00
$\frac{1}{2}$	3.23 3.00	4.56 4.00	3.60 3.50	6.57 6.00

* Lower bound solution.

o Proposed approximate solution.

Figure 4.8

The collapse load is given by

$$C = pl^2/M = 8p^2 + 2\mu + k\sqrt{\mu}p \quad \dots\dots\dots (22)$$

where the value of k is also given in Figure 4.7. The solution is identical to that given by the approximate method with $k = 4$.

Figure 4.8 compares the values obtained from these solutions and the approximate solutions.

(c) Slabs restrained on two short sides.

The moment fields are

$$M_x = M \left[(1 - 8x^2/L^2) + 4k(\sqrt{\mu}/p)(x/L)^4(1 - 4x^2/L^2) \right]$$

$$M_y = 0 \quad \dots\dots\dots (23)$$

$$M_{xy} = k\sqrt{\mu} M (x/L)(y/l)(1 - 4x^2/L^2)(1 + 12x^2/L^2)$$

The collapse load is given by

$$C = pl^2/M = 16p^2 + 2k\sqrt{\mu}p \quad \dots\dots\dots (24)$$

For the range of p between $1/2$ and 2 , the value of k is approximately 2 . The solution is then identical to that given by the approximate method.

The technique of obtaining the moment fields outlined above can be used for cases with different boundary and loading conditions, (e.g. linearly varying load). However, no precise lower bound solution is available for slabs restrained on three or four sides. The difficulty lies in the specification of the twisting moment field.

4.7 CONCLUDING REMARKS

The approximate method presented in section 4.3 readily provides an estimate of the strength of any orthotropic slab, and of the relative importance of various structural actions. The main advantages of the method are the ease of derivation and the simplicity of the solution.

Its main drawbacks are the approximate treatment of the twisting action and the neglect of the interaction effects which makes the solution unsafe. The comparisons made in section 4.4 and 4.5, however, show that the method gives a fairly good estimate of the strength of any orthotropic slabs within the practical range of dimensions.

The moment fields obtained in section 4.6 offer a rational basis for the design of reinforcement and the estimate of the edge forces. The lower bound solutions obtained for slabs with a free edge are believed to be new.

Some further work on slabs can be found in Appendix A2 where an analogy is proposed for picturing the yield line patterns.

CHAPTER V

LOAD CARRYING CAPACITY OF STRUCTURES WITH NO TENSILE STRENGTH

5.1 INTRODUCTION

In this chapter, the strength of structures made of materials having no (or little) tensile strength is examined. In the past, the design of these structures has usually been made based on some form of elastic analysis with a chosen 'safe stress' level. The application of elastic methods to imperfectly elastic structures is not rational. The 'safe stress' design approach does not reflect in any way the load carrying capacity of the structures nor does it give a proper measure of their safety. Heyman has applied the limit principles, derived from plastic analysis of steel frames, to masonry structures (Ref 5.1, 5.2, 5.3, 5.4, 5.5). Heyman's works have provided a better understanding of the structural behaviour and a more rational basis for the design of masonry structures. The two basic assumptions underlying Heyman's approach are: (i) there is no danger of crushing of the material in compression and (ii) sliding failure does not occur. Sliding failures could and did occur under the conditions of reduced arch thrust due to the support movements (Ref 5.6). A proper analysis of sliding failures requires the knowledge of the material and of the support conditions. The assumption that there is no danger of crushing is justified for old stone arch bridges where the stress is relatively small compared with the strength of the material. For highly stressed modern structures, the danger of crushing cannot be overlooked and should instead be allowed for. As Mainstone (Ref 5.6) stated, the thrust line should be made to be "sufficiently within the depths of the arch rib to remove completely the risk of local failures under highly concentrated compressions of the hinge points. The question is: how far within?"

of a plain concrete section under the combined actions of axial load and bending moment is studied. The study results in a rational method of positioning the thrust line at collapse, allowing for the effect of crushing of the concrete. The problem of predicting the strength of masonry walls is then dealt with, using the above method. In the second part, the strength of the Gladesville Arch Bridge is studied for three different loading conditions. Since the arch is slender, the effects of changing geometry and of concrete crushing are included in the calculations. It is believed that this study gives a more realistic measure of safety of this important bridge than the conventional 'safe stress' approach.

5.2 STRENGTH OF A SECTION

The strength of an unreinforced concrete section is analysed. The stress-strain curve for concrete is approximated to the idealized form of Figure 5.1(a). This curve is a well-known approximation recommended by the European Concrete Committee in the "International Recommendations for the design and construction of concrete structures" (F.I.D. Sixth Congress, Prague). It will be assumed in all the following work that the tensile strength of concrete is neglected. For simplicity only a solid rectangular section is analysed, although the principles used are applicable to any other section.

plane sections remaining plane on average, Figure 5.1(c) shows stress distribution patterns for the cracked and uncracked states. The distribution of stress in the concrete follows the stress-strain curve of Figure 5.1(a). The total concrete force must be equal to the applied load P . The moment-thrust-rotation ($M-P-\phi$) relation for the section is derived numerically using the flow chart of Figure 5.2. The ultimate strength is reached when the compressive strain at the outermost fibre is 0.0035; the corresponding bending moment is then the maximum moment that

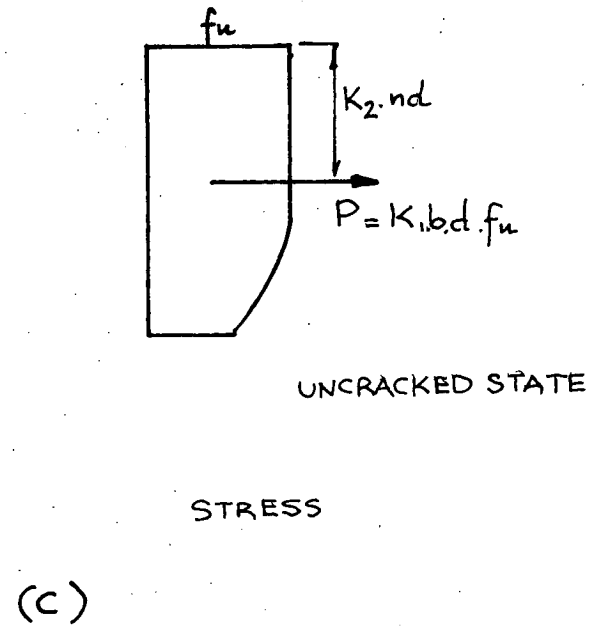
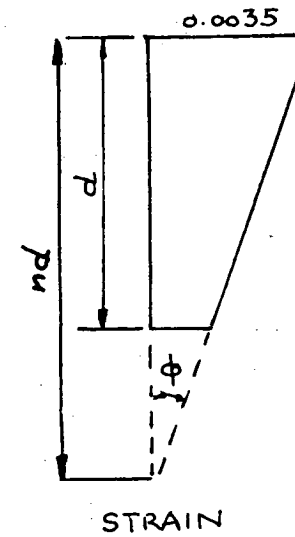
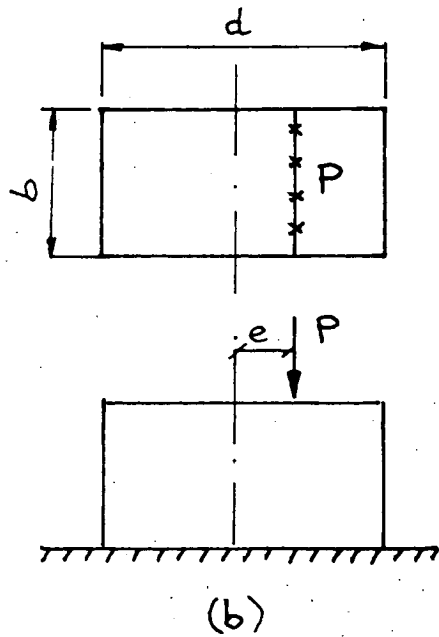
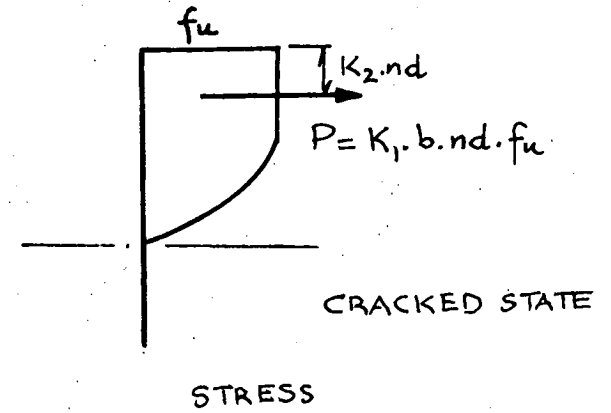
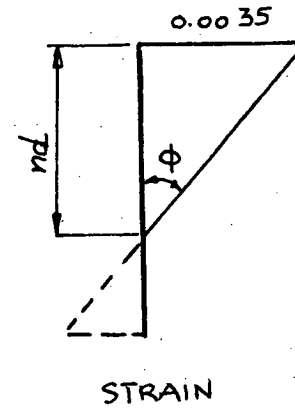
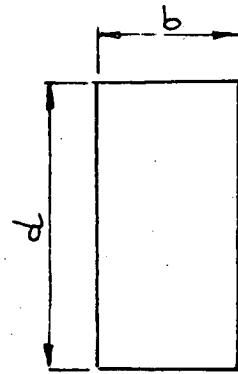
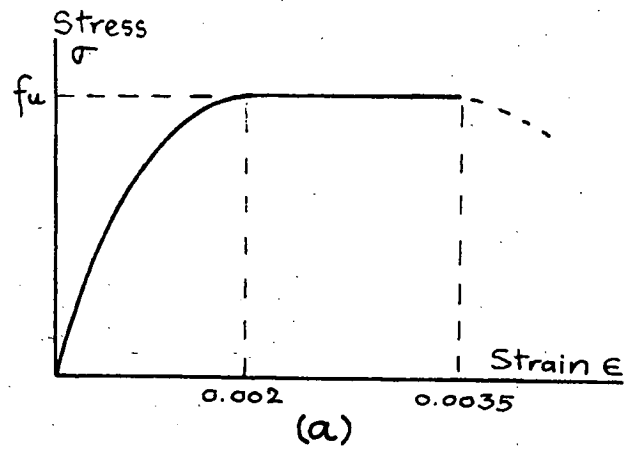


Figure 5.1

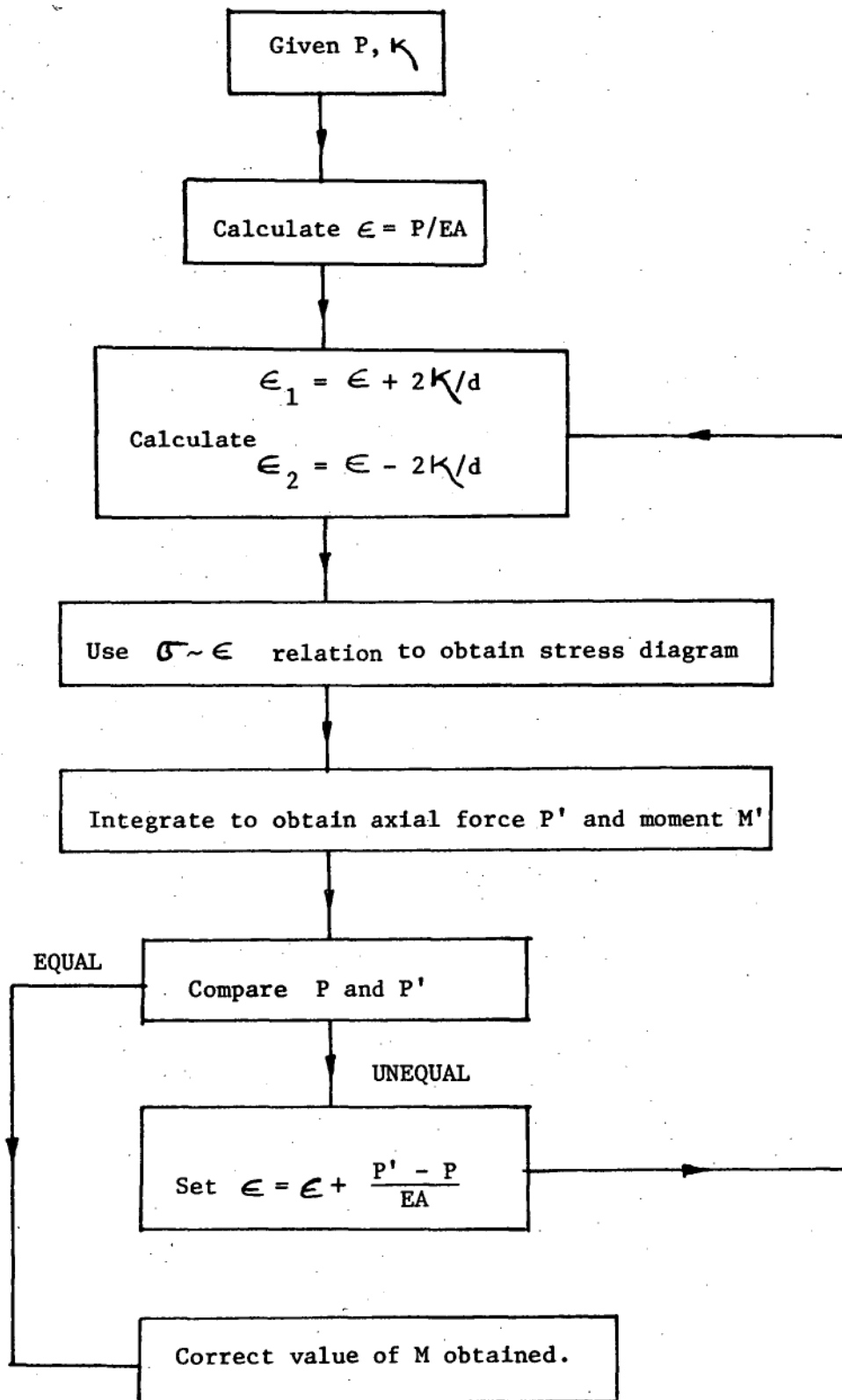


Figure 5.2

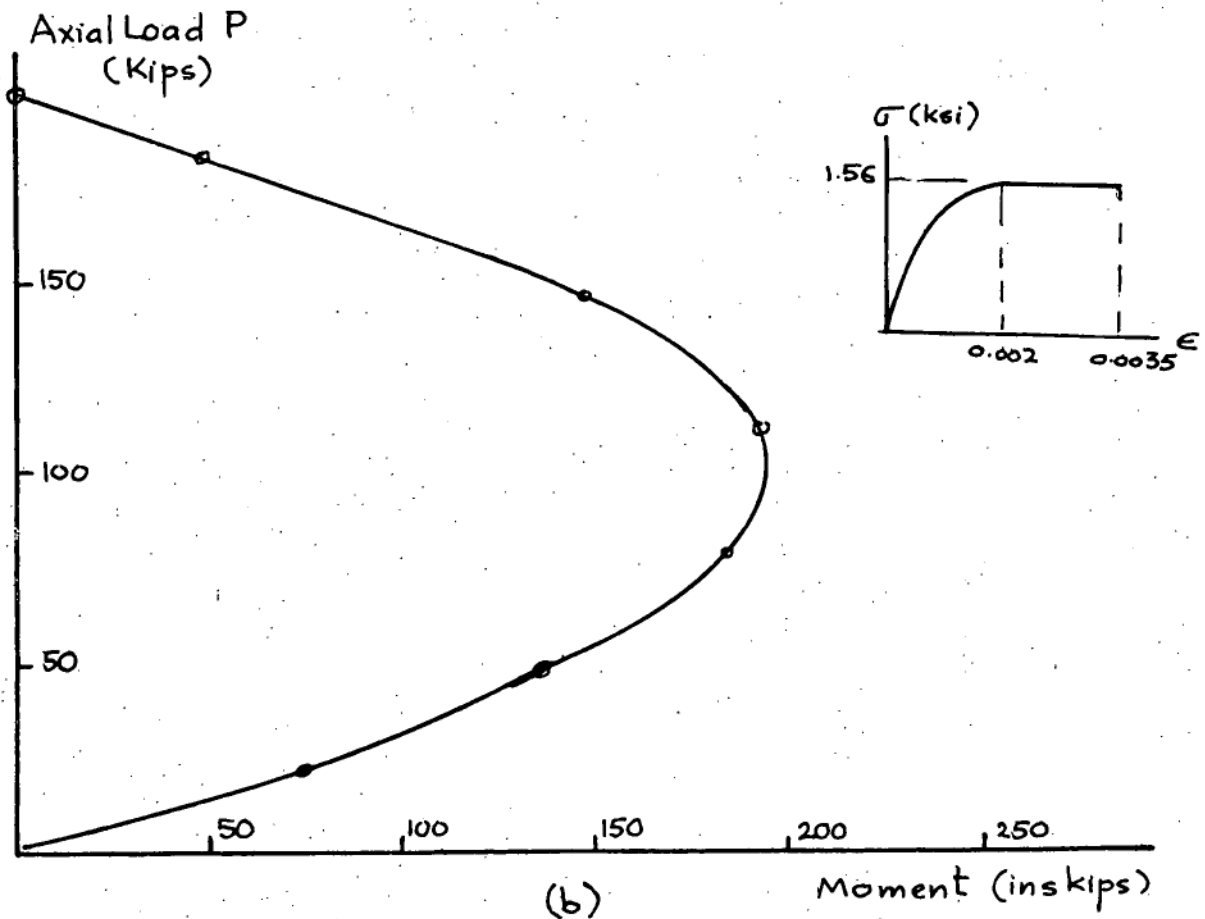
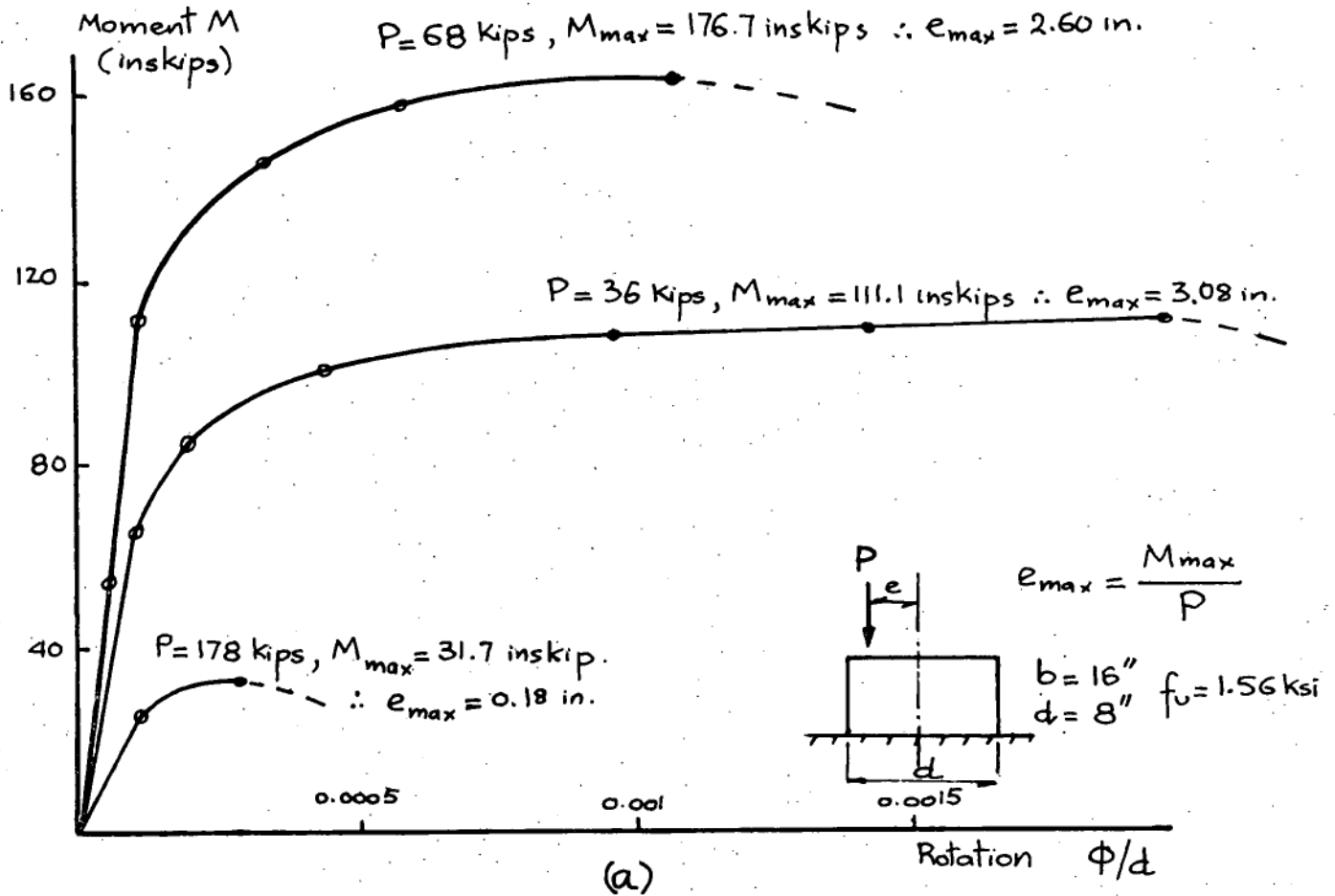


Figure 5.3

can be carried by the section under the considered axial load. From the values of moment and thrust the maximum permissible eccentricity of the thrust is derived.

Figure 5.3(a) shows the $M-P-\phi$ relation for a rectangular concrete section. From the graph, estimate of the maximum permissible eccentricity can be made for any given axial load. The moment rotation relation also indicates whether it is justifiable to use limit principles in the analysis of the structure. For the considered section, the $M-\phi$ curve for the axial load $P = 36$ kips approximates quite well to the ideal 'elastic-plastic' behaviour, while the $M-\phi$ curve for the axial load $P = 198$ kips does not. It may be also noted that the 'middle third' rule, which is based on a linear stress distribution with zero stress at one edge as the limit, has no particular significance. For high axial load the thrust must be placed well within the section (hence the middle third rule is not necessarily safe); while for low axial load, the thrust can be placed very close to the edge of the section.

5.3 STRENGTH OF MASONRY WALLS

This sections deals with the problem of predicting the strength of masonry walls under compressive and transverse loads. The strength of masonry is a combination of the strength of the actual concrete unit and the mortar that binds the units together. The compressive strength of the masonry can be estimated by testing three or five layers of masonry (Ref 5.7 and 5.8). The procedure is similar to those for the testing of standard concrete cylinders. Concrete masonry usually has about 35 to 55% of that of individual block strength; it depends on mortar joint thickness and quality.

Once the average masonry strength is established, the wall can be analysed as a homogenous concrete body. The tensile strength of the joining mortar is neglected. Figure 5.4(a) shows the forces acting on a

section of a masonry wall. The effective wall height is h_e , width b , the axial load is P , and the transverse pressure is p . The thrust is placed at a distance c from the center line of the section; the distance c is determined from the magnitude of the axial load P as outlined in the flow chart of Figure 5.2. Equilibrium analysis of the system gives the following equation.

$$P(c - \delta) + \left(b \cdot \frac{h_e}{2} \cdot p\right) \frac{h_e}{4} = \left(b \cdot \frac{h_e}{2} \cdot p\right) \frac{h_e}{2}$$

in which δ is the central wall deflexion.

The transverse pressure to cause collapse is given by

$$p_{\text{collapse}} = \frac{8P(c - \delta)}{b \cdot h_e^2} \quad \dots\dots\dots (5.1)$$

Figure 5.4(b) shows the position of the thrust line at collapse.

The above analysis is applied to Yokel's experimental work on masonry walls (Ref 5.7). Figure 5.5 shows Yokel's general test set-up and wall dimensions. ~~* The effective height of wall is taken as 0.8h as suggested by Yokel.~~ Figure 5.6 shows a summary of the results of calculations and

* As seen in Figure 5.5, the bottom of Yokel's wall is partially restrained against rotation with a steel channel. The proposed analysis assumes both ends of the wall are free to rotate, therefore an effective wall height must be established for the analysis. Yokel suggested 0.8h as a realistic measure of effective wall height and this value will be used in the following calculation.

using the technique of dynamic relaxation. The outline of the method is

* * The main purpose of the above analysis and calculations is to demonstrate the advantage of the proposed method of placing the hinges at the specified position over the conventional method of placing hinges at the edge of the section. In Figure 5.6 reading downward in each column, it will be observed that there are definite improvements in the estimate of the load capacity.

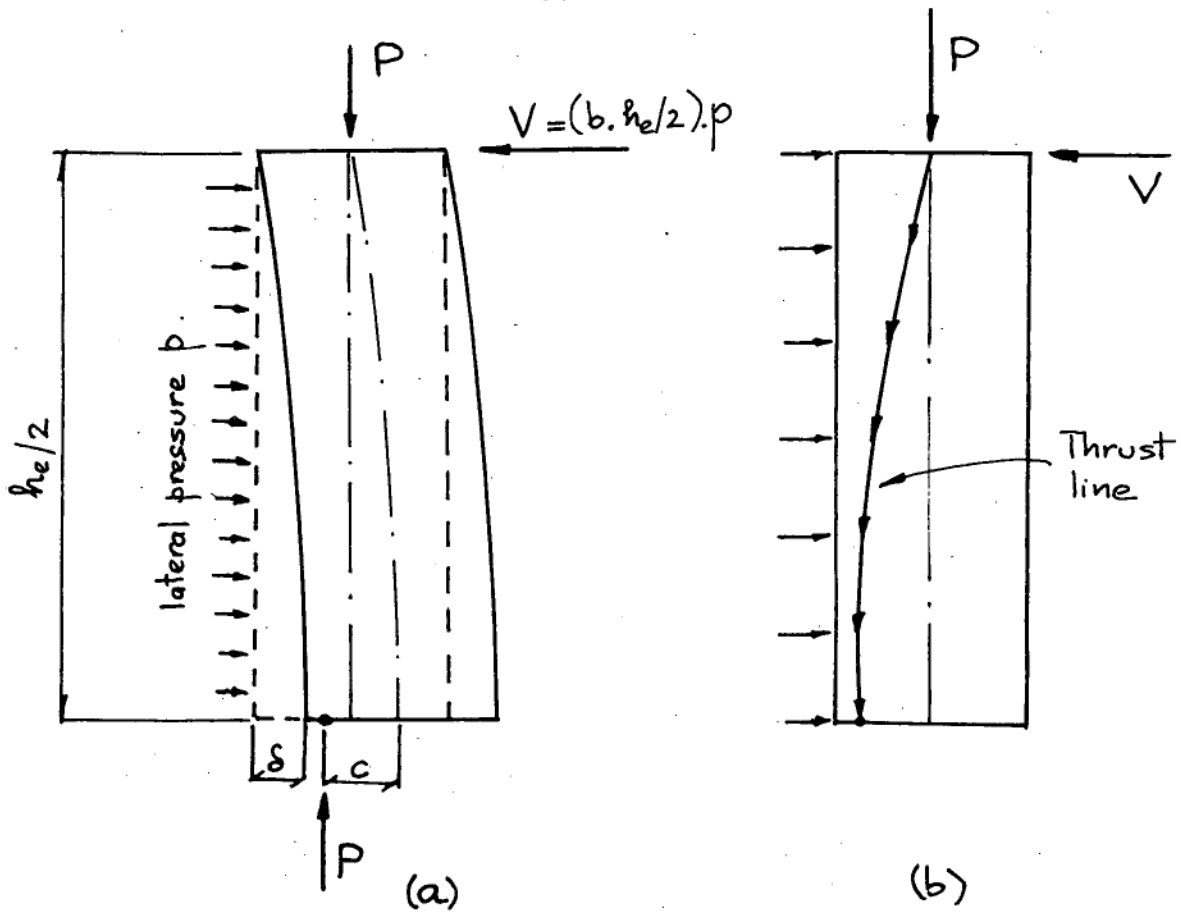


Figure 5.4

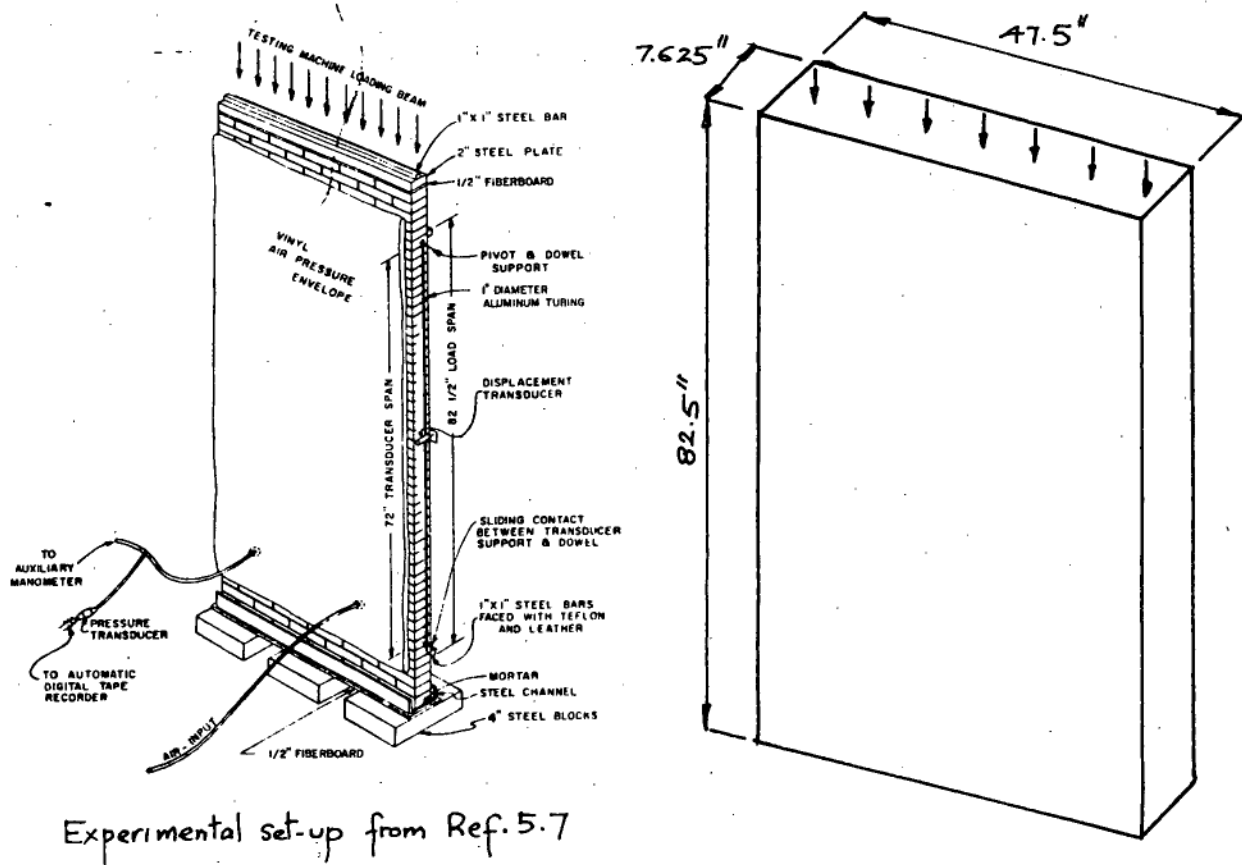


Figure 5.5

WALL DESIGNATION		3-3	3-4	3-5	3-6	3-7*	3-8*	3-9*	3-10
AXIAL LOAD (Kip)		25	50	100	150	200	300	400	500
MEASURED DEFLEXION (in) (at maximum load)		0.49	0.61	0.23	0.79	0.40	0.20	0.19	0.29
MEASURED MAXIMUM TRANSVERSE LOAD (psi)		3.29	5.94	8.17	15.12	15.26	13.80	15.59	6.10
'HINGE' POSITION (AS IN 5.2) (in)		3.65	3.50	3.17	2.85	2.52	1.88	1.25	0.60
PREDICTED WALL CAPACITY (psi)	WITH 'HINGE' PLACED AT EDGE OF SECTION AT ZERO DEFLEXION	3.69 (12.1)**	7.38 (24.2)	14.77 (80.8)	22.16 (46.5)	29.55 (93.6)	44.33 (221.2)	59.10 (279.0)	73.88 (1111.1)
	WITH 'HINGE' PLACED AT POSITION INDICATED AT ZERO DEFLEXION	3.54 (7.6)	6.76 (13.8)	12.30 (50.5)	16.50 (9.1)	19.5 (27.7)	21.9 (58.7)	19.40 (24.4)	11.60 (90.2)
	WITH 'HINGE' PLACED AT POSITION INDICATED AT MAXIMUM DEFLEXION	3.08 (-6.4)	5.60 (-5.7)	11.40 (12.9)	12.10 (-19.9)	16.40 (7.4)	19.50 (41.3)	16.30 (4.5)	6.00 (-1.6)

** Values in bracket = $\frac{(\text{Predicted value} - \text{Measured Value})}{\text{Measured Value}} \times 100$

* Wall did not actually fail, test discontinued.

Figure 5.6

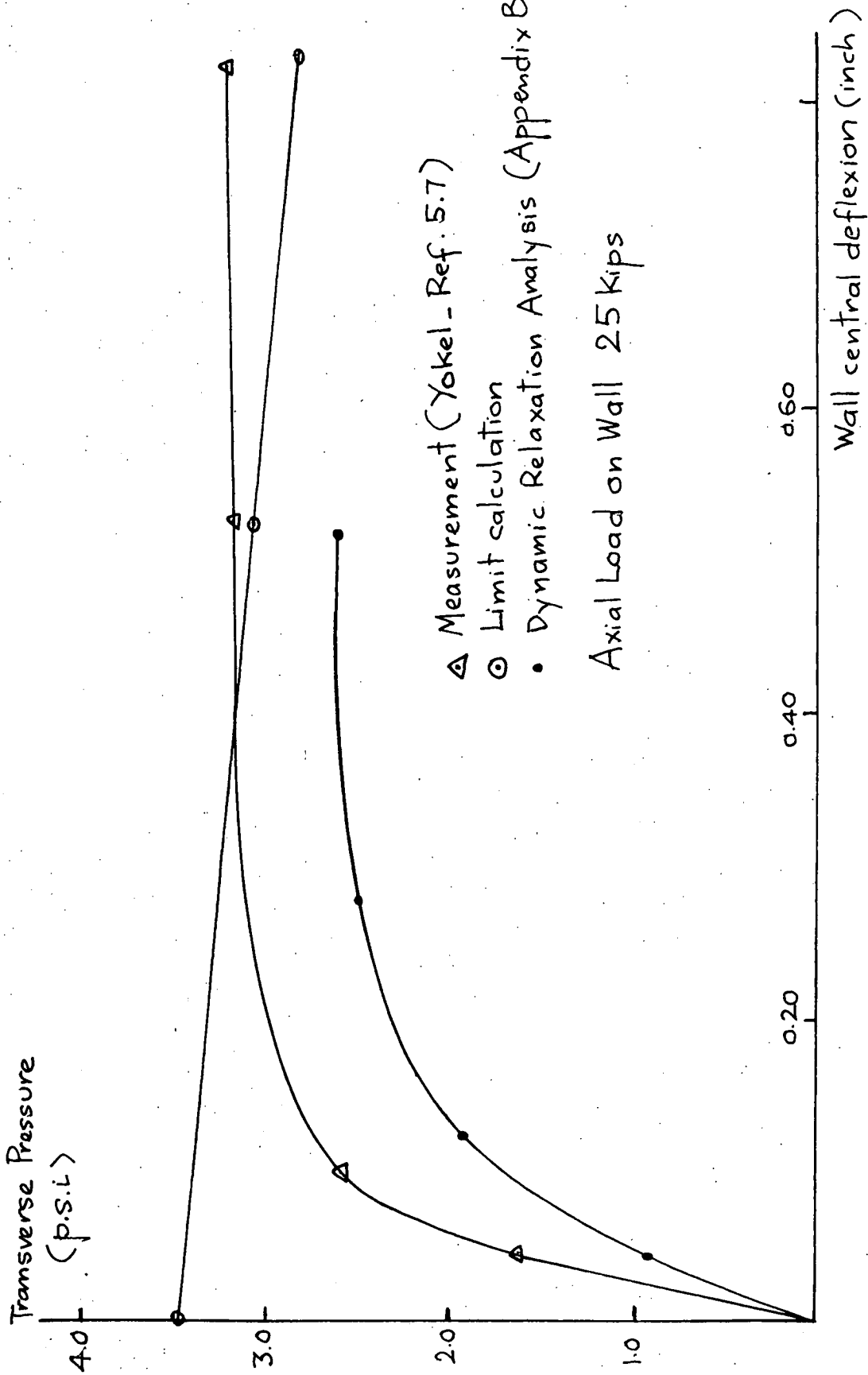


Figure 5.7

5.4 STRENGTH OF GLADESVILLE ARCH BRIDGE

5.4.1 General Description of the arch and the actual design method.

The Gladesville Arch bridge, which spans the Parramatta River between Gladesville and Drummoyne (Sydney, Australia), is the longest single concrete arch span bridge in the world. Its novel design and construction technique have been described fully by the designers in Reference 5.9.

The bridge consists of a concrete arch spanning 1000 ft, supporting prestressed concrete flexible columns and a prestressed concrete beam deck of 100 ft spans. The arch has four ribs, each 20 ft wide and 14 ft deep at the crown, built of hollow concrete voussoirs. The voussoirs were placed upon false work, jointed with insitu concrete, and made into arches by means of flat jacks permanently built into the structure at quarter points to induce thrust. The general geometry of the arch rib is given in Figure 5.8.

The Arch was designed so that it would be made perfectly funicular under its own weight (Ref 5.10). The effect of live load was estimated using an elastic analysis. No estimate was made of the ultimate load-carrying capacity of the structure. The designers stated that the arch had "an enormous factor of safety against failure" and Pippard said "even if tension did occur, the arch would still have a considerable margin of safety"; however, no actual figures were mentioned.

It is interesting to apply the limit principles to establish a measure of safety for this important bridge. Since the stress in the concrete is high in this case, the assumption usually made that there is no danger of crushing of the material is not fully justified. However, allowance for the crushing effects can be made by limiting the thrust eccentricities as proposed in Section 5.2. The calculations made herein assume that the arch is a voussoir arch, as designed and as it was intended to be built.

It is the author's belief that the safety of 'funicular structures' such as this bridge cannot be adequately assessed by the conventional 'safe stress' methods. The application of limit principles to this kind of structure is a more rational approach and calculations similar to the following should be made in all such cases.

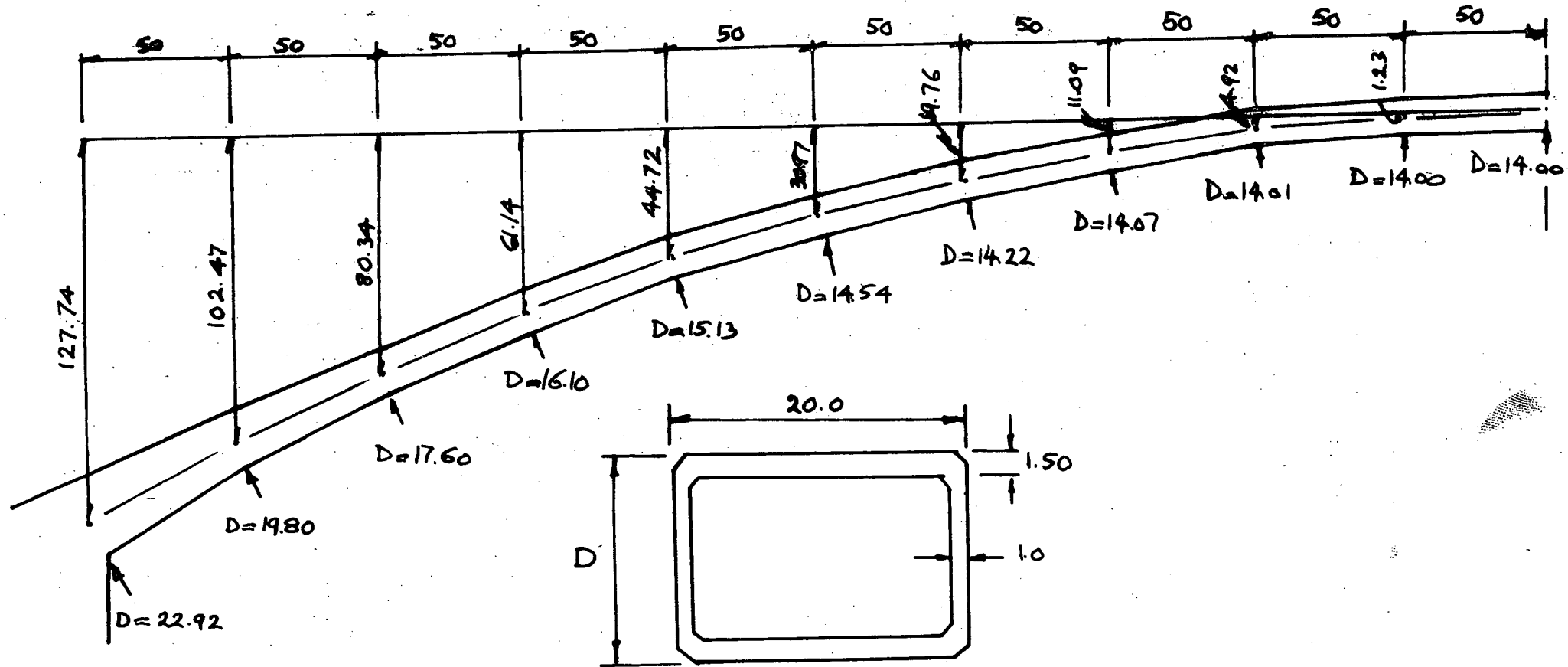
5.4.2 Strength of the voussoir sections

Following the approach in 5.2, the capability of the voussoir sections to carry bending moments under their own dead weight thrusts is investigated. The characteristics of the moment-rotation curves will indicate whether the application of limit principles are suitable to the analysis of this particular arch bridge.

The geometry of the section is given in Figure 5.8. The stress-strain curve for concrete is approximated to a bi-linear relation, Figure 5.10(a). The dead load thrust line is plotted in Figure 5.9, from which the values of the dead load thrusts at the sections are estimated. (Data was gathered from Ref 5.9). The analysis follows the flow chart of Figure 5.2. Figure 5.10 shows the moment-rotation curves of the sections at the estimated dead load thrusts. It is seen that all the moment-rotation curves can be approximated fairly well to the ideal elastic-plastic behaviour (Fig 1.1 - Chapter I). It follows that the application of limit principles are suitable for the analysis of the arch. The positions of the thrust lines will be further modified with the addition of live load in subsequently calculations.

5.4.3 Strength of a single arch rib under point load

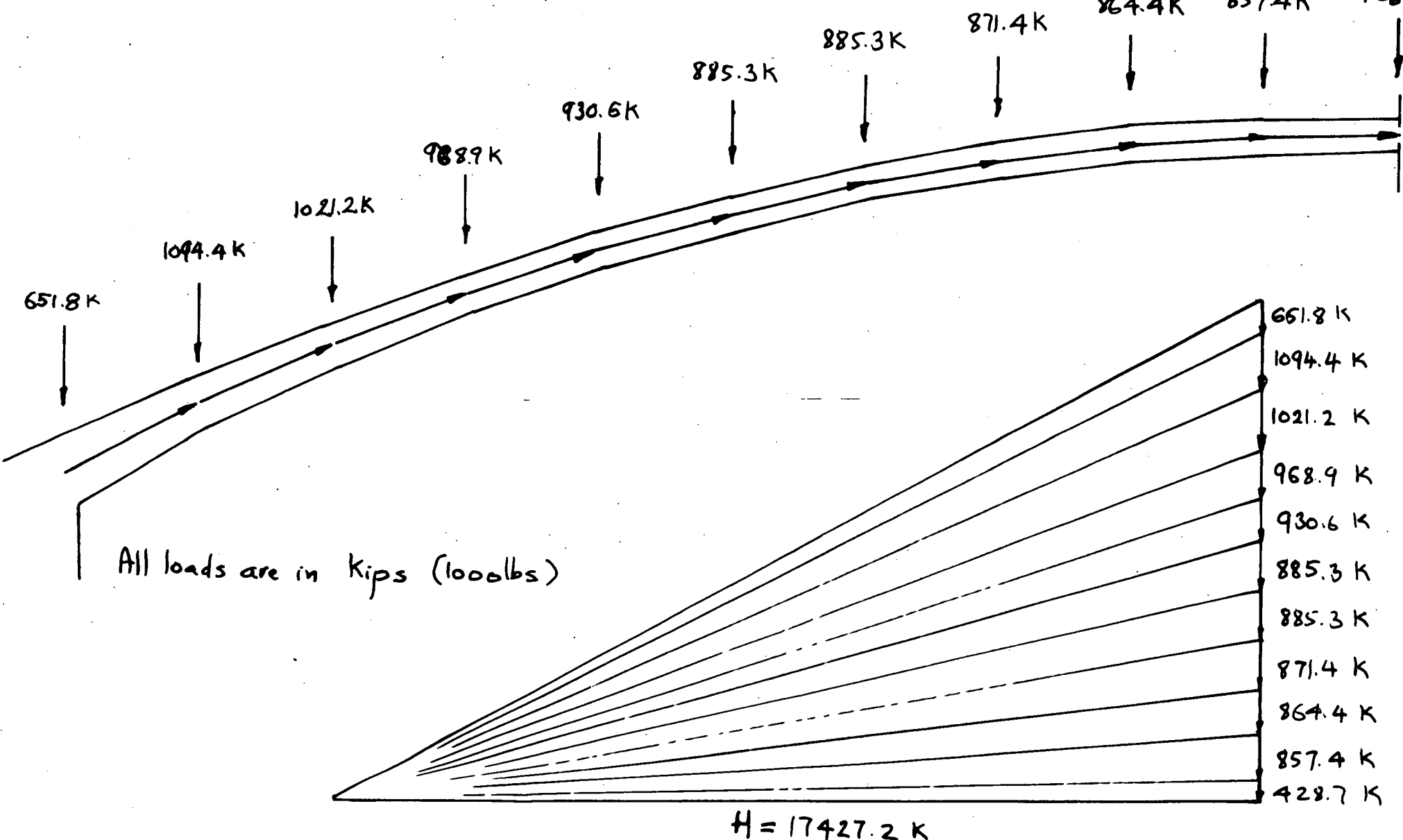
Each arch rib was placed and jacked into position independently before the spandrel columns and crossheads were erected. The strength of an isolated rib under single point load therefore needs to be examined to establish the margin of safety of the rib against a disturbing load which may arise during construction.



All dimensions are in feet

Dimensions of arch rib and voussoir sections.

Figure 5.8



All loads are in kips (1000lbs)

Estimate of dead loads and dead load thrust line.

Figure 5.9

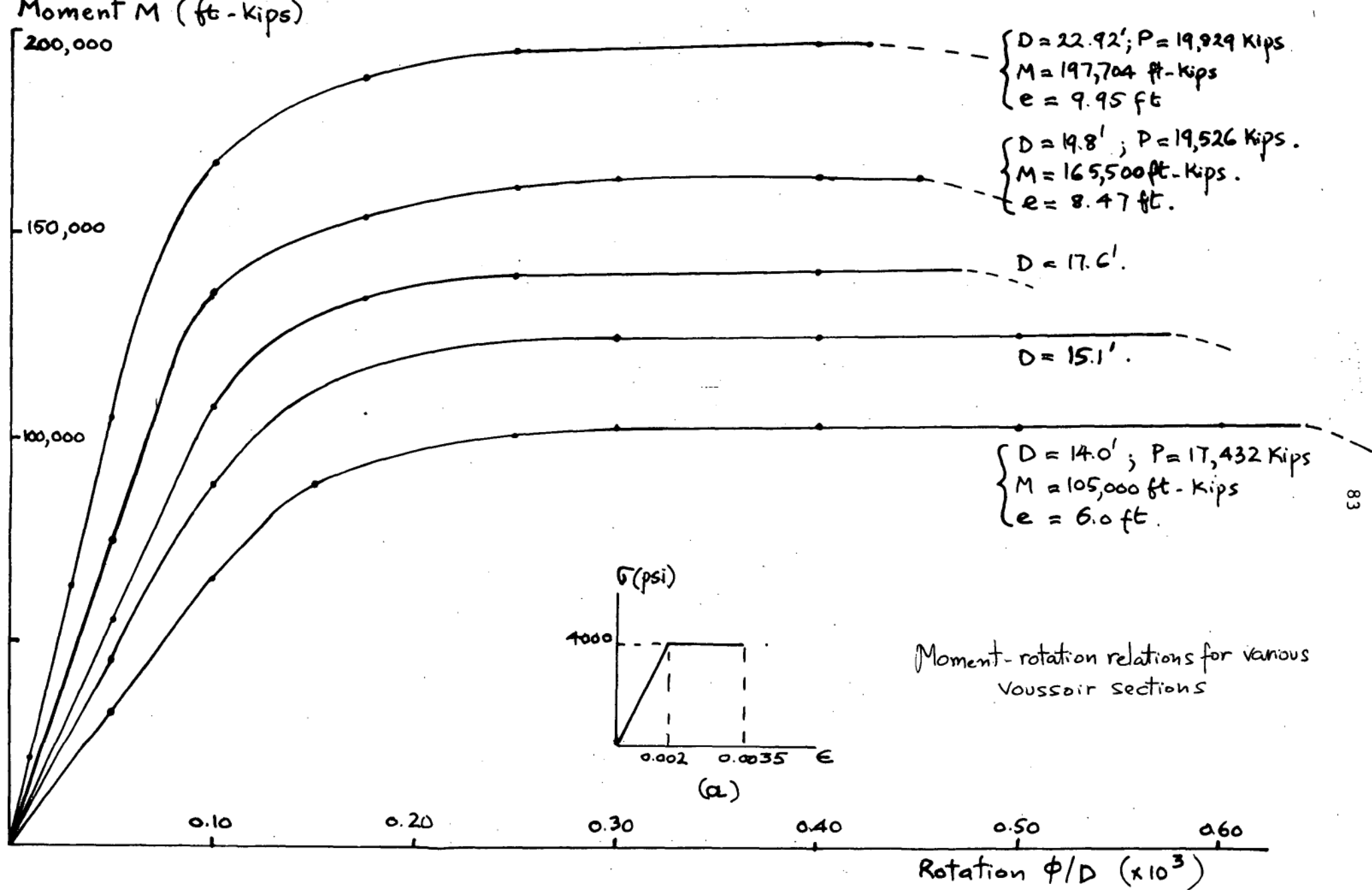


Figure 5.10

The worst condition, that is a single point load acting at a quarter span, is examined. Since the arch was made perfectly funicular under its own weight the positions of the hinges at the collapse of the arch can be located by drawing the point load thrust line (Fig 5.11). The equilibrium of the system is given in Figure 5.12. The following equilibrium equations are used to determine the collapse load:

(i) Sum of moments about points 2 and 3 for the segments 1-2 and 3-4 respectively.

(ii) Sum of moments about 3 for the segment 1-3.

(iii) Sum of the vertical forces and reactions for the entire arch rib.

The equations are

$$\begin{bmatrix} -h'_2 & L_1 & 0 & 0 \\ -h'_3 & L_1 + L_2 & 0 & -L_2 \\ -h'_4 & 0 & L_3 & 0 \\ 0 & 1 & 1 & -1 \end{bmatrix} \begin{bmatrix} H \\ V_1 \\ V_4 \\ W \end{bmatrix} = \begin{bmatrix} \sum_{1-2} \omega_i d_i \\ \sum_{1-3} \omega_i d_i \\ \sum_{3-4} \omega_i d_i \\ \sum_{1-4} \omega_i \end{bmatrix} \quad (5.2)$$

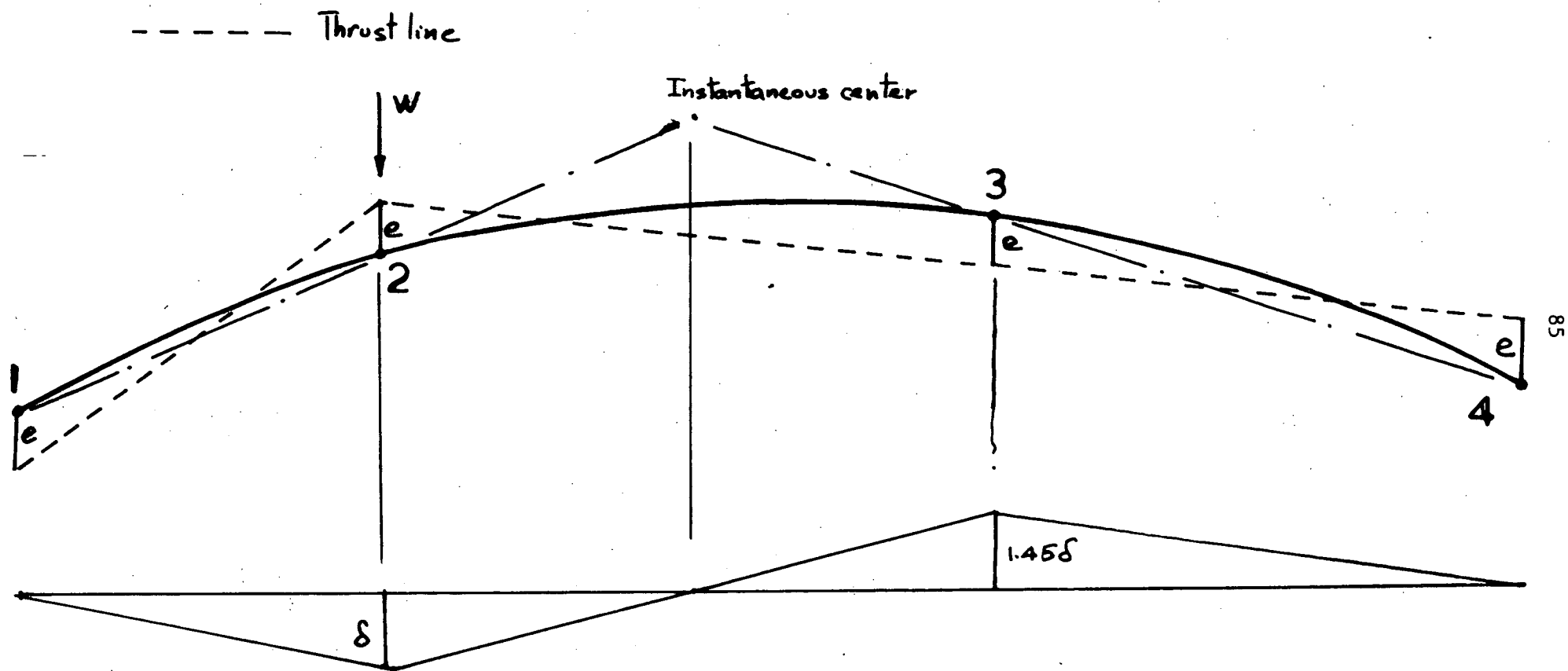
with

$$h'_2 = h_2 + C_1 \cos 26.8 + C_2 \cos 14.0$$

$$h'_3 = h_3 + C_1 \cos 26.8 - C_3 \cos 8.4$$

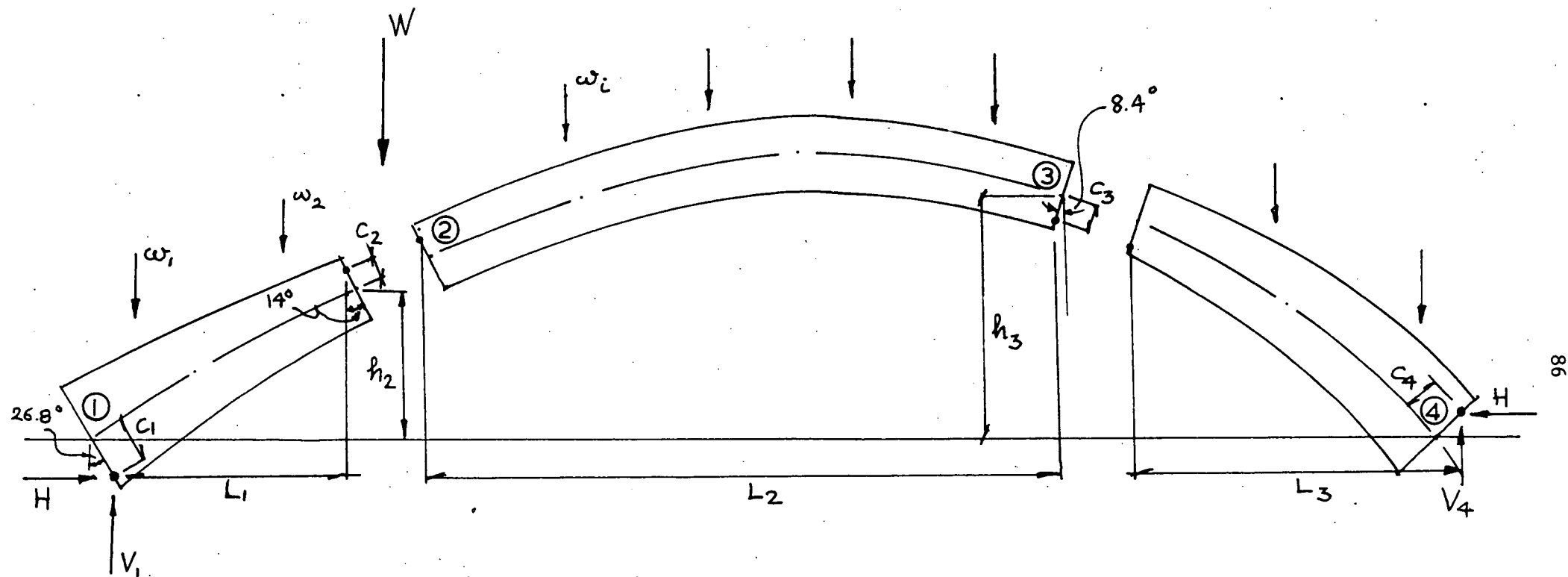
$$h'_4 = h_4 - C_3 \cos 8.4 - C_4 \cos 26.8$$

The symbols are defined in Figure 5.12.



Thrust line for the arch with single point load at quarter span.

Figure 5.11



w_i = distributed dead load
 W = single point load (live load)

Figure 5.12

Effects of deflexion

The effects of deflexion of the arch at collapse can be incorporated into the above analysis. If the point 2 is displaced vertically by a distance δ then point 3 will move upward by 1.45δ (obtained from a simple geometric analysis of the motion of the mechanism, see Figure 5.11).

Therefore the values of h_i in equation 5.2 are replaced by

$$\begin{cases} h'_2 = h_2 - \delta \\ h'_3 = h_3 + 1.45\delta \\ h'_4 = h_4 + 1.45\delta \end{cases}$$

Calculations are made in the following order:

- (i) The hinges are placed at the edge of the section and the collapse load and the reactions are calculated. From these results the

* Figure 5.13 summarizes the results of various calculations on the arch rib with a concentrated load at quarter span. The descending parallel lines in Figure 5.13 are results of various second order rigid-plastic analysis. The slopes of the lines give the rate at which the bridge's load capacity decreases with increased deflexion. The positions of the lines show the effects upon ultimate load calculations of placing the hinges at various positions. The proposed method gives an estimate of the ultimate load 20% - 30% (depending on the magnitude of deflexion) below that given by a conventional rigid-plastic analysis. The non-linear elastic analysis (effect of deflexion included) was performed in the manner proposed in Appendix B1 and solved by the method of dynamic relaxation with the arch divided into 20 elements. The non-tensile non-linear analysis was performed in the manner proposed in Appendix B3. Both of these analyses are believed to be new works. The reliability of these calculations is not known; there are no readily available experimental results to check with. However, all the analyses when plotted together as in Figure 5.13 present a consistent picture, from which the collapse load can be estimated.

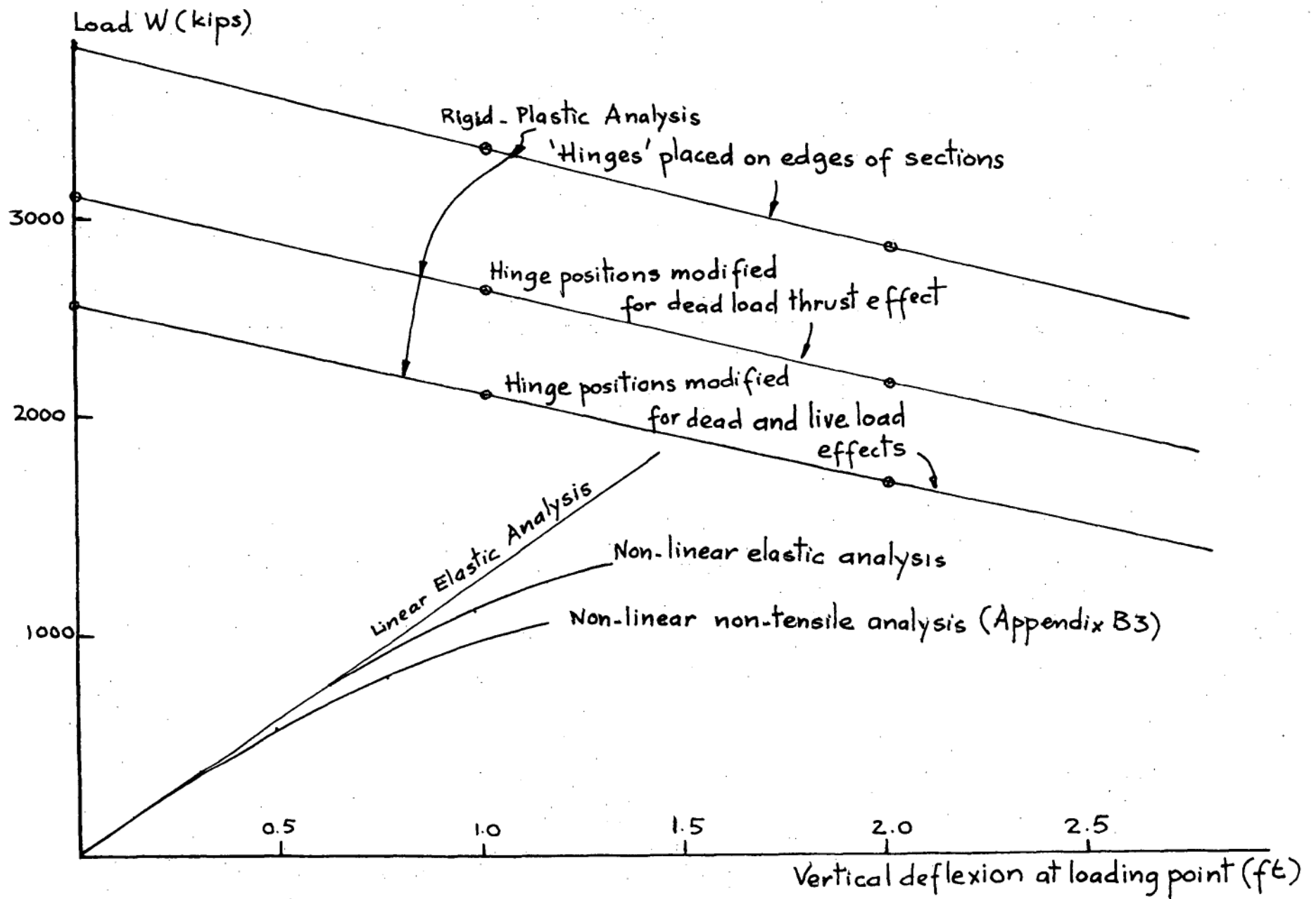
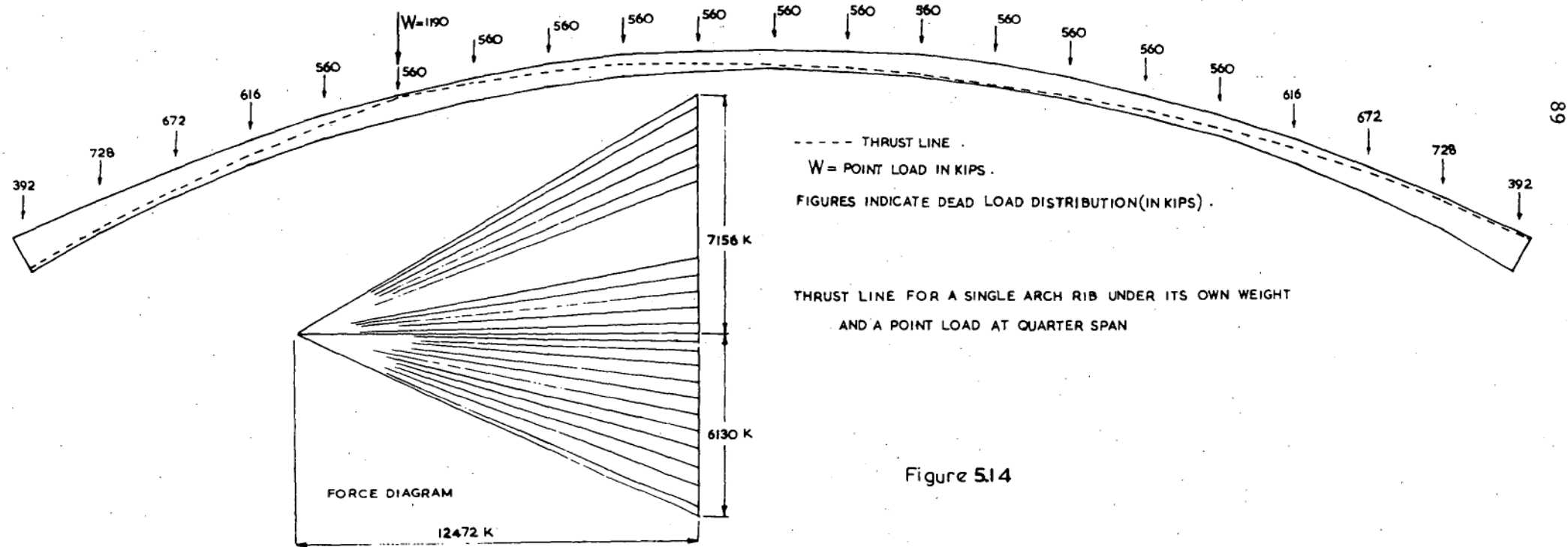


Figure 5.13



CONDITION	δ (ft)	H (kip)	V_1 (kip)	V_4 (kip)	w (k/ft) *
Hinges placed on edge of section	0	26,615	17,209	11,217	19.6
	3	22,161	13,873	10,226	10.9
Hinge positions modified by dead load thrust	0	24,622	15,573	10,813	15.5
	3	20,629	12,626	9,941	7.89
Hinge positions modified by dead and live load thrust	0	23,167	14,360	10,506	12.5
	3	19,718	11,816	9,730	5.8

* Values are for one arch rib.

• SUMMARY OF CALCULATIONS FOR A SINGLE ARCH RIB
UNDER DEAD LOAD AND LIVE LOAD OVER HALF SPAN

Figure 5.15

four ribs, therefore the collapse load factor for this particular loading condition is 6.6.

5.4.4 Strength of the arch bridge under live load over half span.

Similar calculations are performed for the bridge under uniformly distributed live load acting over half of the span. The dead loads now include the weights of the columns, crossheads and the deck. The live load is transmitted to the arch ribs through the spandrel columns, and it is assumed that the live loads are equally shared among the columns. The calculations follow the same process outlined in 5.4.3. Figure 5.15 summarizes the results. It is concluded that each arch rib would collapse at a live load of at least 5.8k/ft acting over half of the span. The design live load is 600 lb/ft in each of the six lanes, thus the collapse load factor for this loading condition is 6.4.

5.4.5 The strength of a single arch rib under lateral load.

The designers have expressed some concern over the lateral stability of a single arch rib during construction. The load capacity of a single arch rib under lateral pressure and its own weight is now investigated. The mode of failure induces three components of force: axial thrust, lateral bending moment and torsional moment. The failure criterion corresponding to these forces is a complicated one, and a full investigation is outside the scope of this thesis. For a monolithic section, most experimenters observed some form of skew bending failure. Failure theories proposed by Cowan, Zia, Swamy (Ref 5.10, 5.11, 5.12) are a combination of Mohr's maximum stress theory and Coulombs internal friction theory.

For our particular problem, the principal factor appears to be the influence of the voussoir joints on the behaviour of the section. This, in turn, depends on the magnitude of the axial thrust at the section.

(i) If the axial thrust is sufficiently high, the influence of the joint may be non-existent and the section behaves as if it is continuous. In this case the standard theory may be used. Swamy (Ref 5.12) stated that a circular interaction curve is a good lower bound approximation and gave the following failure criterion.

$$\left(\frac{M}{M_o}\right)^2 + \left(\frac{T}{T_o}\right)^2 = 1$$

with $T_o = M_{TP} \sqrt{1 + f_{cl}/F_T}$

where M_{TP} is the torsional strength of a plain concrete hollow section

f_{cl} is the stress due to the axial force

and F_T is the tensile strength of concrete.

(ii) If the axial thrust is low, the section may slip at the joint when the maximum frictional resistance is reached. There is no existing theory for this situation. It is proposed to derive the failure criterion as follows:

(a) For a given curvature, with a known axial thrust and with an assumed linear strain distribution, the stress distribution is deduced with cracked regions neglected. (See Section 5.2).

(b) The frictional shear resistance is assumed to be proportional to the normal compressive stress: $\tau = \mu \cdot \sigma$ with $\mu = 0.75$ for finished concrete. (The value of μ can be varied according to the actual condition.)

(c) The torsional moment is assumed to be resisted entirely by these frictional shear forces. It is obtained by taking the moment of the shear forces about the centroid of the area of the section which is in compression.

It is seen that this simple approach accounts for the influence of the cracks due to flexure. This aspect is neglected by the conventional maximum stress theory.

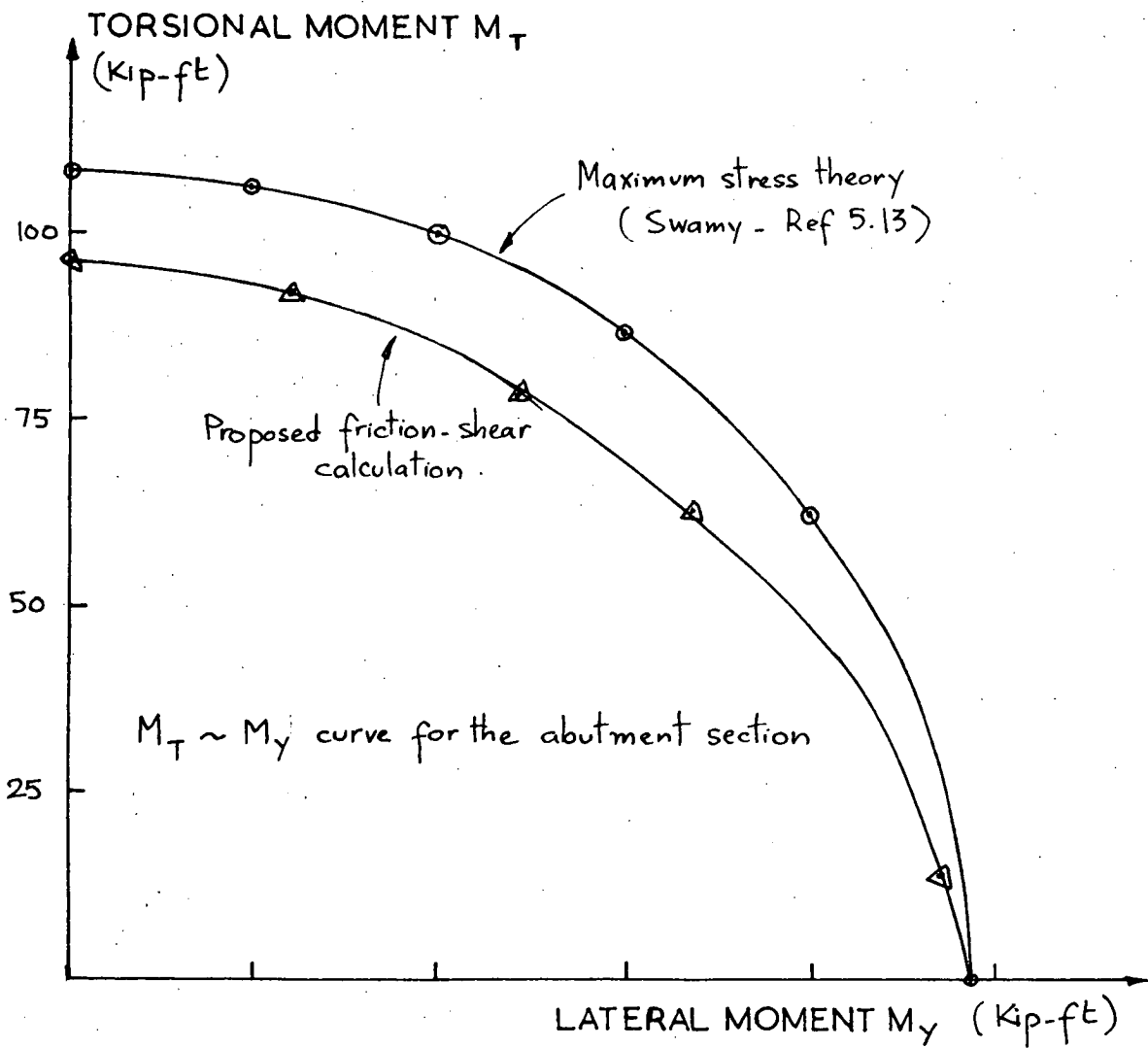
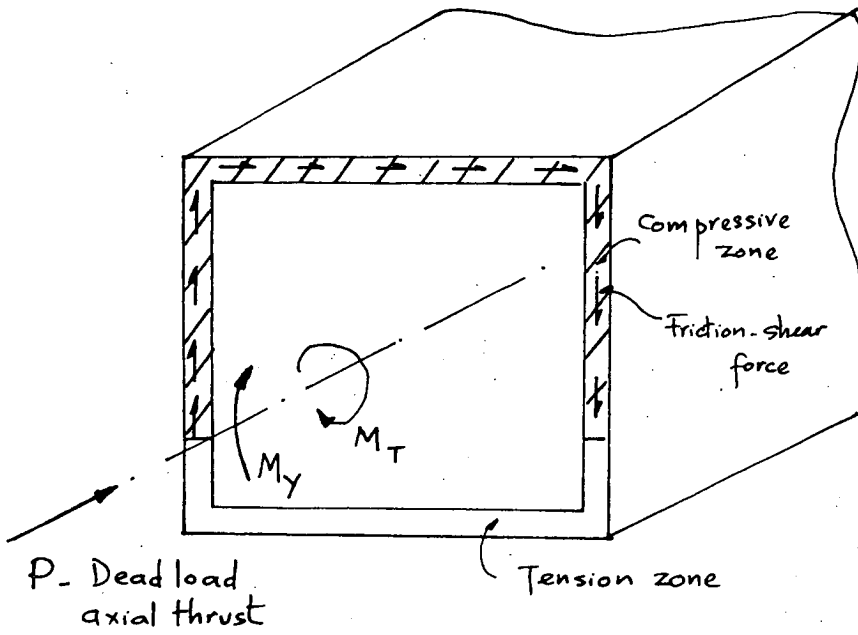


Figure 5.16

* There are no experimental results available for segmental concrete sections under the combined flexure, axial force and torsion. The assumption of a friction failure through the interface is a new one; the assumption was derived tentatively from experimenting with a number of wooden voussoir arches (one was made to scale with the Gladesville Arch). Calculations were performed using both the conventional maximum stress theory and the newly proposed friction-shear theory. For the latter, a value of friction coefficient of 0.75 was selected from a paper by Mast, R.F. "Auxiliary Reinforcement in Concrete Connections" (Journal of Struct. Div. ASCE, Vol 94 No. ST6, 1968).

must still be everywhere safely within the arch (Fig 5.17). Under increasing magnitude of wind load the arch may fail with two, three or four hinges, depending on the ratio of ultimate torsional resistance to the ultimate lateral bending resistance of the cross section. The information required for analysis is presented in Figure 5.18. **

** The treatment of wind as a static problem for this slender arch is rather over-simplified. It can only be considered as a first step towards a solution of this complicated problem.

high, only the collapse modes with 2 or 3 hinges are possible in the Gladesville arch rib.

Referring to Figure 5.19, the lateral component of the reaction at the abutment is R, the thrust line intersects the vertical plane through the center line of the arch at J, (coordinates $\{z_J, y_J\}$ measured from A). The force R, which is equal to half of the total lateral loads, can be considered as acting at the point J. The lateral bending moment and torsional moment at A are

$$M_A = R \cdot y_J \quad ; \quad T_A = R \cdot z_J .$$

For equilibrium in the lateral direction, it is obvious that GJ is parallel to AB, where G is the centroid of the applied lateral load.

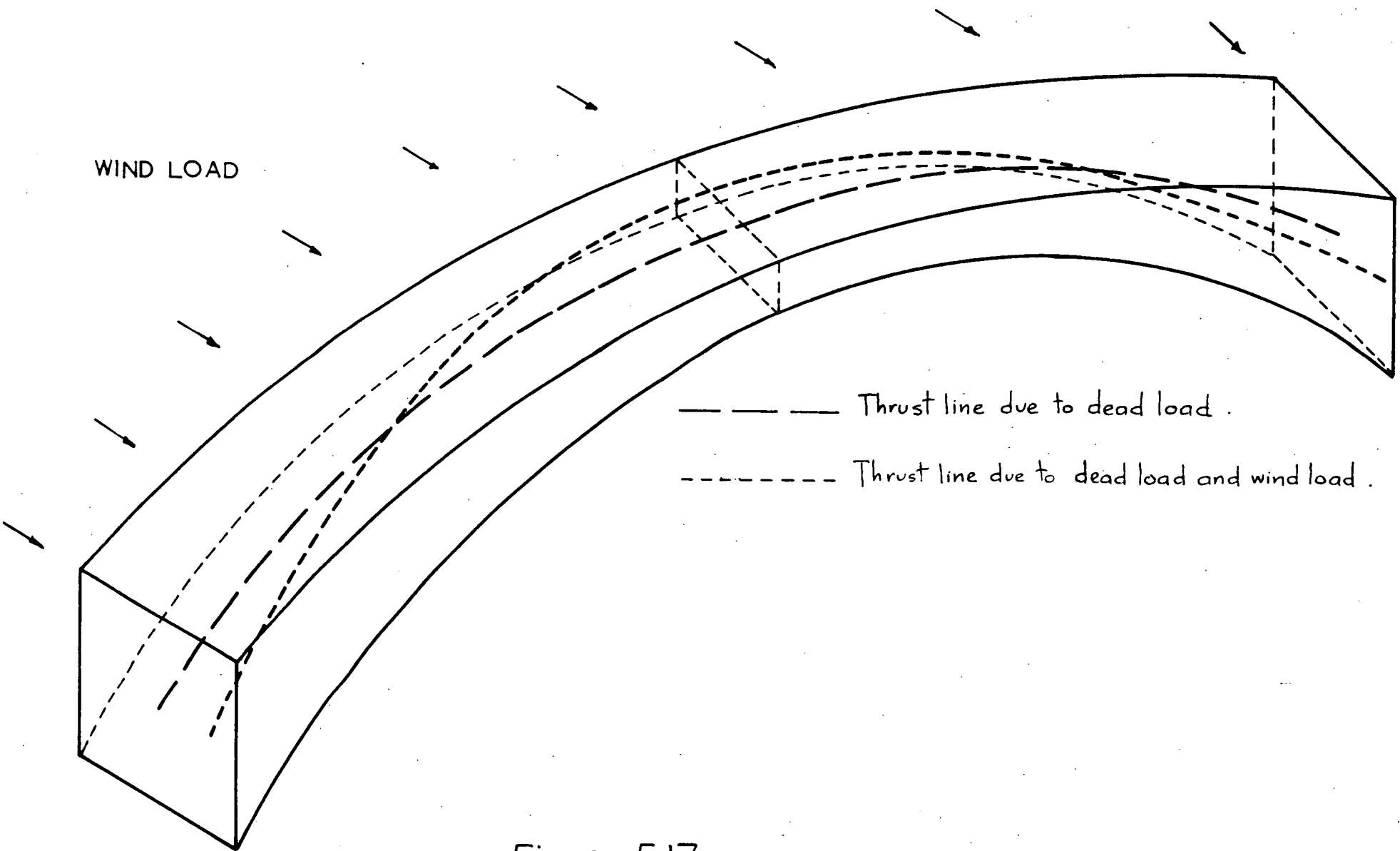
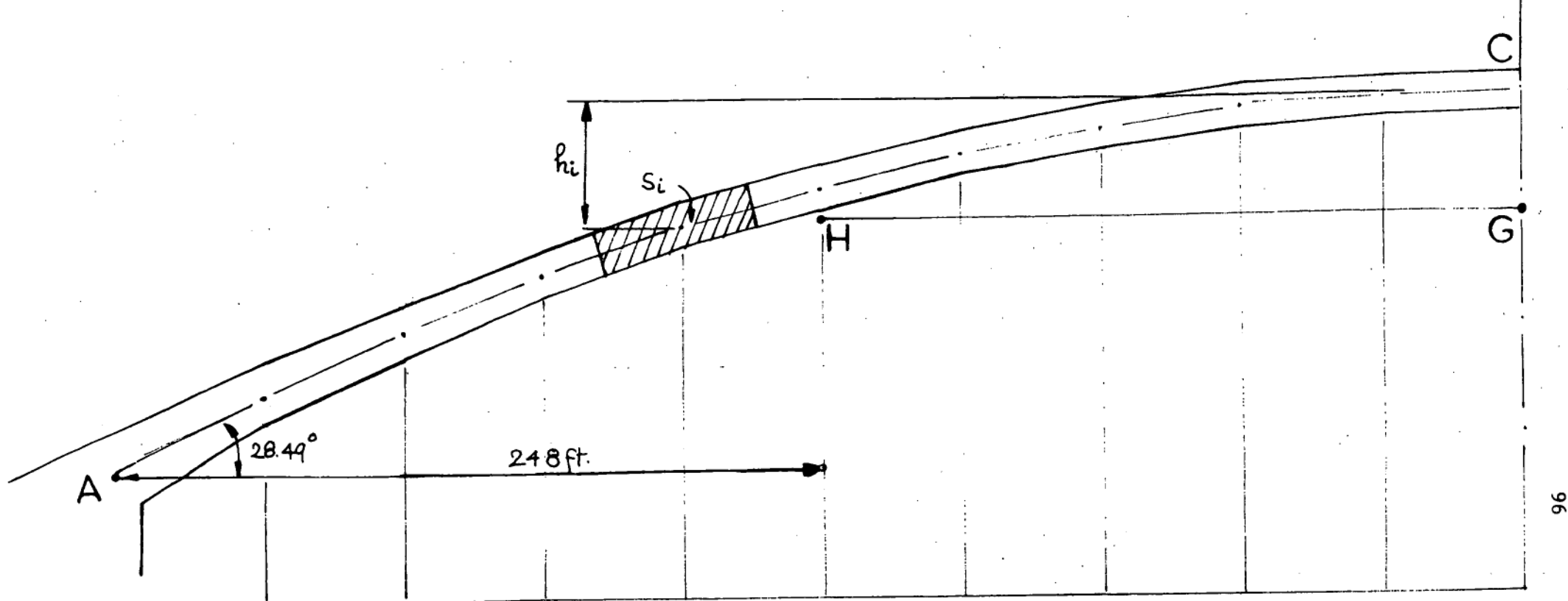
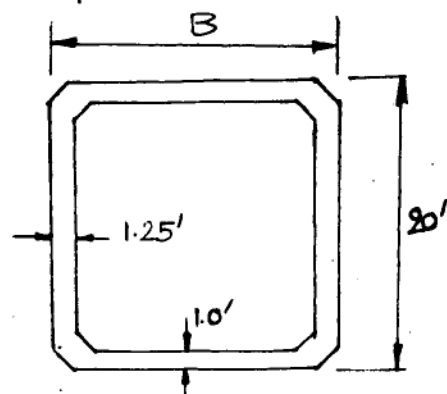


Figure 5.17



96

S_i (ft ²)	987.5	950	805	755	725	710	700	700	700
h_i (ft)	102.47	80.34	61.15	44.72	30.97	19.76	11.10	4.92	1.23



Abutment $B = 22.92'$; $M_{max} = 120,600$ ft-kips ; $P = 12,678$ kips ;
 Crown $B = 14.0'$; $M_{max} = 100,100$ ft-kips ; $P = 11,142$ kips ;

Figure 5.18

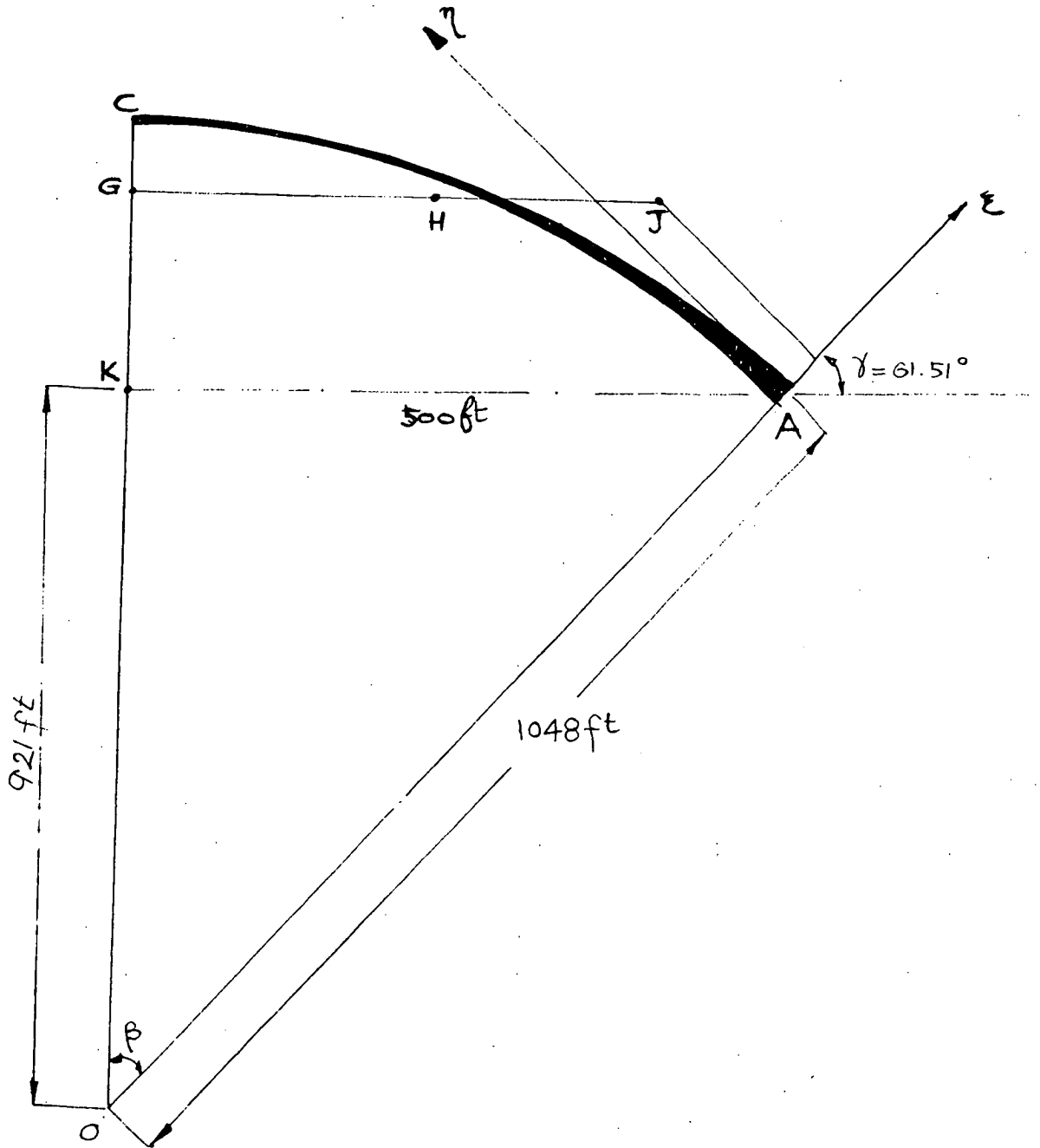


Figure 5.19

From Figure 5.16 we have

$$OG = (OA + \xi_J) \cos \beta + \eta_J \sin \beta \quad \dots\dots\dots (5.3)$$

The failure criterion for the arch cross-section at the abutment A becomes

$$\alpha^2 \eta_J^2 + \xi_J^2 = \left(\frac{T_{max}}{R} \right)^2 \quad \dots\dots\dots (5.4)$$

where $\alpha = \frac{T_{max}}{M_{max}}$

(a) Two hinge mode. The arch may collapse with two hinges, one at each of the abutments A and B (Ref 5.15); the axis of rotation of the collapsing arch is then the line AB. From Hill's principle of plastic work, if γ is the angle between the axis of rotation of the hinge and the normal at the abutment then $\tan \gamma = T/\alpha^2 M$. For the two hinge mode, we have $\gamma = 90^\circ - \beta$ (Fig 5.16).

$$\cot \beta = \frac{T_A}{\alpha^2 M_A} = \frac{R \xi_J}{\alpha^2 R \eta_J} = \frac{\xi_J}{\alpha^2 \eta_J} \quad \dots\dots\dots 5.5(a)$$

Equations 5.3, 5.4 and 5.5(a) are used to solve for the value of maximum lateral pressure. If w is the collapse wind pressure, the equations then become

$$\begin{aligned} R &= (\sum S_i) w = 7382 w ; \quad \alpha = \frac{T_{max}}{M_{max}} = 0.8 ; \\ \frac{\xi_J}{\alpha^2 \eta_J} &= \tan(90^\circ - \beta) = \tan 61.5^\circ ; \\ \alpha^2 \eta_J^2 + \xi_J^2 &= \left(\frac{T_{max}}{R} \right)^2 = \frac{173.7}{w^2} . \end{aligned} \quad \dots\dots\dots 5.6$$

The solutions are:

$$\begin{cases} \xi_J = 66.8 \text{ ft} \\ \eta_J = 56.7 \text{ ft} \end{cases} \quad \text{and} \quad w = 0.163 \text{ k/ft}^2$$

The lateral bending moment at the crown is given by

$$M_c = (HJ) \times R$$

where H is the centroid of the applied lateral load ~~from~~^{from} A to C. Since the position of J is known, HJ can be computed. The bending moment at the crown is found to be $M_c = 275,000$ ft-kip which is far greater than the maximum ultimate value of the moment at the crown 101,000 ft-kip.

This collapse mode violates the failure condition and it is therefore not the correct collapse mode.

(b) Three hinge mode. The hinge at the crown sustains lateral bending moment only (due to symmetry of the mode), while those at the abutments sustain both bending and torsion. Equation 55(a) is now invalid and is replaced by

$$M_c = R.(HJ) = M_p = 101,000 \text{ ft-kip} \quad \dots\dots\dots 5.5(b)$$

$$\text{with } HJ = AH + \bar{x}_J \cos \gamma - \eta_J \sin \gamma$$

The final equations are then

$$\begin{aligned} 0.879 \bar{x}_J + 0.477 \eta_J &= 95.8 \\ 0.64 \eta_J^2 + \bar{x}_J^2 &= 173.7/\omega^2 \quad \dots\dots\dots 5.7 \\ \omega(248 + 0.46 \bar{x}_J - 0.88 \eta_J) &= 13.64 \end{aligned}$$

and their solution, obtained by iterative method, is

$$\begin{cases} \bar{x}_J = 17.0 \text{ ft.} \\ \eta_J = 148.4 \text{ ft.} \end{cases} \quad \text{and} \quad \omega = 0.110 \text{ k/ft}^2$$

Effect of misalignment of voussoirs. It is assumed in the above calculation that the arch is perfectly aligned laterally. Misalignment due to lack of fit between the voussoirs may have some adverse effect on the load-carrying capacity of the arch. The effect of misalignment is equivalent to having the initial thrust line off center. The effect can be allowed for by putting

$$M_c = M_p - H.\delta$$

where H is the horizontal thrust due to dead load and δ is the amount of misalignment.

Equations 5.7 are resolved allowing for various amounts of misalignment

$$\begin{aligned} \text{for } \delta = 1.0 \text{ ft} &\Rightarrow w = 0.105 \text{ k/sq ft} ; \\ \text{for } \delta = 2.0 \text{ ft} &\Rightarrow w = 0.100 \text{ k/sq ft} . \end{aligned}$$

It seems unlikely that the misalignment will exceed 2 ft, so that it may be concluded that the lateral pressure to cause collapse is about 100 lb/sq ft. The design wind pressure in the Sydney area, as laid down in the Australian Standard Loading Code (CA45, pt 2), is 24 lb/sq ft. Thus the collapse load factor for wind load is about 4.2.

5.5 CONCLUDING REMARKS

The load-carrying capacity of structures made of materials having no tensile strength has been investigated. A method of allowing for the effect of crushing of concrete is proposed and used to investigate the suitability of a structure for the application of limit principles. The strength of masonry walls is predicted and compared with actual measurements. The load factors for the Gladesville Arch Bridge are established for three different loading conditions. The thrust line concept is used in all cases to picture the structural action. It is believed that the use of the limit principles, as described above, offers a more rational approach and provides a better understanding of the structural actions of 'funicular' structures than the conventional 'safe stress' approach, and in spite of its shortcomings is more suitable for designing such structures than any other method of which the author is aware.

CHAPTER VI

SOME ASPECTS OF DESIGN OF ARCH DAMS FOR STRENGTH

6.1 INTRODUCTION

The design of an arch dam is, at present, a trial and error process based on some form of elastic analysis. To perform the analysis, the shape of the dam must be guessed, based on general experience. The problem of selecting a suitable dam shape for a given site condition is an important, difficult, and time-consuming part of arch dam design. There are few methods of directly getting a suitable shape. In this chapter an experimental method of directly obtaining a shape for an arch dam is proposed. The method is based on the concept of a thrust surface (an extension of the two-dimensional thrust line).

Since arch dams are 'funicular structures', the accepted definitions of the factor of safety based on stress (i.e. the ratio of the compressive strength of concrete to the maximum stress at design loads) does not reflect at all the load-carrying capacity of the dam. The load-capacity of an arch dam can be estimated using limit principles. Several methods of estimating the load-carrying capacity of arch dams are proposed using the lower bound theorem of plastic theory. The equilibrium approach, attempted herein, provides a relatively simple yet realistic assessment of the strength of arch dams.

The present state of design is first discussed so that the work is viewed in proper perspective.

6.2 STATE OF ARCH DAM DESIGN

An arch dam is a curved dam that carries the major part of its load to the abutments by thrust.

The two primary loads on an arch dam are its weight and the

hydrostatic pressure of the water. These two loads are known with great accuracy once the design is finalized. The effects of gradual application of these loads are sometimes investigated, mainly to prevent cracking or instability of blocks. Additional loads may be imposed by tail-water pressure, deposition of silt, and formation of ice surfaces. Temperature effects are important in arch dams. Expansion and contraction are caused by heat of hydration during construction and temperature differences between the submerged and exposed parts of the dam. Dynamic forces such as seismic action in some areas, or the effect of land or rock slide into the reservoir, are also considered in special cases.

There are other loads which act on the foundations. Seepage of water through rock mass causes uplift which seldom has an important bearing on the safety of the proper dam, although grouting and drainage are most important preparations for the abutments. Deformation of the abutment rock due to the thrust from the dam may have serious weakening effects on the dam (Ref 6.1).

Ideally, an arch dam should transfer all its loads to the abutments by thrust so that the stresses are compressive everywhere. Site condition and construction method make this impossible. Designers therefore attempt to shape and proportion the dam to approach this ideal. Their efforts can be seen through the evolution of the arch dam shape.

Early arch dams are cylindrical in shape and they were designed as a series of arches of constant radius; the arch thickness is increased towards the base to account for the increase in pressure. Since the valley opening decreases towards the base, arches of various radii are then used to reduce the volume of the dam and to improve the reception condition of the thrust to the valley. Although the designers actually used the permissible stress approach, these designs can be considered as limit design based on statically admissible states.

The interaction between various arches causes tension zones to develop near the base of the dam on the upstream face, and on the downstream face in the upper third of the structure. By introducing some vertical curvatures, the weight of the structure tends to reduce these tension zones. Usually, the upstream face is undercut near the base, and the upper portion of the dam is overhung. The amount of vertical curvature is limited by practical construction methods.

Progressive refinement of shape and proper proportioning of arch thickness are the objects of the current state of the art. The design is usually accomplished with the use of one of the following methods of analysis: trial load, shell theory, three dimensional finite element method, or dynamic relaxation method. These methods are all based on elastic theories of structures. The influence of cracks on the state of stress in the dam is usually treated as a local effect.

The development of model tests also contributes greatly to the design of arch dams. The models are usually tested under working load conditions; the test results are used to improve the design or as a check against analytical methods. Only a few of the models are tested to failure.

Design methods have drifted from the early strength design gradually towards the more conventional basis of elastic design. The thinkings of French engineers are more oriented towards strength design; they proposed the theory of "active arches" (voutes actives) which emphasizes the importance of keeping the arches at the bottom of the dam thin (Ref 6.2). Coyne (Ref 6.3) proposed the method of "inclined arches" which takes into account the weight of the structure.

Since cracks must be avoided, especially in the upstream face, an elastic analysis is essential for the final design. However, limit design ideas are helpful in picturing the way the dam carries its load.

Once this picture is formed, it can be used to obtain the dam shape for a preliminary design and to estimate the load-carrying capacity of the dam. These ideas are explored in this chapter.

6.3 PRELIMINARY DESIGN OF ARCH DAMS WITH STRING MODELS

When a highly statically indeterminate structure like an arch dam is to be designed, the use of a simple model is often helpful. The object is to gain some understanding of the structural action and hence to determine whether simple calculations are possible and/or adequate. The view taken here is that of a designer who has a limited amount of geological information of the site on which an arch dam is to be designed.

(a) Picturing the structural action of an arch dam by a thrust surface

Since the main part of the loading in an arch dam is to be carried by direct axial thrust, it is convenient to picture the dam action in terms of a thrust surface (an extension of the two-dimensional thrust line for arch action). If it is assumed that the concrete cannot sustain tensile stresses, then it follows that the surface must be everywhere safely within the dam thickness. Ideally the shape of the dam should be the shape of the thrust surface so that the stress is compressive everywhere. The geometry of such a surface is complex. However, it can be constructed quite readily with the aid of a system of strings and weights as described below.

(b) Description of the set up

A net of strings is set up with pulleys and weights as shown in Figure 6.1. The weights are hung and adjusted to represent hydrostatic loading conditions. The outline of the abutment is represented by the steel frame. The counterweights over the pulleys are adjusted so that the thrust surface enters the abutment at the most favourable angle

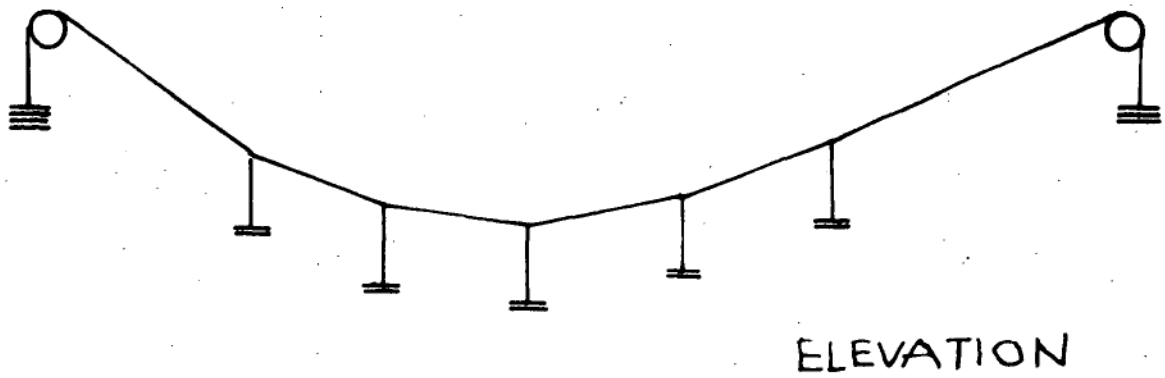
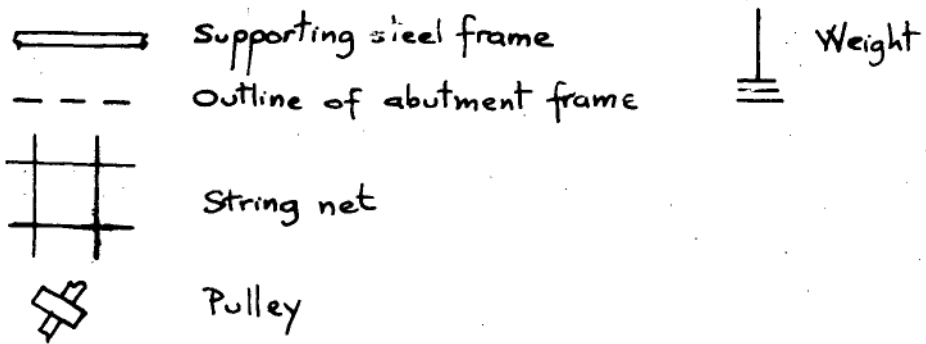
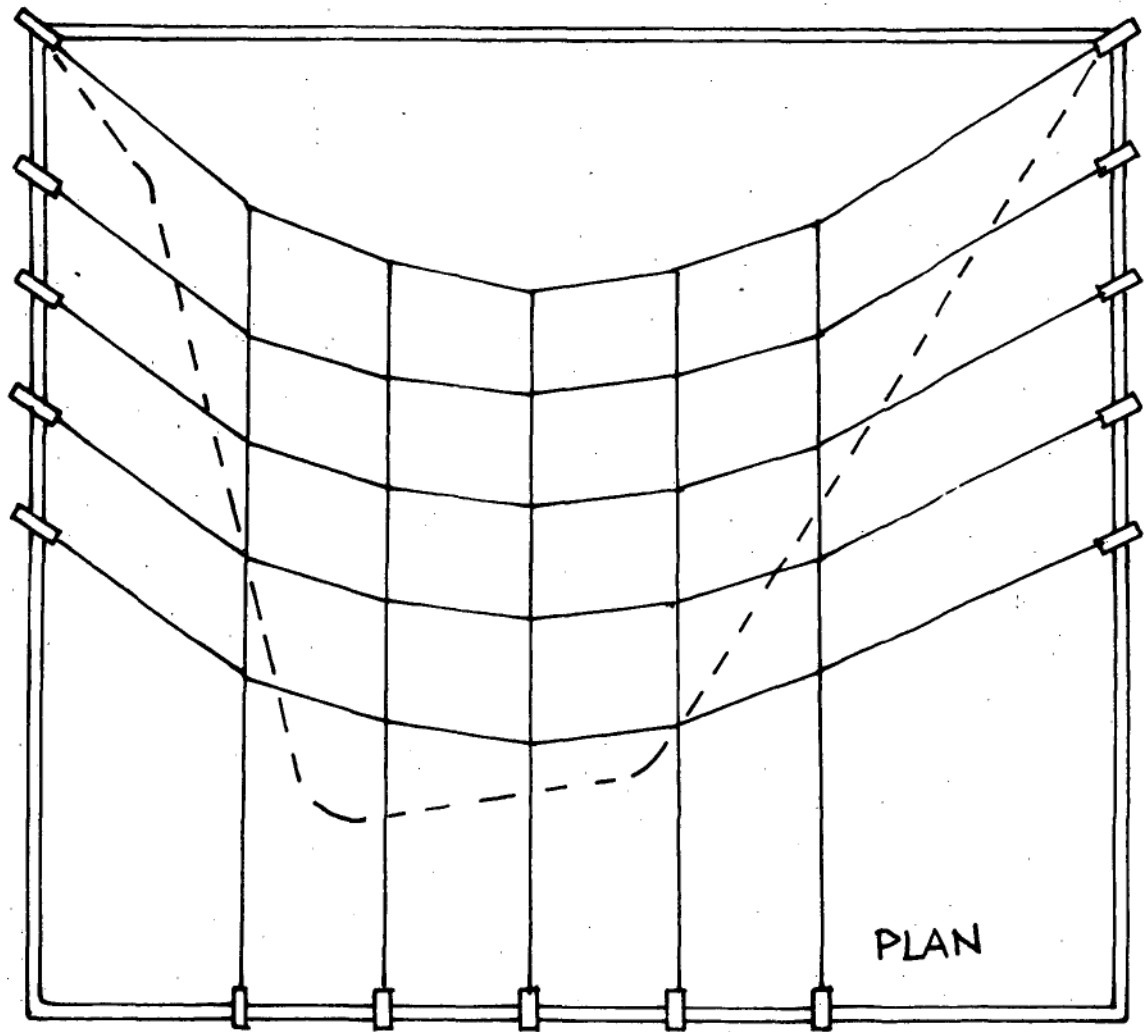


Figure 6.1

(usually from 40° to 50°). The most favourable shape is obtained by adjusting the weights by trial and error. Experience in the process comes quite quickly with practice.

The system provides the following information.

(i) Approximate shape of the thrust surface for certain kinds of loading. In this case it is the hydrostatic load corresponding to a full reservoir behind the dam.

(ii) Magnitude and direction of the abutment thrust for the given loading conditions.

The information is most valuable to the designers particularly in the preliminary design stage.

(c) Test results on the Gordon Dam model

The Gordon Dam is a double curvature arch dam being built in Southern Tasmania (Fig 6.2). Site information as given here was supplied by the Hydro-Electric Commission. A string model of this dam was set up as described in (b) above and adjusted so that the thrust surface angle to abutment was about 45° - 50° (Fig 6.3). The shape obtained is plotted as a series of vertical profiles in Figure 6.4. The actual profile of the dam is included in the same figure for comparison. ~~Graphs of the values of~~

Since the 'experimental' thrust surface is quite close to the actual dam shape, it is expected that the experimental values of thrust are comparable to those calculated by Trial Load Method for the waterload only condition. This comparison is presented in Figure 6.5.

the top of the dam than those given by calculation. The difference in shape between the model and the actual dam at the lower region is due to the omission of the dead weight of the structure on the model. A close inspection of the model profile reveals that the experimental thrust surface correctly indicates the tension zones due to water load. The thrust surface profiles near the abutment do not show the same good agreement

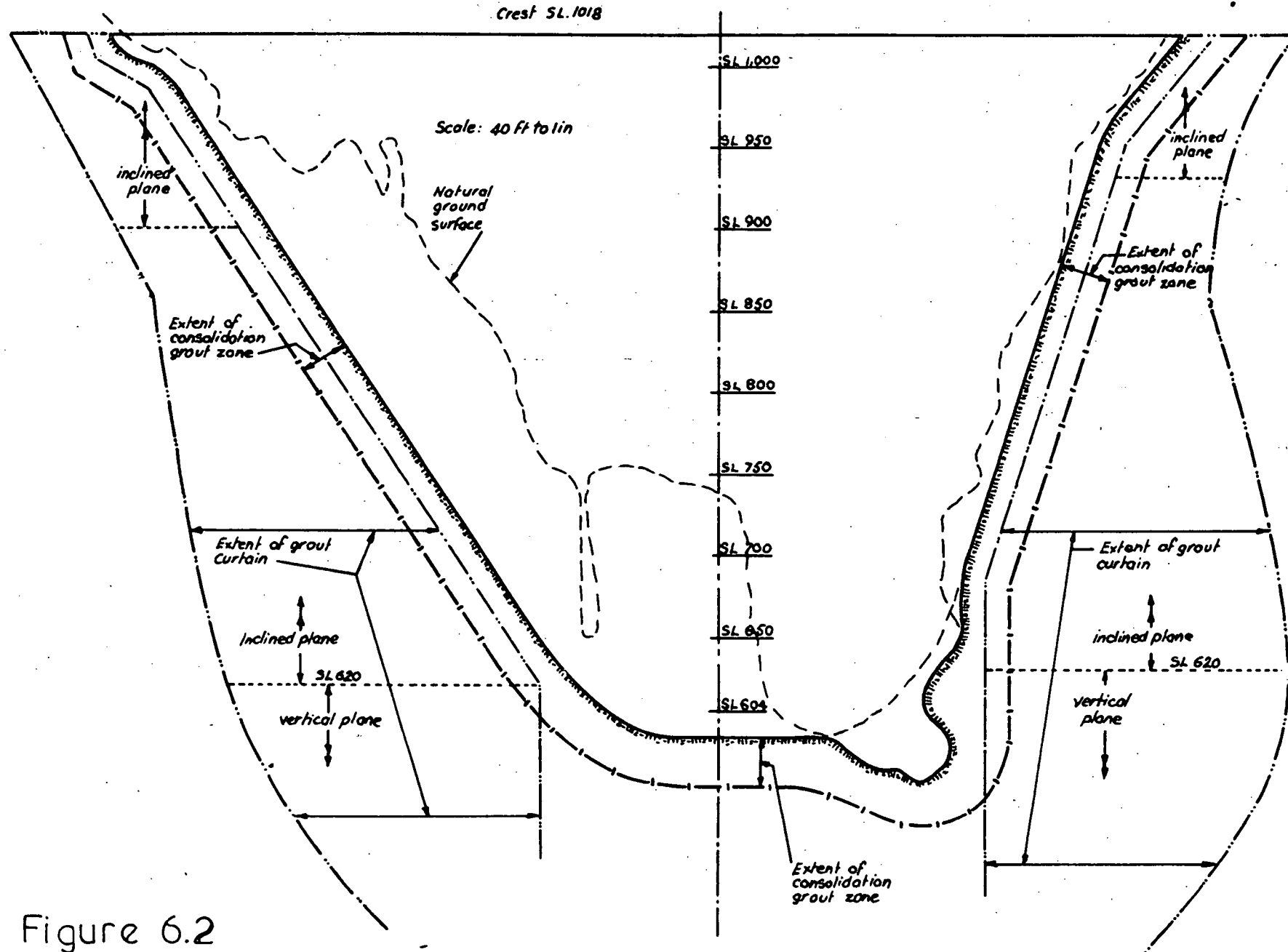
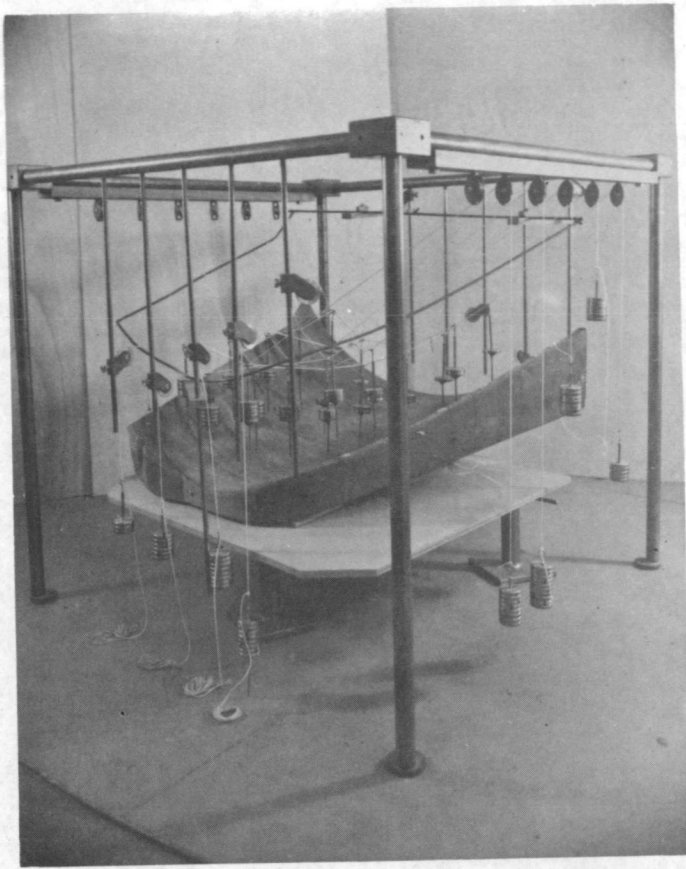
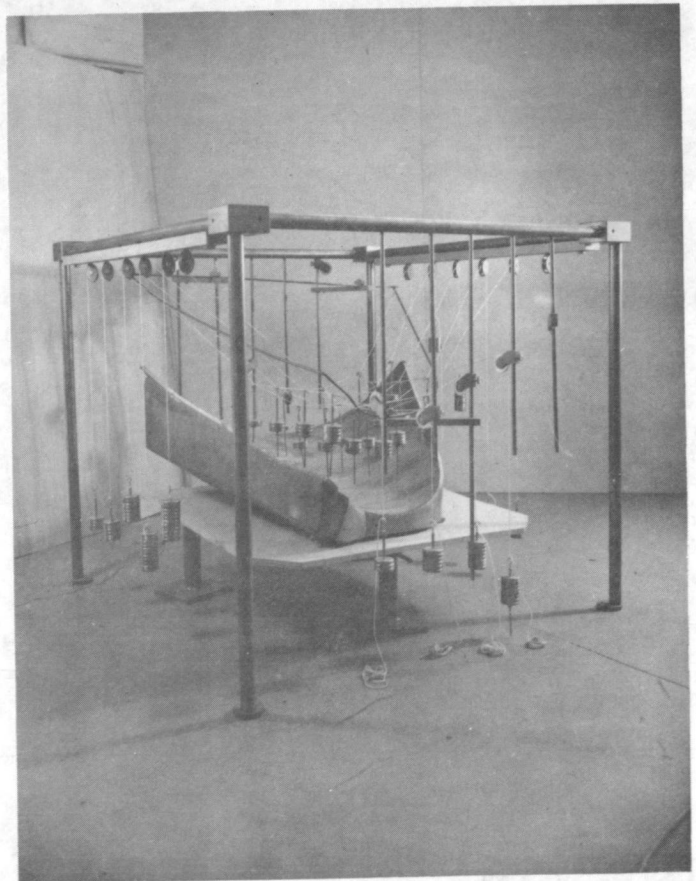


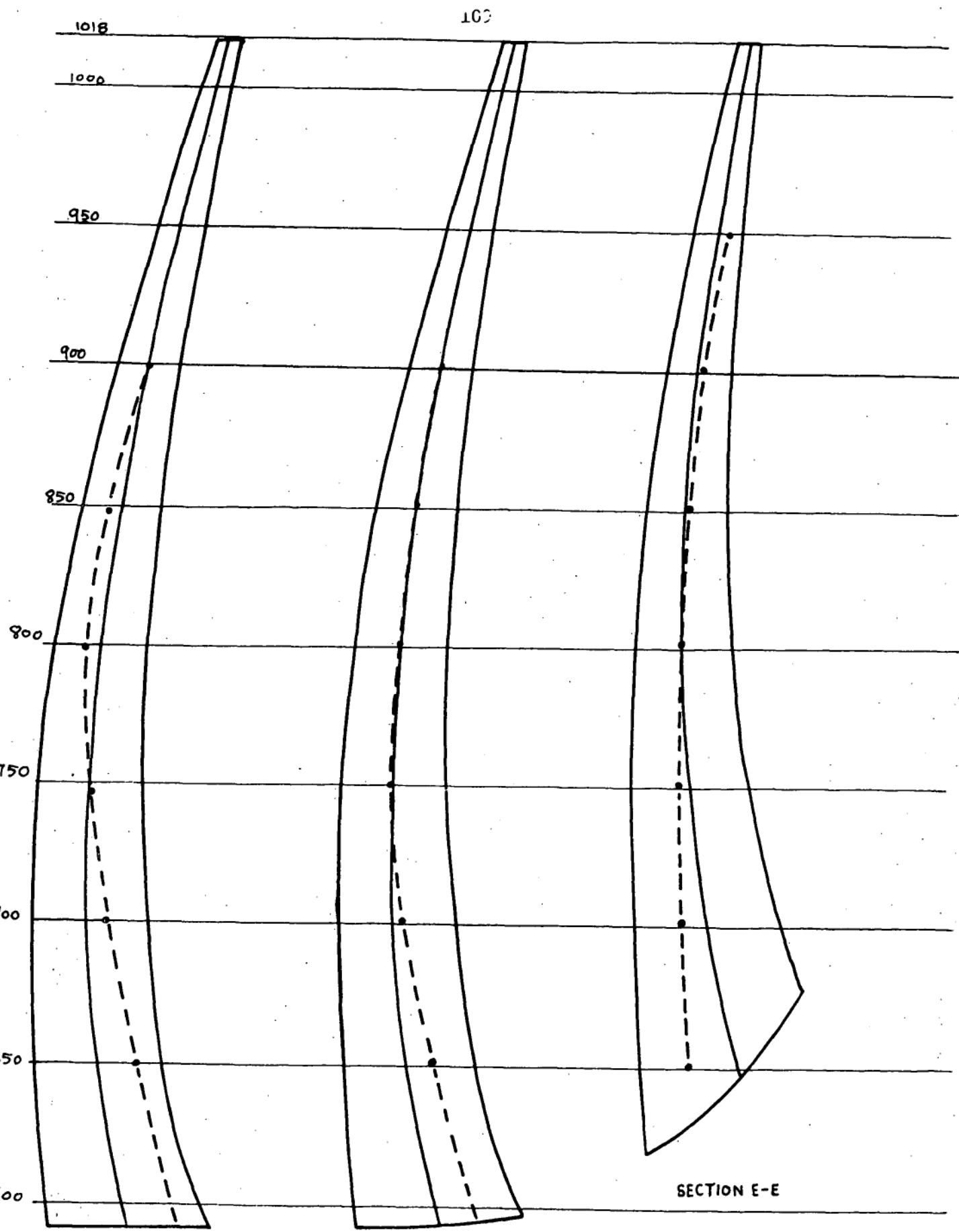
Figure 6.2



String model for the
shape of the Gordon
Arch Dam.

FIGURE 6.3





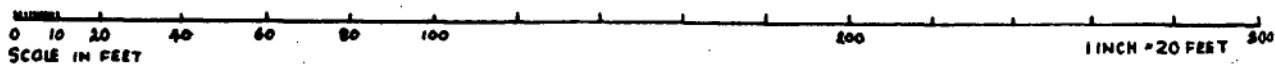
CROWN CANTILEVER

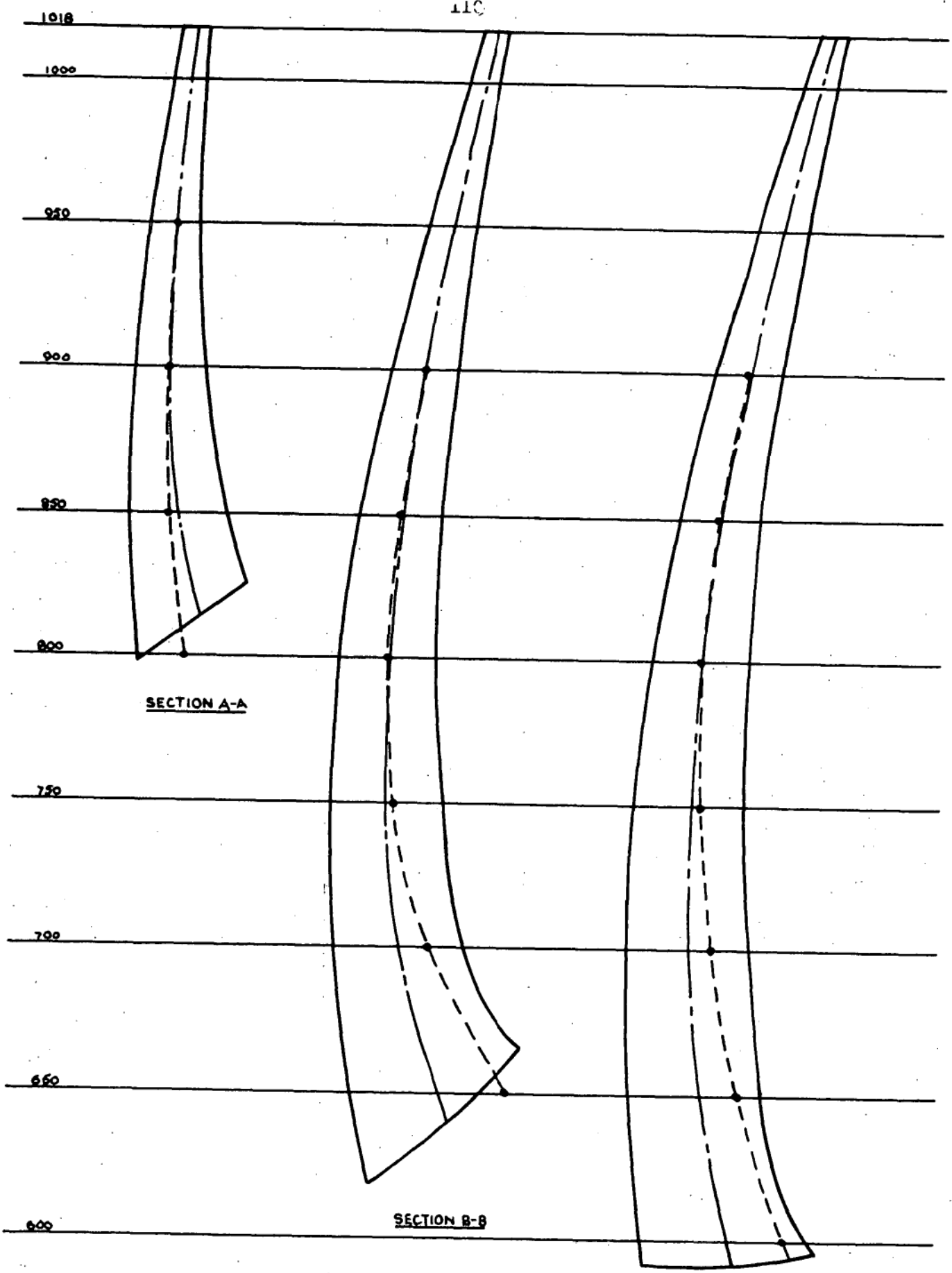
SECTION D-D

— Actual Profile.

--- Profile given by string model.

Figure 6.4(a)





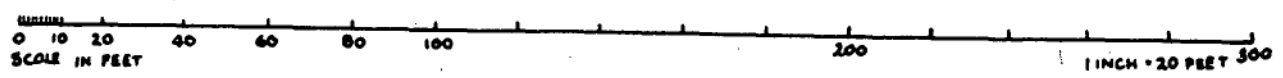
SECTION A-A

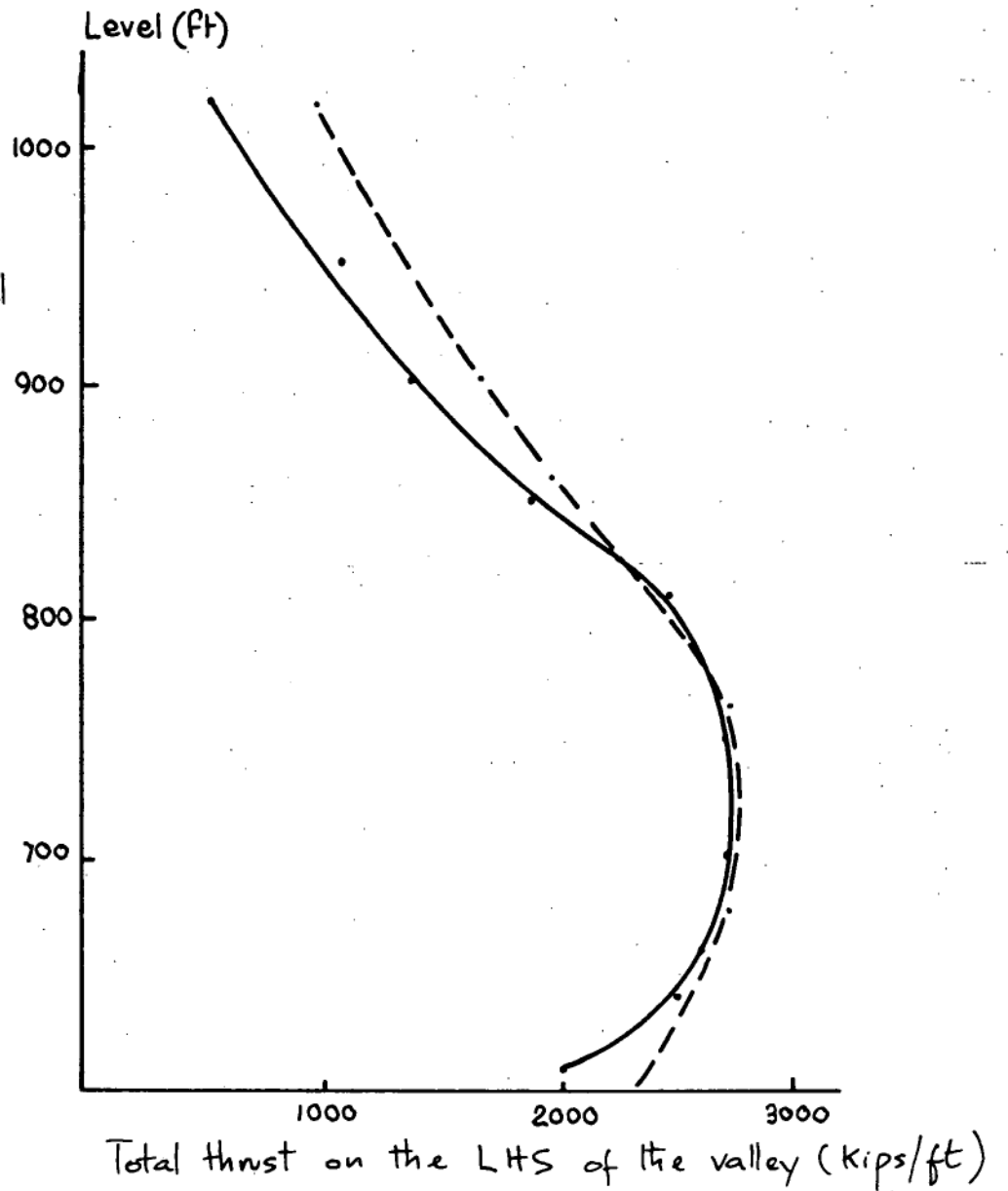
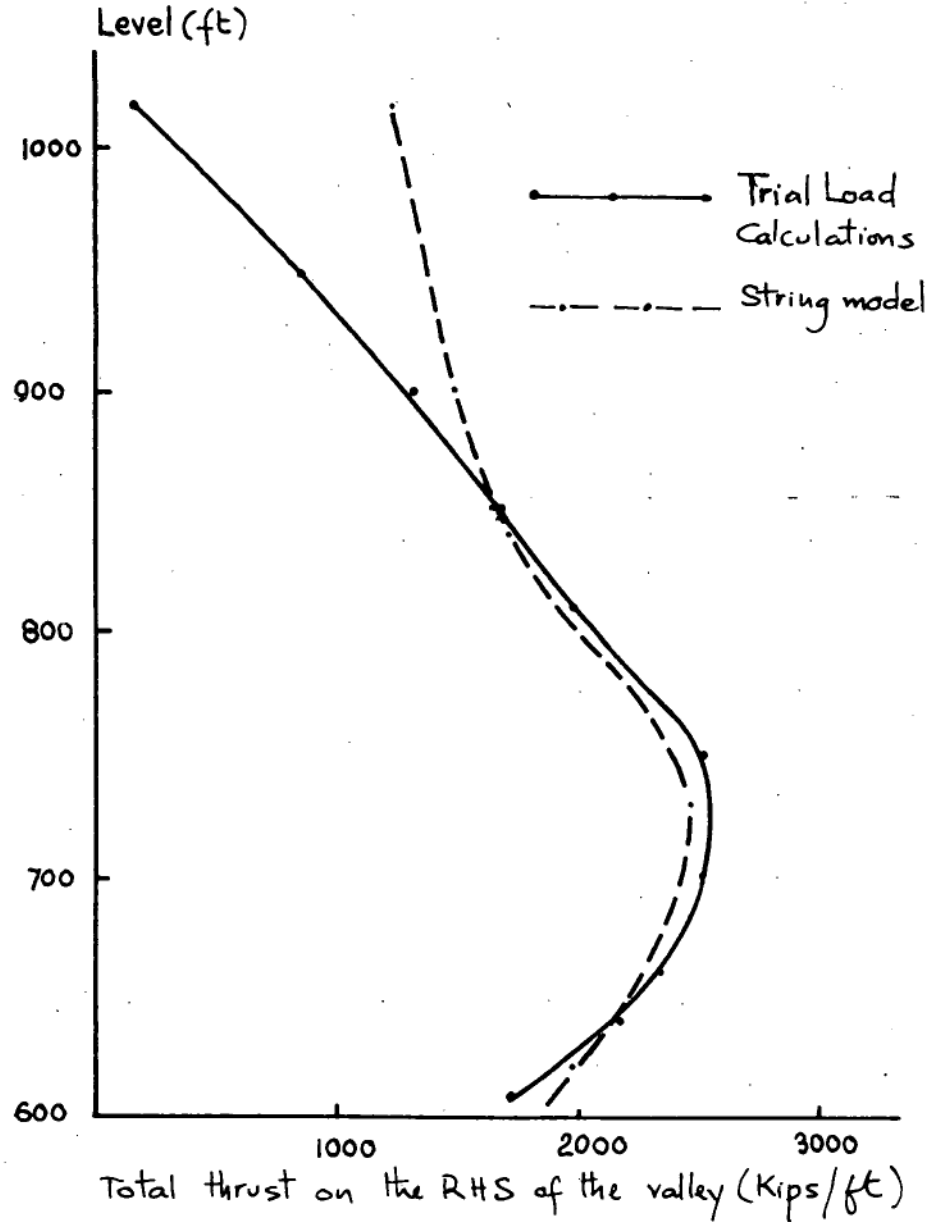
SECTION B-B

SECTION C-C

— Actual Profile
- - - Profile given by string model

Figure 6.4(b)





Comparison of the values of thrust as given by string model and calculations.

Fig.6.5

with the actual dam shape. This is due to the poor representation of hydrostatic pressure on the model in these regions. (The hydrostatic pressure is always acting normal to the upstream face of the dam and this condition is not realized on the model. Possible improvements of the method will be discussed in Section (e)).

(d) Use of the method in the design of arch dams

The experimental method described above has two possible uses in the preliminary design of arch dams;

(i) The thrust surface as constructed above can serve as a guide in the selection of a suitable dam shape. Allowance must be made for the dead weight action to obtain the correct shape. Since the reactions can be varied independently, it is possible to derive the shape that will give the most favourable reaction to the abutment on a given site. The values of the thrust are also useful in determining the dam thickness.

(ii) If a shape has been decided upon, the thrust surface represents a statically admissible state for the given load. If the thrust surface is adequately "covered", i.e. it is everywhere safely within the dam thickness, then the design is safe according to the lower bound theorem of plastic analysis.

(e) Comparison with other methods of shaping the dam

The only other method of shaping the dam that can be found in literature is given by Fiahlo (Ref 6.4). This method uses a rubber membrane with thickness varying similarly to that anticipated for the arch dam. The shape of this membrane under hydrostatic load is used as the shape of the arch dam.

The method proposed in this thesis, when compared with Fiahlo's membrane method shows several disadvantages.

(i) Hydrostatic pressure is not as accurately represented.

(ii) The shape is not completely defined. There is a small region

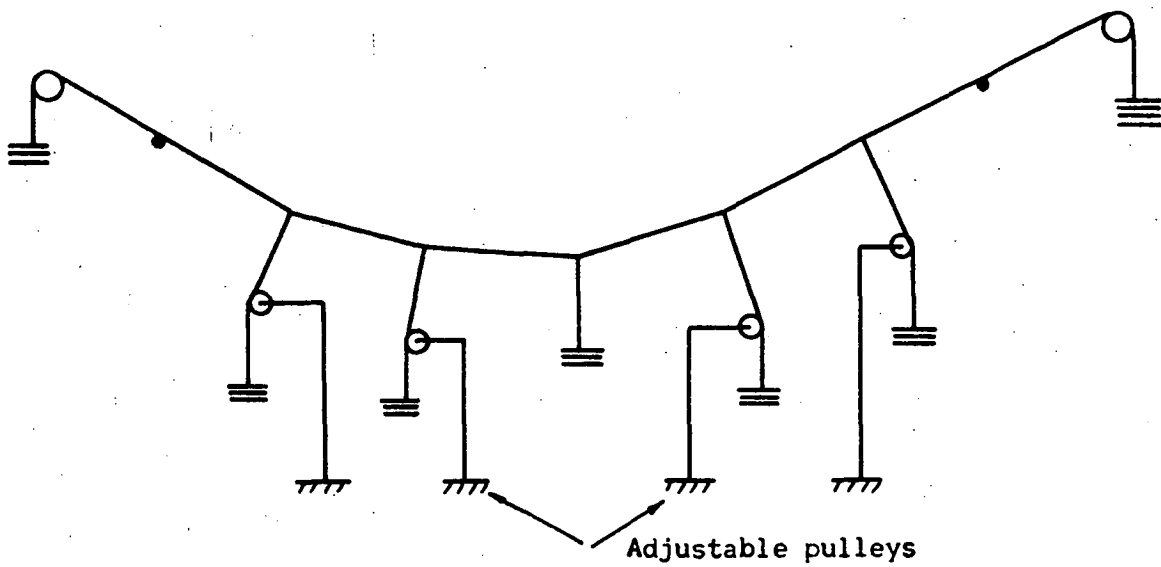


Figure 6.6

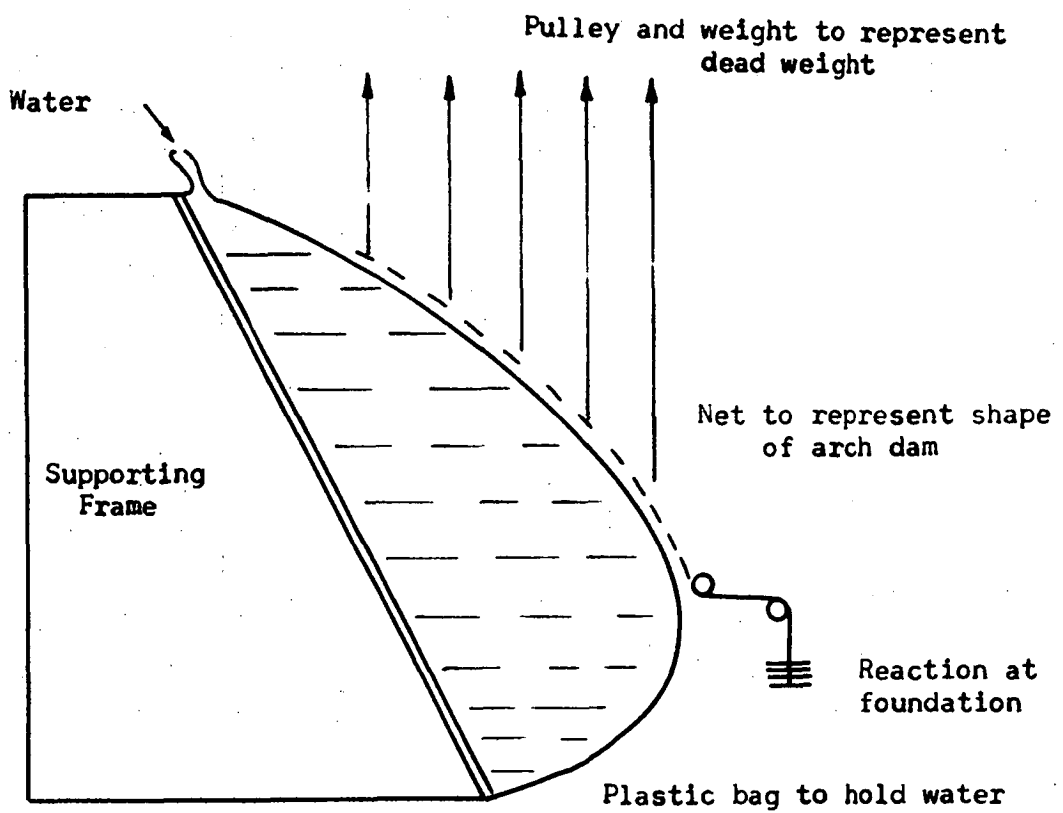


Figure 6.7

near the top of the dam which is not defined by the strings.

However, the following advantages are realized.

(i) Reactions can be varied so that it is possible to vary the shape, especially the angle of the thrust at the abutment. In contrast, membrane models are entirely dependent on the membrane properties; the angle of thrust at the abutment tends to be more acute than the actual site condition permits, and it cannot be changed on the membrane model.

(ii) Estimates of the values of the thrust are directly available from the test in the proposed method, while this information is not directly available in the membrane method.

(f) Possible improvements of the method.

The experimental method of string models presented above is still very crude and it can be improved in many ways. Representation of the hydrostatic pressure can be improved by either using more pulleys and weights arranged as in Figure 6.6, or by using a plastic waterbag as a means of loading with a net representing the dam as in Figure 6.7. Such improvements would lead to a more definite shape for the dam and also provide better estimates of the values of thrust. Gravity load can be introduced with the use of extra weights and strings. However this may not be necessary since corrections for dead weight can be readily calculated once the thrust line for water load is known.

6.4. THE LOAD-CARRYING CAPACITY OF ARCH DAMS

The structural action of arch dams is investigated, using limit principles derived from plastic theory of steel frames. The object is to construct simple statically admissible states, from which the load-carrying capacity of arch dams can be estimated.

The load-carrying capacity of arch dams is investigated here in terms of increasing hydrostatic load. There are two ways of picturing the increasing load: (i) by imagining a gradual increase in the water level

above the design level, or (ii) by imagining a gradual increase in the density of the liquid in the reservoir, (Fig 6.8). Although both alternatives can be produced in the laboratory, neither corresponds to any actual overloading state. This objection does not invalidate the use of a load factor in the design. As pointed out in Chapter I, there need not be a connection between the load factor and the actual overloading state.

The concept of a load factor based on a gradual increase of the liquid density is used since it has been favoured by other investigators (Ref 6.5 and 6.6) and will thus provide the means of comparison with other works. The cylindrical dam models, tested by Bustamente in Reference 6.5, is used as a basis for comparison between various methods of estimating load capacity of arch dams.

6.4.1 Review of existing literature

The problem of the strength of arch dams has not been investigated fully in literature. Two methods however have been proposed.

(a) Bustamente's method (Ref 6.5). The arch dam is divided into two series of arches and cantilevers. The cantilevers are subjected to bending and the arches to axial thrust, Figure 6.9(a). The failure criteria are:

For a section in compression $N_{max} = 0.85 f'_c \cdot t$;

For a section in bending $M_{max} = 0.85 f'_c t^2/8$; (6.1)

For a section in combined bending and compression $\begin{cases} N_{max} = 0.85 f'_c \cdot c ; \\ M_{max} = 0.85 f'_c \cdot c \cdot (t/2 - c/2) ; \end{cases}$

where t is the section thickness, c is the width of the area in compression, N_{max} is the thrust, and M_{max} the bending moment capacity of the section, Figure 6.9(b). Bustamente's failure conditions will be used in all the following works.

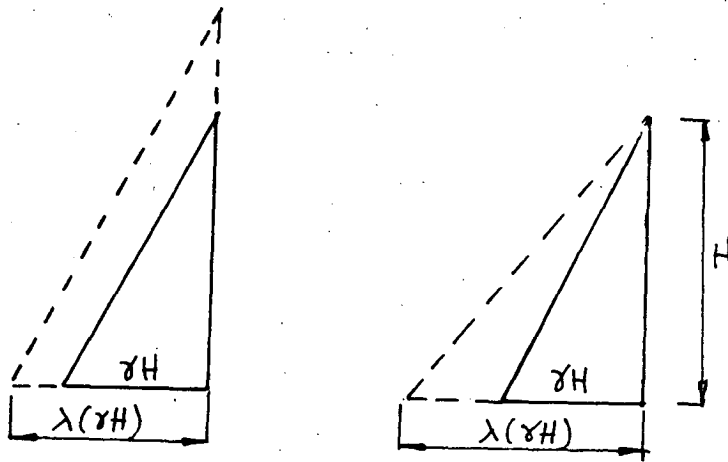


Figure 6.8

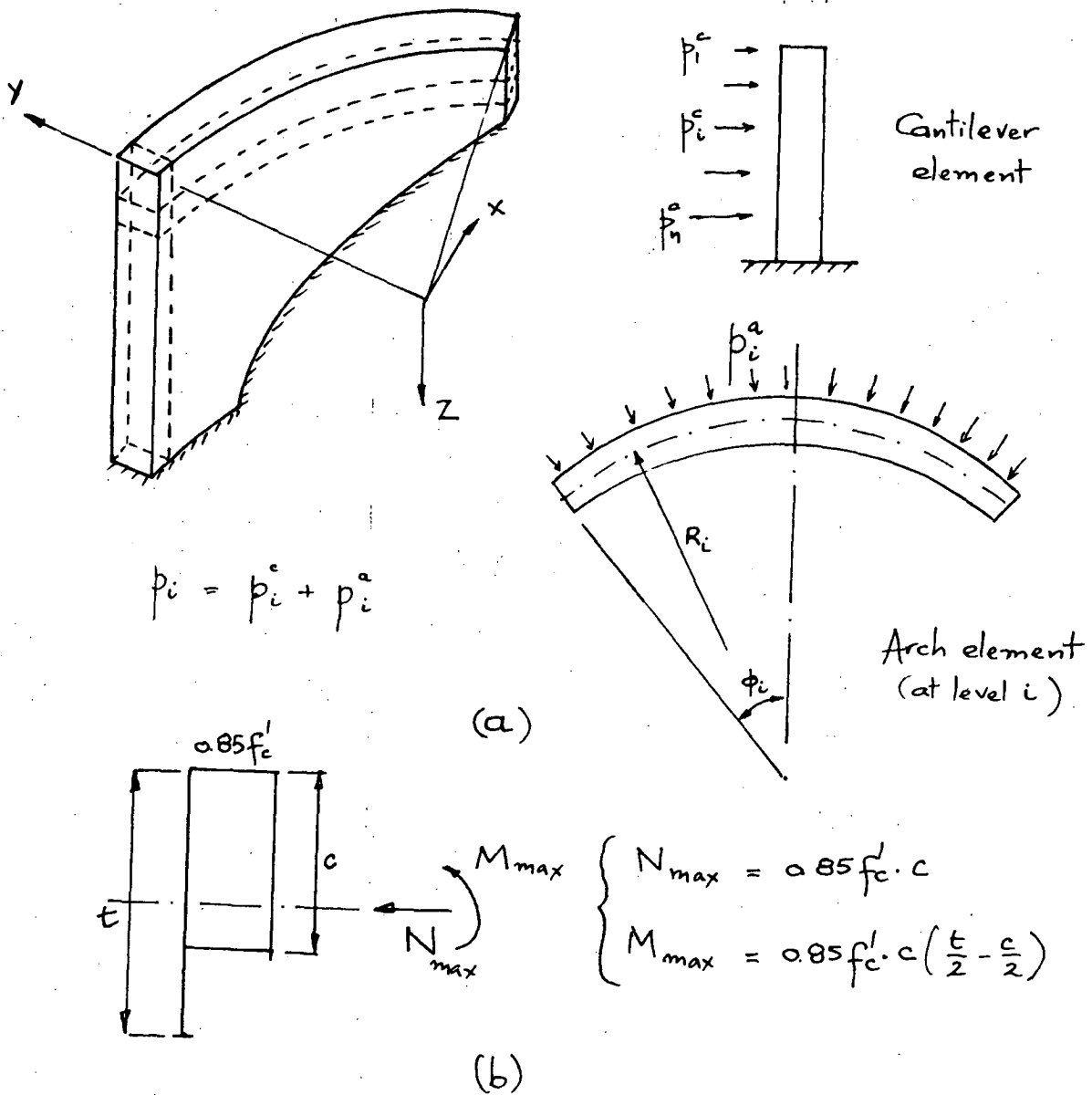
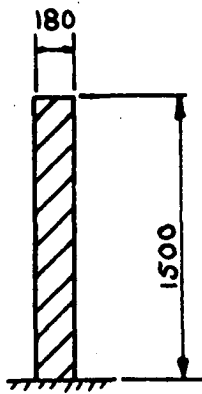


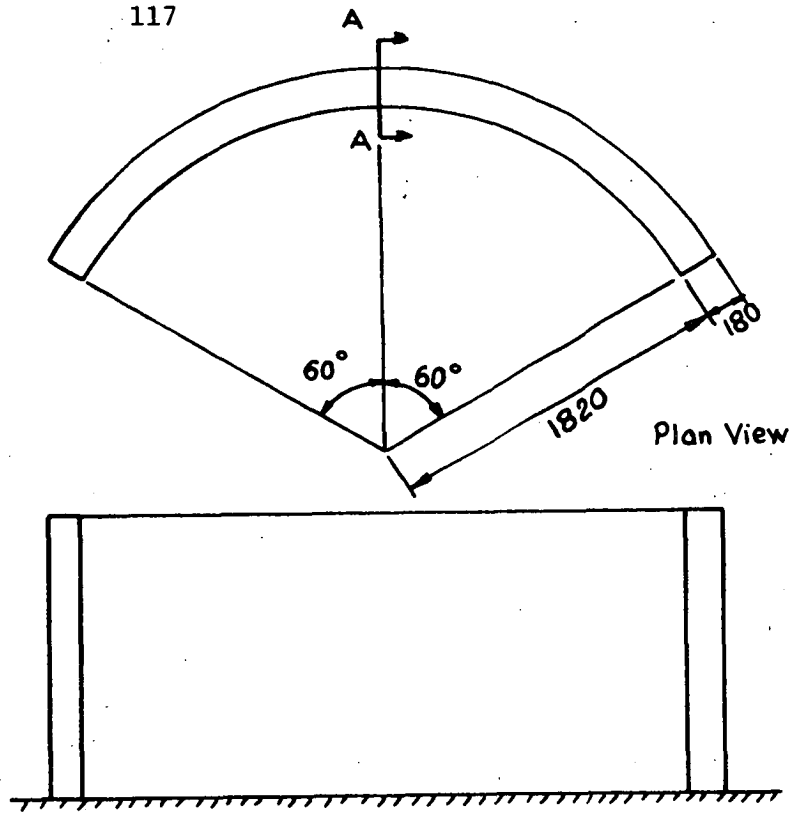
Figure 6.9

$$f'_c = 116 \text{ Kg/cm}^2$$

$$P_{\max} = 18 \text{ Kg/cm}^2$$



Section AA

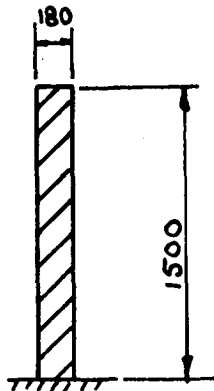


Front View

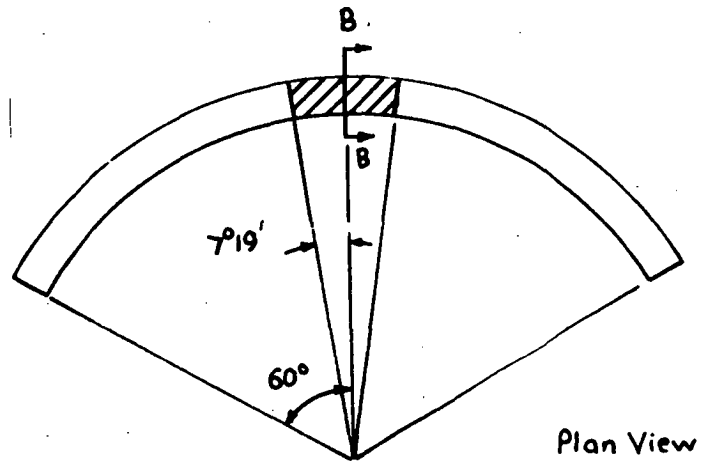
Model I

$$f'_0 = 143 \text{ Kg/cm}^2$$

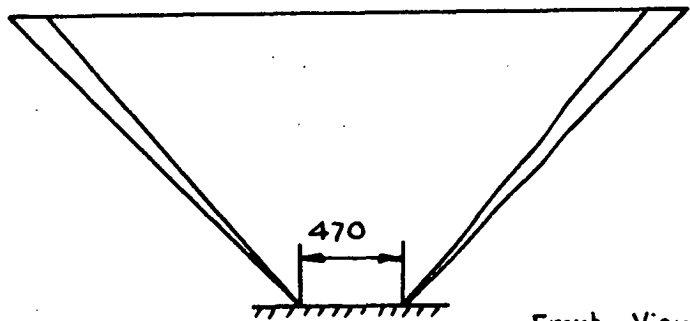
$$P_{\max} = 205 \text{ Kg/cm}^2$$



Section BB



Plan View



Front View

Model II

Figure 6-10

The applied hydrostatic pressure is directly distributed to the arch and cantilever elements. Bustamente used a linear programming technique to determine the maximum load that an arch dam can sustain. The effects of vertical curvature can be included into Bustamente's method of calculation without any difficulty.

The results for his own tested models (Fig 6.10) are:

	Computed values	Measured values
Model I	$p_{\max} = 16.9 \text{ kg/cm}^2$	18.0 kg/cm^2
Model II	$p_{\max} = 21.04 \text{ kg/cm}^2$	20.5 kg/cm^2

(b) Swaminathan's Method (Ref 6.6). The dam is divided into arches and cantilevers as in Bustamente's method. However, the compatibility of deformation of the arches and the crown cantilever is retained. The arches are assumed to be elastic. The hydrostatic pressure is distributed between the arches and cantilevers according to the deformation of the crown section. Swaminathan investigated the effects of gradual increases in hydrostatic pressure and distinguished several stages of failure. The failure criteria used are those adopted by Bustamente, Equation 6.1. Various graphs are given from which the ultimate load capacity can be calculated.

For Bustamente's model I, Swaminathan's method gives the following results:

$$\text{Valley shape factor } \frac{330}{150} = 2.20. \quad \text{Slenderness ratio } \frac{191}{18} = 10.6.$$

$$\text{Pressure required to collapse the dam } p_{\max} = \frac{2.0(0.85f_c')}{10.6} = 18.6 \text{ kg/cm}^2.$$

Bustamente's method and Swaminathan's method are both based on the same statical picture of dividing the dam into arches and cantilevers. Two new methods of estimating the strength of arch dams are now proposed based on different statically admissible states.

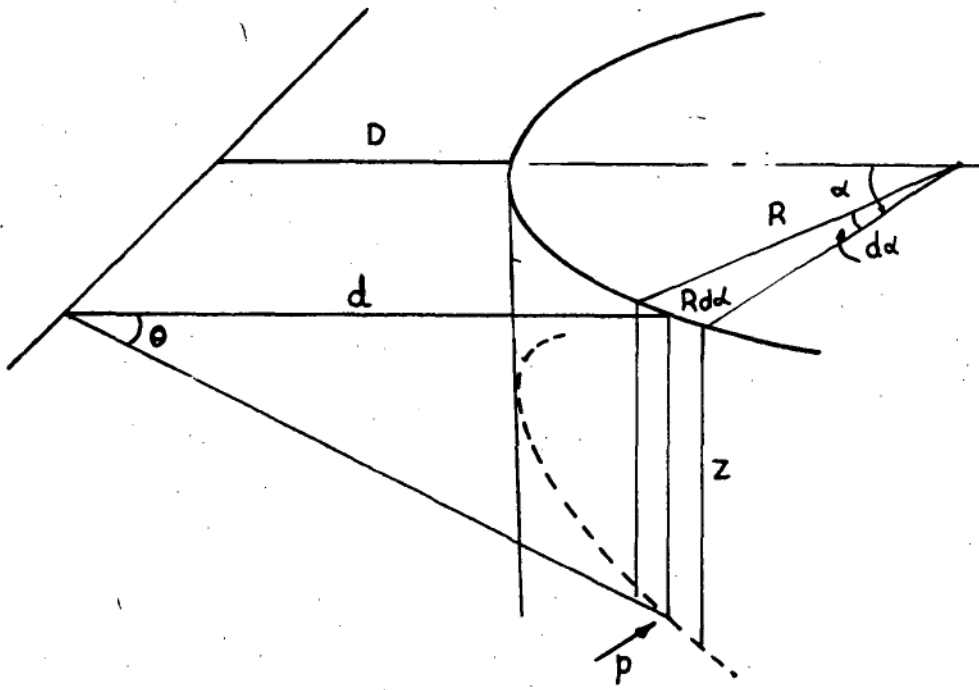
6.4.2 Inclined arch method

The dam is considered as a series of independent arches; each arch slice is considered to support the hydrostatic load independent of the adjacent slices. The arches are obtained by cutting the dam with inclined planes pivoted about a horizontal line located at a distance from the crown at full water level (Fig 6.11). The idea originated from the observation that isostatic lines on arch dam models tend to incline downwards. This idea was first introduced by Coyne (Ref 6.3) in his design of arch dams based on elastic behaviour. The proposal to use the same idea to estimate the ultimate strength is believed to be new. The inclined arches are stronger than their horizontal counterparts because of the extra curvature in their own plane and of the varying cross section areas. The following steps are performed in the analysis.

- (i) The profiles of the arch slices are established, usually by tracing from drawings.
- (ii) The loads on each arch slice are calculated.
- (iii) Thrust lines are drawn for each inclined arch.
- (iv) From the thrust lines the magnitude of the thrust and bending moments are estimated, hence the load factor to cause collapse is calculated.

The analysis must be carried out for various hinge line positions; for each hinge line position, various slices must be investigated in order to obtain the highest possible lower bound.

For Bustamente's models, the inclined arches are elliptical in profile with varying cross section area. A summary of the calculation is given in Figure 6.12. The resultant thrust lines show that there is little bending moment. If the bending moments are neglected, a direct estimate of the horizontal thrust at the crown can be made from equilibrium considerations. For the two models considered, the results are:-



$$p = w.z$$

$$d = D + R(1 - \cos \alpha)$$

$$z = d \tan \theta$$

$$x = R \cos \alpha$$

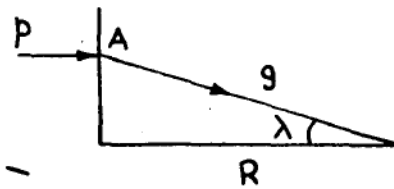
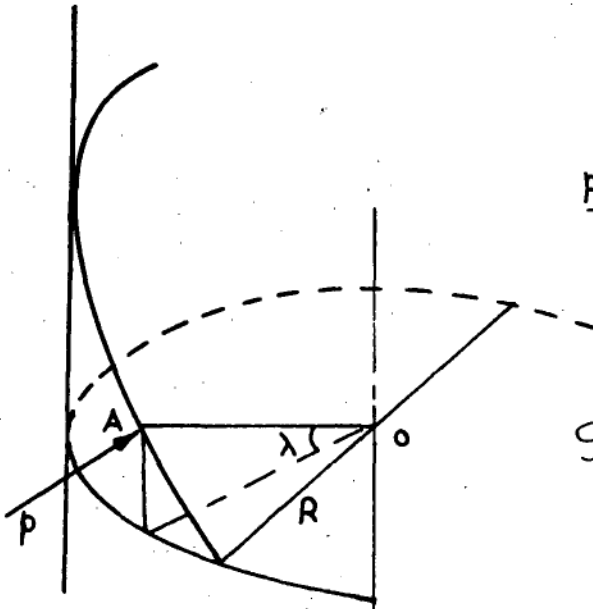
$$y = R \sin \alpha$$

$$z = R \cos \alpha \tan \theta$$

$$r = R \sqrt{1 + \tan^2 \theta \cos^2 \alpha}$$

$$\cos \lambda = \frac{\cos \theta}{\sqrt{\cos^2 \theta + \sin^2 \theta \cos^2 \alpha}}$$

$$g = p / \cos \lambda$$



Geometry of inclined arch slice
(from Ref. 6.2)

Figure 6.11

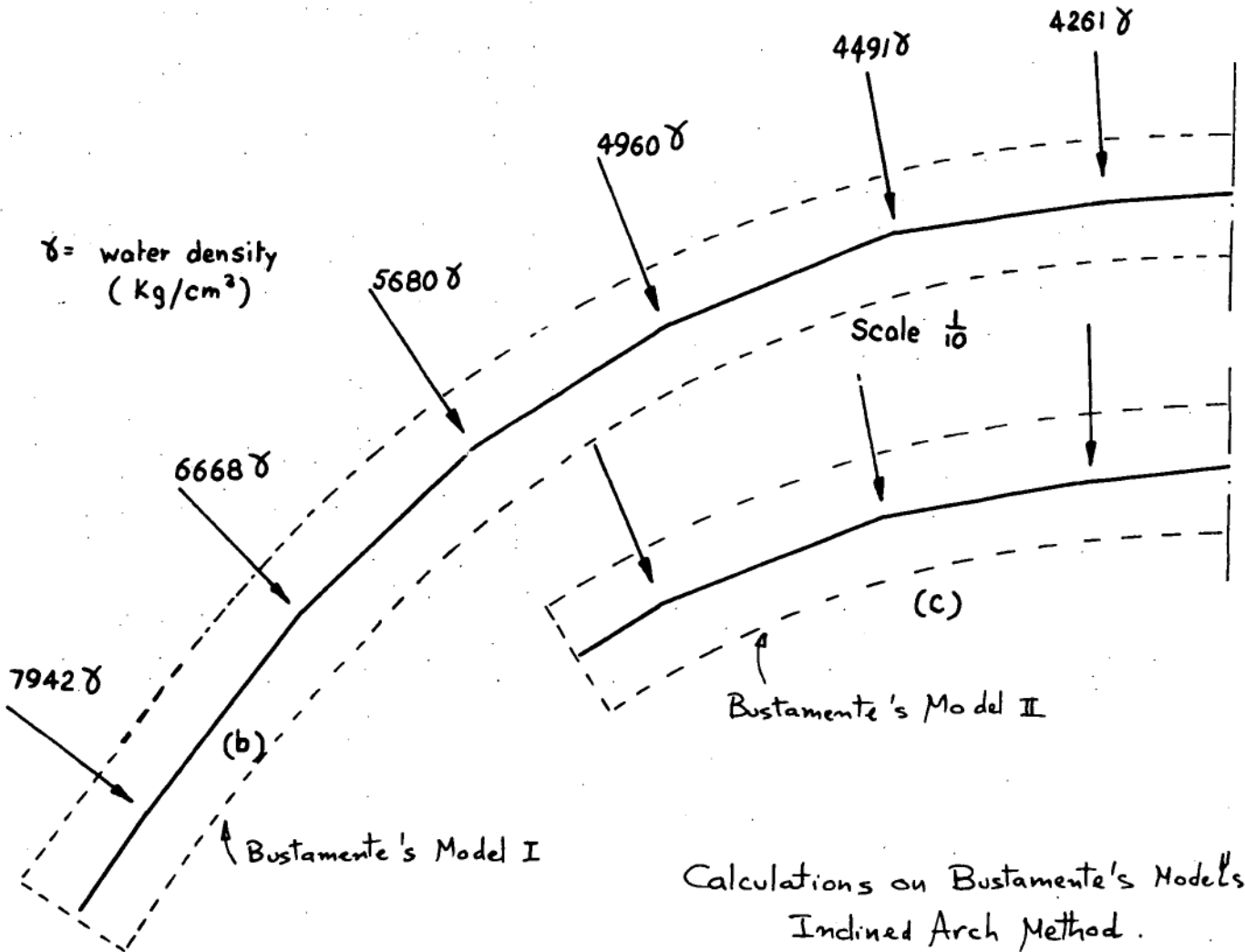
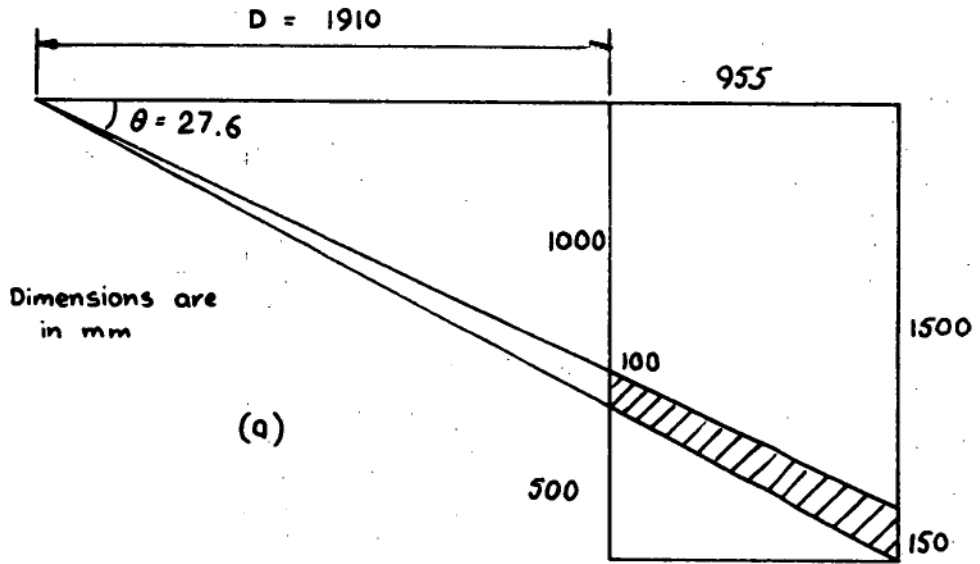


Figure 6.12

Model I $p_{\max} = 13.8 \text{ kg/cm}^2$ (cf. 18 kg/cm^2 experimentally obtained)

Model II $p_{\max} = 19.9 \text{ kg/cm}^2$ (cf. 20.5 kg/cm^2 experimentally obtained).

For comparison, an estimate of the dam capacity is made using horizontal slices. For Bustamente's cylindrical dam models, the maximum hydrostatic pressure is, of course, at the base of the dam. The value of this pressure is given by $p_{\max} = N_{\max} / R$ (circular arch under radial pressure).

The results are

Model I $p_{\max} = 9.29 \text{ kg/cm}^2$ (cf. 18 kg/cm^2 experimentally obtained)

Model II $p_{\max} = 11.45 \text{ kg/cm}^2$ (cf. 20.5 kg/cm^2 experimentally obtained).

It is clear from the above figures that the inclined arch method gives a better estimate of the load capacity than the horizontal arch method.

6.4.3 "Tumbler*" method

An alternative method of obtaining a statically admissible state for the arch dam is to treat the dam as part of a shell of revolution under hydrostatic load. The general forces acting on an element of a shell of revolution will be as shown in Figure 6.13.

Following Flugge (Ref 6.7), the equations of equilibrium for an element of a shell of revolution under hydrostatic load can be reduced to

$$Q_x - \frac{\partial M_x}{\partial x} = 0 ;$$

$$-\left(\frac{N_x}{R_x} + \frac{N_y}{R_y} \right) - \frac{\partial Q_x}{\partial x} + p_z = 0 \quad \dots\dots\dots (6.2)$$

Physically, it means that the hydrostatic load is resisted mainly by direct thrust in the horizontal direction, and by direct thrust and

* The name "Tumbler" was first used to describe the approximation of arch dams as part of a shell of revolution by Pippard et al in the elastic analysis of Dokan Arch Dam (Ref 6.8).

bending moment in the vertical direction. For single curvature dams, these actions are reduced to arch action in the horizontal direction and bending action in the vertical direction.

The above equations of equilibrium are used as the basis for the estimate of the load capacity. These are two alternative methods of solution.

(i) Algebraic method. This method is similar to the method used in the analysis of load-carrying capacity of slabs (Chapter IV). The moment and force fields are described by functions which satisfy the equilibrium equations 6.2. The failure condition, Equation 6.1, is then used to calculate the ultimate pressure.

For the Bustamente's cylindrical dam models, the following expressions for the force and moment fields are proposed.

$$M_x = -K \frac{t^2}{8} \left(\frac{x}{H} \right)^3 + C \left(\frac{x}{H} \right)^3 \left(1 - \frac{x}{H} \right) \left(\frac{H^2}{12} \right);$$

$$N_y = -RC \cdot \left(\frac{x}{H} \right) \left(2 - \frac{x}{H} \right);$$

where K and C are constants to be determined so that the failure conditions are satisfied everywhere. Using equation 6.1 as the failure condition, the maximum pressure (at the base of the dam) is found to be

$$p_{\max} = \frac{6Kt^2/8}{H^2} + \frac{3C}{2};$$

For Bustamente's model I, we find

$$p_{\max} = 15.1 \text{ kg/cm}^2. \text{ (cf. } 18 \text{ kg/cm}^2 \text{ experimentally obtained).}$$

(ii) Graphical method. The equilibrium equations can be handled graphically in the following manner.

Draw a loading diagram $p(x)$.

Guess a distribution of N_y such that the failure criterion is

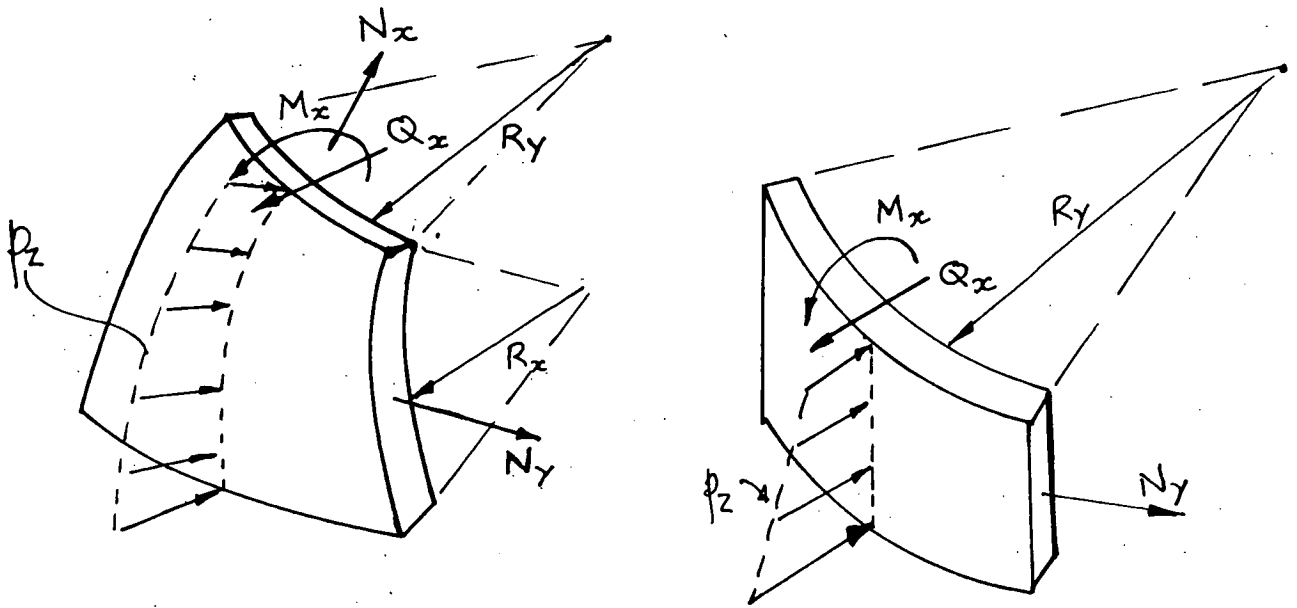
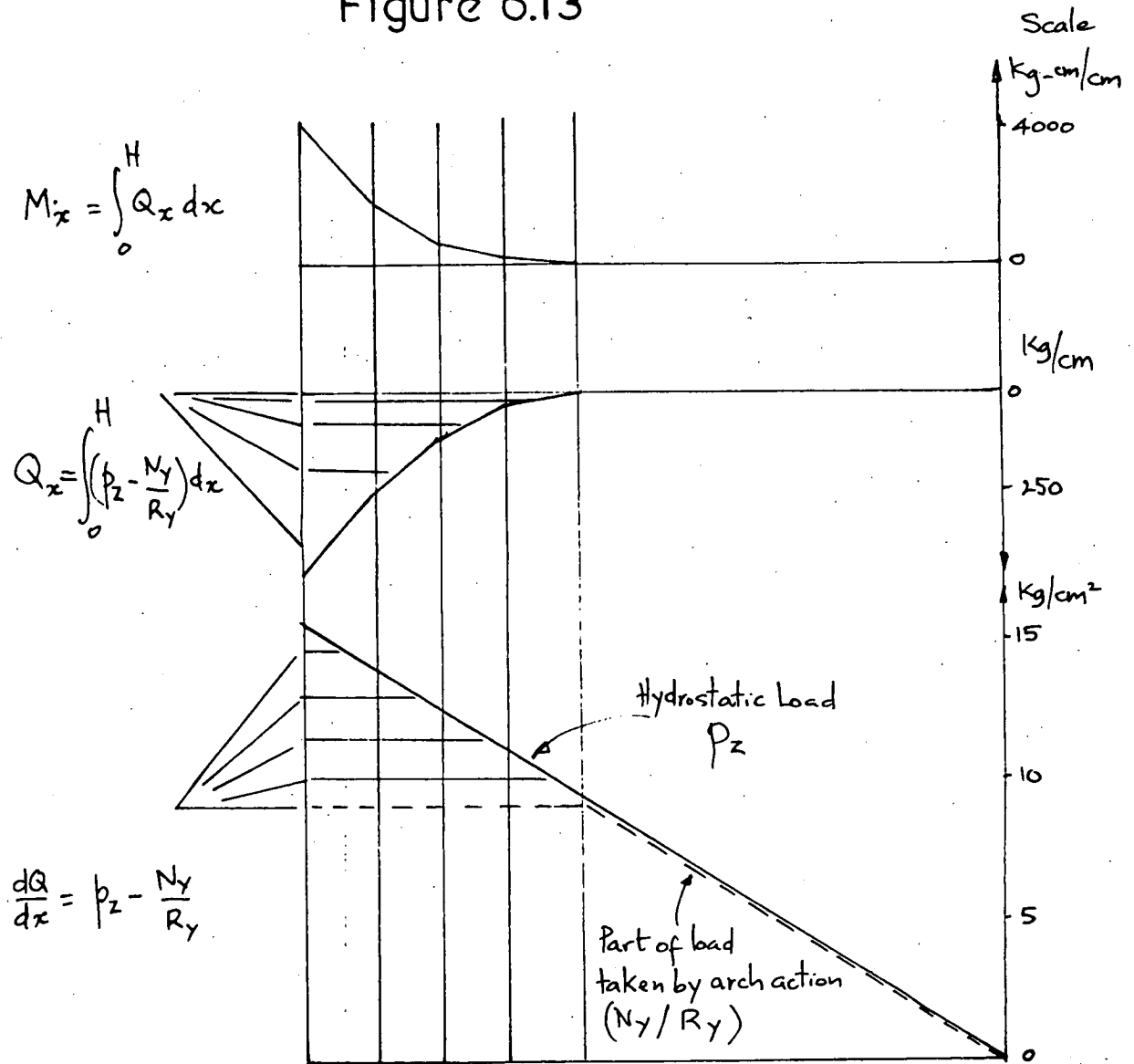


Figure 6.13



Graphical Solution using "Tumbler" theory

Figure 6.14

observed.

Determine $\frac{dQ_x}{dx}$ from the equilibrium equations.

Graphically integrate $\frac{dQ_x}{dx}$ to obtain Q_x .

Graphically integrate Q_x to obtain M_x .

Check combined failure condition in the vertical direction.

Appropriate boundary condition must be inserted and the calculation is repeated until both failure and equilibrium conditions are observed. Calculation for Bustamente's Model I is given in Figure 6.14.

The graphical method is far more flexible than the algebraic method in dealing with varying boundary conditions, non-uniform thickness, etc.

6.5 CONCLUDING REMARKS

Some aspects of the design of arch dams for strength have been discussed. An experimental method of directly obtaining the dam shape for a given loading and site condition is proposed using strings and weights. The method is based on the concept of a thrust surface. The load-carrying capacity of arch dams is then investigated by construction of various statically admissible states.

Further work can be found in Appendix A3 where the test of a shell is reported and an approximate 'elastic-plastic' method of analysis is proposed and applied to various dam models.

CHAPTER VII

DEFLEXION, BUCKLING, AND STRENGTH

7.1 INTRODUCTION

The limit design method of picturing statically admissible states described in previous chapters enables a design to be made to sustain a given load. The calculations are reliable only if deflexions do not have any marked effects on the equilibrium conditions and local (and overall) stability is assured. The effects of deflexions and buckling on the strength of structures are discussed in this chapter. ~~In particular,~~

The influence of deflexion on the load capacity of structures has been commented upon in previous chapters where particular structures are analysed. Various new methods of estimating deflexion are proposed in the Appendices B1, B2, and B3. The statements on deflexion in this chapter recapitulate the works presented elsewhere in the thesis. Buckling of structures is a large subject and is not within the scope of the thesis. This chapter discusses, with the help of a simple example, the relevance of the Euler type stability analysis in the assessment of the strength of structures.

7.2.1 Deflexions which do not affect the strength of structures.

These deflexions, under working load, must be estimated so that the structure is acceptable for service. For frames which support their loads mainly by bending moment, deflexions are basically given by a double integration of the bending moment diagrams. For a statically admissible state design, the bending moment diagrams can be easily estimated and the deflexions can be calculated with the use of the virtual work equation or complementary energy methods (Ref 7.1 and 7.2). In this connection, it should be noted that to predict accurately the deflexions for a frame with a particular loading condition (past the first yield) is practically

impossible; the calculations are so sensitive that minor differences in stress-strain relations could cause major differences in the results. What is wanted in the design is the estimate of the load that a structure can carry at a particular deflexion. This deflexion can be easily estimated by approximate methods. The argument can be best seen from a typical load-deflexion graph for a frame. (Fig 7.1).

In Appendix B1, an iterative method of estimating deflexion in elastic-plastic framed structures is proposed using dynamic relaxation technique. The method differs from other methods in assuming that the yielded regions are spread out instead of being localized. The results, however, are in close agreement with other methods and experimental measurements.

The deflexion question can sometimes be avoided altogether; e.g. for slabs, the deflexion requirement can be satisfied by the selection of proper thickness such as recommended by the Codes (Ref 7.3).

7.2.2 Deflexions which affect the strength of structures.

These problems occur when the equilibrium equations are sensitive to the effects of deformation, particularly with compression members. In many cases, these deflexions can be included in the limiting equilibrium equation, and an estimate of the reduction in load-carrying capacity can be easily made. An analysis of this kind together with some form of elastic analysis often gives a very good indication of the likely form of the load-deflexion curve as seen in Figure 7.2. Calculations of this kind have been done for the Gladesville Arch in Chapter V and for various models in Appendix A1. The possibility of performing these calculations should be investigated for all designs.

7.3 BUCKLING

The term "buckling" is used here with its traditional meaning: the widely diverse behaviour of practical structures, in the field and in

5% difference in P causes 20% in δ at A
 5% difference in δ causes $\leq 1\%$ in P at A

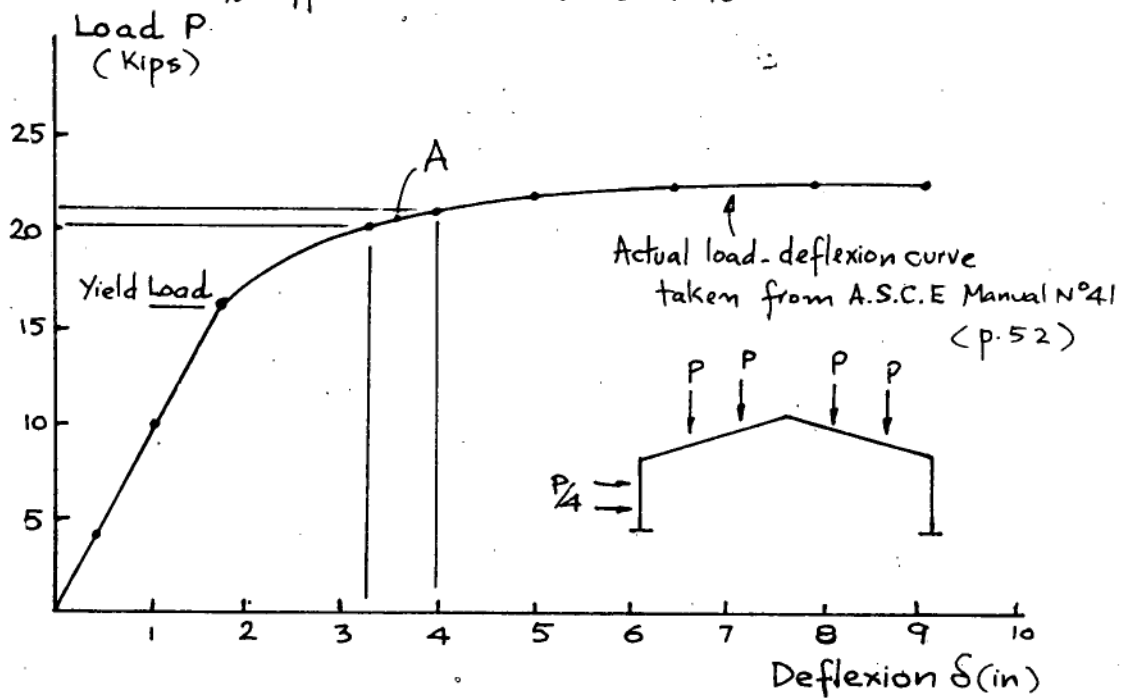


Figure 7.1

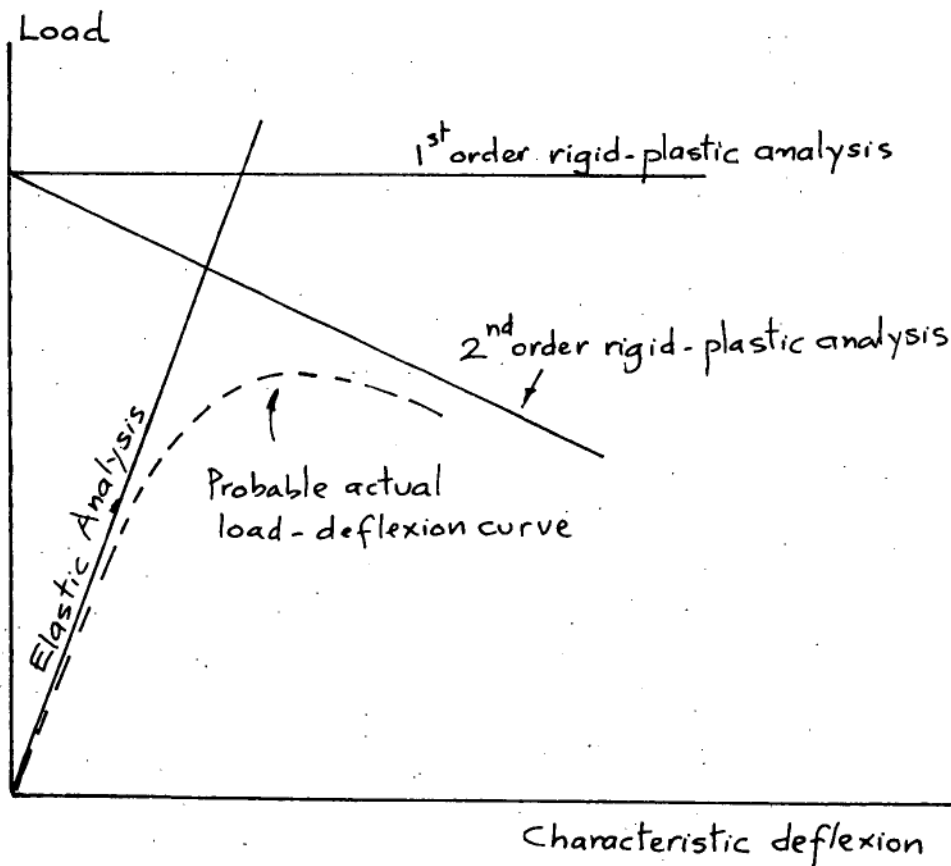


Figure 7.2

laboratory tests, where the effects of change of geometry influence the load carrying capacity of the structures or members. A full treatment of this subject is well outside the scope of this thesis; this section intends only to examine the relevance of stability analysis of the Euler type, to the assessment of strength of structures.

7.3.1 EULER AND NON-EULER BUCKLING

The ultimate capacity of many metal structures and elements is limited by some kind of instability. Most of the present stability theories have their roots in the Euler analysis of a pin-ended column. The theories are, therefore, applicable only if the underlying assumptions in the Euler-type theories are satisfied. There are structures, such as arches, over-braced frames, and shells, which do not conform to the Euler type theory. In these structures, the internal forces that cause buckling are not statically determinate and redistribute markedly as buckling deformations occur.

The basic differences in the behaviour of the two types of buckling may now be considered.

(a) Euler-type buckling

The term Euler-type buckling is used here to denote the elastic behaviour of structures characterized by the load-deformation relation of Figure 7.3. This applies to both in-plane and lateral buckling. A large amount of work and writing has been devoted to instability and buckling behaviour using this approach; such studies have the following characteristics in common.

Physically, the major internal forces in the structures, such as the axial forces in braced frames, or the bending moments in beams liable to lateral buckling, are often statically determinate, or almost so. This may imply at times that the deformations of the structure are fairly small, but, more importantly, that there are no marked redistributions, as the

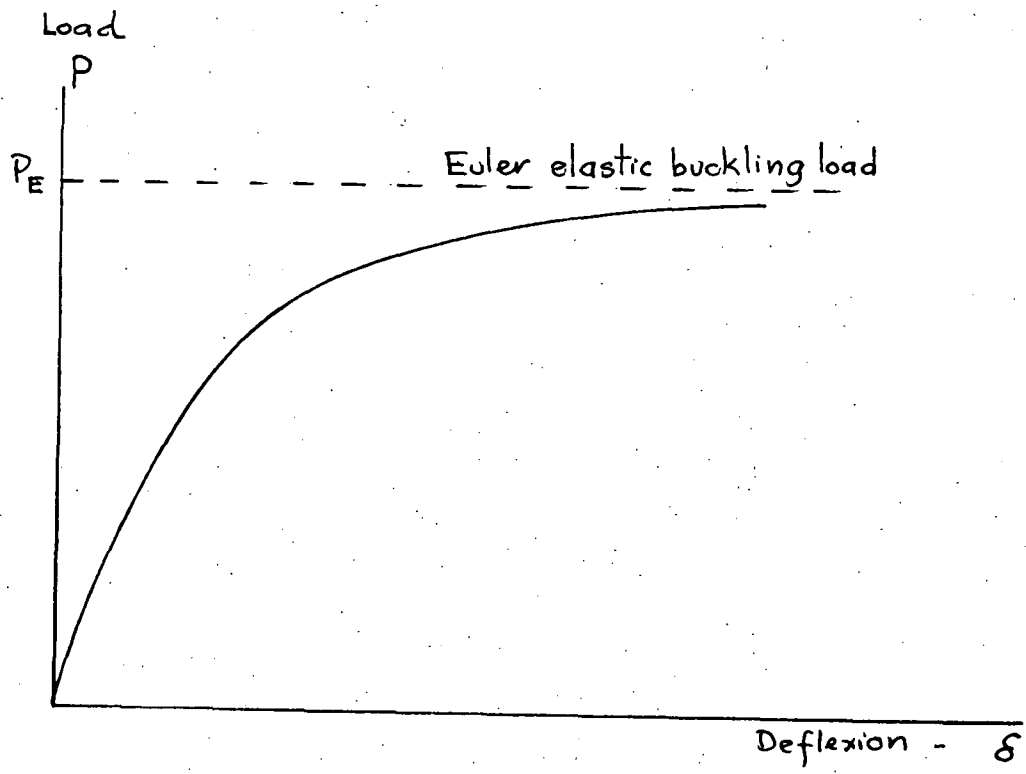


Figure 7.3

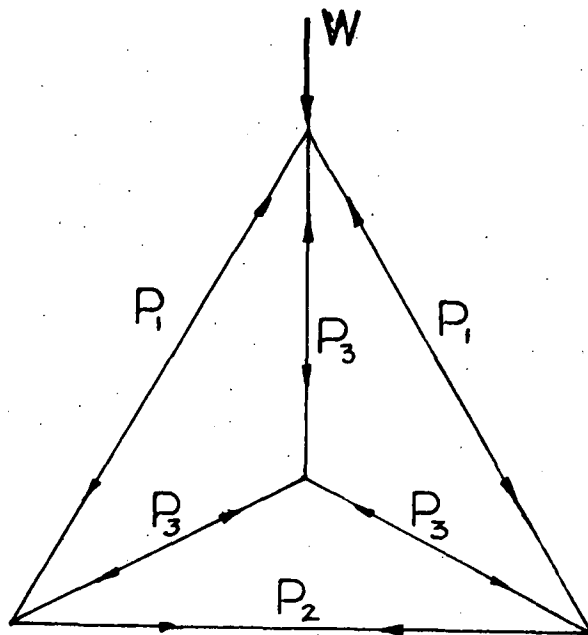


Figure 7.4

buckling deformations occur, of the major internal forces causing buckling. Most of the structures so treated are not exactly statically determinate: however, for these structures, the internal forces or bending moments are normally easily obtained and there is little redistribution of them. For example, as a braced frame buckles, in or out of its plane, the curvature of the members indicates the existence of bending moments and therefore end shears; these affect the equilibrium of the joints but not enough to alter greatly the axial forces in the members until very large deformations occur. For unbraced frames, for example, a portal frame buckling in a sway mode, the redistribution may be somewhat greater, but its effect is still not very important.

Mathematically, it is often found that the associated differential equations are linear and reducible to a single governing differential equation. This reduction is possible because the force and displacement variables are often separable. The problem can be identified as an eigenvalue problem and the buckling modes are orthogonal.

Experimentally, Euler-type buckling is associated with the Southwell plot technique for analysing measured deformations which participate in the buckling mode. A linear Southwell plot is often obtained (depending mainly on whether the structure is deforming in a well-defined mode), which gives an estimate of the corresponding critical load. Kjar (Ref 7.4) established the rules under which the Southwell technique can be used to obtain the critical load. These rules have the same mathematical properties as those mentioned above.

(b) Non-Euler Buckling - An example.

The load-deformation behaviour of the simple over-braced frame of Figure 7.4 is described here to illustrate the non-Euler buckling behaviour.

The frame is one degree over-braced. For any external load W , the

distribution of the internal forces P_1 , P_2 , P_3 is not known; however, if one force is assumed, say P_3 , then others can be estimated from equilibrium condition. The distribution of the forces, which is determined by the conditions of geometrical compatibility, can be derived iteratively using dynamic relaxation. The complete numerical analysis is given in Appendix B2. Figure 7.5 shows a typical load-deformation graph and Figure 7.6 an internal force distribution graph.

The following observations were made:

(i) The internal forces P_1 , P_2 , P_3 varied non-linearly with the load as buckling developed. There is marked redistribution of the forces as shown in Figure 7.6.

(ii) The load-deformation graph, Figure 7.5, did not have the characteristics described for Euler-type buckling. The deflexion appeared to run away at some lower load but then the curve started to rise before running away again at some higher value. It is suggested that the cause of this behaviour is the redistribution of the axial forces in the frame.

The same kind of behaviour has been observed previously in the laboratory for the above frame (Ref 7.5) and for the thin arches liable to lateral buckling (Ref 7.6).

7.3.2 RELEVANCE OF EULER-TYPE ANALYSES IN THE PREDICTION OF STRENGTH OF STRUCTURES

It can be stated that, in general, Euler-type analyses are applicable to the elastic portion of the loading path of a structure only if the internal forces that cause buckling do not redistribute markedly as buckling deformations occur.

Thus, Euler analyses are relevant in the assessment of the ultimate strength of statically determinate structures of suitable stiffness, such as columns, beams, braced frames, and trusses, and for some classes of

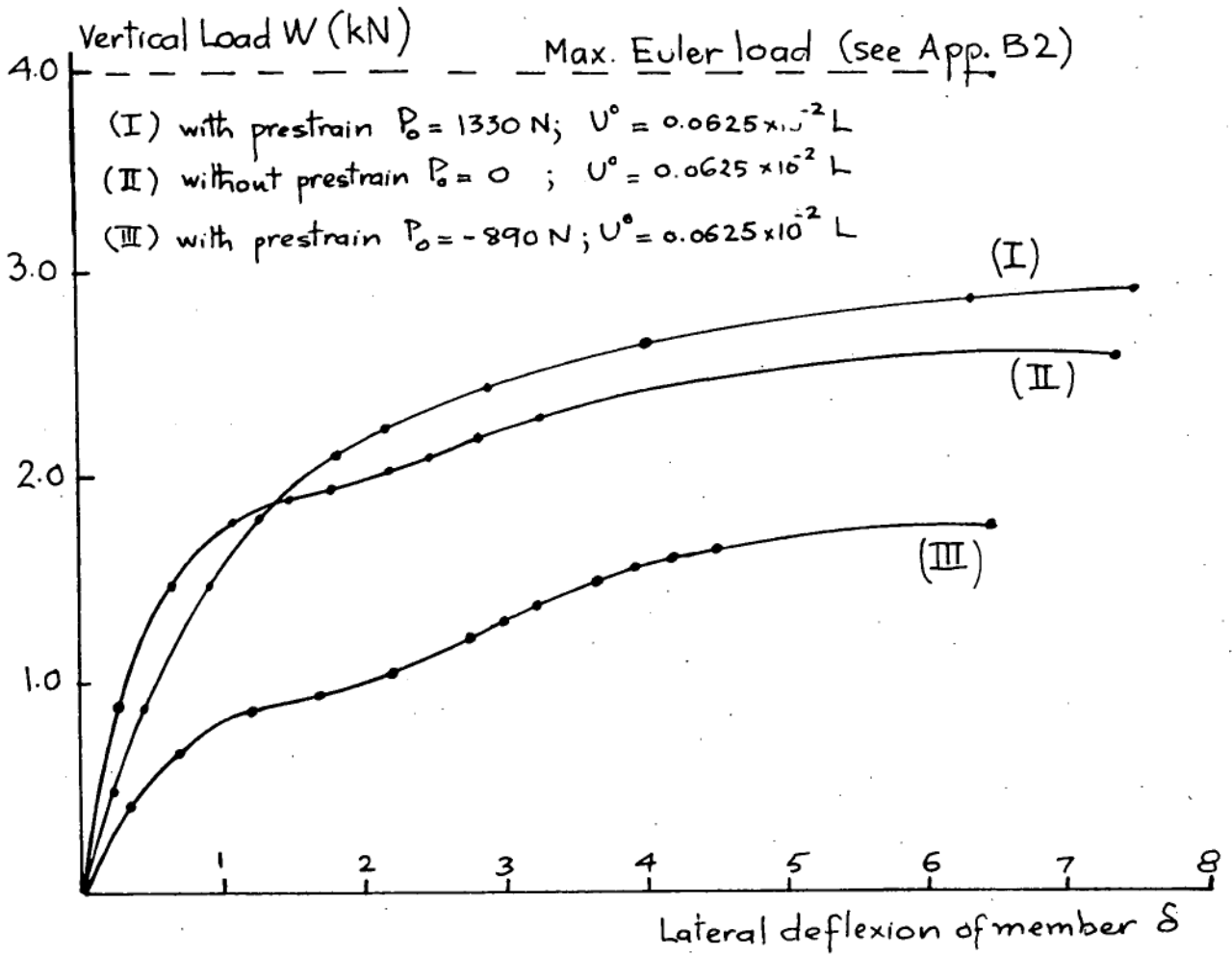


Figure 7.5

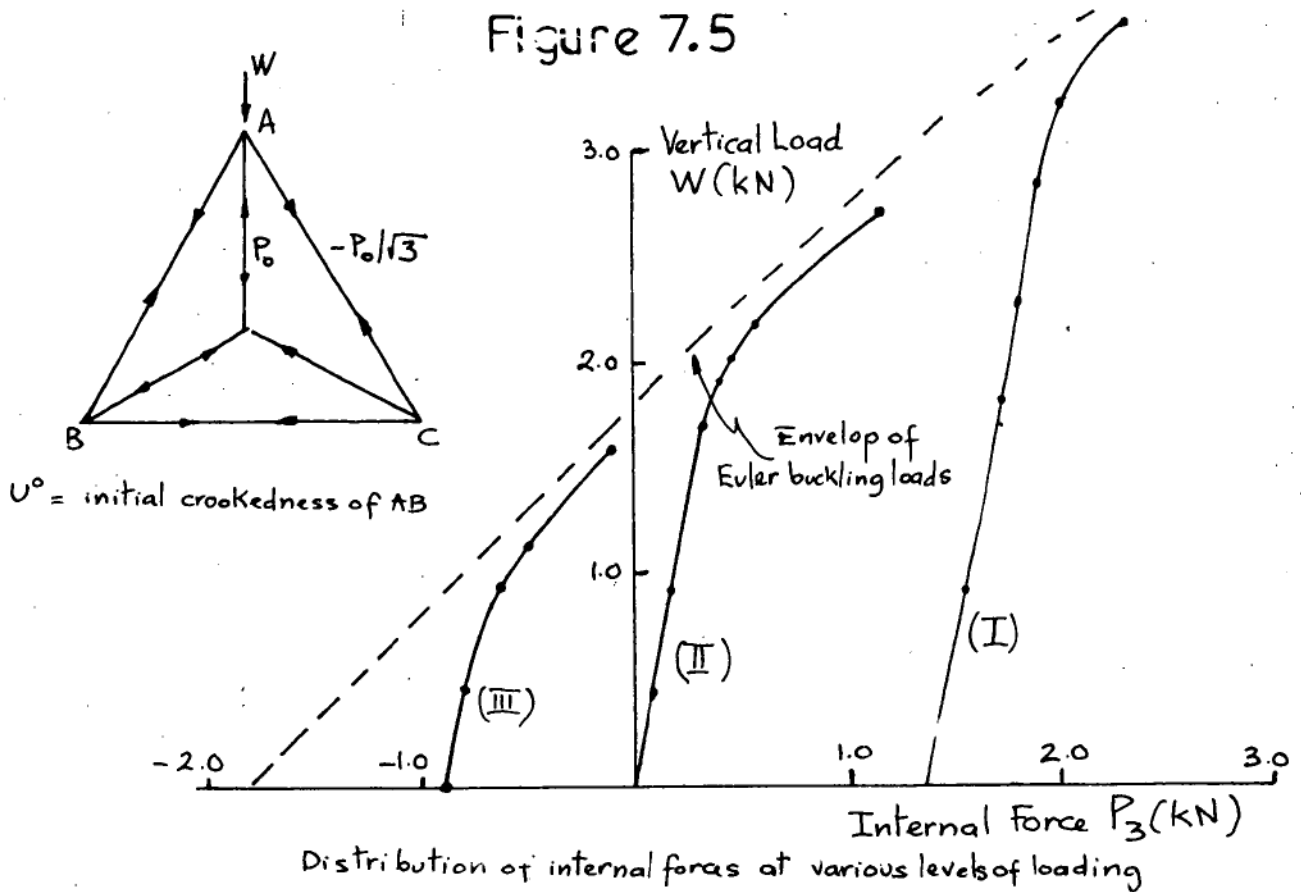


Figure 7.6

statically indeterminate structures where the major internal forces causing instability change only marginally as buckling develops. Arches, over-braced frames, and statically indeterminate structures in general, do not behave in the Euler fashion. (It is a matter for laboratory and field testing to determine if an Euler-type study is approximately suitable, as it may be for lateral buckling of continuous beams.) The redistribution of internal forces seems to have a beneficial effect in many cases.

For plates, and structures containing large plate element, such as thin webs of girders, deck plates of bridges, and the hulls of ships, the relevance of an Euler-type analysis depends on the type of boundary support. Plates with edges free to move have little reserve of strength after the Euler load is reached, while plates whose edges are restrained against pulling in have large post-buckling strength, and failure can occur only after yielding of the most highly stressed region as buckling progress. The Euler critical load has little physical significance in this case.

Shells form a class of their own, where the redistribution of internal forces as buckling deformations occur has a weakening effect on the structure. The behaviour of an axially loaded thin circular cylinder is well-known, but difficult to describe with any clarity as there are now so many mathematical treatments designed to fit the results of tests. In any case, this particular theory gives only limited guidance to designers of other types of thin shells.

7.4 CONCLUSION

The relations between deflexion, buckling, and strength have been briefly discussed. In particular, the relevance of the stability analysis of the Euler type to the assessment of strength of structures has been examined. The foregoing notes present a view point which differs somewhat from that accepted. The structural engineer must never take the stability

of a structure for granted. The possibility of buckling during erection or in service must be envisaged and prevented. Furthermore, if buckling is a problem, the designer should not assume that ideas and methods based on Euler type analyses are wholly satisfactory in coming to grips with what really happens.

CHAPTER VIII

PRACTICAL DESIGN CONSIDERATIONS

8.1. INTRODUCTION

In the application of limit design methods, just as in any other design method, there are a number of important practical design factors

* The thesis has discussed the design of structures for strength. The discussion is not complete if the factors which may limit strength are not presented.

detailed design of joints. **

** The topics, which appear to be disjointed, are in fact intimately connected from the practical design point of view. Joints are most likely to be highly stressed regions and the material problems such as brittle or fatigue failure in steel or creep and shrinkage cracks in concrete often occur at the joints.

these topics, to indicate the problems for which neglect may lead to misleading results, and to outline some design approaches by which these problems can be taken into consideration.

*** The materials presented in this chapter are available in most text books; some statements are rather trivial or self-evident from a theoretical point of view. However, these factors should always be in the designer's mind since they do set limits on any design. The materials are therefore well worth repeating even if the coverage may be inadequate.

steel in a different manner: extremely rapidly and with little deformation. This type of failure occurs more frequently at low temperature under static or impact loading and is often induced by a crack or a notch. Notch sensitivity of a metal is its resistance to the starting

and the propagating of a crack at the base of a standardised notch. The Charpy V-notch test is most often used to determine this notch toughness (Ref 8.1).

Fatigue of steel is a progressive failure caused by large variation in stress (especially with a reversal of stress) over a period of time. The average stress across the section may be well below yield point, but the non-uniformity of the stress distribution may cause yielding in a small region which eventually produces minute cracks; the cracks further increase the non-uniformity of the stress distribution which in turn cause the cracks to propagate. Fatigue failure occurs with the application of large numbers of loading cycles with large variations in stress or with local stress concentration (Ref 8.2).

Although both types of failure exhibit little ductility, brittle fracture resistance decreases with temperature while fatigue resistance does not. Cracks propagate slowly and intermittently in fatigue failure while brittle fracture cracks propagate at high speed.

8.2.1 Design against brittle fracture

As mentioned above, the Charpy V-notch test has been used most often in assessing notch toughness of metal. Other tests such as the Tipper notch tensile test and the Pellini test are sometimes used to determine the suitability of a metal or a welding process for a particular situation. Brittle fracture failure is most likely when there is a combination of low service temperature together with (i) thick plates or thick sections, (ii) severe stress concentration resulting from poor connections and details and (iii) defects in welding such as cracks or lack of fusion, (Ref 8.3). Naturally, the above combinations should be avoided if possible. The safeguard against brittle fractures thus lies in three factors.

(i) The proper selection of materials. Materials should be selected with regard to service temperature and plate thickness (Ref 8.4). The steel should be impact-tested, such as recommended in Reference 8.5.

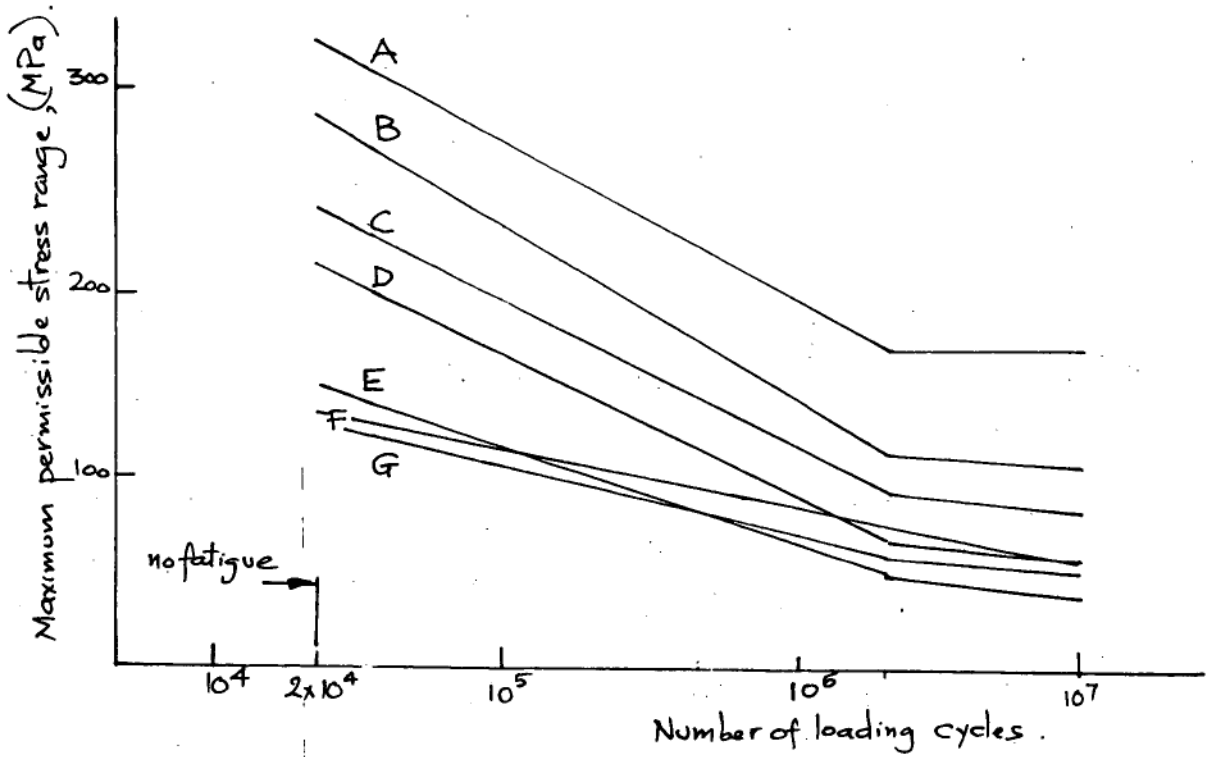
(ii) Correct welding procedure. Another major essential for notch toughness is that the correct welding procedure must be followed. This problem will be further discussed in the detailed design of welded joints.

(iii) Good fabrication technique and careful supervision.

8.2.2 Design against fatigue

The results of fatigue tests are usually presented as graphs of nominal stress causing failure against the number of cycles (for laboratory specimens of simple shape). The designer should be aware of how these numbers are obtained, as there are many types of fatigue tests, loadings, and specimens. There is a growing tendency to do a full scale fatigue test under representative loading conditions when fatigue is a major design consideration.

The 'classical' type of fatigue response involves a dropping range followed by a runout range (known as the endurance limit). Figure 8.1 shows the maximum permissible stress range plotted from Reference 8.3. In all modern fatigue rules, the fatigue strength is considered to be independent of the yield stress of the material. The design against fatigue is therefore based on the reduction of permissible stress with loading conditions. The concept of load factors for fatigue has been attempted but without any clarity (Ref 8.7). From Figure 8.1 it is seen that no fatigue is predicted for less than 20,000 cycles (two applications per day for 25 years). It follows that fatigue will rarely be a problem in most civil engineering structures (with the exception of crane structures). Wind loads are excluded from fatigue consideration in the A.S. Codes of Practice (Ref 8.3) although low, frequently occurring winds



Stress Category	Exemplary Situation	Illustration
A	Base metal with rolled or cleaned surfaces	
B	Weld metal in complete-penetration butt-welded splices of rolled and welded sections having similar profiles.	
C	Weld metal in complete-penetration butt-welded splices, with or without transitions having slopes < 1:2.5, weld soundness is not established by examination.	
D	Weld metal in complete-penetration butt-welds in tee or cruciform joints.	
E	Base metal adjacent to longer fillet welded attachments	
F	Continuous or intermittent longitudinal or transverse fillet welds and continuous fillet welds subjected to shear parallel to the weld axis	
G	Shear on plug or slot welds	

Extracted from Ref. 8.6 . For complete listing see the original .

Figure 8.1

associated with aerodynamic resonance can conceivably cause fatigue problems.

Detailed design of joints are particularly important in fatigue consideration. From Figure 8.1 it is seen that the fatigue strength varies considerably with the type of detail used. Improved fatigue strength can be obtained by detail design, such as avoiding abrupt change of section by large fillet radius, stress relieving grooves, or, in cases of cut-outs, by providing suitable reinforcement. Tolerances, edge distances of holes, surface finish and effects of machining processes, should be watched so that stresses introduced by misalignment, shrinkage and other causes are reduced to a minimum. In making design modifications to avoid fatigue failures, it should be watched that the procedure does not simply transfer the problem to another location. This may result in more damage without any increase in overall fatigue life (Ref 8.6).

8.3 CREEP AND SHRINKAGE OF CONCRETE

When concrete is stressed to a low or moderate intensity by a constant and sustained load, an immediate deformation occurs (called instantaneous elastic strain) followed by a gradual deformation at a continuously diminishing rate (called creep strain or simply creep). The two effects are not separable by ordinary testing methods; the terms are used in a descriptive sense only. It is not known definitely whether creep strain will ever settle, but the rate of change diminishes in such a way that a limiting value seems to exist. Creeping strain varies with the age of the concrete at which the load is applied. McHenry (Ref 8.8) observed that if deformation due to several loads applied simultaneously or successively is considered, then the resulting deformation at any time is given by the sum of deformation of each

individual loading up to that time. This 'superposition' principle made possible the practical problem of determining time-varying stresses and strains in concrete structure.

Shrinkage is caused by the loss of moisture by evaporation while concrete is drying, and also by the chemical change in the hydration of cement (the former factor is predominating). In reinforced concrete even uniform shrinkage causes strains: compression in steel, tension in concrete. In mass concretes shrinkage appears to confine almost exclusively to the outer skin of concrete.

8.3.1 Effects of creep and shrinkage on structural behaviour

Creep and shrinkage cause time-dependent deflexion in reinforced concrete members. However, the most important effect of creep and shrinkage on the structural behaviour is that they can produce a differential deformation between various parts of a structure. This differential deformation causes extra stresses in the structural members apart from the normally computed dead, live, and wind load stresses. The redistribution of the internal forces in a structure caused by creep and shrinkage may or may not affect the strength of the structure. The following factors are relevant to the design consideration.

(i) Creep and shrinkage are affected by the environment. Temperature and humidity effects are important because they affect the volume change of concrete. The exposed and submerged face of a dam or the interior and exterior columns in a building have different creep rates. Differential deformation between these parts is possible.

(ii) Creep and shrinkage are also affected by the volume-surface ratio. Thus, differential deformations may occur between the shear wall core and adjacent columns, causing differential settlement in the slabs and supporting beams (Ref 8.9).

(iii) Creep is also affected by the magnitude of stress and the amount of steel reinforcement. Both of these factors may cause differential shortening in columns.

(iv) Lastly, creep is affected by the time factor. Creep is greater the younger the concrete at the time of loading. This point is important since the effects of creep on a structure depends just as much on construction technique as on the design.

The effects of shrinkage is most critical in the design of reinforced concrete water retaining structures. In these structures, shrinkage may cause unacceptable cracks. In prestressed concrete structures the effect of creep and shrinkage are especially significant as they cause loss of prestress. The problem is further complicated by the relaxation of the prestressing steel.

While in most cases creep and shrinkage do not substantially affect the strength of structural members, in long and slender compressive members creep can produce deformations leading to instability so that the load-carrying capacity of the member is reduced. Creep buckling of long columns is a recognised problem, although it is still imperfectly understood. Effects of creep on arches and arch dams can also be quite critical. These structures are designed so that the load is carried mainly by axial compression, the thrust line for the arch (or the thrust surface for arch dams) nearly coincides with the centerline of the structure. Creep strains deform the structure and increase the eccentricity of the thrust line (or surface). This, in turn, increases the stresses in the structure. The stress increase is followed by some creep increase. If the load is sufficiently high, it is conceivable that the structure may deteriorate to the point of collapse. In the design of the Gladesville Bridge, Sydney, creep is considered in detail and measurements are still being made to assess its effects (Ref 8,10).

The effects of creep, however, are not always adverse. The effects of creep on a beam and column arrangement, for example, are self correcting. The differential shortening in the columns induces moments and shears in the beams. The beams in turn respond by reducing the load on the column which settles most. The columns which settle less will receive additional loads from the columns which settle more. This redistribution creates a new modified stress level for creep. There are also the beneficial effects of creep in the relief of stress concentration with time.

8.3.2 Design to avoid creep and shrinkage effects

The most common method to avoid the problem is by inserting contraction and expansion joints. Proper detail designs can eliminate differential creep and shrinkage such as recommended by Fintel and Khan (Ref 8.9); interior columns should be designed to have the same steel percentage and volume surface ratio; slabs should be hinged around the stiffer shear wall core. Note that fixity attracts and increases volume change and should not be made more than necessary.

8.3.3 Design to allow for creep and shrinkage effects

For structures in which the loads are carried mainly by axial compressive forces developed in the concrete such as columns, arches, and arch dams, the effects of concrete creep and shrinkage cannot be avoided altogether. Some designers take the concrete behaviour as visco-elastic, i.e. a delayed elastic behaviour. Stress-strain relations are still written in linear form identical to elastic behaviour with the elastic constants replaced by integral operator. In simple form this becomes an elastic analysis with a reduced effective elastic modulus (Ref 8.12). More precise analysis requires expressions for predicting creep. These expressions contain a number of empirical and quasi-rational coefficients. Neville (Ref 8.12) reviewed six different types of expressions for the creep

functions and presented various methods of creep analysis for structural members. It is noted that all treatments for creep are, at present, limited to working loads. There are no guides to the problem of creep at ultimate load.

In massive concrete structures such as dams the effect of creep on the stress development in the structure is difficult to predict (especially if considerations are given to the foundation which has different creep properties). Fortunately, from effective modulus elastic calculations, it has been observed that a wide variety in properties results in limited effects on stresses and deformations (Ref 8.11).

Finally, the problems of creep and shrinkage can be alleviated somewhat by quality control of concrete. Strong concrete creeps less. However, if the quality of the concrete is inconsistent, the differential creep may be greater. Curing is important in reducing shrinkage cracks.

8.4 DETAILED DESIGN FOR DUCTILITY

Many experienced designers have observed that most of the failures in steel and concrete structures have been of a brittle type. Special attention must be given to the detail design of joints as these are often the regions of high moment and shear. Local weakness at these points will govern the structures capacity to carry loads. Precise solutions for the strength of joints are not necessary provided that they are on the lower bound; more attention should be given to the detailing of joints. The aim is to achieve ductility, i.e. ability to undergo deformation beyond the elastic range while still maintaining loads. Ductility provides safeguard against overload and impact since it allows large redistribution of forces in the structures (Ref 8.13).

8.4.1 Concrete detailing

- (1) Shear failures in concrete are quite sudden and without

warning and they should be avoided at all stages. Members should be checked for shear so that up to ultimate capacity (flexural) no shear or diagonal failures can take place. Shear re-inforcement must be adequate up to ultimate capacity without relying on concrete capacity to take shear.

(ii) Anchorage. Particular attention should be given to the anchorage of the main bars especially at regions near to columns. Splicing should be far from regions of high stresses and must be staggered. Anchorage for transverse reinforcing, stirrup hooks, should be checked.

(iii) Confinement of concrete in high axial load members is useful in maintaining ductility. This is done by providing high yield steel hoops closely spaced. The higher the axial load, the more confinement of concrete is necessary.

(iv) Quality of steel and concrete. Concrete crushing must be avoided by adequate steel provision (a limit of 2.5% is usually used for design). High yield steel reduces ductility while high strength concrete increases it.

(v) Ductility requirement for beams and columns. For a beam to have adequate ductility, the steel percentage must be kept well below those for "balanced elastic design". Over reinforced beams have little ductility as the concrete may crush before the steel yields. For a column to possess ductility, the maximum compressive force should be below one quarter of the ultimate compressive strength of the column section. This requirement can easily be seen from a typical column interaction curve (Fig A1.10, Appendix A1).

8.4.2 Steel detailing

(i) Joint layout. Simple joint layout is important. The cost of fabrication is usually high for joints. The number of pieces which

require marking out, cutting and fitting, special edge preparation, should be minimised. The two most common methods for joining metals together are bolting and welding. Welding is still the main method used in the shop, and with modern methods of inspection works of very high standard can be expected. Bolting has largely replaced riveting with the development of high strength bolts, and is popular in the field. The general trend is to have all the pieces welded in the shop where high quality welding is possible and bolted in the field for ease of erection. A combination of bolting and field welding is sometimes used such as in column-beam connection. Another obvious point in designing joint layout is to make the job accessible for welding or bolting; this feature is sometimes overlooked by the designer.

(ii) Welded joint. The following points should be watched when a welded joint is designed.

Selection of welding process and precautions. Arc welding is a fusion process in which the electrodes are melted to provide the filler metal. The difference in welding with or without flux should be noted. The heat affected zone on the parent metal is likely to cause cracks and this should be eliminated with proper precautions. For carbon steel, weldability decreases with the increase of carbon contents. For low alloy steel the main danger is underbead cracking. High alloy steel is susceptible to embrittlement from grain growth at high temperature. Each steel must be considered separately and weldability is related to the type of joint used.

Effects of distortion and residual stresses. Due to the presence of the heat in welding, the dimension of the end product will change; this causes distortion and stresses. Thus over welding must be avoided. Preheating helps to eliminate some distortion and stresses. Normally the effects are not important as they can be absorbed by plastic

deformation, unless precautions are not taken and the welded joints become brittle. Stress relieving procedures usually alleviate these problems.

Service conditions. Joints which are excellent for one job may not be adequate for others because of different operating conditions. The nature of the stress in the joint must be considered; tension, shear, torsion, bending...since different joint design is suitable for different stress application.

Weld selection. Fillet and lap welds are easier to make than butt welds. Automatic welding is fast and reduces the cost of deposit metal. Shop welding is good and reliable. Field welding is expensive and should be kept to a minimum, preferably replaced by bolting. Continuous single run fillet welding is desirable, especially when corrosion is to be considered.

(iii) **Bolted Joint.** With the development of high strength bolts, the use of bolted joints has largely replaced riveted joints in structures. The advantage is of course the ease of erection. The tightening procedure by counting the turn of the nut has been shown to be reliable, easily used and inspected in the field. Research has shown the superiority of bolts over rivets in both fatigue and static tests. Tests on large bolted joints showed that the strength of the fastener in shear far exceeds the strength of the section. Misalignment and condition of the surface have little effect on the joint efficiency. For moment connections it has been shown that bolted joints can accommodate large rotational displacement if flexible end plates are used. There is only one failure of bolted joints reported in literature; the cause is attributed to corrosion and overtightening effect.

The design of bolted joints should be made so that the failure is

forced into the connected material rather than the bolts themselves, since this type of failure is more ductile.

8.5 CONCLUDING REMARKS

Various aspects of practical design consideration have been discussed. The discussion is by no means complete and is limited by the author's own practical experience. The prime purpose is to achieve ductility in the members and the structure. Most of the problems can be avoided by careful and suitable detailing, particularly in the detailed design of joints. Thorough supervision is required since so much depends on common sense and good construction practice. The successful completion of a job depends on many persons. However, the prime responsibility rests with the designer. He must issue adequate instructions on drawings and specifications to ensure that the structure will be properly built since he is the only one with the most comprehensive view of the project.

SUPPORTING EXPERIMENTAL STUDIES

APPENDIX A1

TESTS OF ARCHES AND RELATED CALCULATIONS

INTRODUCTION

Tests on three series of arches (steel, reinforced concrete, and plain concrete) were made to study the behaviour of arches under increasing vertical loads. Both symmetrical and unsymmetrical loading arrangements were used.

All arches were loaded to collapse. Deflexion and strain measurements were taken at all stages of loading; thrust lines were plotted from experimental data, and the collapse modes were studied.

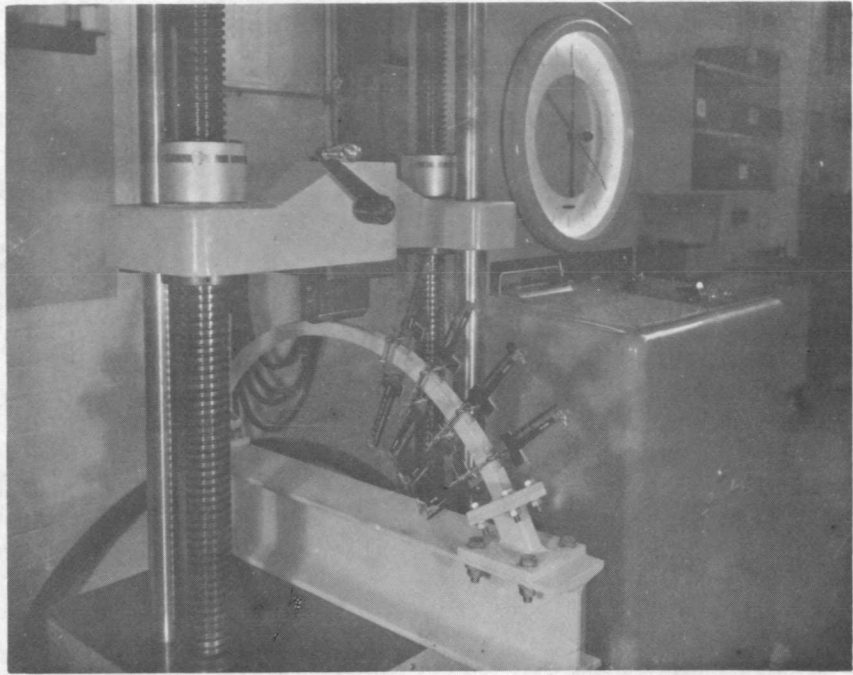
GENERAL DESCRIPTION OF TEST SET-UP AND EXPERIMENTAL PROCEDURE

All arches were mounted on specially designed steel beams. Tests were performed in (i) an Amsler testing machine, (ii) a Shimadzu testing machine, and (iii) a specially designed loading rig with Roberts mechanism which allowed the arches to sway freely. The general loading arrangements were shown in Figure A1.1(a), (b), (c), and (d).

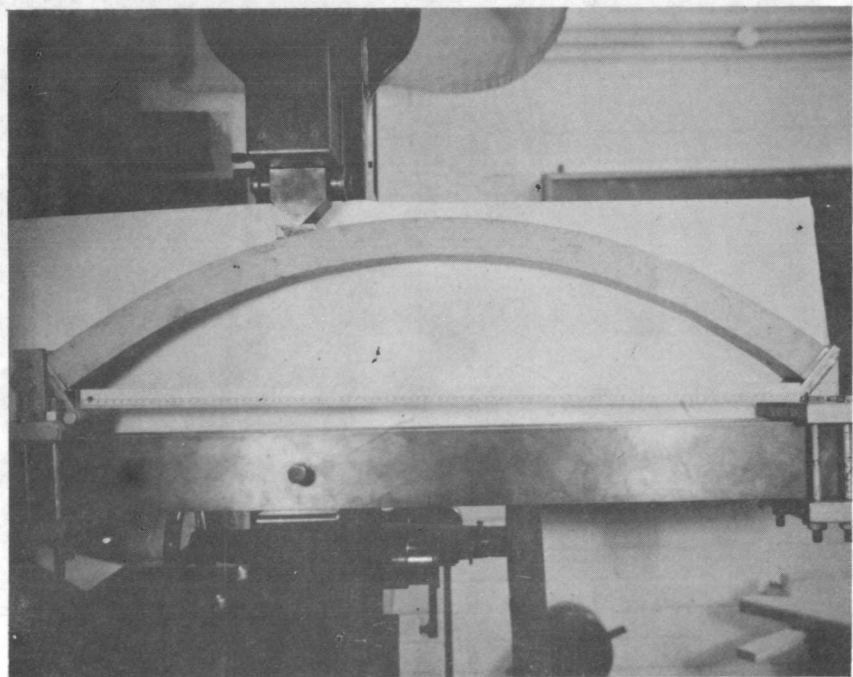
Measurements were made with dial gauges for deflexions, Huggenberger mechanical gauges for strains in steel and concrete. Electrical strain gauges were also used at places inaccessible to the Huggenberger gauges.

All arches were loaded to collapse; measurements were made at all stages of loading. The collapse modes were studied.

Properties of the materials were obtained in the usual way; tensile tests for the steel specimens made from the same batch of steel, and compression tests for the standard 6" cylinder concrete specimens made from the same mix as the experimental models. In addition, the plastic moment for the steel section was obtained from simple beam tests, and the yield surface for the reinforced concrete section, subjected to combined

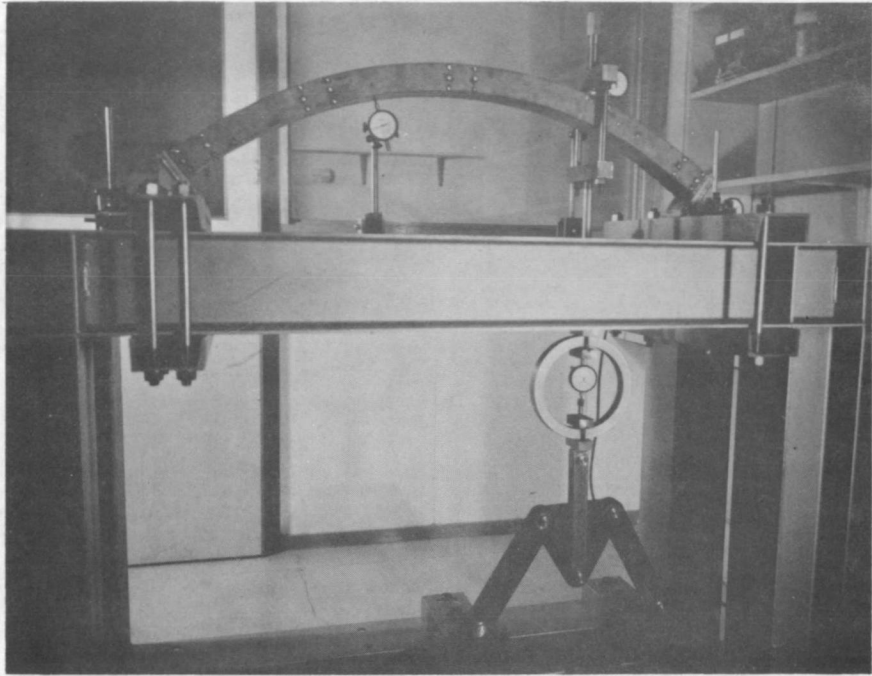


(a) General loading arrangement on the Shimadzu testing machine.

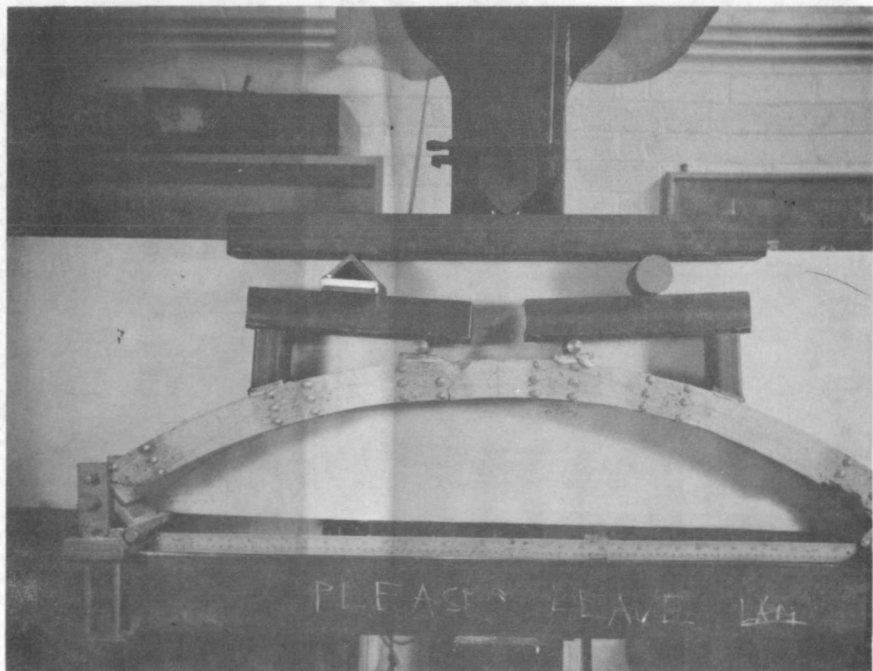


(b) General loading arrangement on the Amsler testing machine.

FIGURE A1.1



(c) General loading arrangement with proving ring and Roberts mechanism for free horizontal movement.



(d) General arrangement for symmetric loading condition.

bending and axial forces, was obtained from a series of tests of columns (of the same section) under eccentric loadings

From the strain readings at a certain load level and the stress-strain curves for the materials, bending moments and axial forces were calculated for various locations on the arches; the thrust line for that load was plotted to obtain an overall equilibrium check. While the overall equilibrium condition is satisfactory, detail comparisons of the thrust and bending moment values often show poor agreement. The shift of the thrust line under different load levels was also observed.

EXPERIMENTAL RESULTS, RELATED CALCULATIONS, AND DISCUSSIONS

STEEL ARCHES

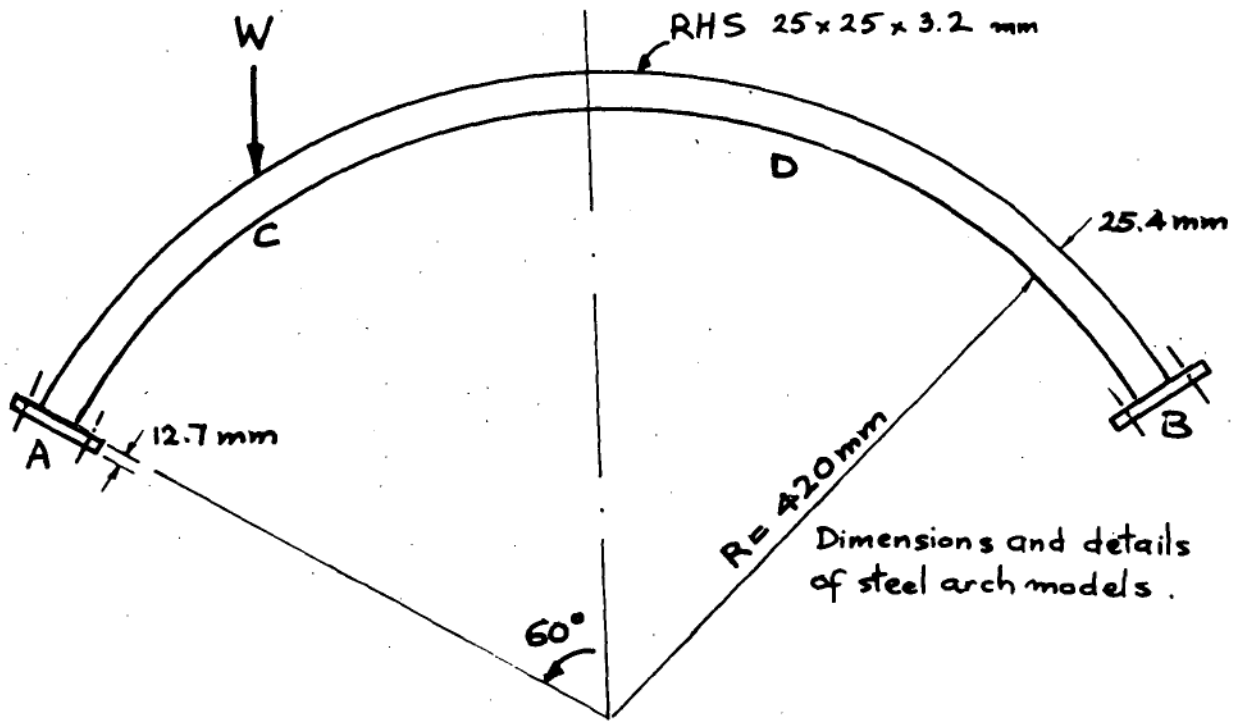
The dimensions and other details of the steel arches are given in Figure A1.2(a). The arches are made from 1" x 1" x 1/8" rectangular hollow section, bent to the desired circular shape, then annealed before testing. Half inch base plates are welded to the arches and bolted to the supporting beams. After yielding occurs, difficulties were experienced in maintaining a steady load while readings were taken.

ARCHES UNDER SINGLE POINT LOAD AT QUARTER SPAN

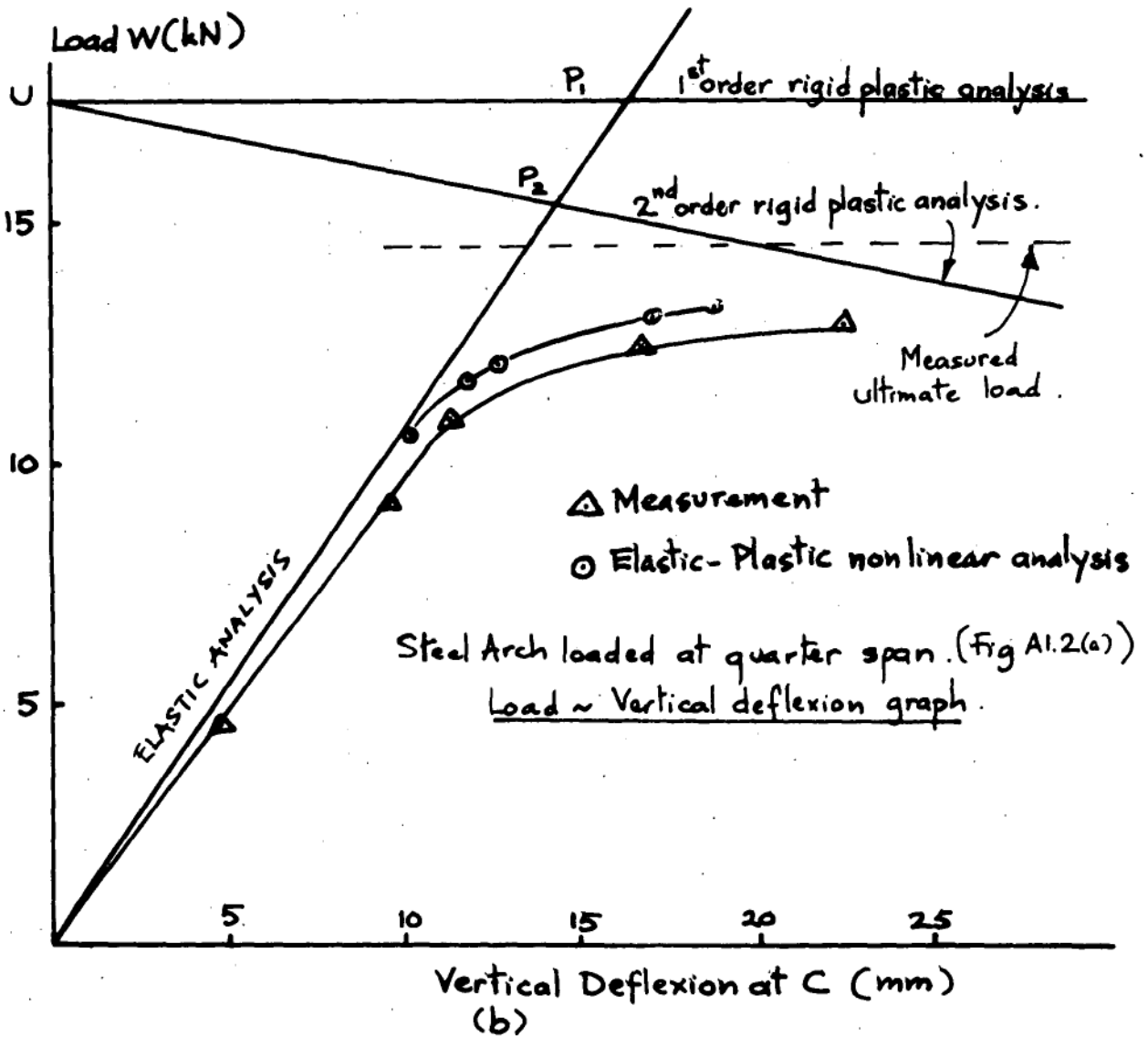
A typical load-deflexion graph is presented in Figure A1.2(b), together with related calculations. Yield was first reached under the point of loading C, then at the support A, then at the region D, and finally at the support B. There was considerable spreading of the yielded regions A, C, and D, while the support B remained elastic for most of the test's duration.

From the strain readings, thrust lines were plotted in Figure A1.3. A picture of the collapsed arch is in Figure A1.4(a).

CALCULATIONS. The axial force in the arch is small and the load is resisted mainly by flexural action. A simple plastic analysis is



(a)



(b)

Figure A1.2

performed by drawing the plastic thrust line for the point load. The calculated ultimate load is 17.2kN, well above the measured 14.2kN. The effect of vertical deflexion is taken into account as shown in Figure A1.5 and A1.6. The result is the sloping line UP_2 in Figure A1.2(b). The measured ultimate load is higher than this estimate; strain hardening of the section with increasing deformation is thought to be the cause of the difference. An elastic-plastic analysis using dynamic relaxation (Appendix B1) is also performed and shown on the same graph, Figure A1.2(b).

ARCHES UNDER SINGLE POINT LOAD AT THE CROWN

The results of tests and calculations are presented in Figure A1.7. The picture of the collapsed arch is in Figure A1.4(b). It is seen that there is considerable spreading of the yielded regions B, C, and D, while the supports A and E remain elastic for most of the test's duration. It can be said that the 'hinges' at A and E were not properly formed. The reason can be easily seen in Figure A1.7; most of the deformation occurs in the regions B-C-D. The influence of deflexion on the load-carrying capacity is quite marked as shown on the second order rigid-plastic analysis, Figure A1.7.

EFFECT OF STRAIN HARDENING

Some unannealed arches were also tested to study the effect of strain hardening. The results are compared in Figure A1.8. The unannealed arches were considerably stiffer and consequently the ultimate load capacity was much higher. However, while the annealed arches could hold ultimate load with increasing deflexion, the unannealed ones could not. The arches were under the conflicting influences of strain hardening and deflexion. For the unannealed arches, the influence of deflexion (which decreases the load-carrying capacity) is offset by the influence of strain hardening (which increases the load capacity). For the unannealed arches,

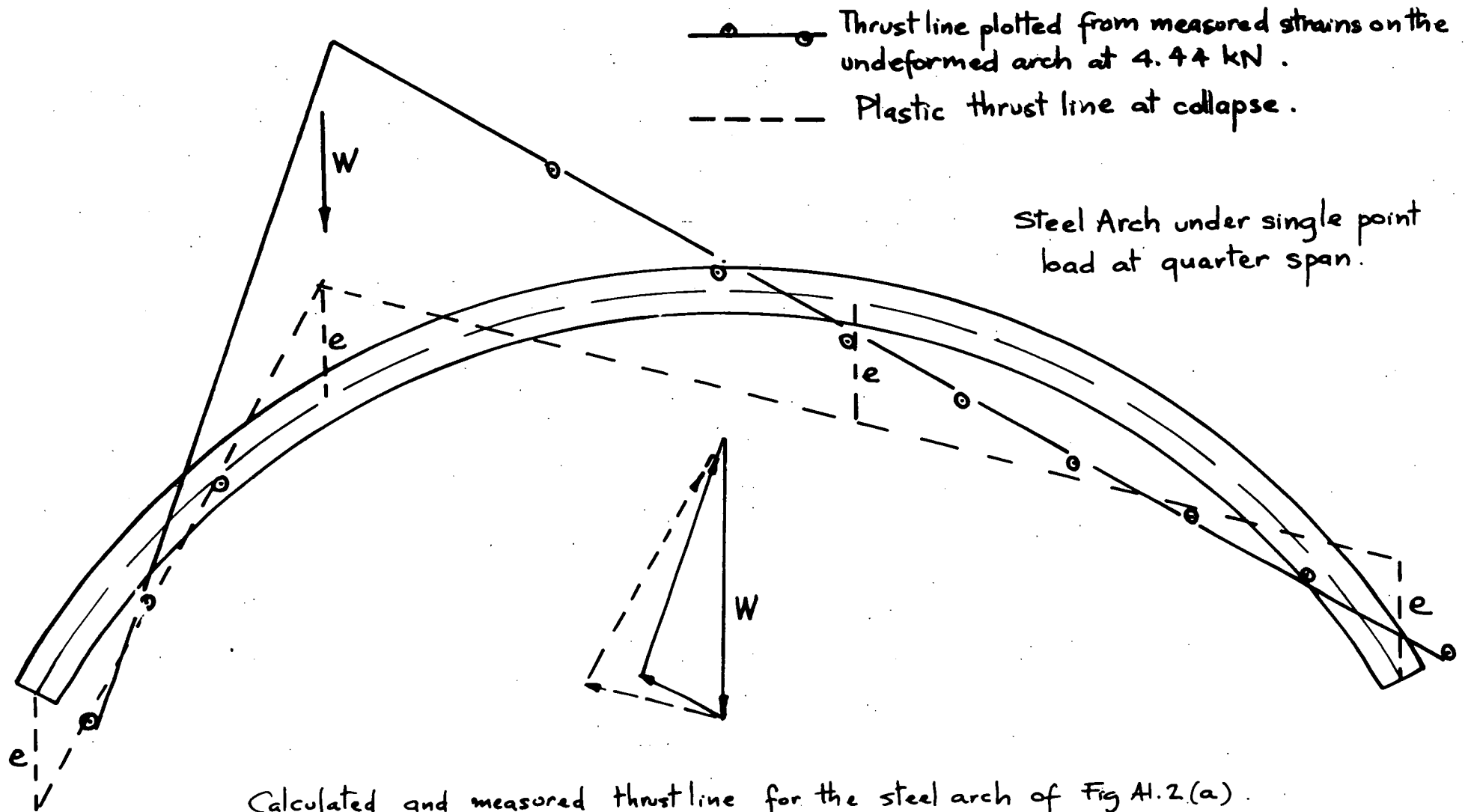
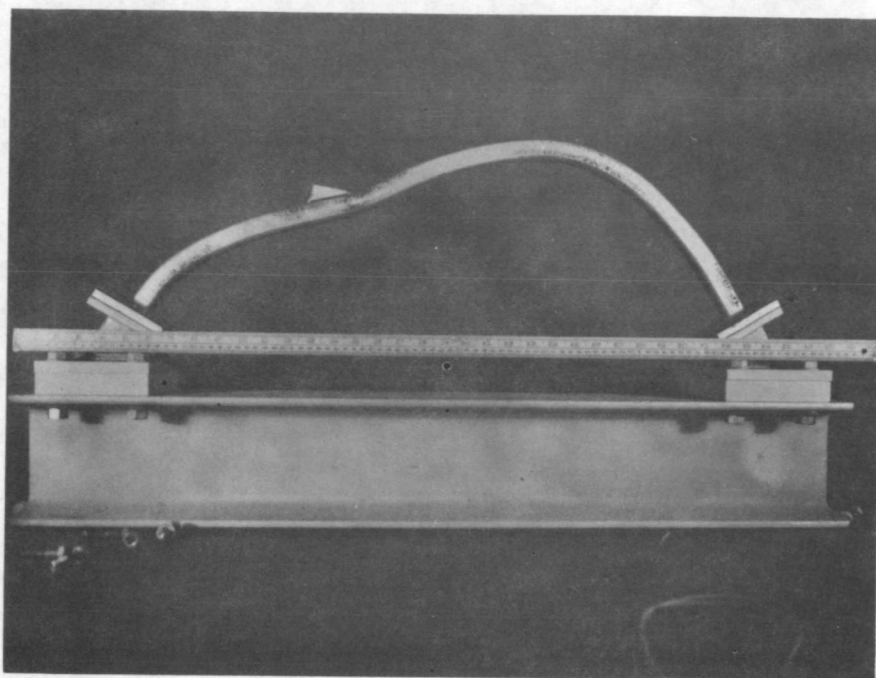
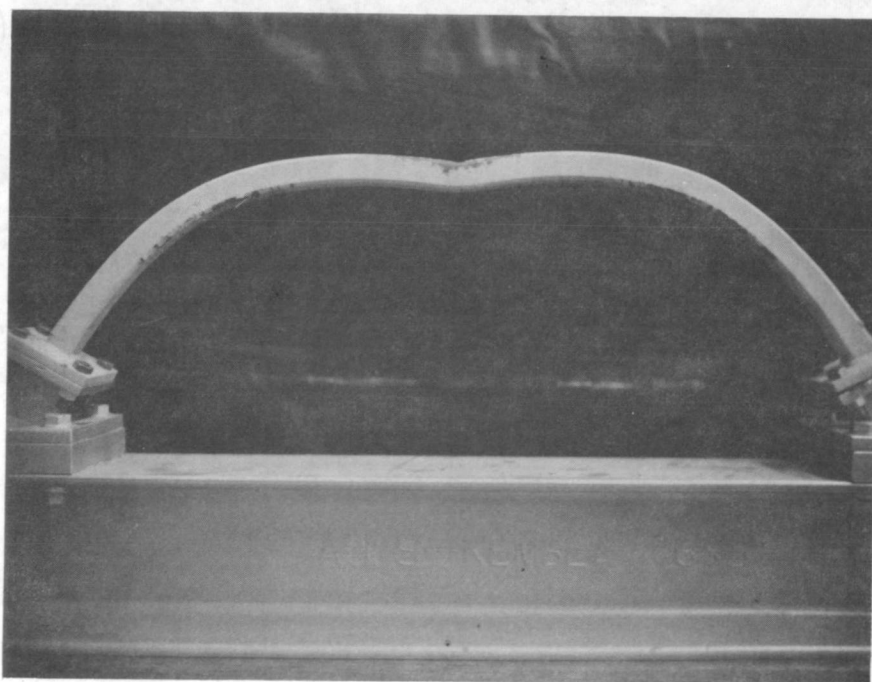


Figure A1.3



(a) The collapse of a steel arch under one single point load at one quarter span.



(b) The collapse of a steel arch under one single point load at the crown.

FIGURE A1.4

$e = 63 \text{ mm}$
 $M_p = 0.52 \text{ kN-m}$
 $\delta = 0 \quad W_o = 17.2 \text{ kN}$
 $\delta = 25 \text{ mm} \quad W_o = 13.6 \text{ kN (see Fig. A1.6)}$

Instantaneous Center

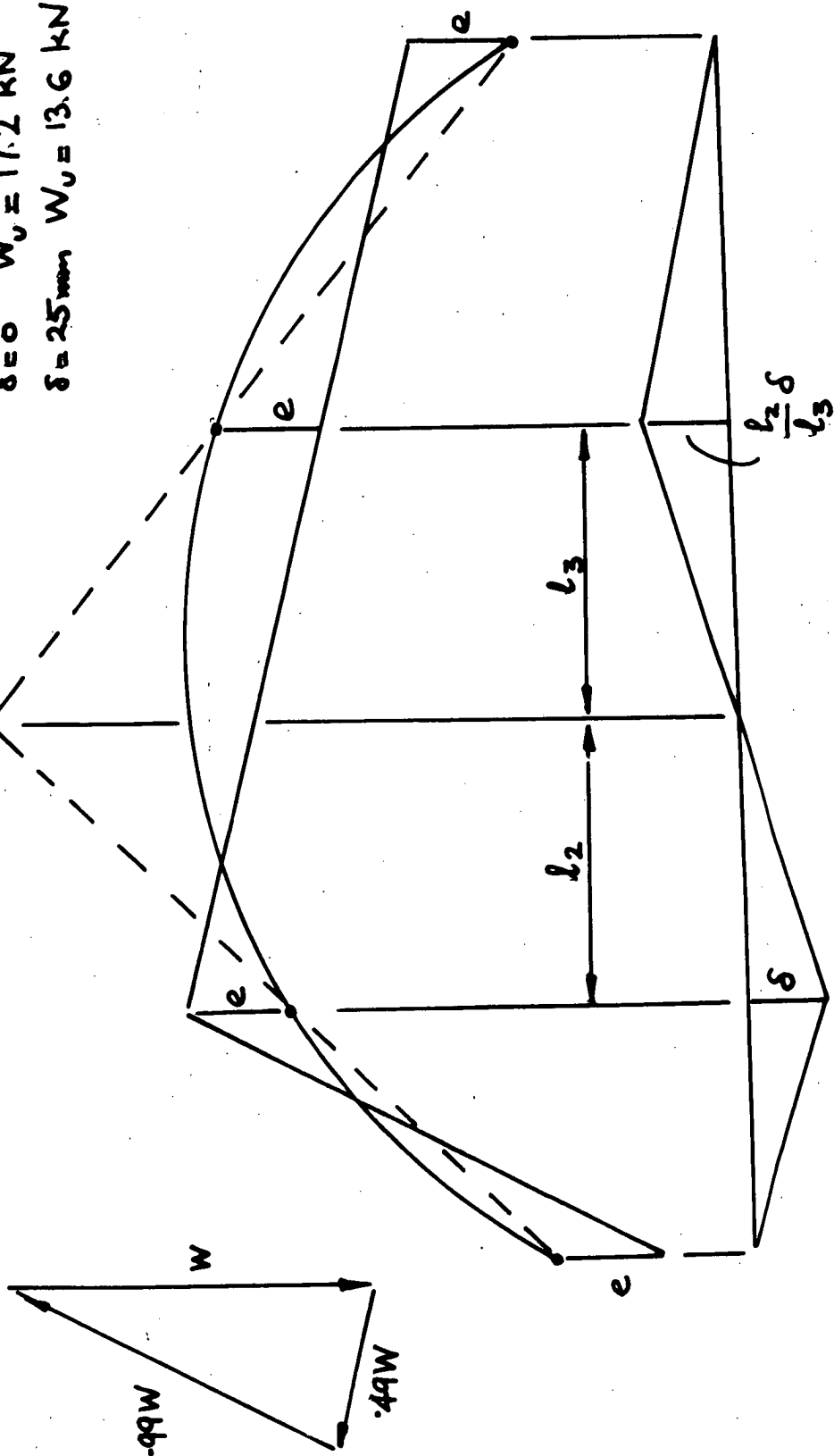
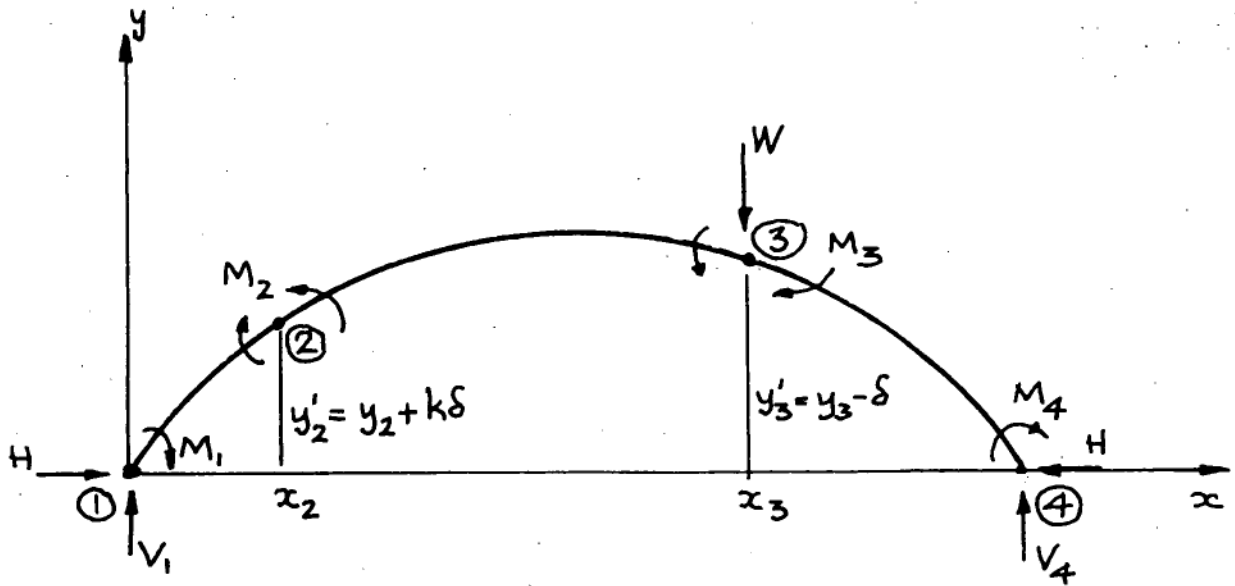


Figure A1.5



$$\sum V = 0 \Rightarrow V_1 + V_4 - W = 0$$

$$\sum_{1-2} M = 0 \Rightarrow H y_2' - V_1 x_2 - M_1 - M_2 = 0$$

$$\sum_{3-4} M = 0 \Rightarrow H y_3' - V_4 (L - x_3) + M_3 + M_4 = 0$$

$$\sum_{1-3} M = 0 \Rightarrow H y_3' - V_1 x_3 - M_1 + M_3 = 0$$

Solutions are :

$$V_1 = \left\{ (M_1 - M_3) / y_3' - (M_1 + M_2) / y_2' \right\} / (x_2 / y_2' - x_3 / y_3')$$

$$V_4 = (M_1 + M_4) / (L - x_3) + x_3 V_1 / (L - x_3)$$

$$H = V_1 x_2 / y_2' + (M_1 + M_2) / y_2'$$

$$W = V_1 + V_4$$

Solutions for arch under single point load - effects of deflexion are included in the calculations.

Figure A1.6

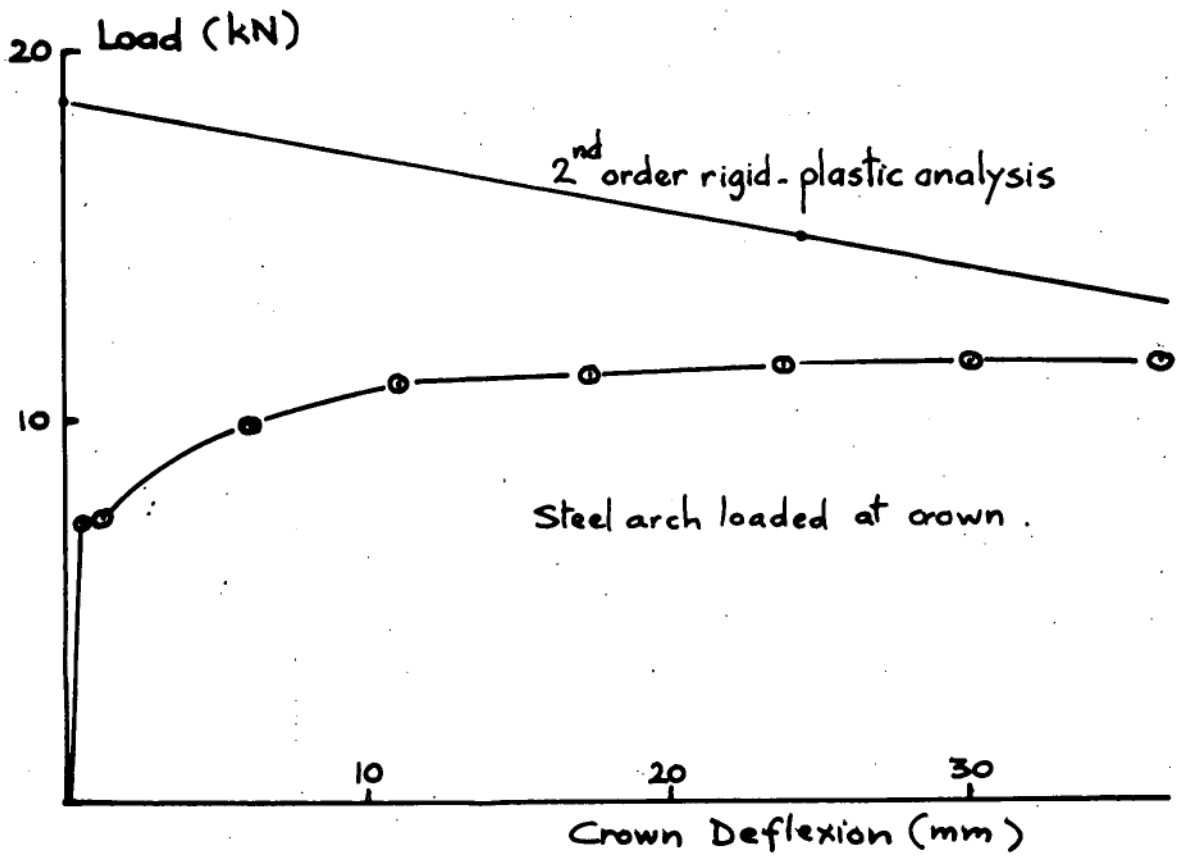
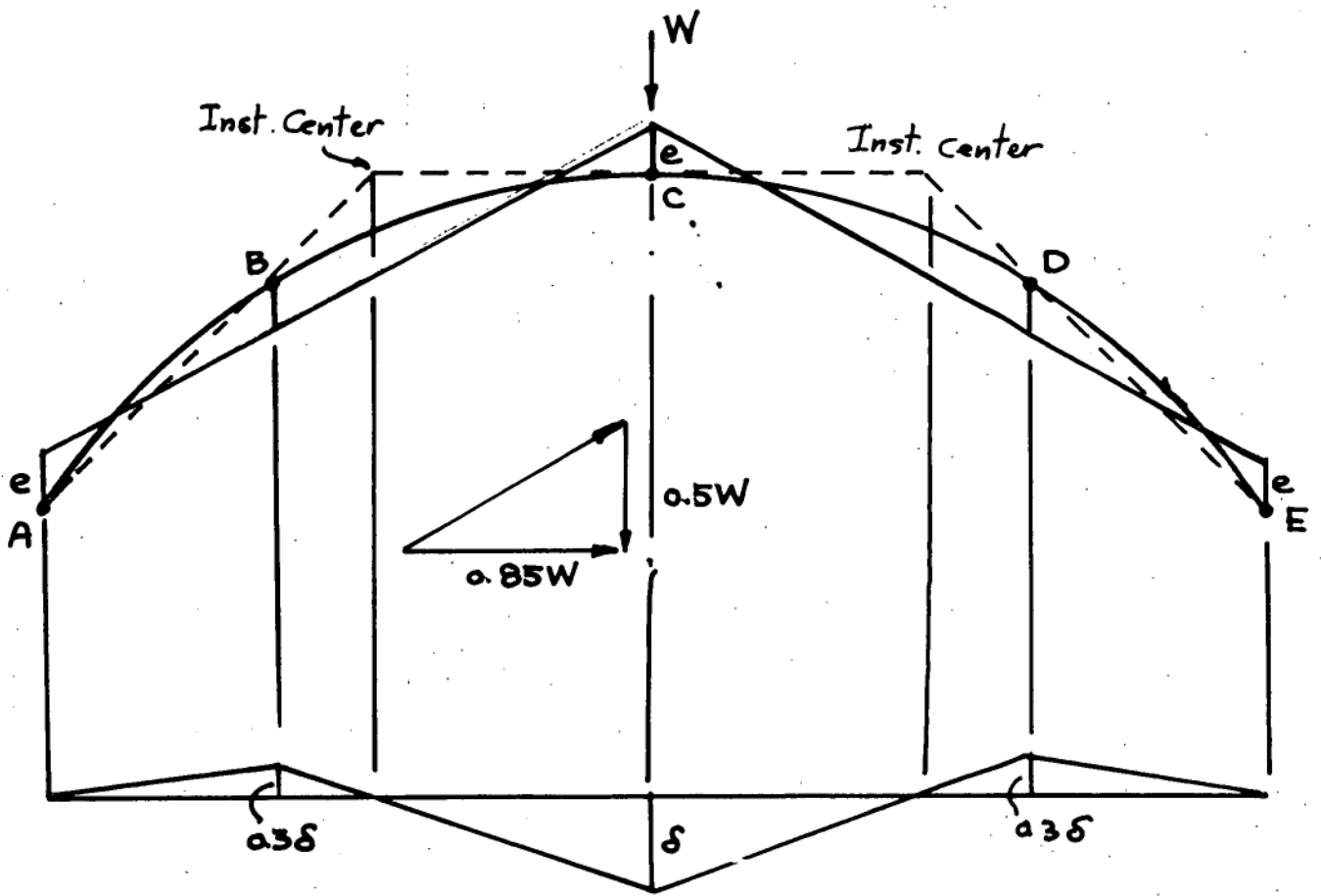


Figure A1.7

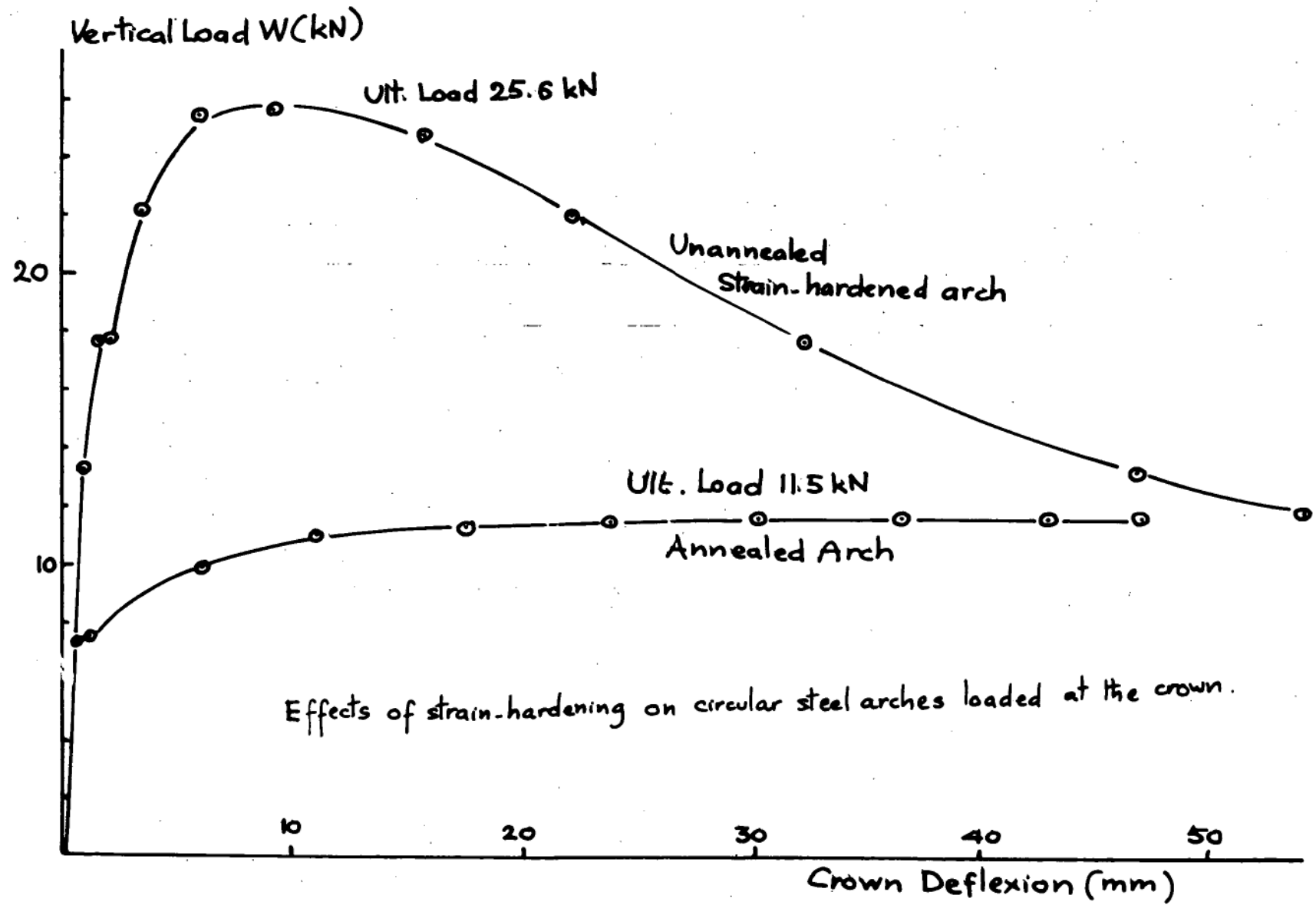


Figure A1.8

there are no further strain hardening effects after the ultimate load is reached, and the increasing deflexion causes the load capacity of the arch to drop (Ref A1.1).

REINFORCED CONCRETE ARCHES

The dimensions of the arches and the details of reinforcement are given in Figure A1.9. The reinforcements (4-3/16" wire) are welded to the base plates. The base plates have four steel bolts on their other sides, enabling the arch to be mounted on the supporting beam.

Strains were measured both on the concrete and steel reinforcement with Huggenberger strain gauges. From these data, thrust lines were plotted for various loading levels to obtain overall equilibrium check. A series of reinforced columns were made from the same mix with the arches and tested under varying eccentricities to obtain the yield surface for the section; the results are presented in Figure A1.10.

ARCHES UNDER SINGLE POINT LOAD AT QUARTER SPAN

A picture of the collapse arch is in Figure A1.11(a); only three regions of extensive deformation are observed. Cracks were formed quite early in the test. Concrete crushing only occurred when the arch nearly reached its ultimate capacity; there was a drop in the load capacity when the concrete started to crush. The calculated and measured thrust lines are plotted in Figure A1.12(a). Calculations were performed as in the steel arches, i.e. a simple plastic analysis, then corrections were made for the effects of axial loads (from the interaction curve Figure A1.10) and deflexions (from the analysis) of the motion of the mechanism, Figure A1.12(b). The equilibrium conditions are as given in Figure A1.6. The load-deflexion graph is in Figure A1.12(c). The difference in the measured and calculated values is due to the incomplete redistribution of moments. The calculations assume that the ultimate moment as given by

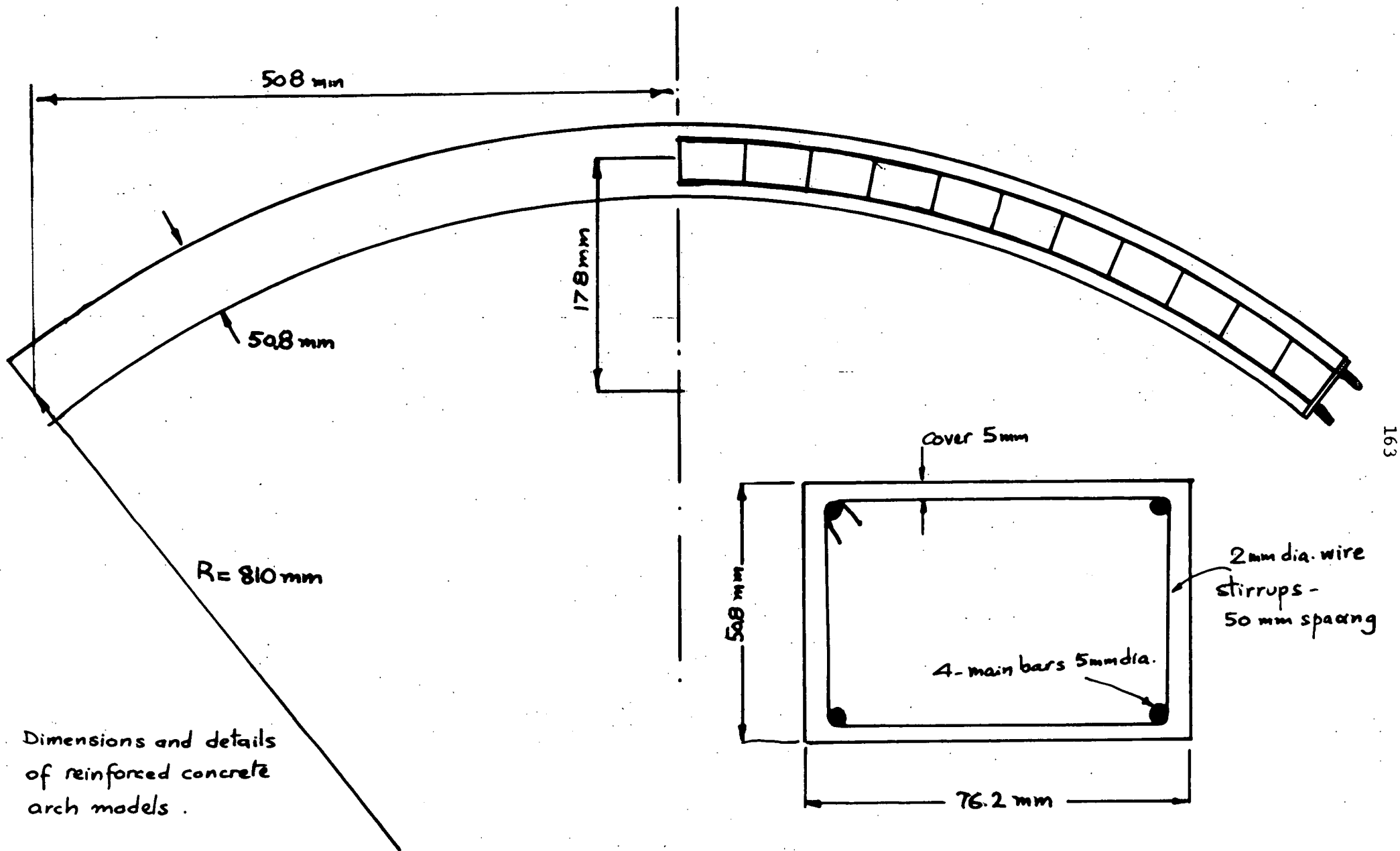
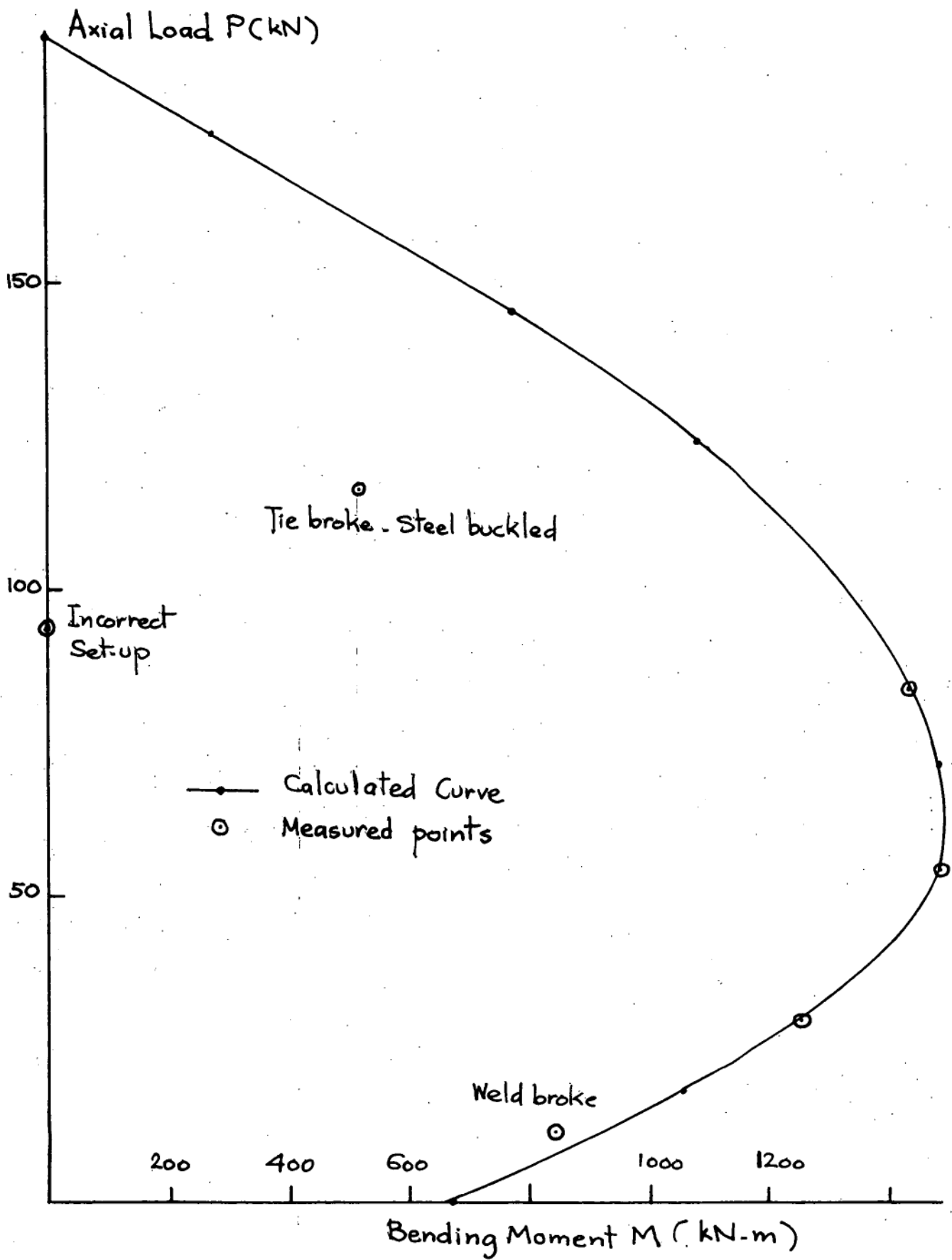
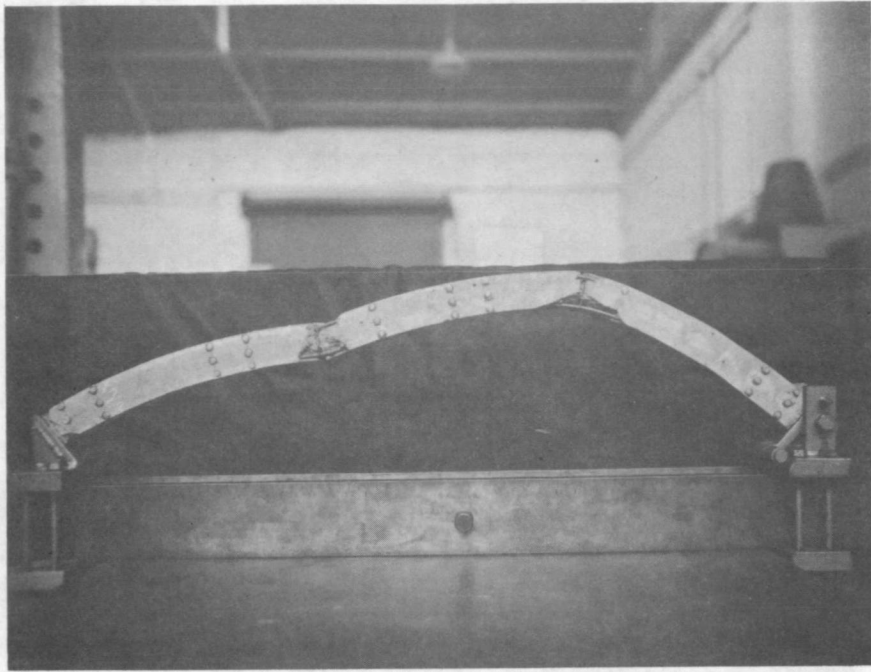


Figure A1.9

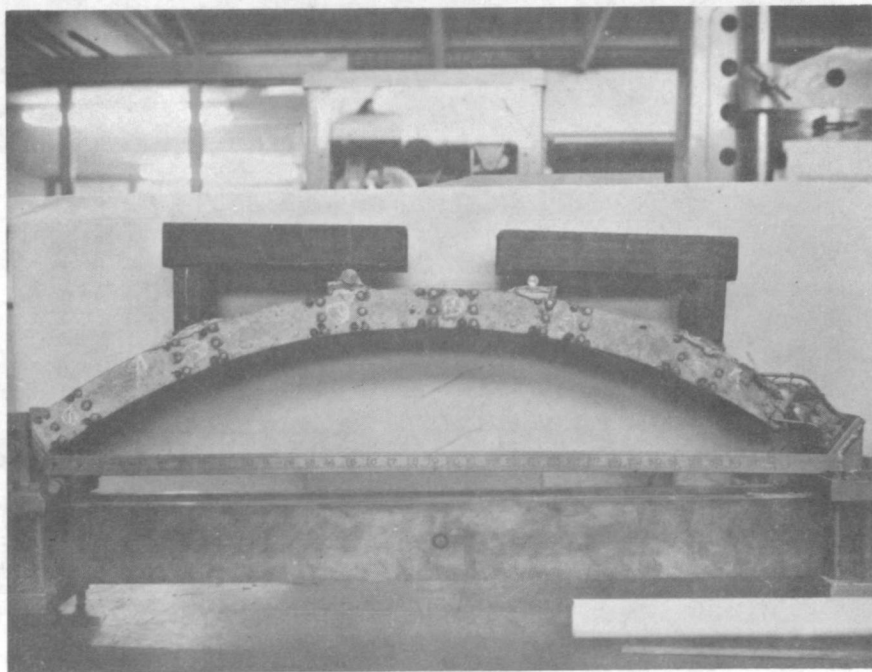


Yield surface for the reinforced concrete arch section.

Figure A1.10

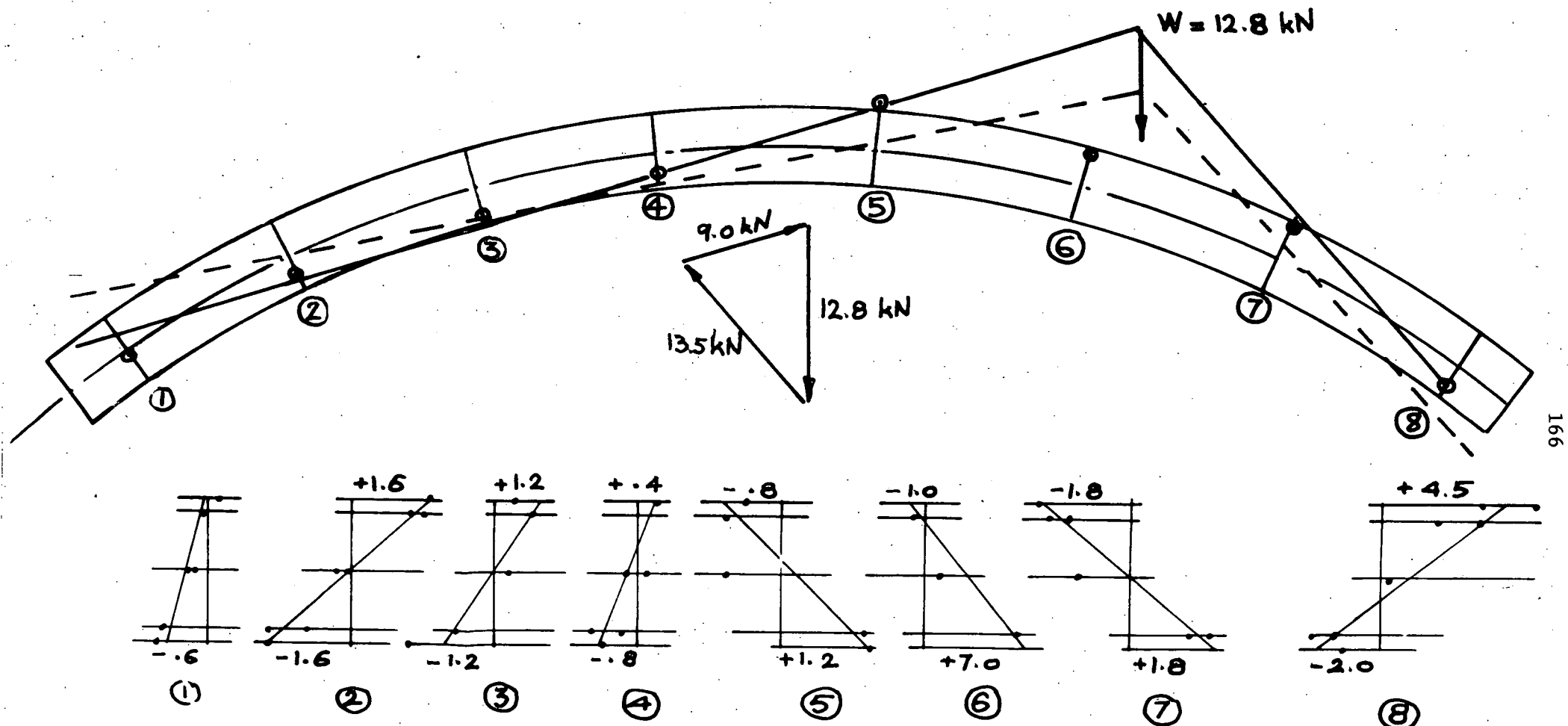


(a) The collapse of a reinforced concrete arch under one single point load.



(b) The collapse of a reinforced concrete arch under four symmetric point loads.

FIGURE A1.11



—— Measured thrust line at 12.8 kN.

---- Calculated thrust line at $\delta = 8\text{mm}$.

Strain figure $\times 10^3$ +ve tension
-ve compression

Measured and calculated thrust line for the reinforced concrete arches loaded at quarter span.

Figure A1.12(a)

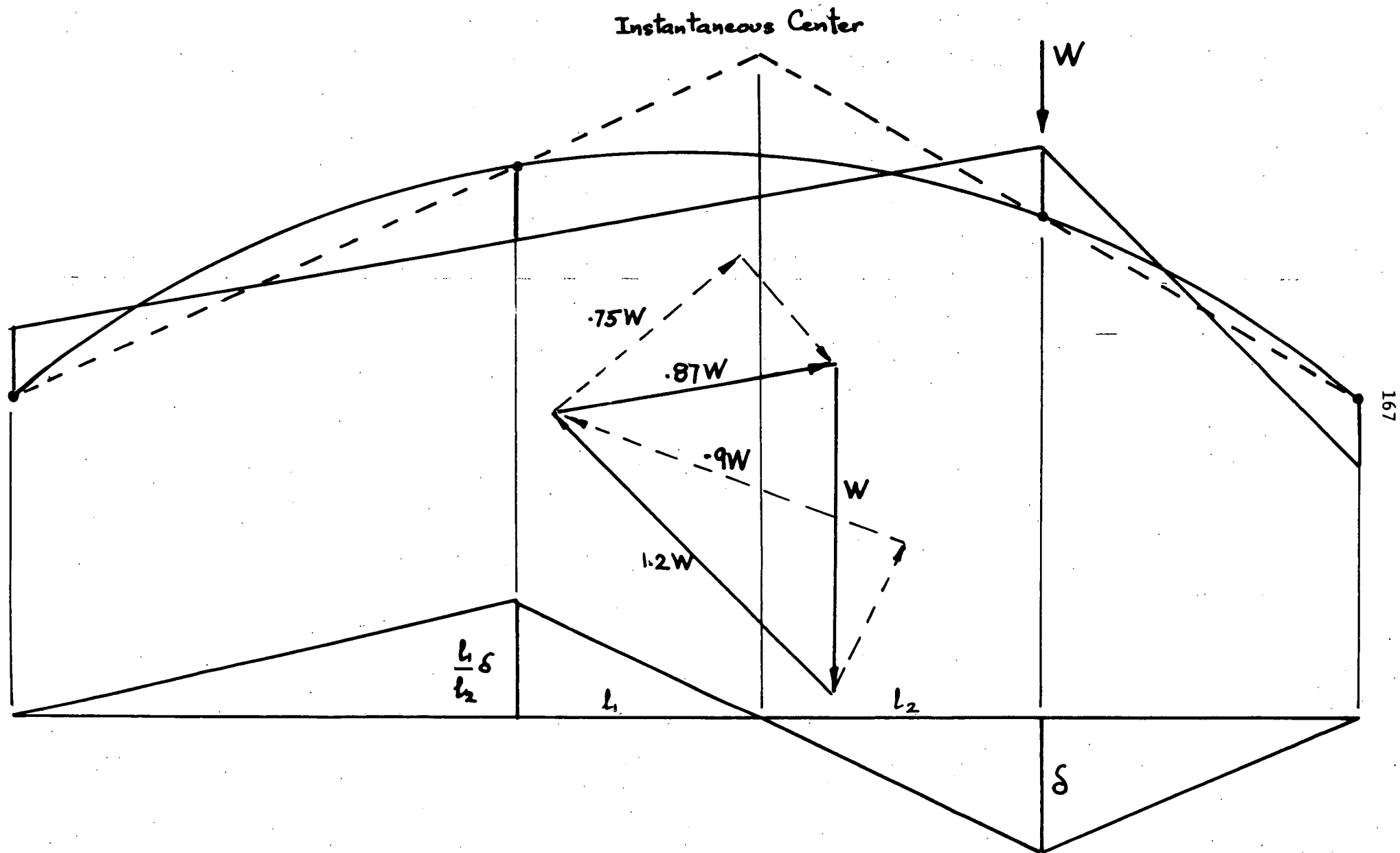


Figure A1.12(b)

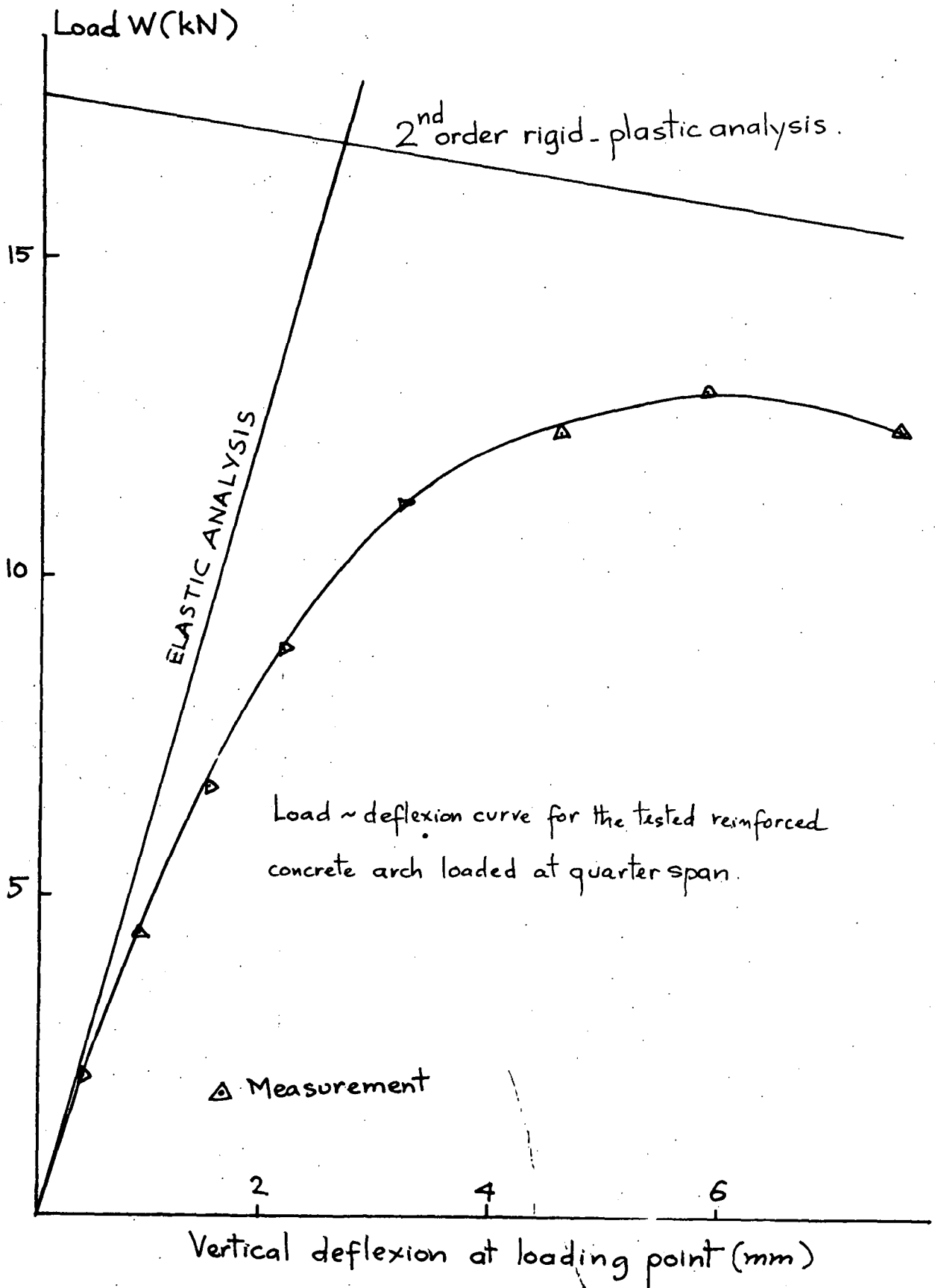


Figure A1.12(c)

the yield surface can be maintained with increasing deformations while actually there is a drop in the capacity of the sections with increasing deformation (Ref A1.2, A1.3).

ARCHES UNDER FOUR SYMMETRICAL POINT LOADS

The arches failed locally near the support with broken ties and the main reinforcement was buckled. No other cause of failure was visible. The thrust lines for the arch are in Figure A1.13, the picture of collapse in Figure A1.11(b).

PLAIN CONCRETE ARCHES

The dimensions of the arches are the same as those of the reinforced concrete arches.

ARCHES UNDER SINGLE POINT LOAD AT ONE THIRD SPAN

The behaviour of the arches is influenced by the tensile strength of the concrete. After cracks have formed, the arches can carry very small loads. The arches fail with four hinges as pictured in limit theory, Figure A1.14(b). However, with some support movement it is possible that the slipping failure would occur near the loading point as observed in some tests at our laboratory.

ARCHES UNDER FOUR POINT SYMMETRICAL LOADS

Since the thrust line lies within the arch and there is little bending moment, failure could only occur with extensive crushing of the concrete. There are only three regions of extensive crushing when the ultimate load is reached, Figure A1.14(b). A four hinge mechanism type of failure is not possible as can be seen from the position of the thrust line, Figure A1.15.

CALCULATIONS. There is no standard treatment of this mode of failure. The following scheme of lower bound calculation is proposed.

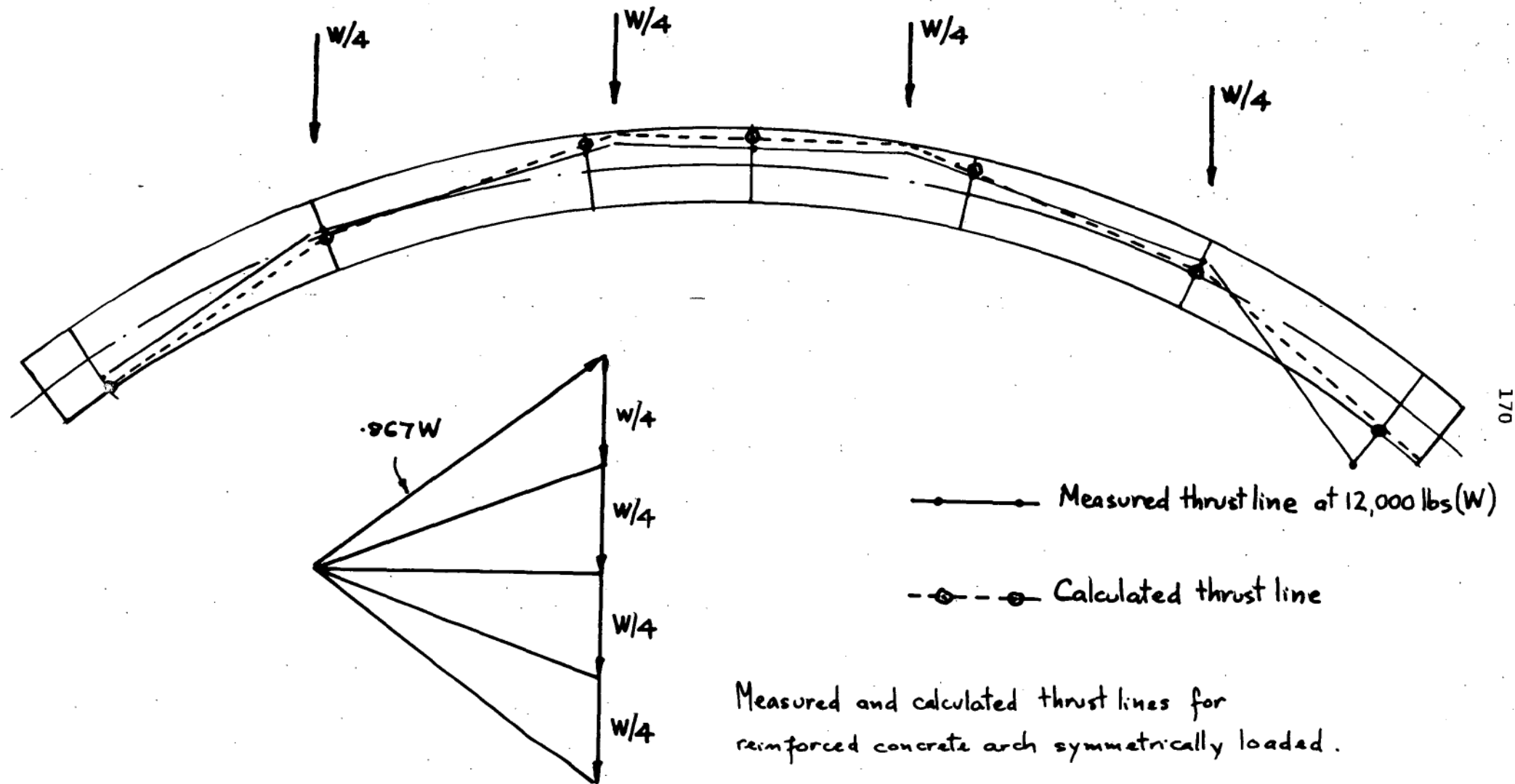
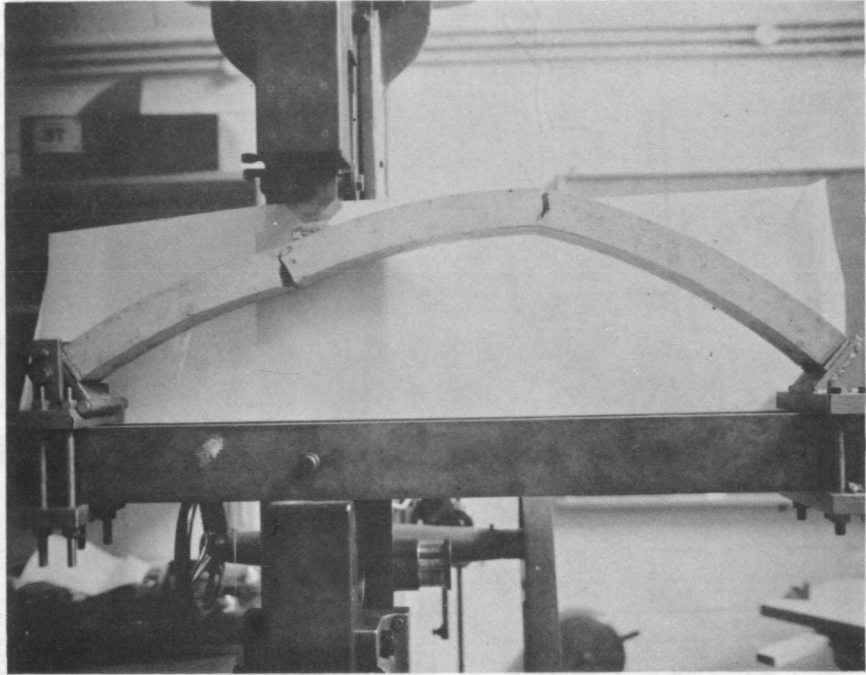
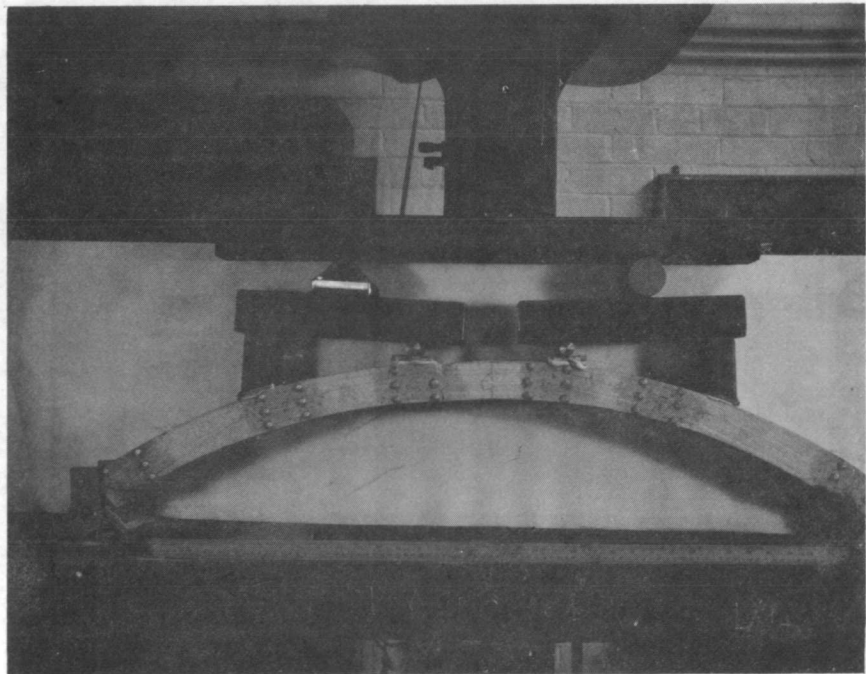


Figure A1.13



(a) The collapse of a plain concrete arch under one single point load.



(b) The collapse of a plain concrete arch under four symmetric point loads.

FIGURE A1.14

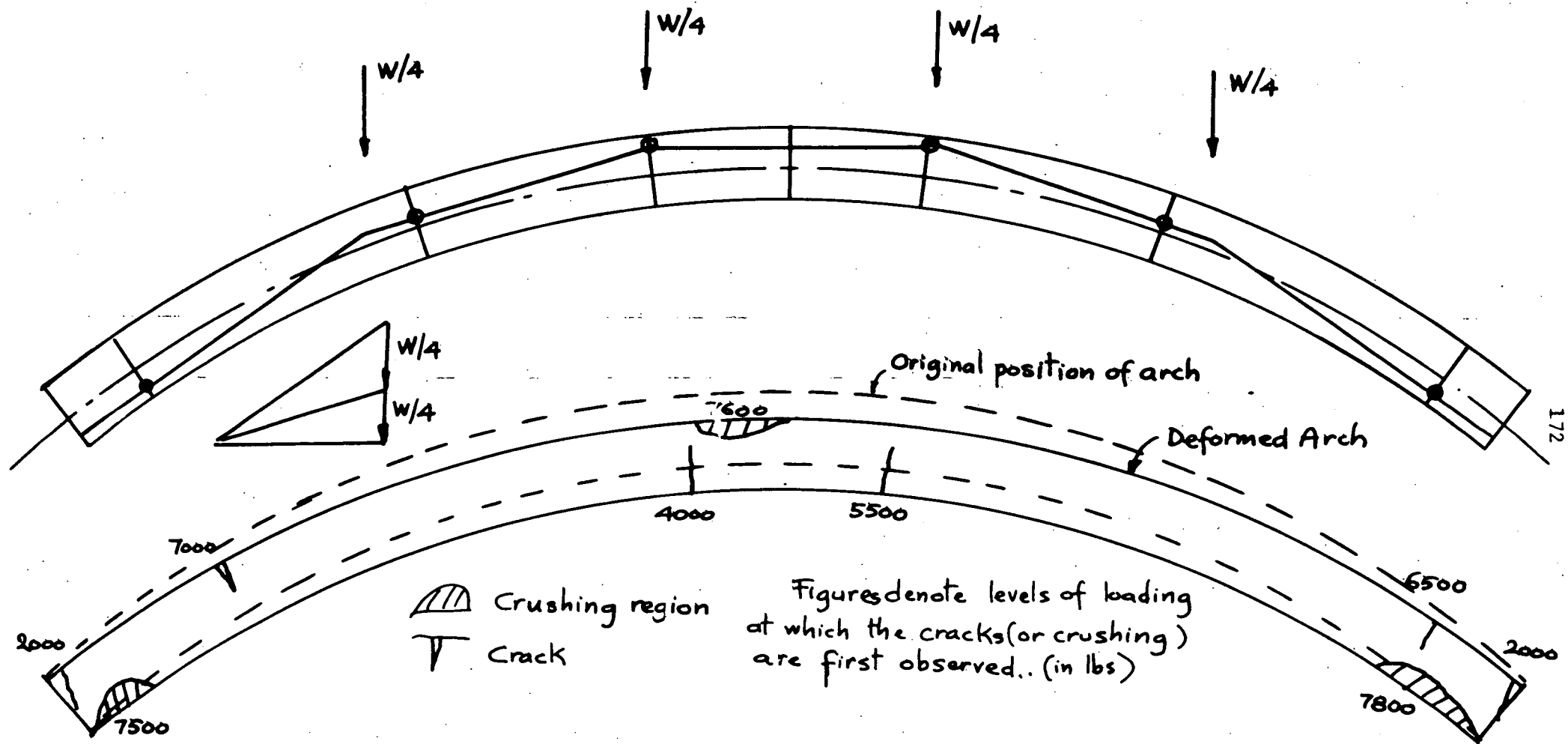


Figure A1.15

The value of thrust and moment at a section is given by

$$N = 0.85 f_c' \cdot c \quad ; \quad M = 0.85 f_c' \cdot c \left(t/2 - c/2 \right) ;$$

where t is the section thickness, c is the width of the stress block.

Trial values of thrust and moment are guessed at the two failing sections, the equilibrium of the system is checked, and the value of the collapse load obtained. The iterative procedure, which is presented in the flow chart of Figure A1.16, is repeated until satisfactory agreement is reached. The effect of the crown deflexion can also be included in the scheme of calculations as shown in Figure A1.16.

The results of the calculations are:

With no deflexion: At the crown $c = 1.74''$)
) . $W = 2.01 \cdot (0.85 f'_c)$
 At point C $c = 1.98''$)

With 1" deflexion
at point C : At the crown $c = 1.84''$)
At point C $c = 1.99''$) $W = 1.80 \cdot (0.85 f'_c)$

The measured ultimate load is $W_u = 8000$ lbs, with crown deflexion 1".

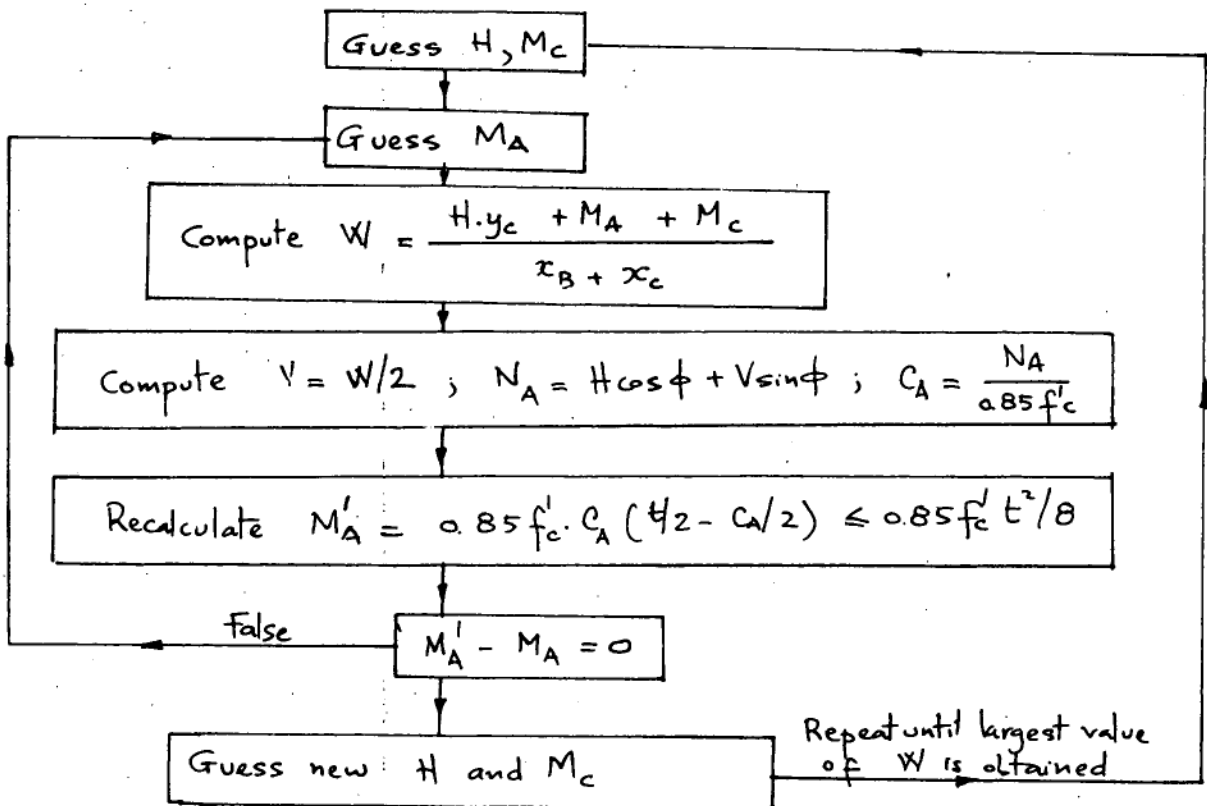
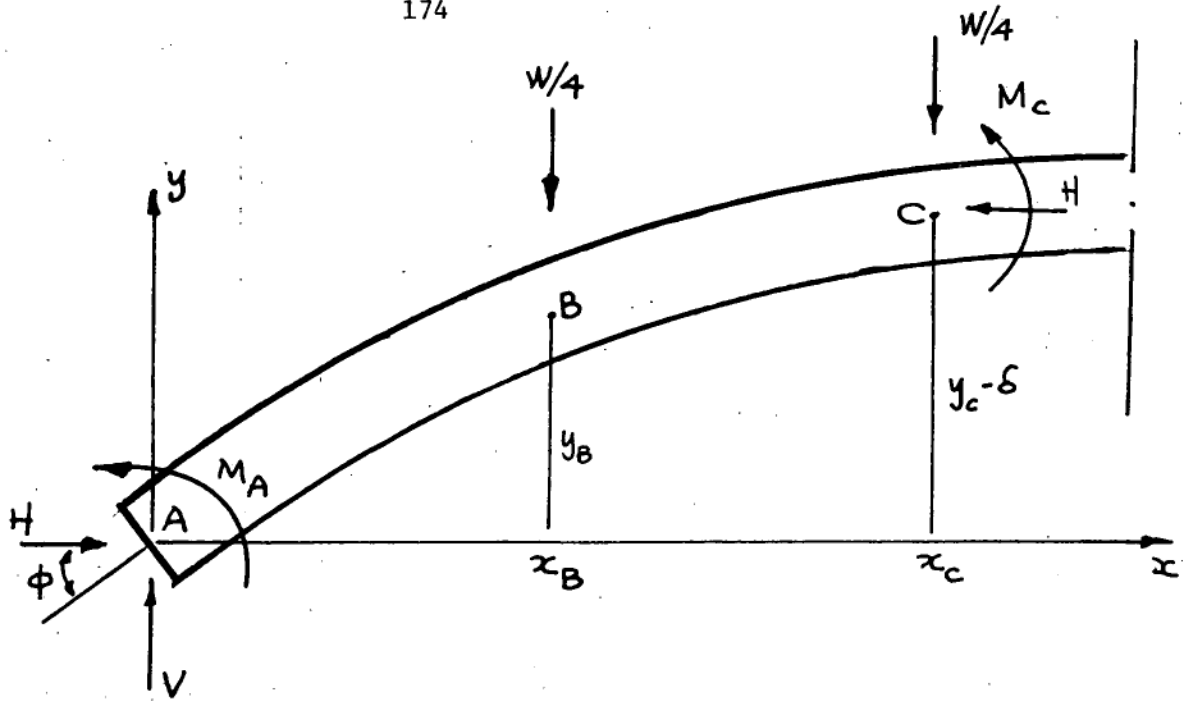
The strength of concrete is $f'_c = 5500 \text{ lb/in}^2$ (from cylinder tests);

therefore $W(\text{collapse}) = 9300 \text{ lbs (no deflexion)}$, $W = 8400 \text{ lbs (1" deflexion)}$.

The calculated value of the collapse load is only 5% different from the measured value. It is envisaged that the proposed method of calculation can be suitably applied to the problems of arches under symmetrical load.

CONCLUSION

The results of tests on steel, reinforced concrete, and plain concrete arches were reported. Various aspects of the collapse behaviour are



Flow chart for calculating the collapse load of plain concrete arch symmetrically loaded.

Figure A1.16

discussed and related limit calculations are performed. The actual redistribution of moments and the collapse load can differ significantly from plastic limit theory. The differences are due mainly to the limited redistribution of moment in the arches, particularly reinforced concrete arches. Deflexion is another major factor for the discrepancies between theory and observed behaviour; however a second order rigid-plastic analysis (which includes deflexion effects) can usually be performed easily. Connection detailed designs are particularly important as they may cause major changes in the behaviour of the arches. In all, the tests provide an insight into the basic structural behaviour of steel, reinforced concrete, and plain concrete arches.

APPENDIX A2

YIELD LINE PATTERNS OF SLABS AND THE ROOF ANALOGY

INTRODUCTION

Three slabs of different dimensions and boundary conditions were tested under uniformly distributed load. The aims were to observe the collapse behaviour and to compare the yield line patterns with a proposed roof analogy.

GENERAL DESCRIPTION OF TEST SET UP AND EXPERIMENTAL PROCEDURE

The dimensions, support conditions, and details of the reinforcement of the slabs are given in Figure A2.1. All slabs are 25.4 mm thick; reinforcements are made of 1.6 mm diameter wire 25.4 mm spacing placed centrally both ways.

The uniform loading is provided by a rubber bag loaded with either air or water pressure. The pressure is measured with demountable pressure gauge; the total load on the slab is obtained from proving ring readings. A picture of the test set up is presented in Figure A2.2(a).

Deflexions were measured with dial gauges. Strains were measured with electric strain gauges. The strain readings were difficult to interpret due to the presence of cracks.

OBSERVED COLLAPSE BEHAVIOUR

Due to the high tensile strength of concrete and the light centrally placed reinforcement, it is difficult to tell whether the reinforcing steel has any influence on the behaviour of the slab.

Two types of cracks are formed. The major cracks which divide the slab into portions; extensive deflexion and rotations are observed along these cracks; they are usually termed the yield lines. With each region

divided by the major cracks, there are minor cracks which allow the slab to deflect to conform with the deformation pattern provided by the major cracks. The corner effects, i.e. the branching of the major cracks as they enter a corner, are also observed.

THE ROOF ANALOGY

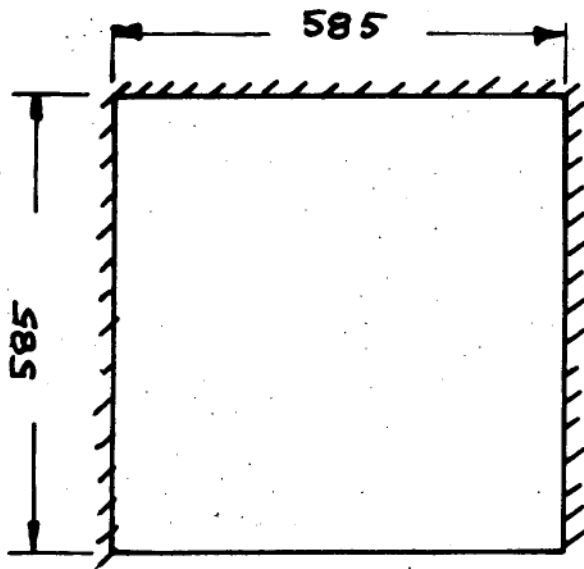
A simple way of picturing the yield line pattern is obtained from the following roof analogy.

The slab is considered as the area to be covered by a roof. A supported edge of the slab is equivalent to a side of the roof with rain gutter. A free edge is equivalent to a side of the roof without rain gutter. A column support is equivalent to a down pipe.

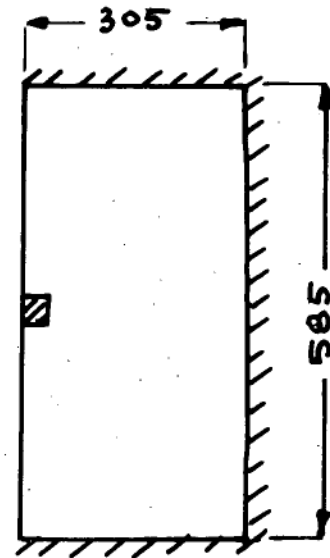
If a roof pattern is devised so that the rain water can flow down the prescribed way, then the projection of the ridges is a possible yield line pattern.

COMPARISON OF YIELD LINE PATTERNS AND ROOF ANALOGIES

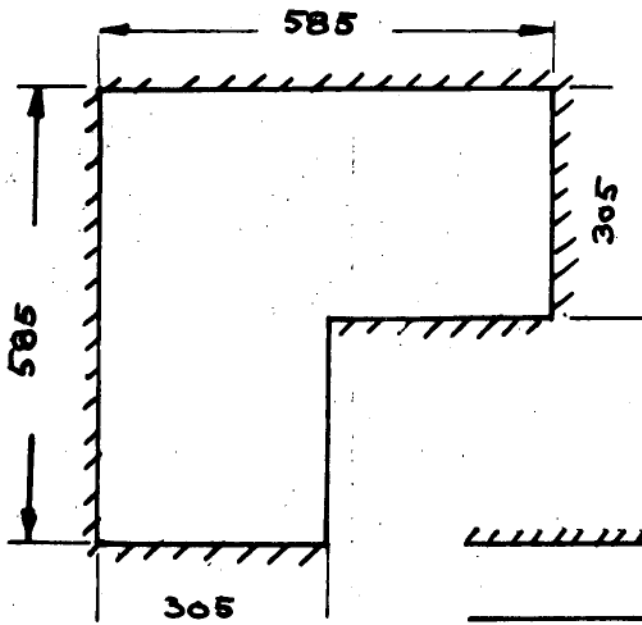
Figure A2.4 presents the roof patterns and the corresponding yield line patterns of the three tested slabs. Figure A2.2(b), Figure A2.3(a) and Figure A2.3(b) show the actual yield line patterns. The overall agreement is fairly good. A major difference is found in Slab No. 3 where a circular yield line is obtained around the column support instead of the predicted square pattern. However, the former can be considered as a limiting case of the latter (Ref A2.1).



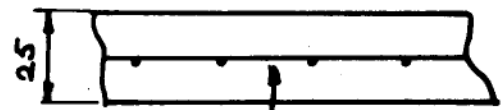
Slab N°1



Slab N°3



Slab N°2



square mesh 1.6 dia. wire
25 spacing

Simply supported edge

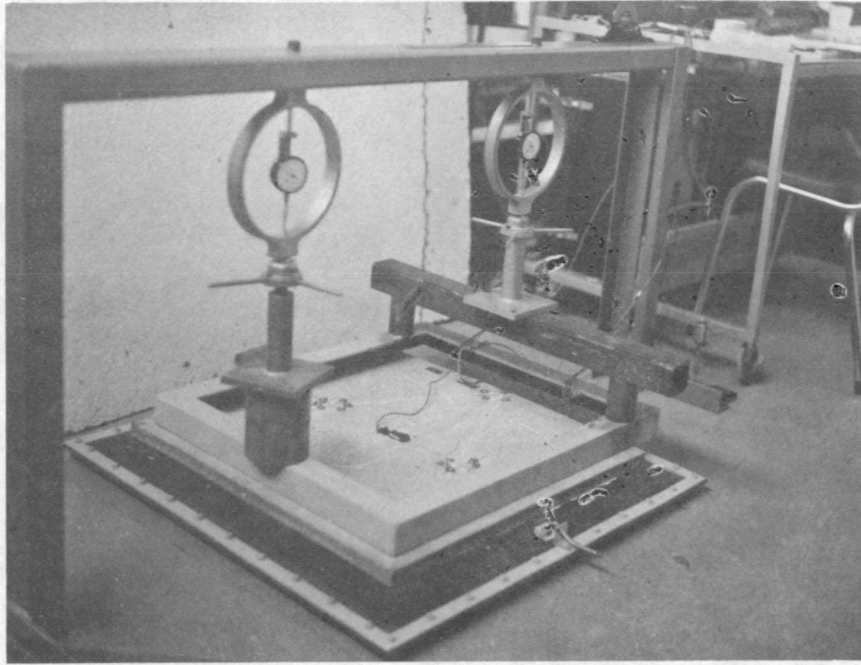
Free edge



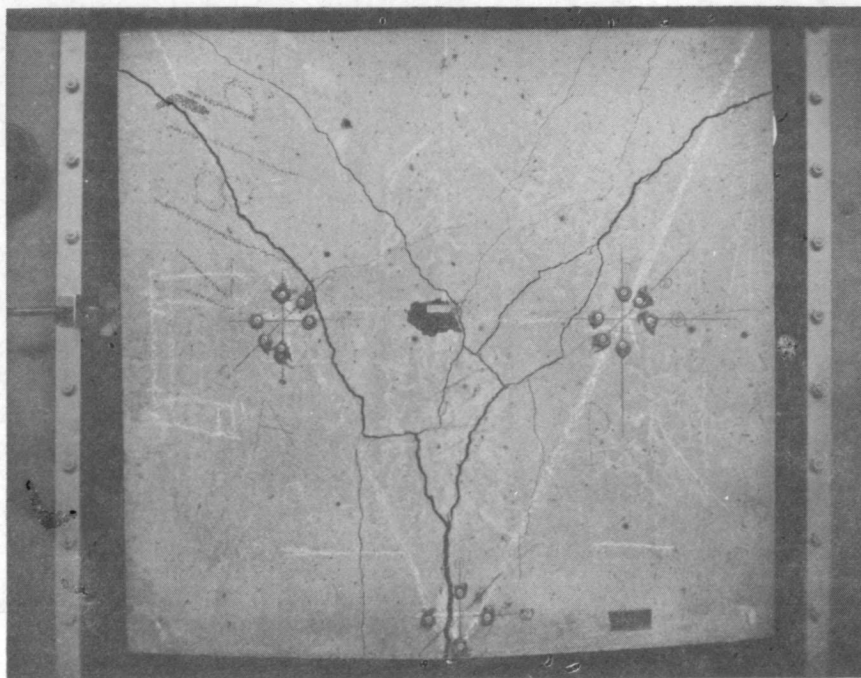
Column

All dimensions are in mm.

Figure A2.1

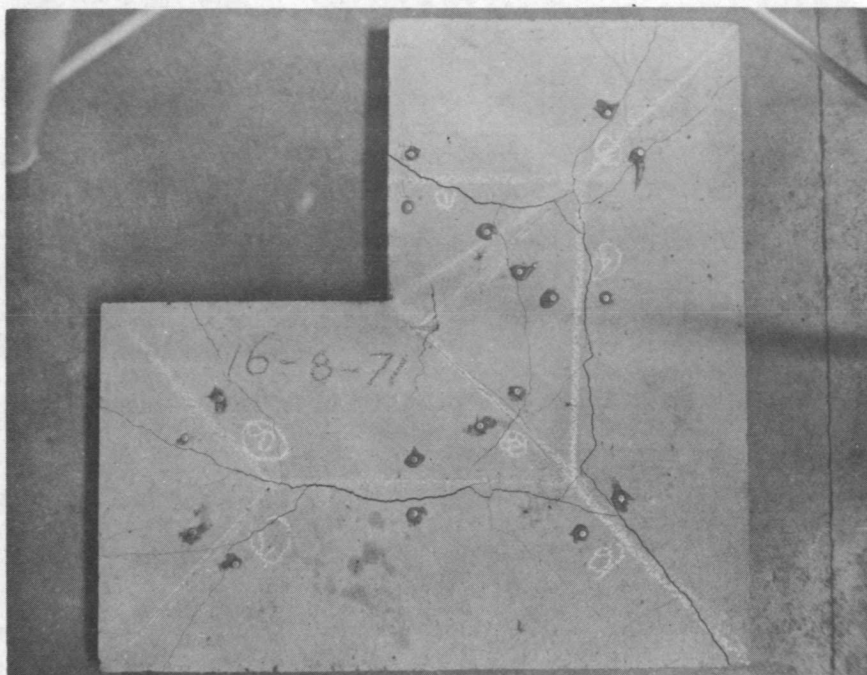


(a) General set up for the testing of slabs.

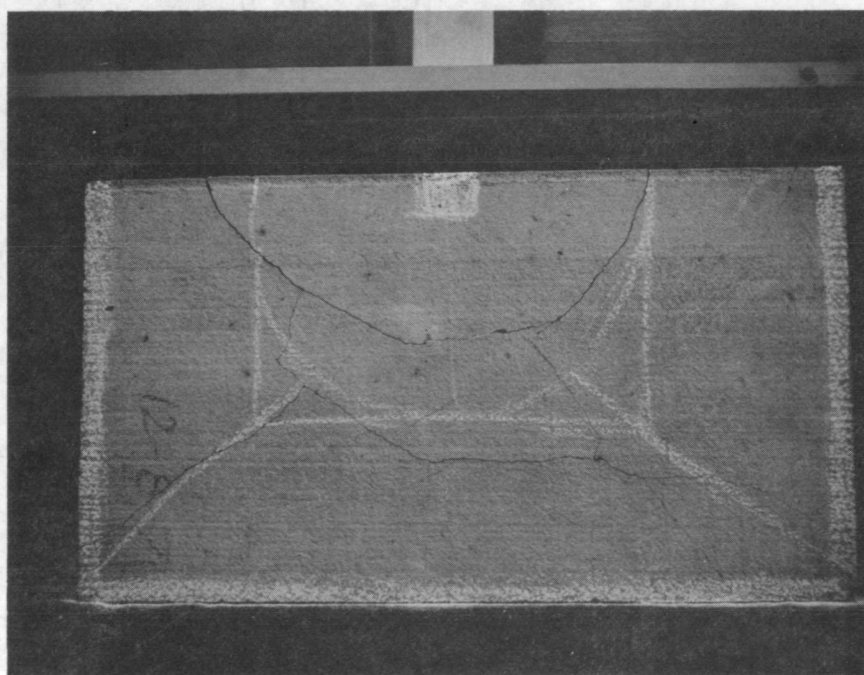


(b) Failure pattern of Slab No. 1.

FIGURE A2.2



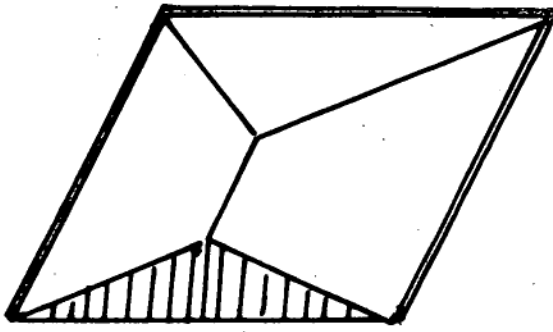
(a) Failure pattern of Slab No. 2.



(b) Failure pattern of Slab No. 3.

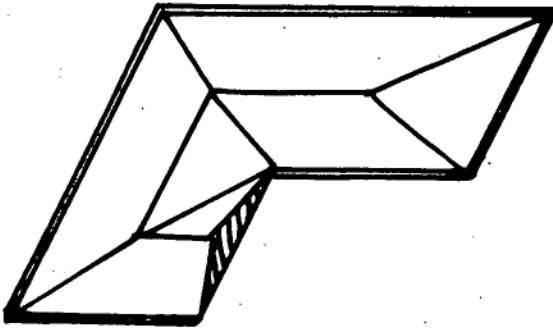
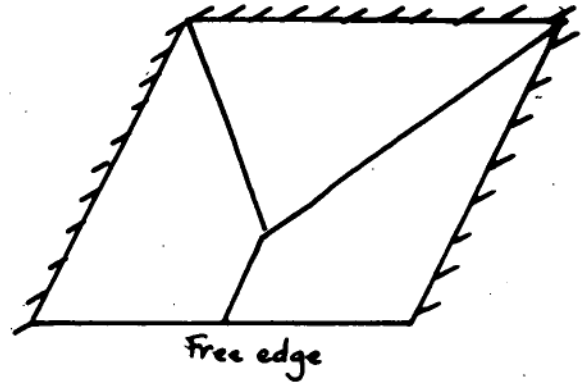
FIGURE A2.3

Roof Patterns

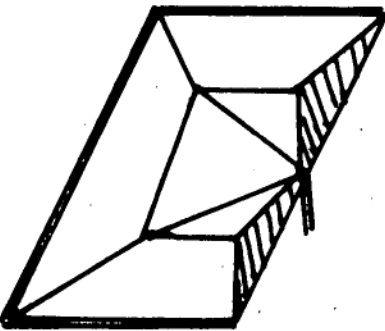
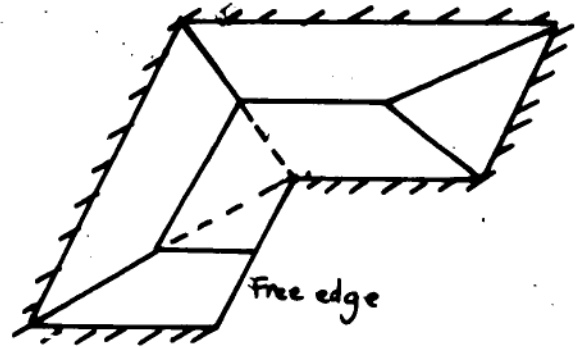


Slab N°1

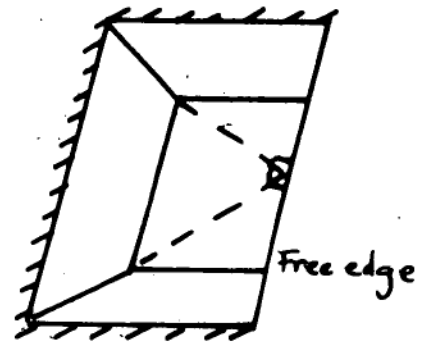
Yield Line Patterns



Slab N°2



Slab N°3



== Gutter

|| Down pipe

Vertical face

Simply supported edge

□ Column

Figure A2.4

APPENDIX A3

TEST OF A SHELL AND RELATED CALCULATIONS

INTRODUCTION

A concrete circular cylindrical shell supported on three sides was tested under uniform radial loading condition. The test was performed as a preliminary step in the investigation of the strength of shell structures in general, and of arch dams in particular.

GENERAL DESCRIPTION OF TEST SET UP AND EXPERIMENTAL PROCEDURE

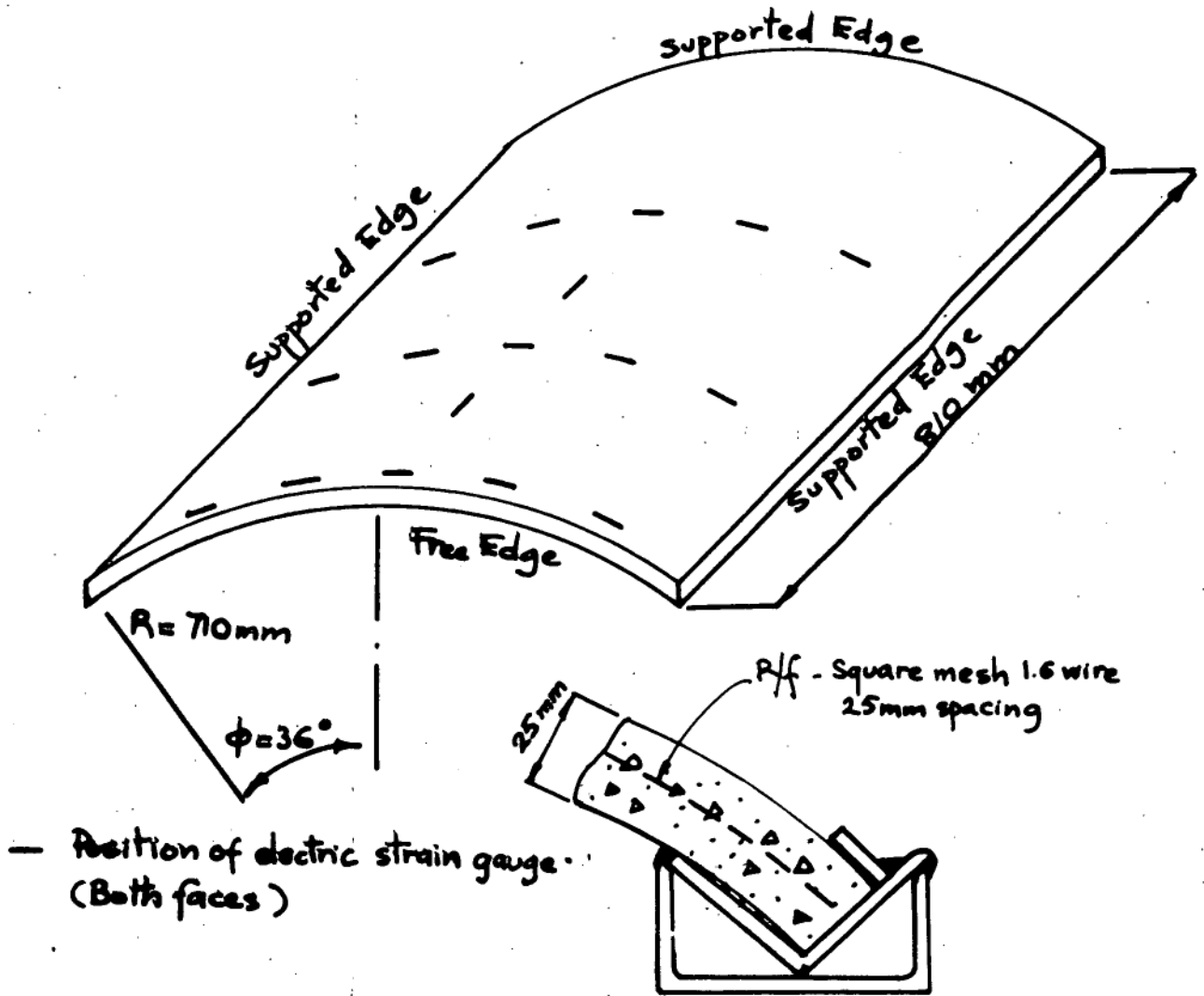
The dimensions and the supporting conditions of the shell are presented in Figure A3.1(a). The shell is 25.4 mm thick; reinforcements are made of 1.6 mm diameter wire, 25.4 mm spacing placed centrally both ways.

The general arrangement of the test set up is sketched in Figure A3.1(b). The uniform radial pressure is provided by a curved rubber bag, especially designed for the test, loaded with water pressure. The pressure is measured with demountable pressure gauge; the total load on the shell is measured with four proving rings placed at four corners of the supporting frame. A picture of the test set up is presented in Figure A3.2(a).

Deflexion was measured with dial gauges placed at various positions along the crown of the shell. Strains on the concrete were measured with electric strain gauges placed on both faces of the shell, Figure A3.1(a).

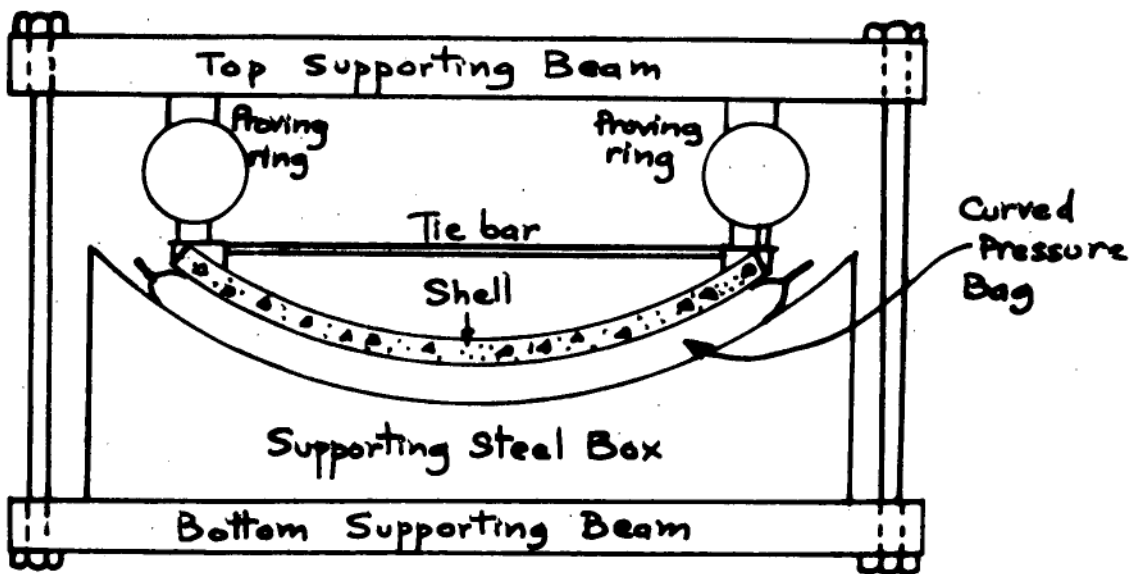
OBSERVED BEHAVIOUR

The high tensile strength of concrete and the light reinforcement made it difficult to assess the effects of the reinforcement on the behaviour of the shell. The exact supporting condition was not known; fully hinged restraint was originally intended but it was observed



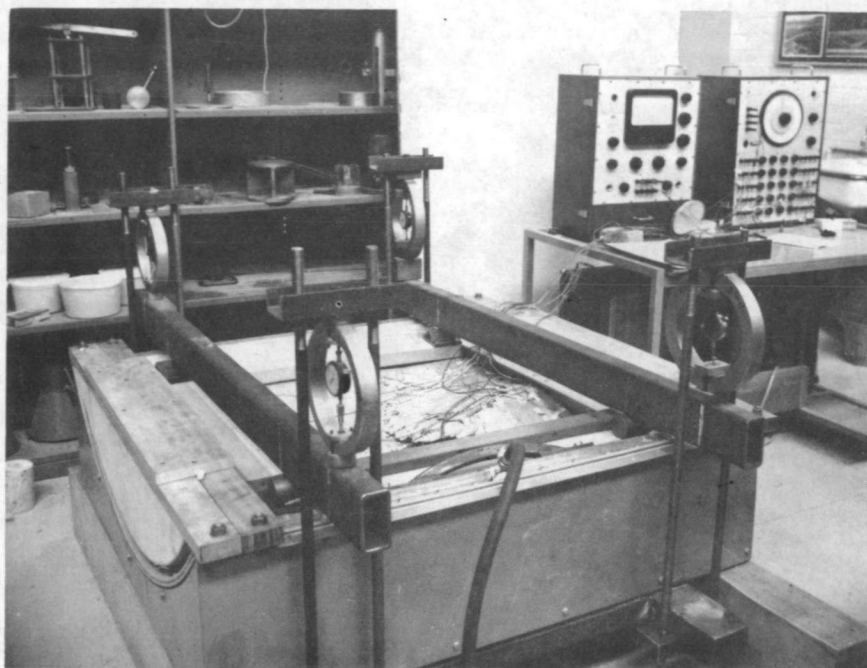
Details of shell support arrangement

(a)
Details of shell model.

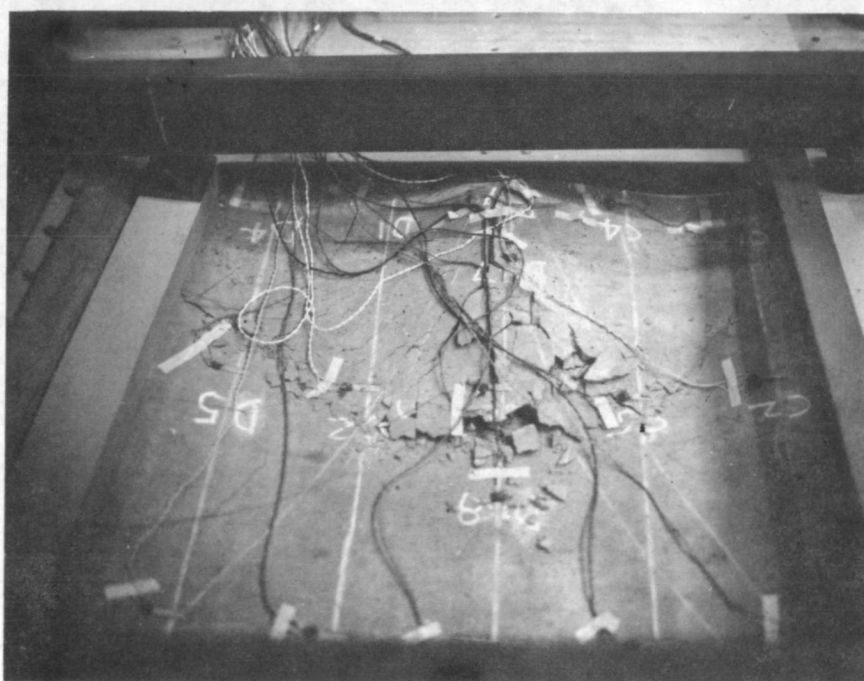


(b)
Loading Arrangement.

Figure A3.1



(a) General set up for the testing of a shell under uniform radial load.



(b) Picture of shell after collapse.

FIGURE A3.2

subsequently that partial sliding actually occurred.

The load-crown deflexion graph is presented in Figure A3.4. At low pressure (under 60 kPa), there was no crack and the shell behaviour was elastic and repeatable. The pressure was taken up to 60 kPa, then reduced to zero three times. Consistent readings of deflexions and strains were recorded. As the load increased, the behaviour became non-linear. Cracks were formed and the movements of the support observed. Sketches of cracking patterns are presented in Figure A3.3 for various loading levels. The cracks originated from the straight edges and were thought to be caused by the deformation of the supporting rig. There was crushing of the concrete at the crown and the supports in the transverse direction at high pressure. The final collapse was sudden, the upper part of the shell (near the free edge) caved in; the instability was caused by extensive crushing of concrete and large deflexion. A picture of the collapsed shell is presented in Figure A3.2(b). The ultimate pressure was 138 kPa.

CALCULATIONS

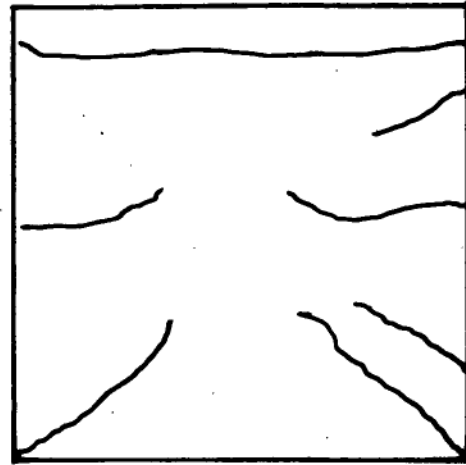
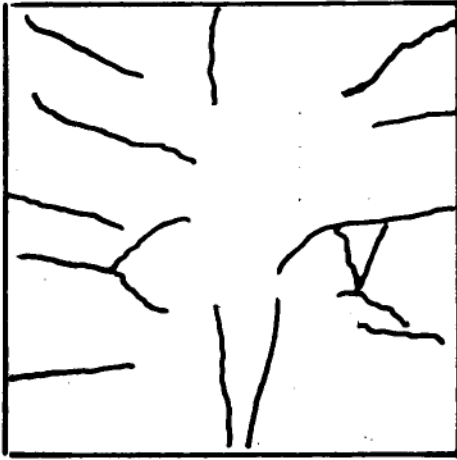
Calculations were done on the basis that the steel reinforcement had no influence on the load-carrying capacity.

For the uncracked state, an elastic analysis by Finite Element method, (Ref A3.1), represented by the line OA in Figure A3.1, shows fairly good agreement with the measured data (Ref A3.1).

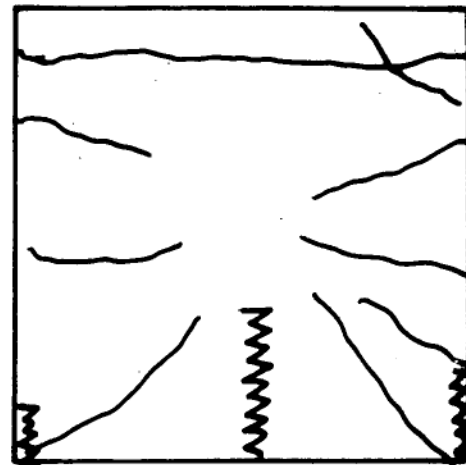
For the ultimate loading test, it was observed that the supporting rig had been deformed permanently and the edge conditions had changed from hinge to free to slide. An approximate elastic-plastic analysis of the shell following the line suggested in the next section was performed, and the results represented by the line OCD in Figure A3.4.

FREE FACE

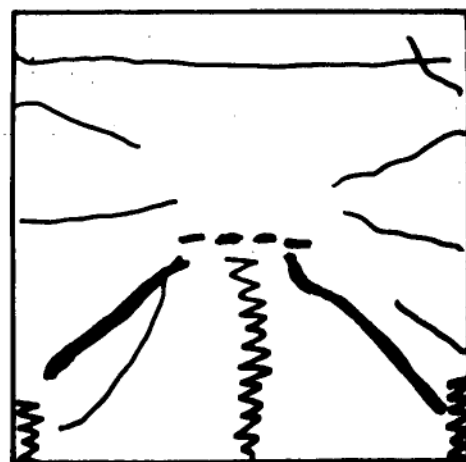
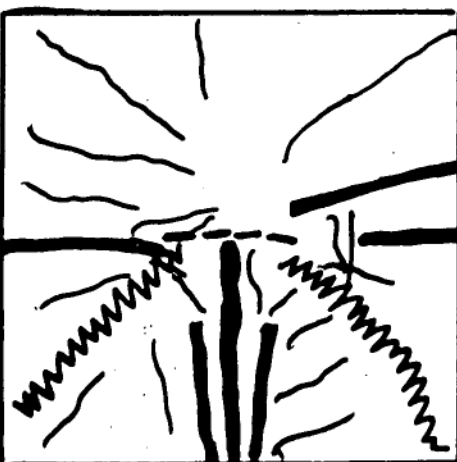
LOADED FACE



Cracking pattern at 75 kPa



Cracking pattern at 120 kPa



Cracking pattern at 138 kPa

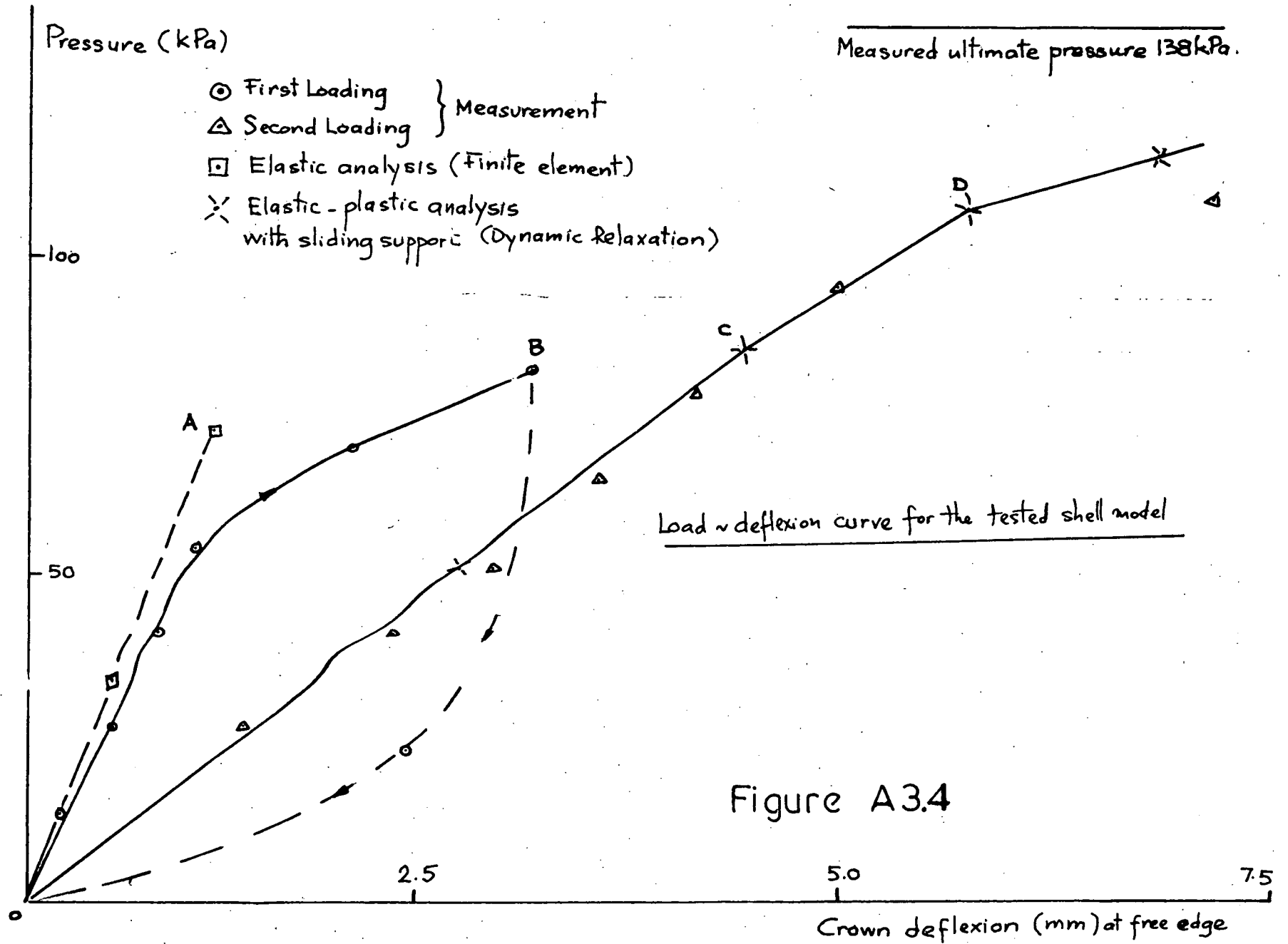
— Fine Crack

— Major Crack

MMM Crushing zone

---- Shearing zone

Figure A 3.3



APPROXIMATE ELASTIC-PLASTIC ANALYSIS OF CYLINDRICAL SHELL UNDER RADIAL LOADS

Following Tolke's simplified method of elastic analysis of arch dams (Ref A3.2), the following approximate elastic-plastic analysis of cylindrical shell under radial loads is proposed. The method is most suitable for the analysis of arch dams.

The shell is divided into a series of horizontal arches. The arches are assumed to resist the radial loads elastically until the combined axial thrust and bending moment reach the combined failure condition; then it is assumed that the arch will not take any further extra load. The failure condition for the concrete arch section is

$$N_{max} = 0.85 f'_c \cdot c \quad ; \quad M_{max} = 0.85 f'_c \cdot c \cdot (42 - d2) \quad ;$$

where c is the width of compressive part of the section and t is the section thickness (Fig A3.5). The crown deflexion of an arch w_c under uniform radial pressure p is proportional to the pressure $p = K \cdot w_c$

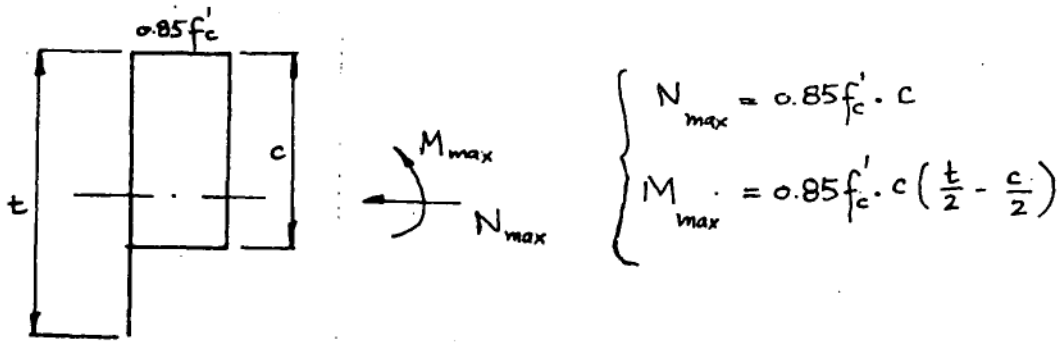
The factor K is found from elastic theory of arches (Ref A3.3). K can be made to accommodate various boundary conditions including the changing shape of the supports (triangular, rectangular, trapizoidal, etc...), the deformation of the support, and the degree of fixity at the shell edges. The factor K can be different for different slices of the shell.

Consider a strip of unit width along the crown of the shell in the vertical direction. This strip is imagined as being placed on a non-uniform elastic foundation provided by the arches, and is analysed as such. The strip is assumed to be elastic and to carry its loads by bending moment until the failure condition is reached. For a concrete section, the failure condition is

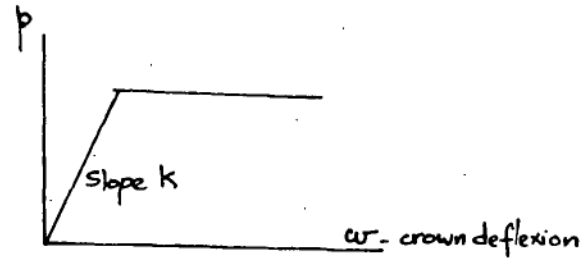
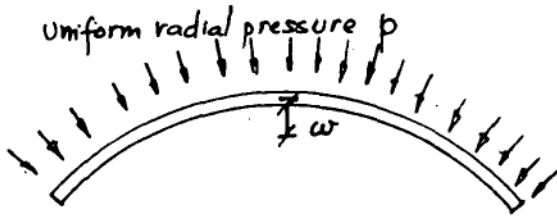
$$M_{max} = 0.85 f'_c \cdot t^2 / 8$$

where t is the shell thickness.

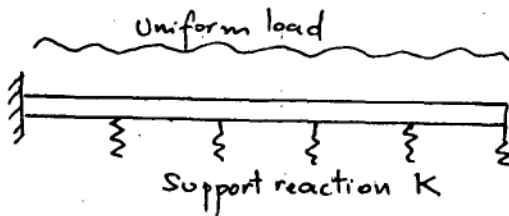
The analysis of the shell is thus reduced to the analysis of a strip



Assumed failure condition for a concrete section

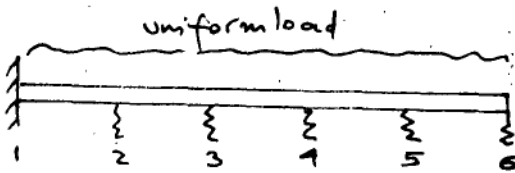


Assumed $p \sim w$ relation for individual arch slice



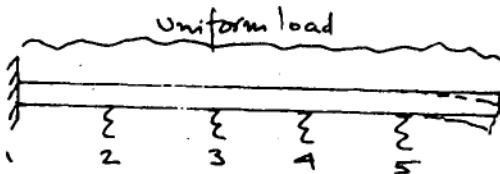
$$\begin{cases} E = 2 \times 10^6 \text{ kg/cm}^2 \\ t = 25 \text{ mm} \\ R = 710 \text{ mm} \end{cases} \left\{ \begin{array}{l} \text{From elastic arch theory} \\ K = 550 \text{ kPa/mm} \end{array} \right.$$

Beam equivalent of the tested shell model



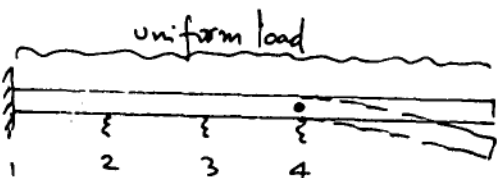
Stage 1 - All arches are elastic

$$p_{max} = 82.7 \text{ kPa}$$



Stage 2 - Progressive failure of arch slices starting from the free edge

$$\Delta p = 25.9 \text{ kPa} \\ (\text{for all arch slices from 5-6})$$



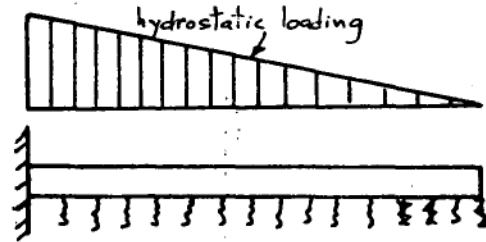
Stage 3 - Max. moment reached at position 4

$$\Delta p = 23.7 \text{ kPa}$$

Final collapse pressure $p_{max} = 132.3 \text{ kPa}$

Figure A3.5

"Elastic-plastic" calculation for the tested shell model

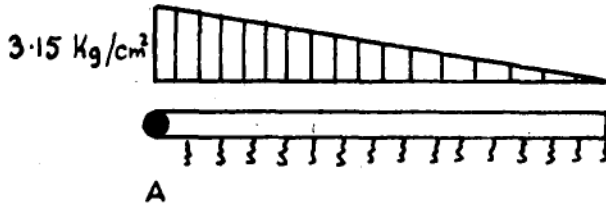


Elastic Support $K = 54.8 \text{ Kg/cm}$
Equivalent Beam for Bustamente's model arch dam I.

Bustamente's model II (Chapter VI)
Fig. 6.10

$$E = .21 \times 10^6 \text{ Kg/cm}^2$$

$$t = 18 \text{ cm}$$

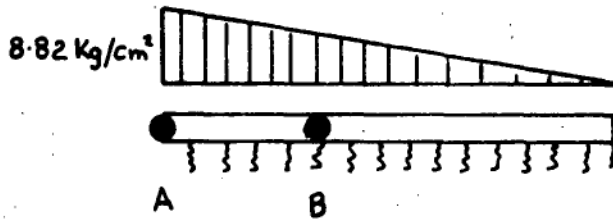


End of stage 1

$$M = M_{\max} \text{ at base}$$

$$p_1 = 3.15 \text{ Kg/cm}^2$$

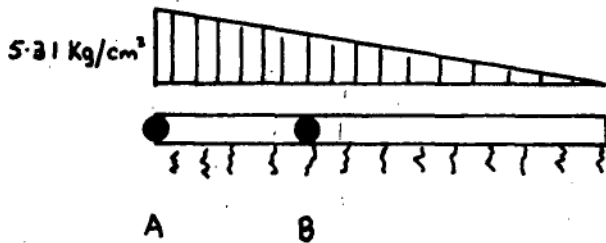
All arches still elastic



End of stage 2

$$M = M_{\max} \text{ at A and B}$$

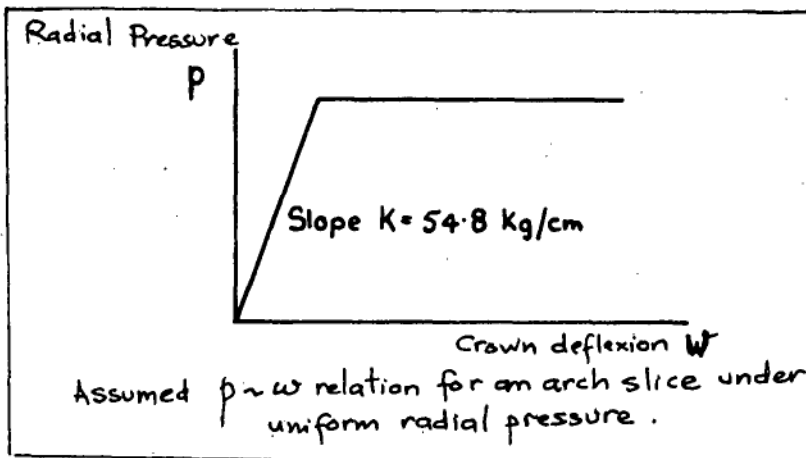
$$p_2 = 8.82 \text{ Kg/cm}^2$$



End of stage 3

Arch slice at B reaches its ultimate capacity

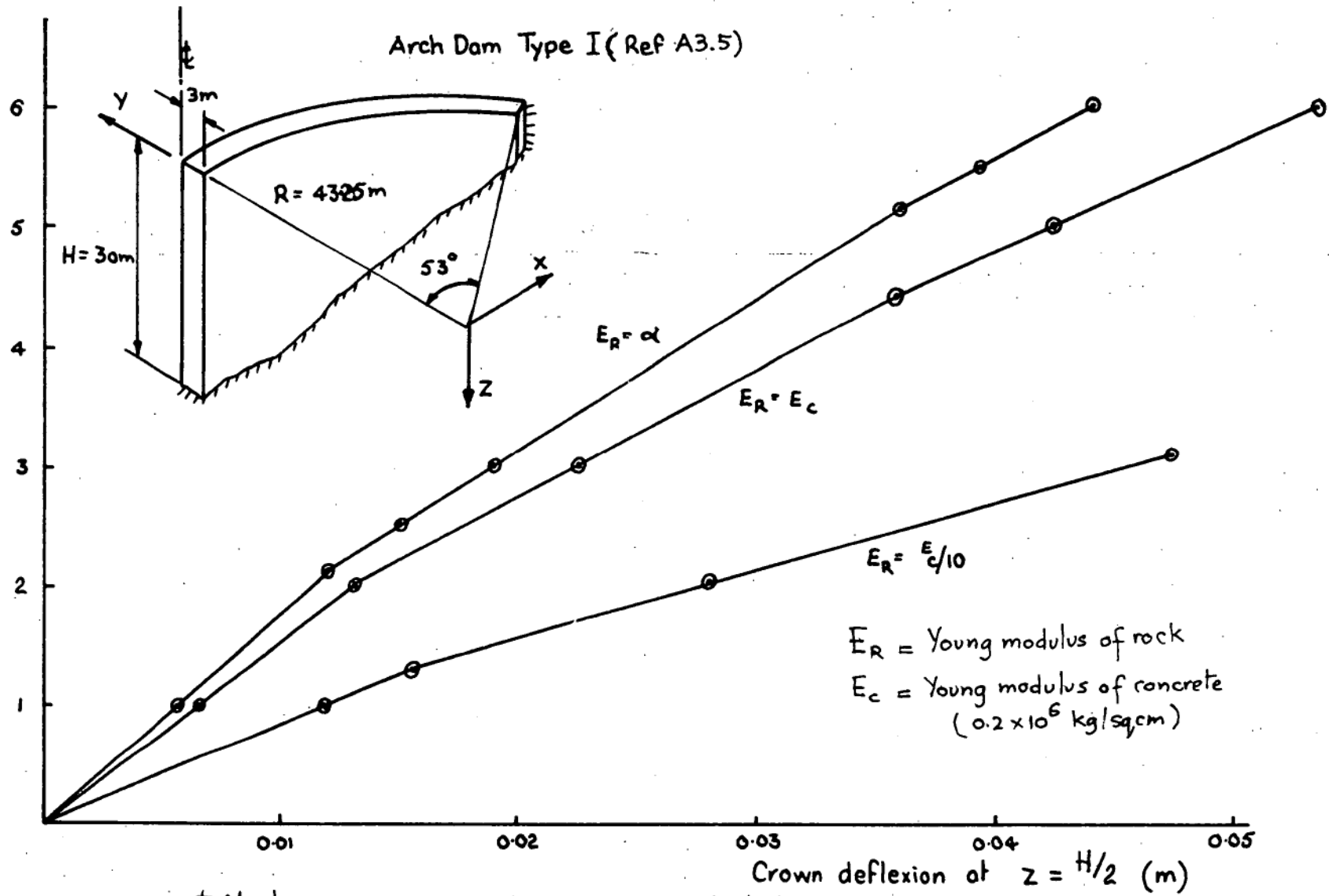
$$p_3 = 5.31 \text{ Kg/cm}^2$$



$$\text{Total } p_{\max} = 17.37 \text{ Kg/cm}^2$$

Figure A3.6
"Elastic-plastic" calculation for Bustamente's model arch dam

Factor of full water load



Effects of varying rock modulus on the behaviour of arch dam.

Figure A3.7

on elastic foundation. The deflexion of the strip at a particular level determines the pressure which acts at that level. The magnitude of the thrusts and moments are determined from the value of the pressure, using the elastic theory of arches. With increasing load, either the vertical bending moment in the strip at a section reaches its ultimate value (a hinge is then formed at that section) or the combined bending and thrust on an arch section reach the failure condition (the 'elastic' support is then considered as absent for any further increase in load).

The calculations are performed in the following order:

- (i) the elastic analysis of all arch slices to determine the arch stiffness factors at the crown using elastic arch theory.
- (ii) the analysis of the beam on 'elastic' support. This analysis can be done either analytically or numerically. Due to the changing properties of the sections, it is best to use a numerical technique such as Finite Element or Dynamic Relaxation to solve the problem.

The calculations for the tested shell model are summarized in Figure A3.5. It is seen that despite the drastic simplification made, the results agree fairly well with the measured data.

Similar calculations are performed for the Bustamente's arch dams model (Ref A3.4 and Chapter VI). The results are summarized in Figure A3.6.

One of the advantages of the proposed method is that it can be used to assess the load-carrying capacity of arch dams with elastic abutment. One of such analysis is performed for the arch dam type I (Ref A3.5), the results are presented in Figure A3.7.

CONCLUSION

Test of a shell with boundary conditions similar to those of an arch dam under uniform radial loads is presented. An approximate elastic-plastic method of analysing such a shell is proposed. The method is then used to analyse some arch dams with rigid and elastic abutments.

SUPPLEMENTARY NUMERICAL STUDIES

APPENDIX B1

DYNAMIC RELAXATION TREATMENT OF DEFLEXION
IN ELASTIC-PLASTIC FRAMED STRUCTURES

SUMMARY

Deflexions of framed structures loaded into the elastic-plastic range can be estimated using the technique of dynamic relaxation.

The calculation is made simple if a cubic function is used to describe the deformed shape of the frame element. The method differs from other methods in assuming that the yielded regions are spread out instead of being localized. The results are compared with those given by Heyman (Ref B1.4).

INTRODUCTION

Treatments of deflexions in elastic-plastic framed structures have been given by Symonds and Neal (Ref B1.1), Lee (Ref B1.2), Stevens (Ref B1.3) and Heyman (Ref B1.4). The treatment given below differs in assuming that the yielded regions are spread out instead of being localized at the hinges. Consequently there is no plastic hinge discontinuities. This assumption is supported by experimental observations as reported in Appendix A1. Localized deformation is dominant only when the ultimate load is reached. The use of dynamic relaxation technique allows the separation of equilibrium and geometrical conditions, and results in a very simple computing procedure. The results are in close agreement with other methods and experimental measurements.

FORMULATION OF THE METHOD

(a) Geometry. Consider the member AB in flexural action only (Figure B1.1). A cubic function is used to describe the deformation of the member:

$$w = ax^3 + bx^2 + cx + d$$

If the end rotations of the members are θ_A, θ_B , and the end deflexion w_A, w_B , the curvature expressions for the ends A and B are

$$\left. \begin{aligned} \kappa_A &= \left(\frac{d^2 w}{dx^2} \right)_{at A} = 4(\theta_A/l) + 2(\theta_B/l) + 6(w_A - w_B)/l^2 \\ \kappa_B &= \left(\frac{d^2 w}{dx^2} \right)_{at B} = 2(\theta_A/l) + 4(\theta_B/l) + 6(w_A - w_B)/l^2 \end{aligned} \right\} \dots\dots\dots (1)$$

(b) Moment - Curvature relation. Any established moment-curvature relation can be used. For simplicity the elastic-perfectly plastic moment curvature relation is used here.

$$\left. \begin{aligned} M_i &= (EI) \kappa_i \quad \text{for } \kappa_i \leq \kappa_y \\ M &= M_p \quad \text{for } \kappa_i > \kappa_y \end{aligned} \right\} \dots\dots\dots (2)$$

(c) Equilibrium. Both the equilibrium of the joints and the equilibrium of the members are considered. For frames which carry the loads mainly by bending moment, the equilibrium of the joints results in two sets of equations.

$$\left. \begin{aligned} \text{Sum of the moment at a joint } \sum M &= 0 \\ \text{Sum of the forces at a joint } \sum V &= 0 \end{aligned} \right\} \dots\dots\dots (3)$$

The equilibrium of each member gives the value for the end shears

$$Q_A = -Q_B = (M_A + M_B)/l \dots\dots\dots (4)$$

(d) Dynamic relaxation iterative procedure. The general scheme of calculation is given in the flow chart of Figure B1.2. One starts with an initial guess for the deformation of all joints, (w_i, θ_i) . Curvatures are computed from (1), end moments from (2), end shears from (4). Overall equilibrium check is given by (3). If equilibrium is not reached, the deformations are relaxed as in standard dynamic relaxation process and the calculation repeated until convergence is reached.

EXAMPLES

(a) Fixed end beam. The load-deflexion graph for a fixed end beam under one single point load is given by Figure B1.3 and is compared with that given by Heyman (Ref. B1.4). It is seen that the deflexion given by our method is less than that by Heyman's for the same load, the reason being the omission of hinge discontinuities. As observed by Gregory (Ref. B1.4) it is not possible to calculate the deflexion for a given load with any good agreement with the experimental results. The question is "At a given deflexion, what is the load that can be supported?". In this sense the two methods show fairly good agreement.

(b) Portal Frame. The portal frame, tested by Baker in Ref. B1.6 is analysed. The results are presented in Figure B1.4. The analysis used both elastic-perfectly plastic and elastic-strain hardening moment curvature relation. The agreement is fairly good.

CONCLUSION.

A simple method of estimating the deflexions of framed structures in the elastic-plastic range has been presented. The model used in the analysis allows the spreading of the yielded regions along the member length instead of localized hinges. It is noted that the two models (localized hinges or spread out yielded regions) are only approximations of the actual physical condition, which is perhaps somewhere in between. The developed model is useful in the analysis of concrete structures where unlimited hinge rotations are not possible, and tests have shown considerable spreading of the failure region.

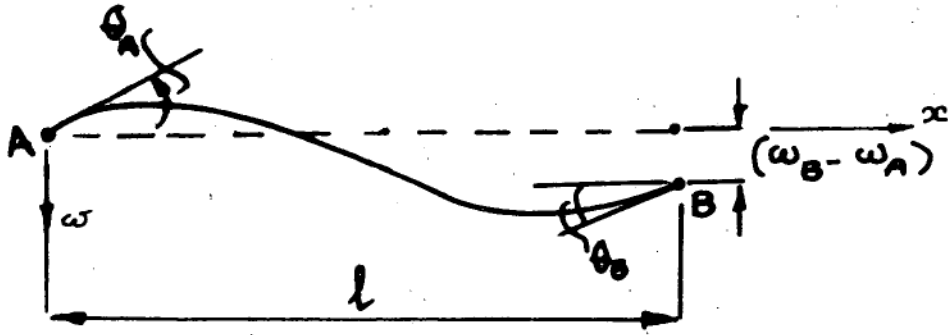


Figure Bl.1

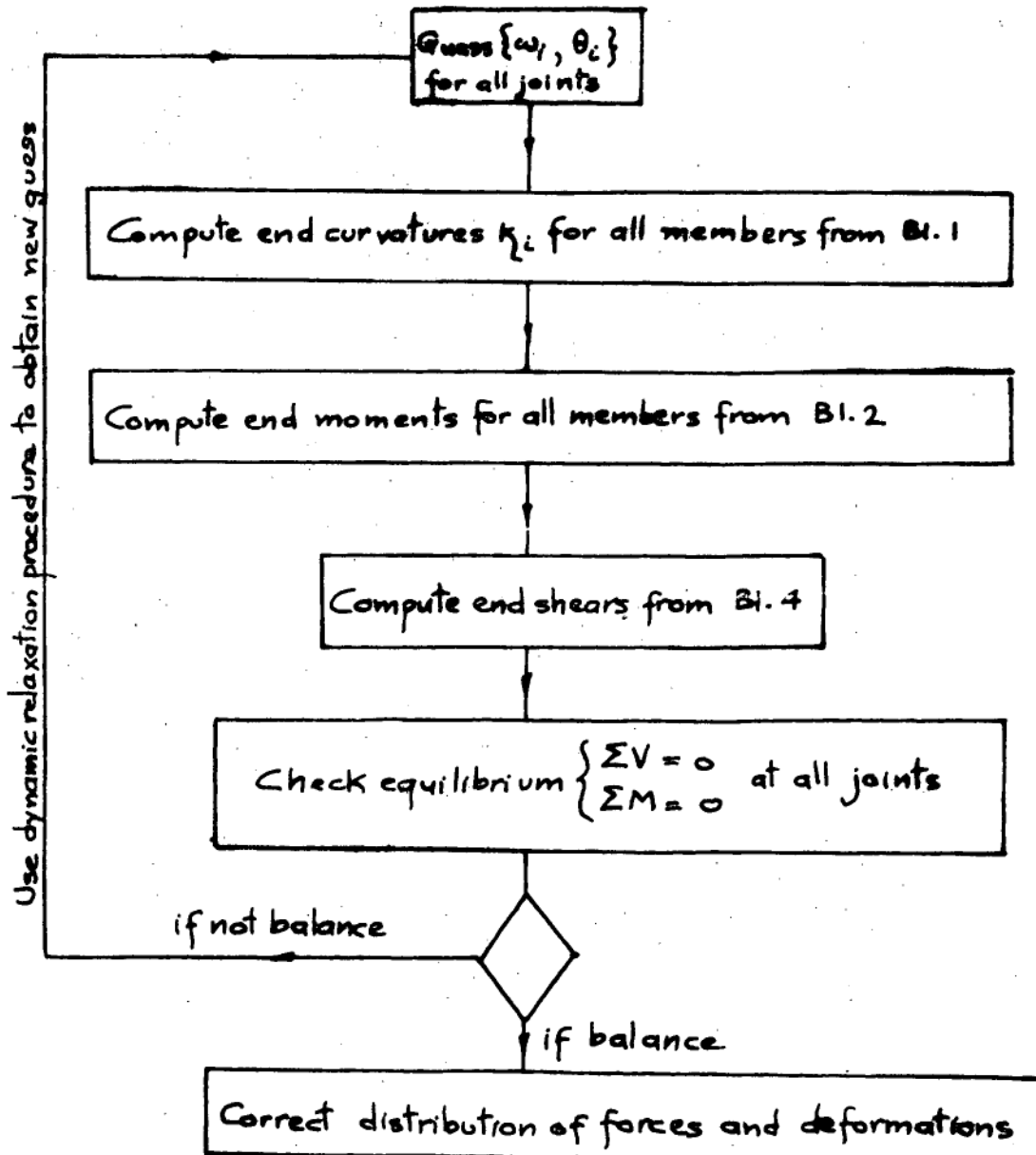


Figure Bl.2

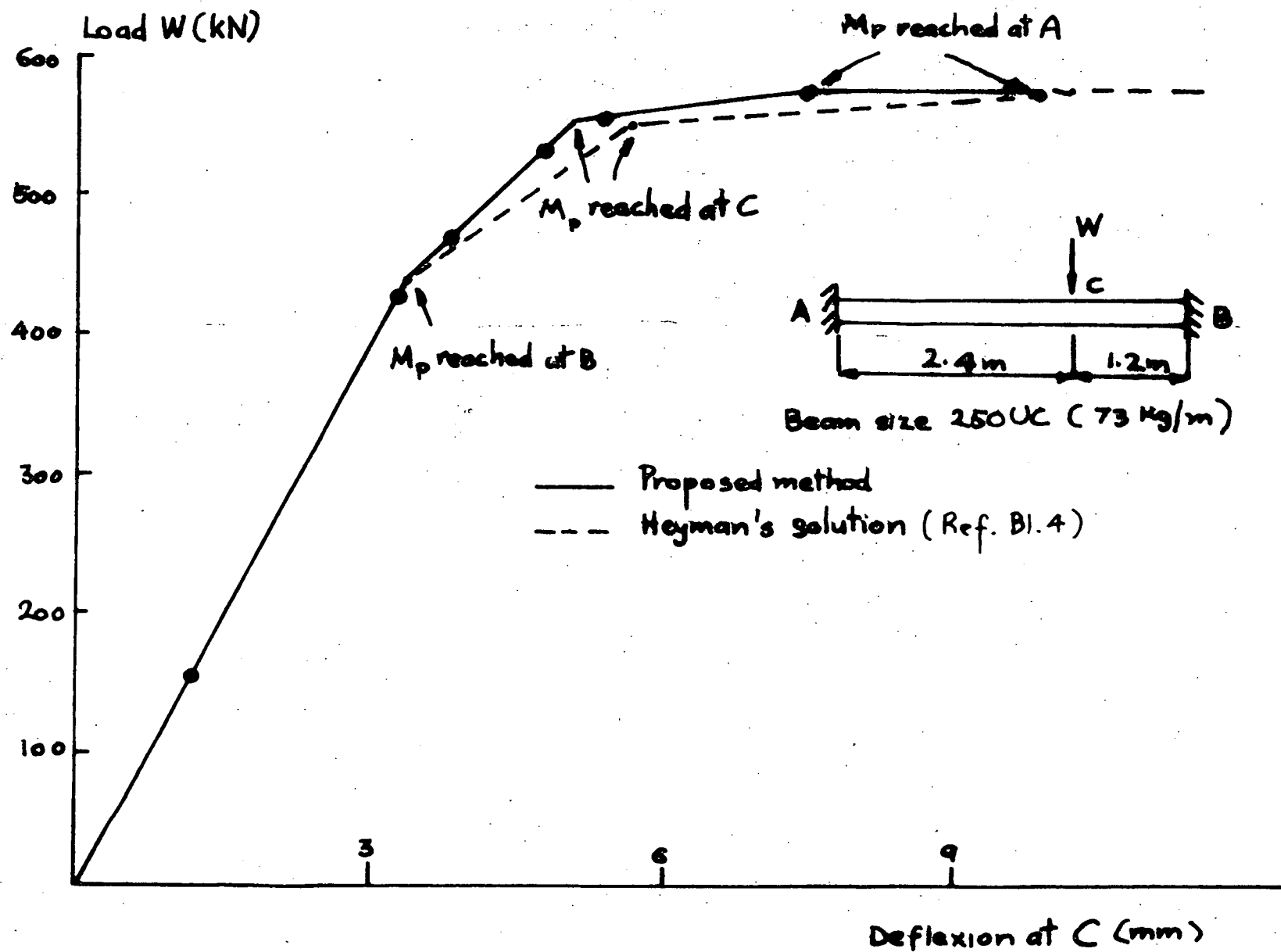


Figure Bl.3

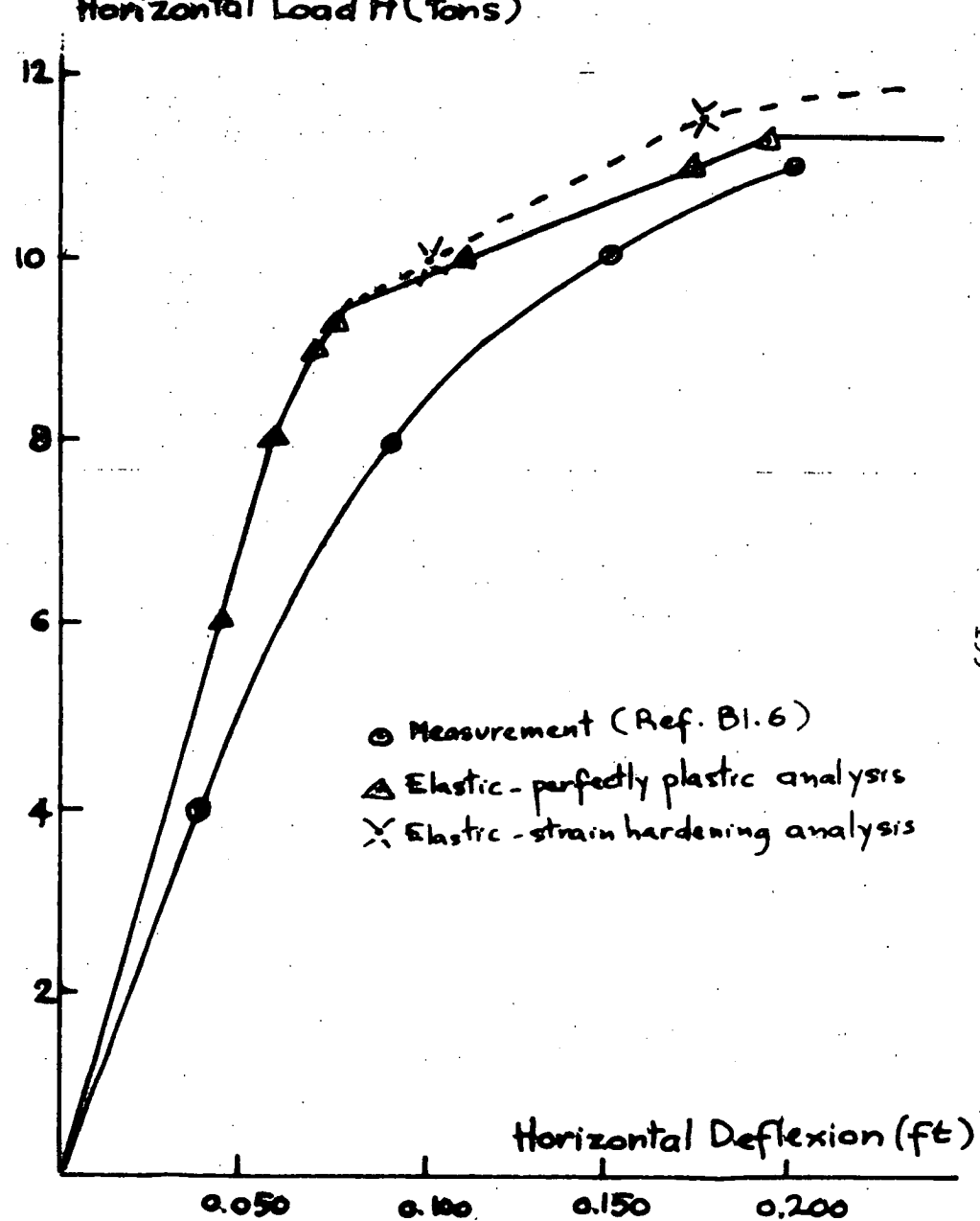
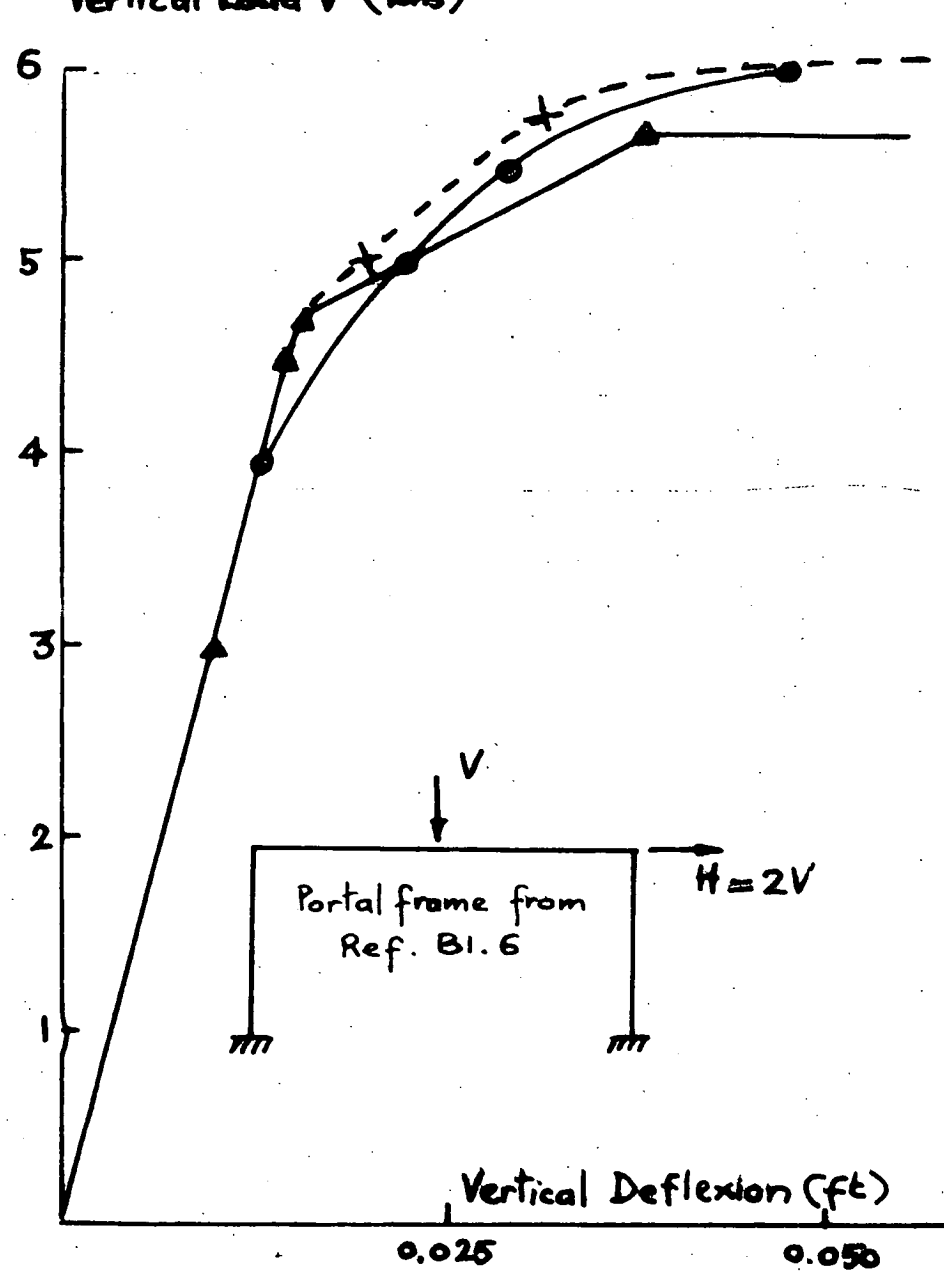


Figure B1.4

APPENDIX B2

DYNAMIC RELAXATION TREATMENT OF ELASTIC STABILITY

PROBLEMS IN OVERBRACED FRAMES

SUMMARY

A numerical study of the load-deformation behaviour of overbraced frames by the method of dynamic relaxation is presented. The results show that the major internal forces causing buckling in overbraced frames are not statically determinate and redistribute markedly as buckling deformations occur. The ordinary stability analysis of the Euler type is not adequate to describe the behaviour of such frames.

INTRODUCTION

The overbraced frame of Figure B2.1 is used to demonstrate the application of the method of dynamic relaxation to problems of elastic stability. The method is flexible, allowing for the inclusion of the effects of crookedness and prestrain. Dynamic relaxation uses a damping technique to solve a structural problem by a process of iteration between the equations of geometrical compatibility and the equations of equilibrium. The basis of the method has been fully explained by Otter et al (Ref B2.1) and will not be repeated here.

FORMULATION OF THE PROBLEM

The rigidly-jointed triangulated frame of Figure B2.1 has the internal axial force distribution (as yet unknown) as defined in Figure B2.2. To solve the problem iteratively, nine degrees of freedom are used to describe the deformation of the frame. They are six joint rotations and three mid-span displacements, Figure B2.3(a). The corresponding forces are moments at the ends of members M_1 to M_{18} , and shear forces at the ends of members Q_1 to Q_6 , Figure B2.3(b).

Only the elastic behaviour of the frame is studied. the general form of the moment-displacement relation for a straight member AB Figure B2.3(c) is

$$\begin{aligned} M_A &= (EI/l) \{ (S + SC)U/l + S\theta_A + SC\theta_B \} \\ M_B &= (EI/l) \{ (S + SC)U/l + SC\theta_A + S\theta_B \} \end{aligned} \quad \dots\dots\dots \text{B2.1}$$

where S, SC are the stability function coefficients (Ref B2.4) which depend on the axial force P in the member.

The equations of equilibrium are:

- (i) Sums of end of member moments equal to zero at joints 1 - 7.

$$\left. \begin{aligned} M_{2i} + M_{2i+1} + M_{i+3} &= 0 \quad i = 2, 4, 6 \\ M_{2i} + M_{2i+1} &= 0 \quad i = 1, 3, 5 \\ M_{12} + M_1 + M_{13} &= 0 \\ -M_{14} + M_{16} + M_{18} &= 0 \end{aligned} \right\} \dots\dots\dots \text{B2.2}$$

- (ii) Sums of forces normal to the member at joints 2, 4, 6 equal to zero

$$\left. \begin{aligned} Q_6 - Q_5 &= 0 \\ Q_4 - Q_3 &= 0 \\ Q_2 - Q_1 &= 0 \end{aligned} \right\} \dots\dots\dots \text{B2.3}$$

- (iii) The shear forces are obtained by taking moments of each member about its end.

$$\left. \begin{aligned} Q_1 &= [M_1 + M_2 - P_1(U_1^0 + U_1)]/(L/2) \\ Q_2 &= [M_3 + M_4 + P_1(U_1^0 + U_1)]/(L/2) \\ Q_3 &= [M_5 + M_6 - P_2(U_3^0 + U_3)]/(L/2) \\ Q_4 &= [M_7 + M_8 + P_2(U_3^0 + U_3)]/(L/2) \\ Q_5 &= [M_9 + M_{10} - P_1(U_2^0 + U_2)]/(L/2) \\ Q_6 &= [M_{11} + M_{12} + P_1(U_2^0 + U_2)]/(L/2) \end{aligned} \right\} \dots\dots\dots \text{B2.4}$$

where U_i^0 is the initial crookedness and U_i is the lateral displacement of the point i. Note that the last terms of equations B2.4 represent the non-linear effect of axial load on lateral displacement.

For compatibility calculations, it will be necessary to calculate the shortening of each member due to axial forces and bending moments.

The axial shortening, due to axial force P, is given by

$$\delta_a = P.L / EA \quad \dots\dots\dots B2.5$$

The bending shortening is given by

$$\delta_b = \frac{1}{2} \int_0^L \left(\frac{dy}{dx} \right)^2 dx$$

If the deformed shape of the member is assumed to be

$$y = A \sin(\sqrt{\rho} \pi x / L) + B \cos(\sqrt{\rho} \pi x / L) + Cx + D$$

where $\rho = P/P_E$ and A, B, C, D are constants to be determined from the

boundary condition: $(y)_{x=0} = (y)_{x=L} = 0$; $(dy/dx)_{x=0} = \theta_A$;

$(dy/dx)_{x=L} = \theta_B$; the bending shortening then becomes²

$$\delta_b = -(L/\pi^2) \left(\frac{1}{2} F_1(\theta_A^2 + \theta_B^2) + F_2 \theta_A \theta_B \right) \quad \dots\dots\dots B2.6$$

where F_1, F_2 can be shown to be the derivatives, with respect to ρ , of the stability functions S and SC respectively (Ref B2.2).

The total shortening of the member is then

$$\delta = \delta_a + \delta_b \quad \dots\dots\dots B2.7$$

For any external load W, the distribution of the axial forces in the frame are not known. However, if one is assumed, say P_3 (Fig B2.2), then the others can be deduced from statics, and hence the deformation of the whole frame can be calculated using equations B2.1 - B2.4.

If the frame is thought of as consisting of two parts, the star frame (inner part, Δ) and the delta frame (outer part, Δ), then the displacements Δ_1 and Δ_2 of point A relative to the line BC (Fig B2.4) of the two parts are compatible only if the correct values of axial forces distribution are used in the calculations. The values of Δ_1 and Δ_2 are given by

$$\begin{aligned}\Delta_1 &= 2\delta_1/\sqrt{3} - \delta_2/2\sqrt{3} \quad (\text{delta frame}) \\ \Delta_2 &= \delta_3 + 2\delta_4 - \delta_2\sqrt{3}/2 \quad (\text{star frame}) \quad , \quad \dots\dots\dots \text{B2.8}\end{aligned}$$

where $\delta_1, \delta_2, \delta_3, \delta_4$ are the total shortening of the members 1, 2, 3, 4 as shown in Figure B2.4.

The scheme of calculation is shown in the flow chart of Figure B2.5.

EFFECTS OF CROOKEDNESS AND PRESTRAIN

(i) Crookedness. Any required amount of crookedness can be imposed upon the frame by specifying the values of U_1^0, U_2^0, U_3^0 . Note that various modes of buckling can be stimulated by appropriate specification of the crookedness values.

(ii) Prestrain. Prestrain can be included as a set of constant forces which are in equilibrium with themselves without any external loading, Figure B2.6. Note that the values of crookedness and prestrain are not necessarily independent. If an attempt is made to specify them separately, the values of prestraining forces will alter the values of initial crookedness at no load.

SUMMARY OF RESULTS OF CALCULATION

Calculations for the first mode only are presented here. Figure B2.7 shows the effects of crookedness on the behaviour of a frame free of prestrain. Load-deformation graphs are shown for crookedness values of (a) $0.0625 \times 10^{-3}L$ (b) $0.0625 \times 10^{-2}L$ (c) $0.0625 \times 10^{-1}L$. It is clear that the behaviour does not follow the usual Euler type buckling behaviour of a pin-ended column. Obviously a Southwell plot cannot be used to obtain the buckling load.

Figure 8 shows the effect of prestrain upon frames with crookedness of $0.0625 \times 10^{-2}L$ and $0.0625 \times 10^{-1}L$. It should be noted that the amount of prestrain affects the onset of large deformation and therefore can be made beneficial or otherwise.

Figure B2.9 shows the distribution of internal forces at various levels of loading. It is seen that the distribution is linear at low load where the deformations are small but becomes non-linear at higher load where large deformations develop. The dotted curve gives the buckling load of the frame obtained by the usual Euler approach at various levels of distribution of axial forces. It is called the interaction curve (Ref B2.3). It is noted that as the internal force distribution becomes non-linear, it appears to head for the peak of the interaction curve.

CONCLUSIONS

- (i) The behaviour of overbraced frames cannot be described by the usual Euler-type stability analysis. The reason is that the internal forces causing buckling are not statically determinate and redistribute markedly as buckling deformations develop. (Euler-type analysis always assume that the distribution of internal forces causing buckling remains constant at all level of loadings.)
- (ii) Initial crookedness has large effects on the behaviour of the frame. Large crookedness cause the redistribution of internal forces to occur earlier.
- (iii) Prestraining forces control the onset of large deformation. Their effects can be predicted in any particular case.
- (iv) If the frame remains elastic, it appears that the ultimate buckling load is independent of both crookedness and prestrain and is given by the peak of the interaction curve.
- (v) In any real frame, due to the large deformation, the frame will probably yield well before the ultimate elastic buckling load is reached. It is, therefore, necessary to study the whole load-deformation behaviour of the frame in the manner carried out above. It may also be noted that the effect of yielding can be included in the above scheme of calculation without difficulty.

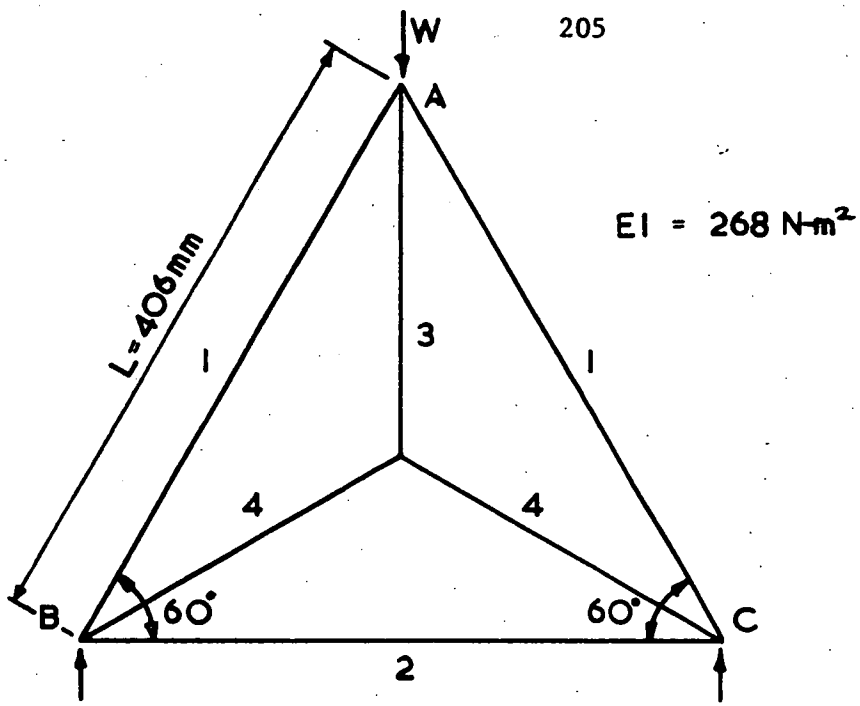


Figure B2.1

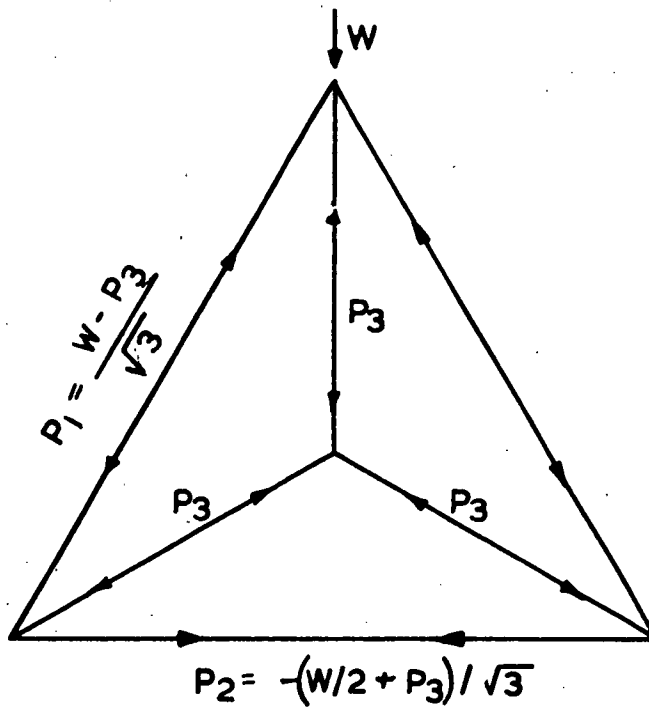


Figure B2.2

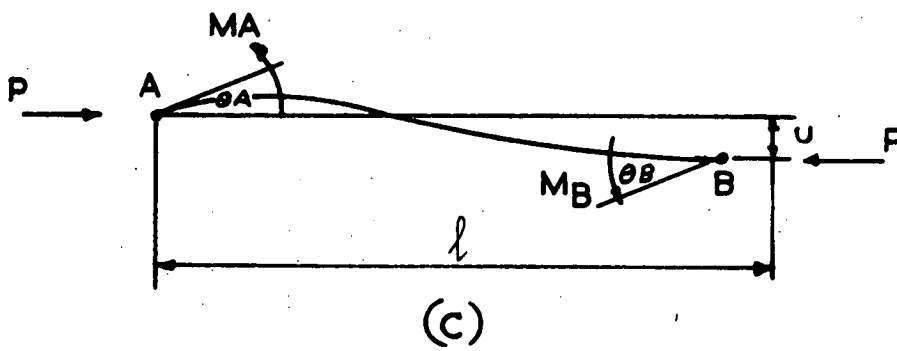
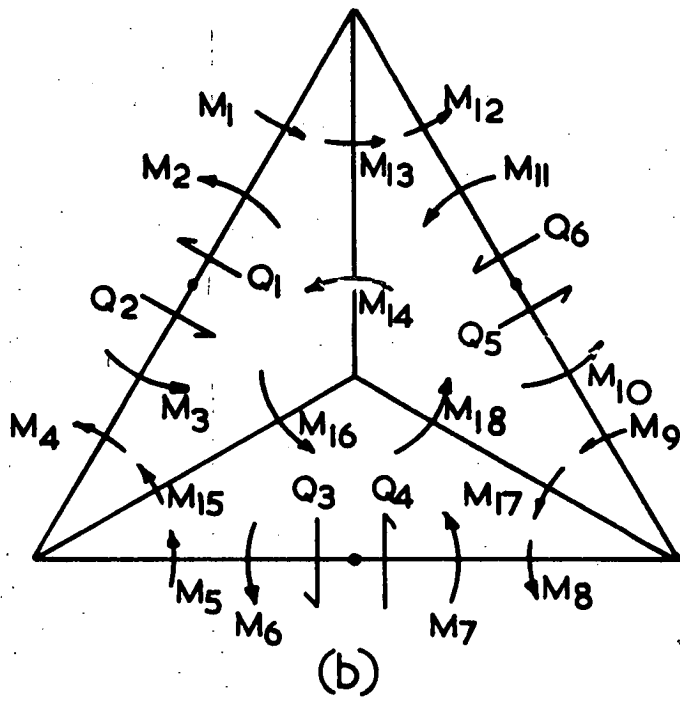
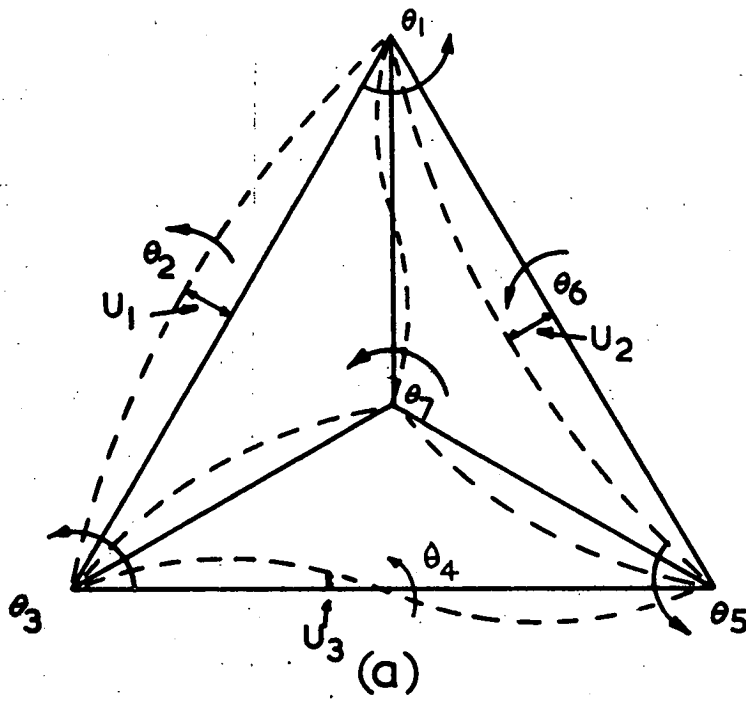


Figure B2.3

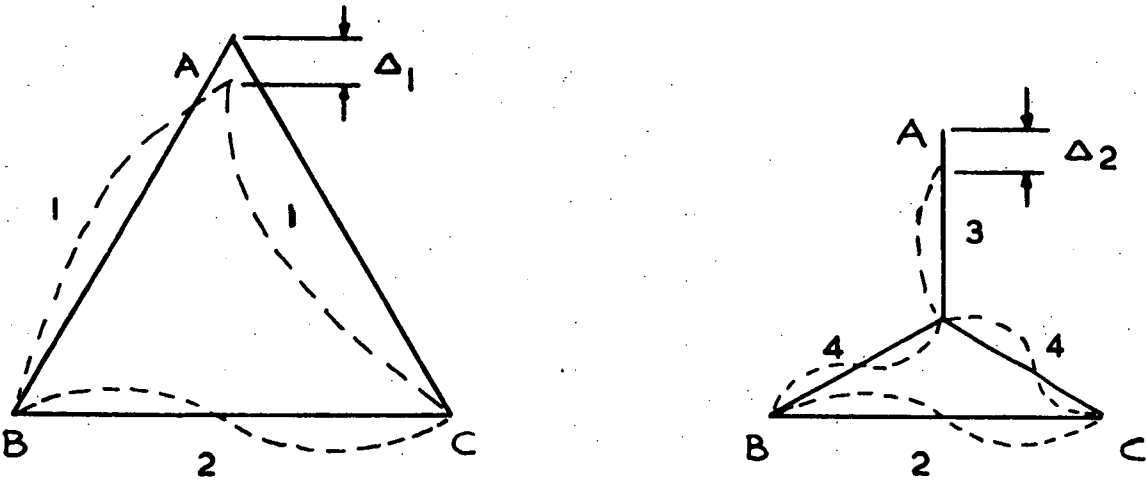


Figure B2.4

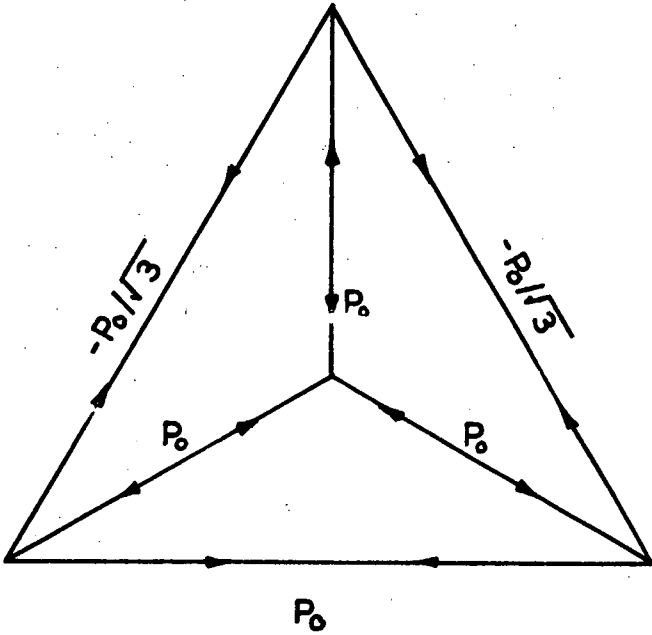


Figure B2.6

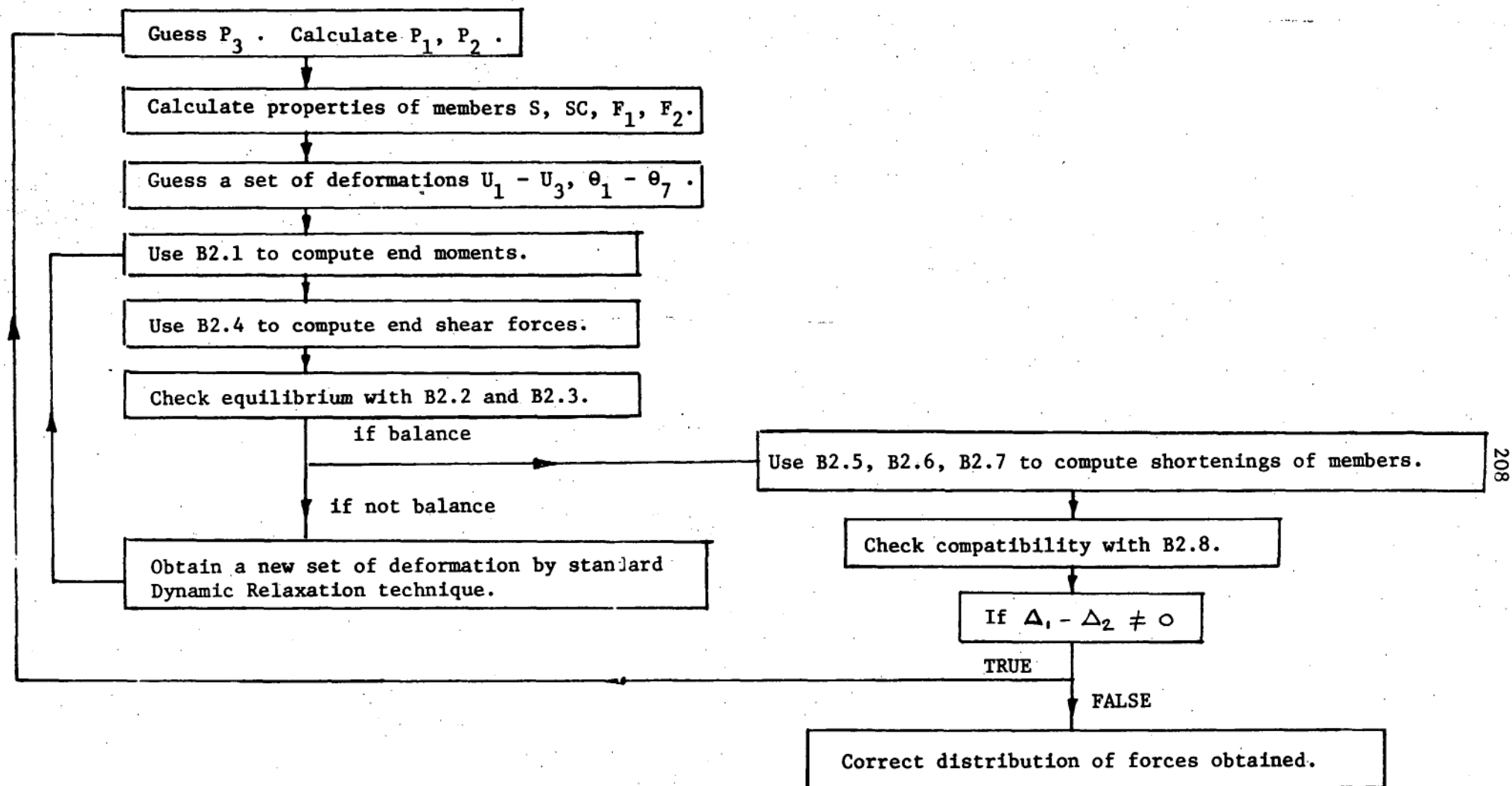


Figure B2.5

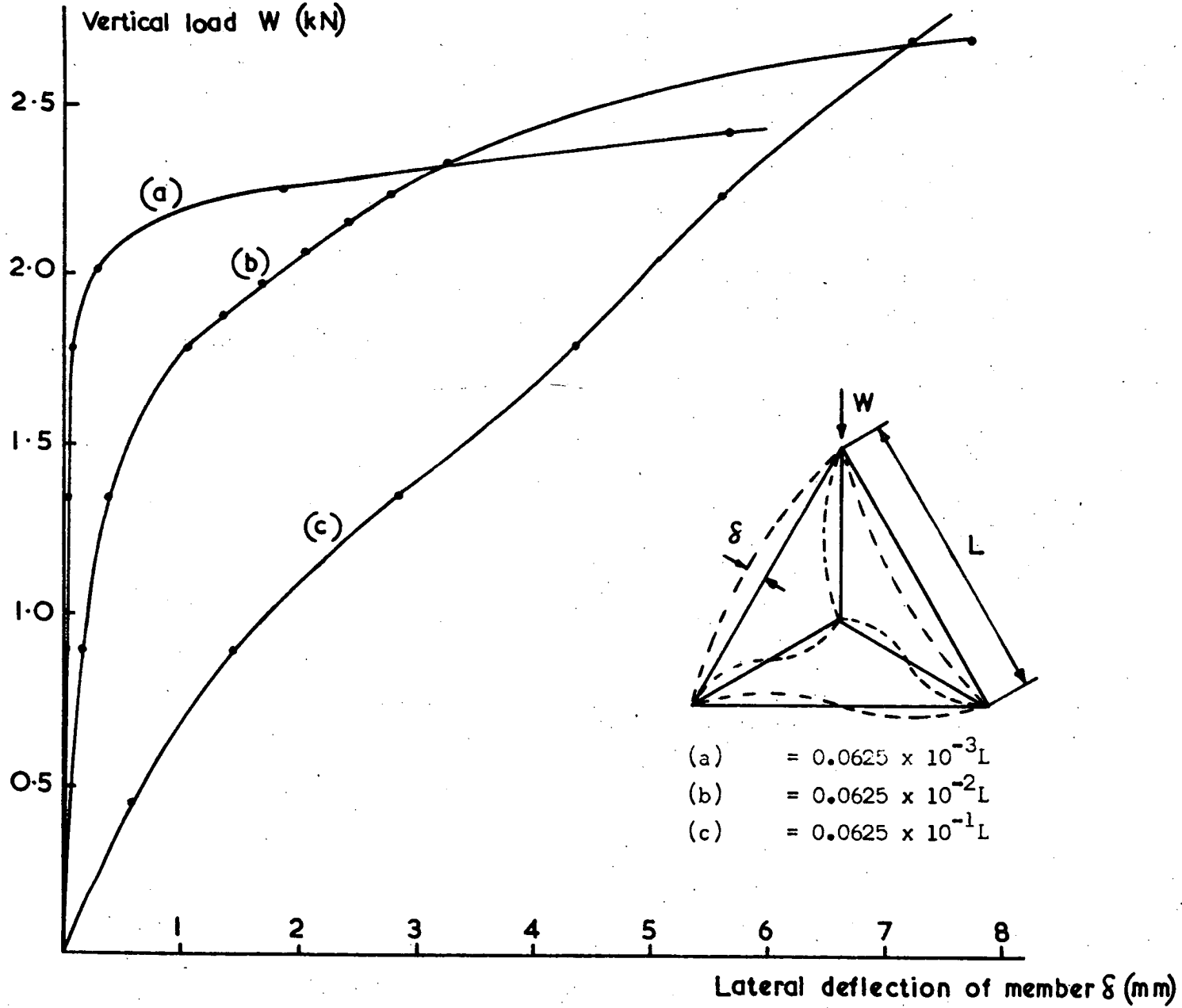


Figure B2.7

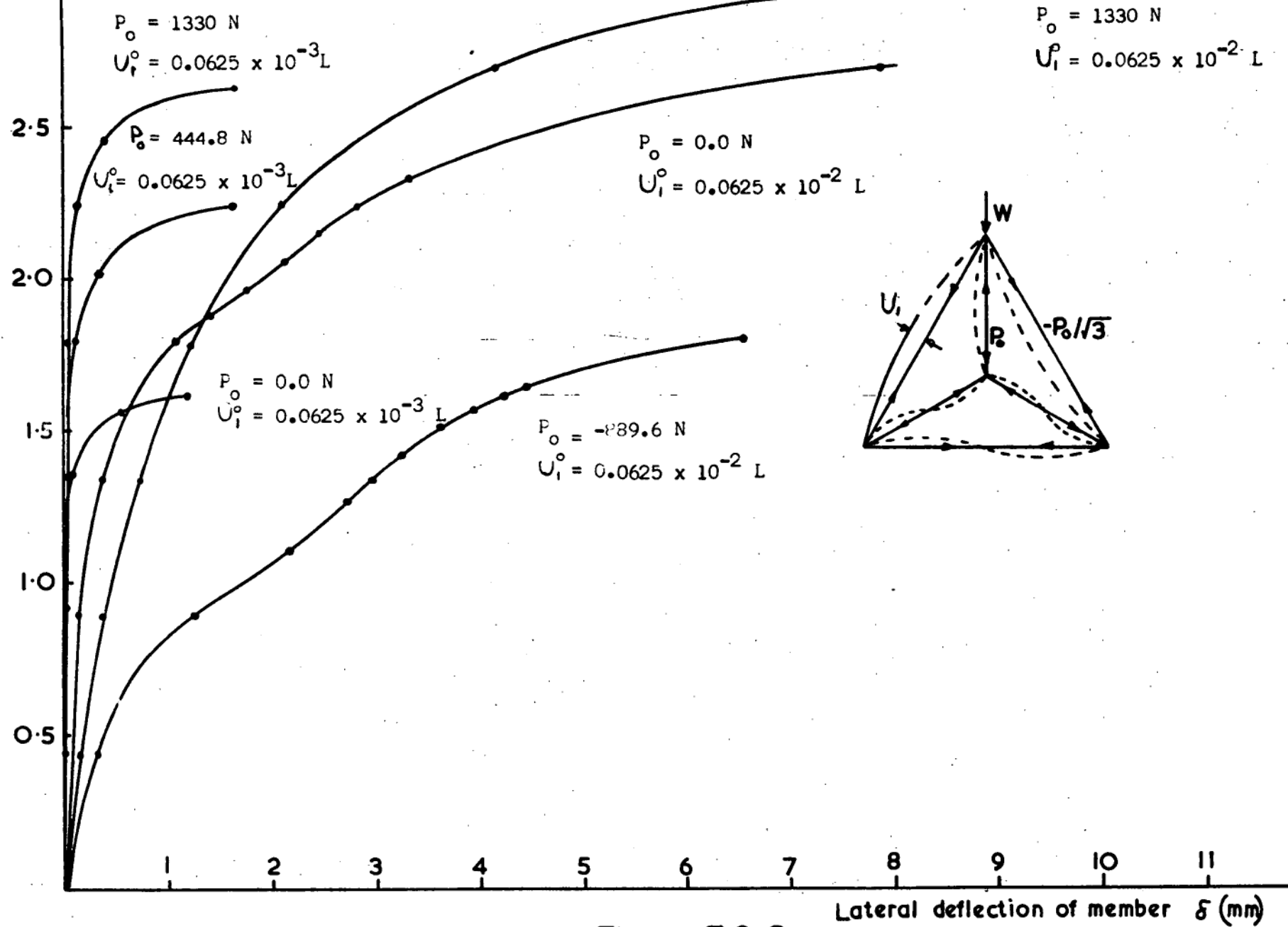


Figure B2.8

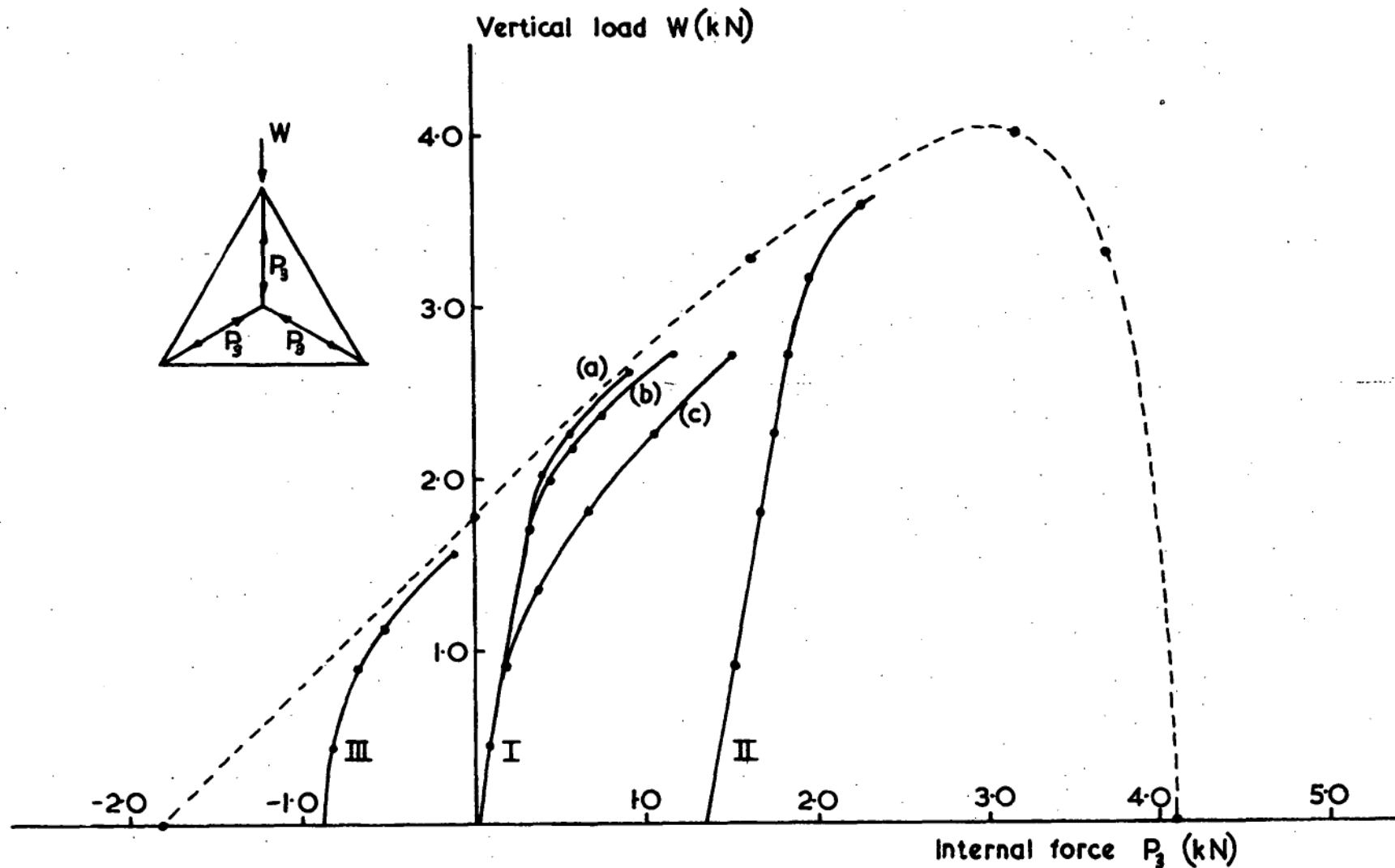


Figure B2.9

DISTRIBUTION OF INTERNAL FORCES AT VARIOUS LEVELS OF LOADING

(I) No prestrain (1) $U_1^0 = 0.0625 \times 10^{-3} L$ (b) $U_1^0 = 0.0625 \times 10^{-2} L$ (c) $U_1^0 = 0.0625 \times 10^{-1} L$

(II) With prestrain $P_0 = 1330 \text{ N}$ $U_1^0 = 0.0625 \times 10^{-2} L$

(III) With prestrain $P_0 = -889.6 \text{ N}$ $U_1^0 = 0.0625 \times 10^{-2} L$

APPENDIX B3

DYNAMIC RELAXATION TREATMENT OF STRUCTURES WITH NO
TENSILE STRENGTH

SUMMARY

Behaviour of structures which have no tensile strength is studied numerically by the method of dynamic relaxation. The standard approach of estimating the flexural stiffness EI and correcting it with reference to the moment-thrust-curvature ($M-P-\kappa$) diagrams requires large numbers of stored $M-P-\kappa$ curves. The present method dispenses with this storage. Direct use is made of the stress-strain diagrams which can be either linear or non-linear. Calculations are done for a prestressed wooden beam and a voussoir arch as examples.

INTRODUCTION

Treatment of cracks and their influence on structures is normally an iterative process based on an elastic analysis. The standard approach for beams and frames is to estimate the flexural stiffness EI of the members and to analyse the structure elastically. The values of EI are then corrected (by the removal of the tension zones) with reference to the moment-thrust-curvature diagrams ($M-P-\kappa$). The structure is then re-analysed.* The process is repeated until satisfactory convergence is reached. This treatment requires large numbers of stored $M-P-\kappa$ diagrams. The method proposed below dispenses with this storage. Direct use is made of the stress-strain relations which can be linear or non-linear. The method uses the iterative technique called Dynamic Relaxation which iterates between the equations of geometrical compatibility and the equations of statical equilibrium. The basis of dynamic relaxation has been fully explained by Otter et al and will not be repeated here.

* (Ref B3.1)

FORMULATION OF THE METHOD

Consider the member 1-2 (Fig B3.1). Under the action of moment M , axial force P and shear force Q , the member deforms and cracks. The centre line of the member is chosen as the reference line which is independent of cracking. The axis of centroids of the compression zone, on the other hand, is determined by the extent of cracking which may vary considerably across the depths of the section and along the lengths of the member.

The deformations of the member may be described by those of the reference line: two displacements u , v and a rotation θ at each end of the member (Fig B3.2). A cubic function is used to describe the variation in v , normal to the member and a linear function for u , along the member. The expressions for curvatures and strain become:

$$\left. \begin{aligned} K_1 &= 6(v_2 - v_1)/l^2 + 4\theta_1/l + 2\theta_2/l \\ K_2 &= 6(v_2 - v_1)/l^2 + 2\theta_1/l + 4\theta_2/l \\ \epsilon &= (u_2 - u_1)/l \end{aligned} \right\} \dots\dots\dots (B3.1)$$

where K_1, K_2 are the curvatures at ends 1 and 2 of the member, ϵ is the average axial strain in the member.

The problem is to relate these expressions of curvatures and strain (which are defined on the centre line only) to the actual forces, P and M , acting on the cross-section. This is done by integrating the stress-strain diagram across the section to obtain the forces. Consider the member 1-2 of Figure B3.3. If the axial strain ϵ and curvatures K_1, K_2 are given, then the axial forces P_1 and P_2 and moments M_1 and M_2 at ends 1 and 2 of member can be calculated. The diagrams of Figure B3.4 are obtained for linear stress-strain relation. In general, it is seen that P_1 and P_2 are not equal if this section cracks. This inequality results from the difference in the position of the centroidal axis and the reference line

upon which deformations are defined. Equilibrium of the element is not satisfied; to proceed any further one has to find a way of recovering the equilibrium of the member. Two alternatives are available:

- (i) If the axial force P in the member is statically determinate or known, as it may be for a prestressed beam or masonry wall, the problem is then to relate the curvature κ to the moment M such that the total force across the section is P . This problem can be solved iteratively with the flow chart of Figure B3.5.
- (ii) If P is statically indeterminate such as in a voussoir arch, then the problem is to find a value of P for the member such that equilibrium is recovered. This can be done by either

- (a) Setting $P = EA \epsilon$ then proceeding as in (i) to find the relation between M and κ , or

- (b) Integrating the stress diagram as in Figure B3.3, then setting

$$P = \frac{1}{2}(P_1 + P_2).$$

It is seen that both approaches are only approximate. The only way to find out whether they will give satisfactory results is to apply them to particular problems and to compare the results with experiment.

PRESTRESSED WOODEN BLOCK BEAM

Consider the wooden block beam of Figure B3.6. Such a structure is easily made and tested, and the results are informative. The prestressing force is P acting at a distance e from the centre line. The load W is applied at mid span. The structure is analysed by dividing it into a number of elements of length DX . Then equilibrium of the element gives (Fig B3.7).

$$Q_1 = Q_2 = (M_1 + M_2)/DX - P(v_2 - v_1)/DX \quad \dots\dots\dots (B3.2)$$

The second term on the right represents the non-linear effect of

axial force upon the deformation. Equilibrium of each joint give $\sum M = 0$. Since the axial force on the member is known, the alternative (i), defined previously, is used. A solution is obtained following the iterative scheme of Figure B3.8. Figure B3.9 shows the results of the calculation. The graphs of load against central deflections are shown for (i) experimental measurement, (ii) elastic calculation, (iii) non-tension calculation. The differences between calculated and measured behaviour are due to the lack of fit between the wooden blocks, and to slippage between the blocks, due to shear forces, as cracks open.

VOUSSOIR ARCH

The voussoir arch of Figure B3.10 is analysed for the loading shown. The structure is statically indeterminate, the axial force distribution in the structure is not known, and alternative (ii), as set out previously, is used. Either of the approaches given in section (ii) gives approximately the same results. However (b) converges more quickly than (a).

Figure B3.11 shows the stresses on the intrados and on the extrados of the arch; the results are compared with those from elastic calculation for the uncracked state. It is seen that the influence of cracks on the structure is fairly local. Figure B3.12 compares the deformations of the elastic and cracked arches. It is seen that cracked structures deform more than those which behave elastically and do not crack.

CONCLUSION

A simple workable approach to the non-linear analysis of structures made of materials which carry no tension has been given above. The method dispenses with large storage of the M-P- κ diagrams of members, normally required for such analysis. Reasonable agreement with experimental data is obtained. The common design practice of considering cracking as a

local effect and allowing for the increase of stress only at or near that cross-section is seen to be justified to some extent.

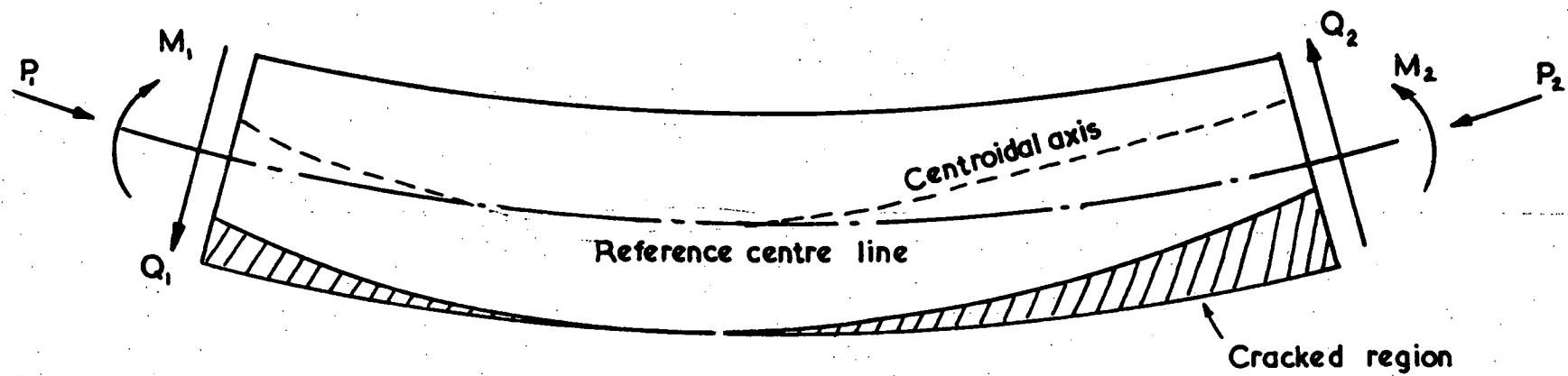


FIGURE B3.1

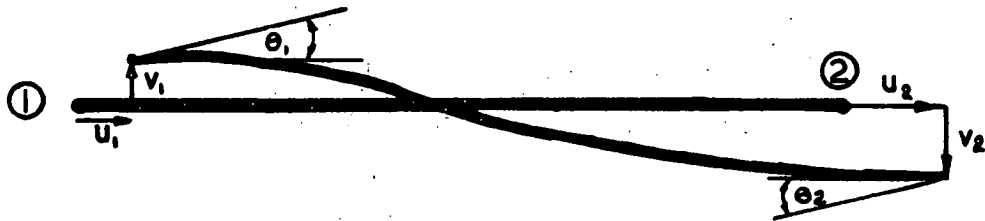


Figure B3.2

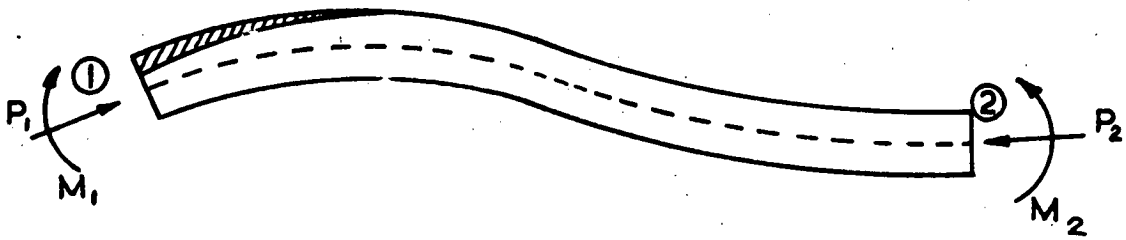


Figure B3.3

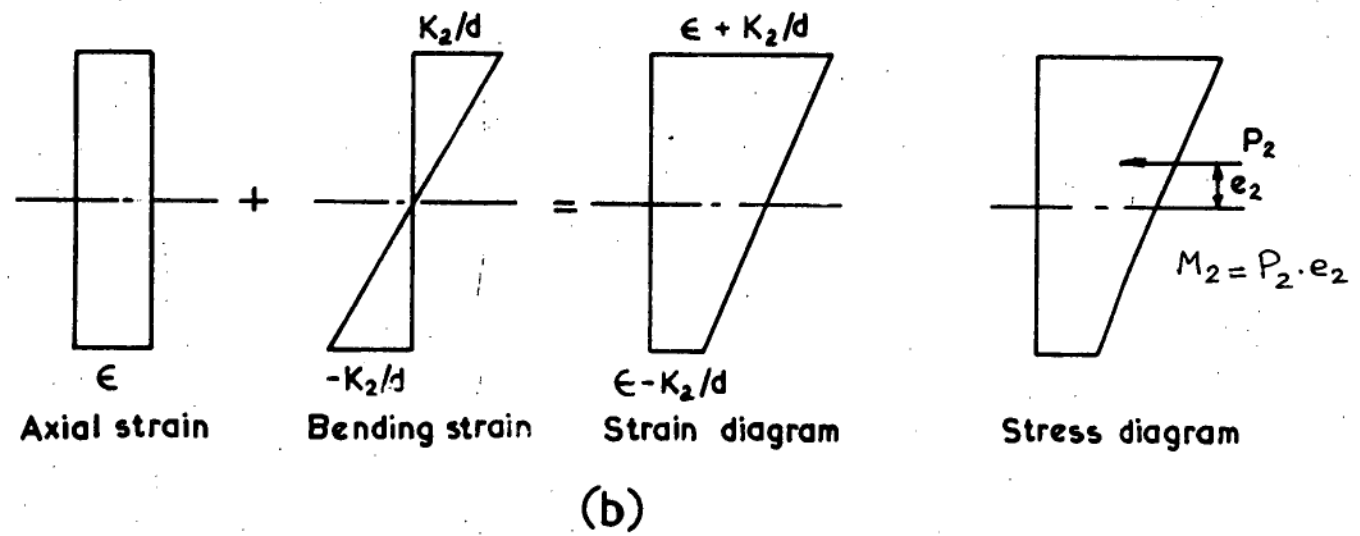
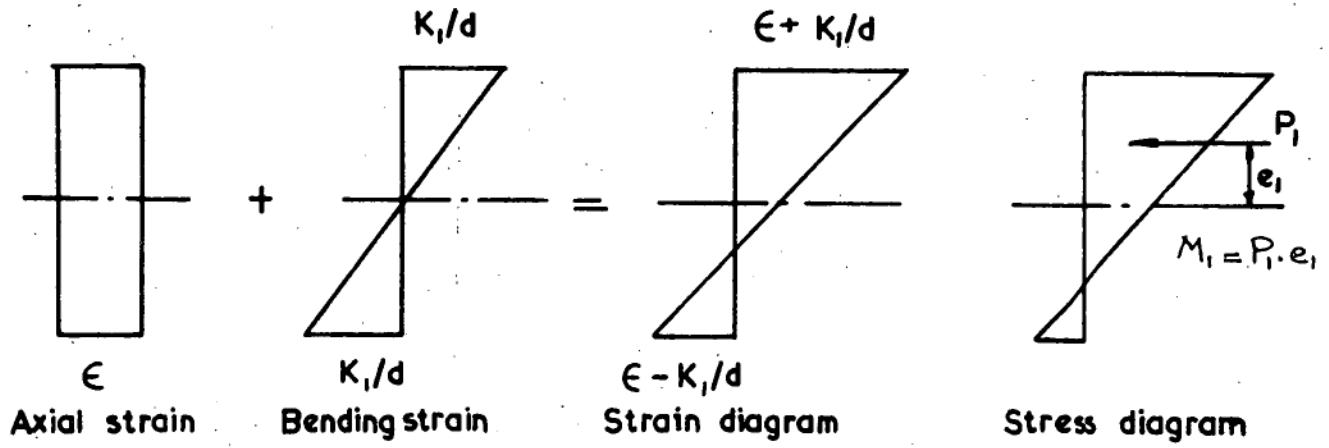


Figure B3.4

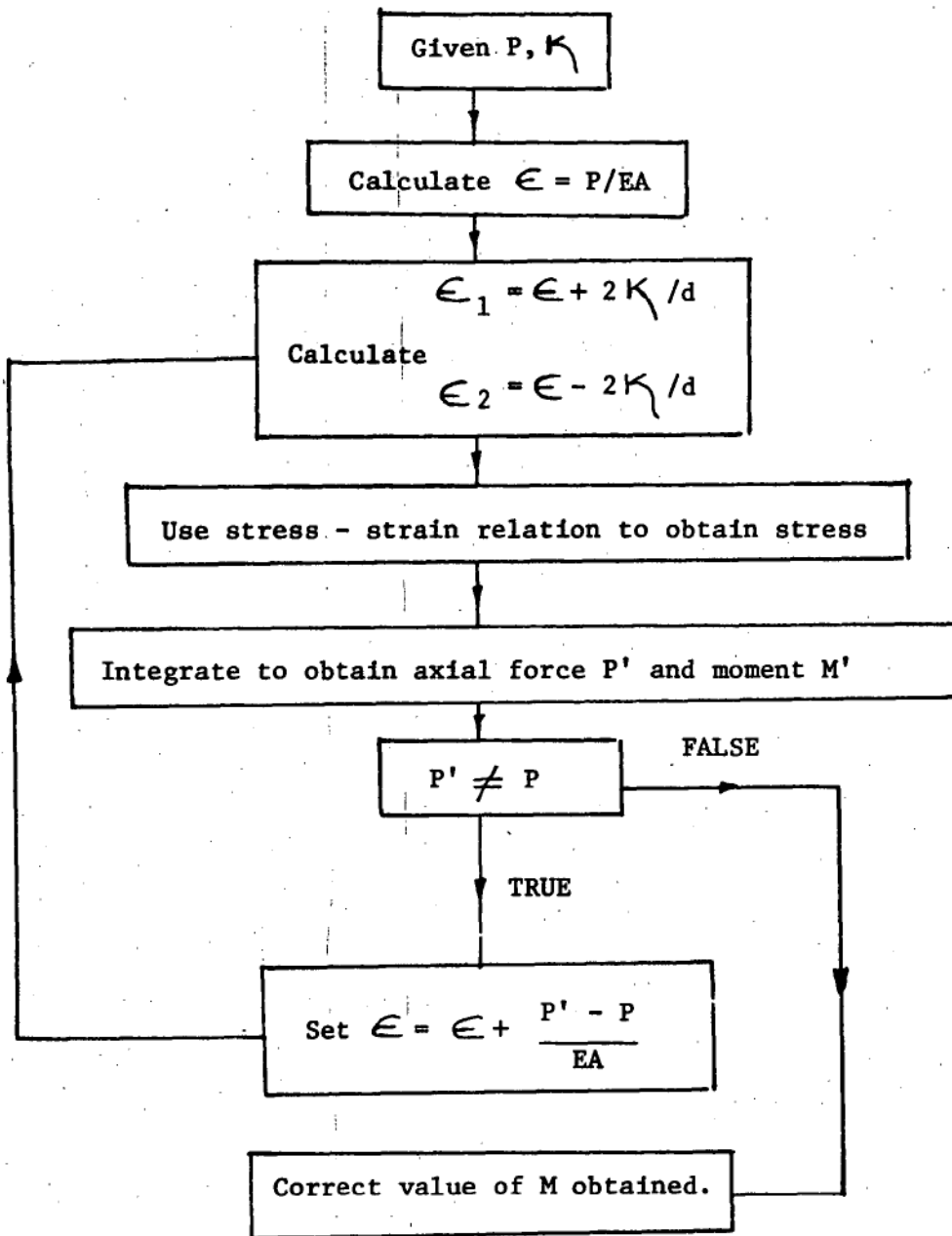


Figure B3.5

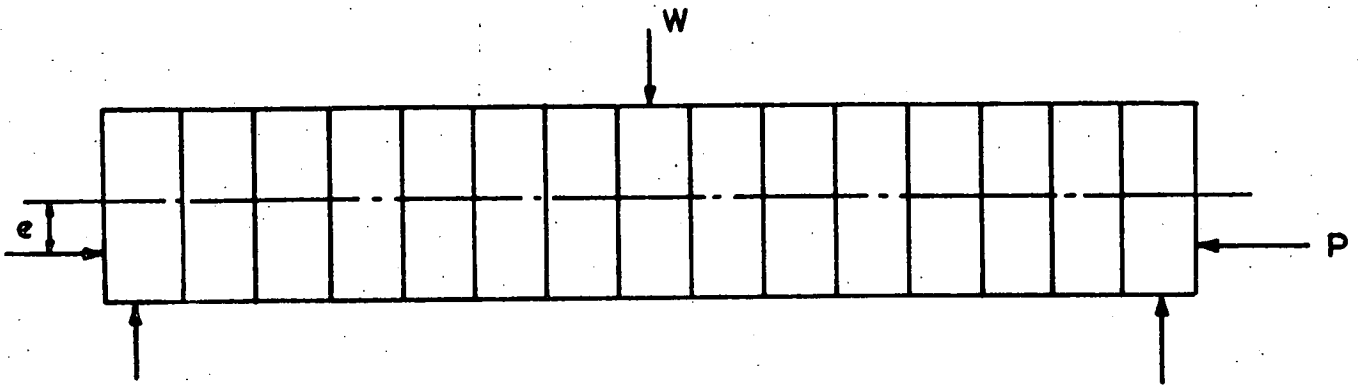


Figure B3.6

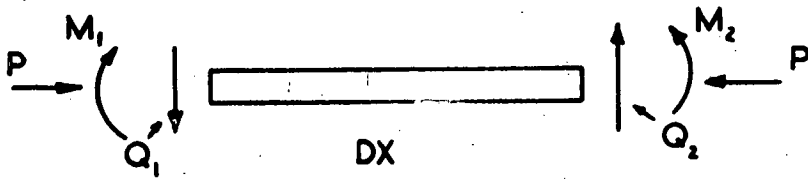


Figure B3.7

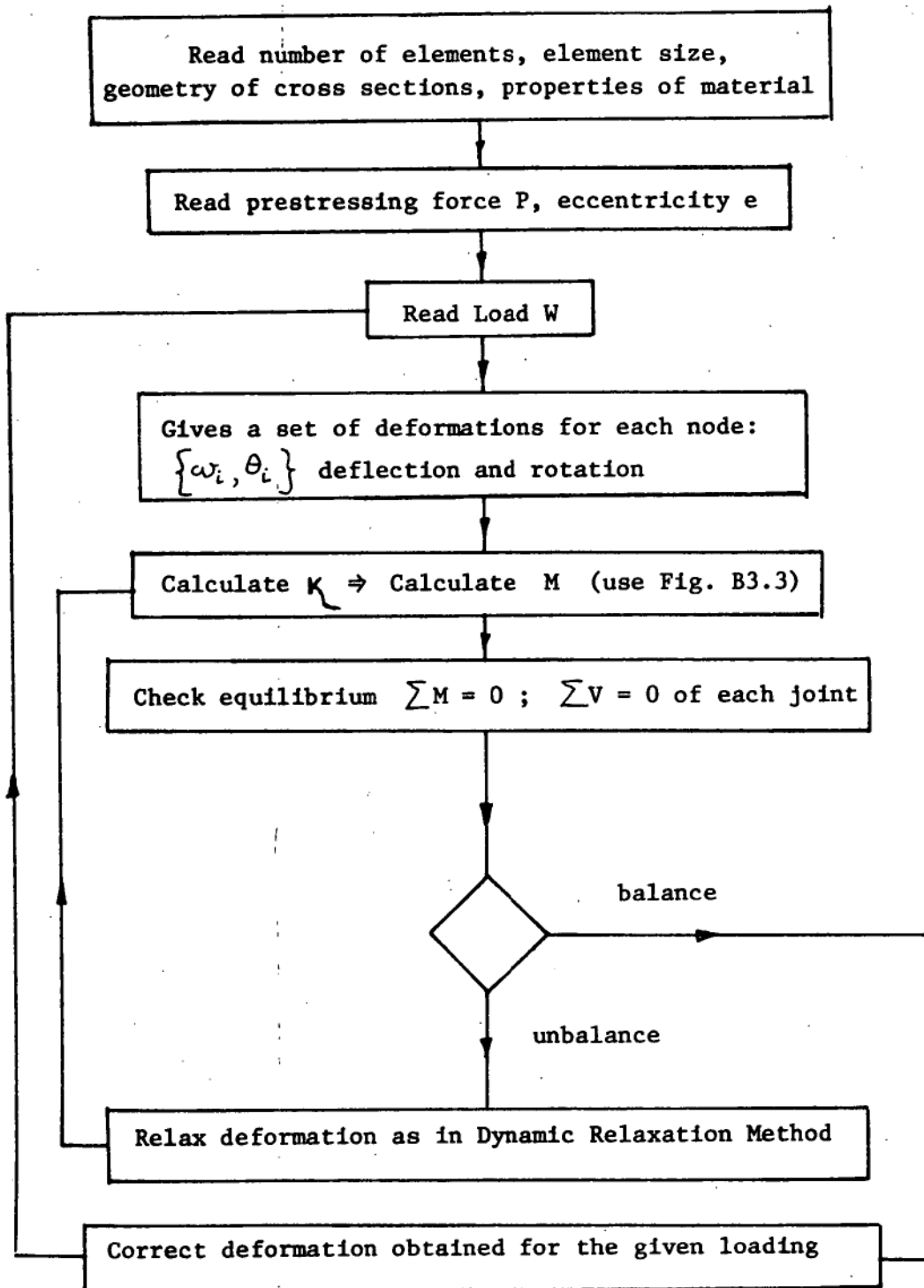


Figure B3.8

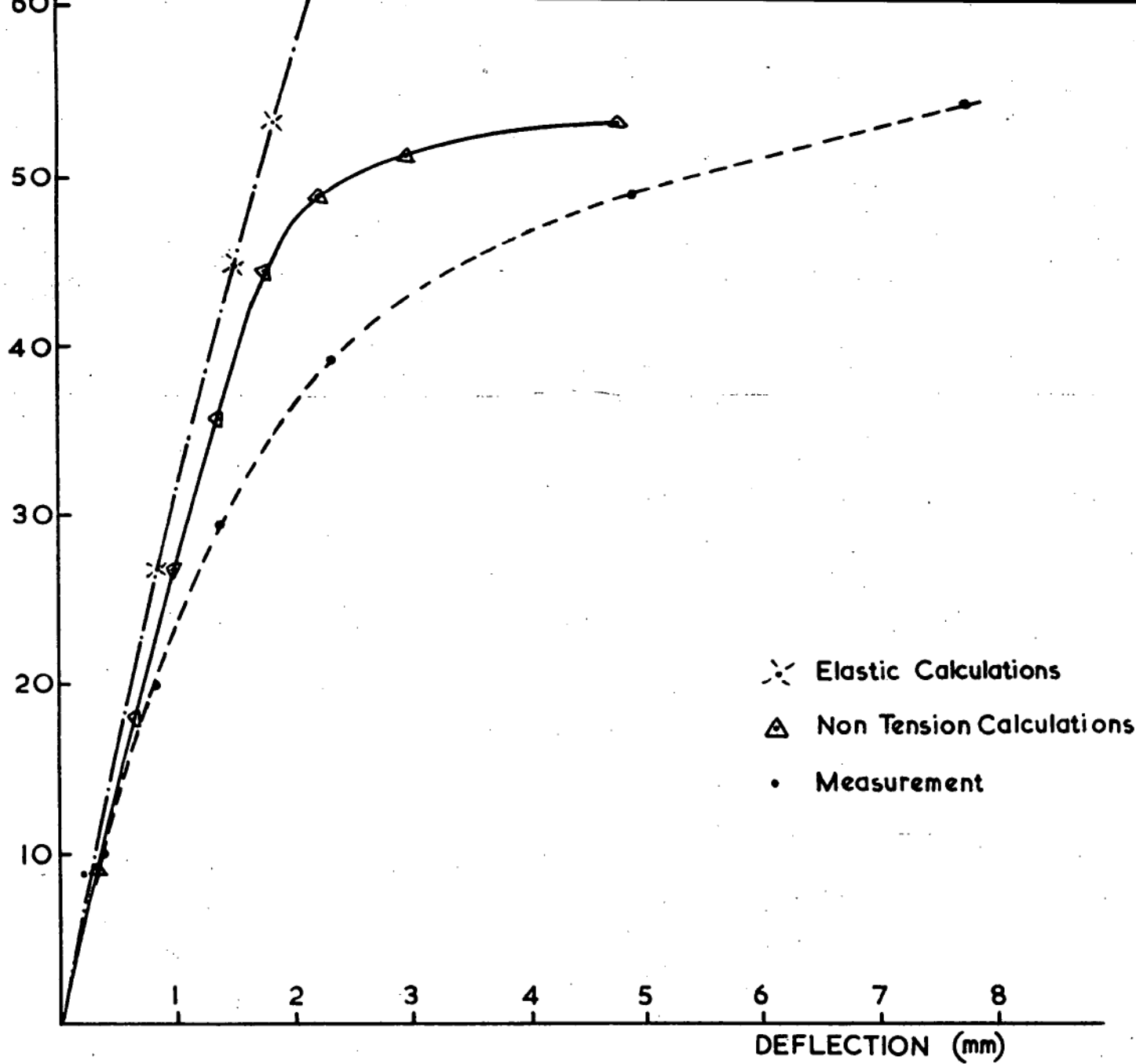


Figure B3.9

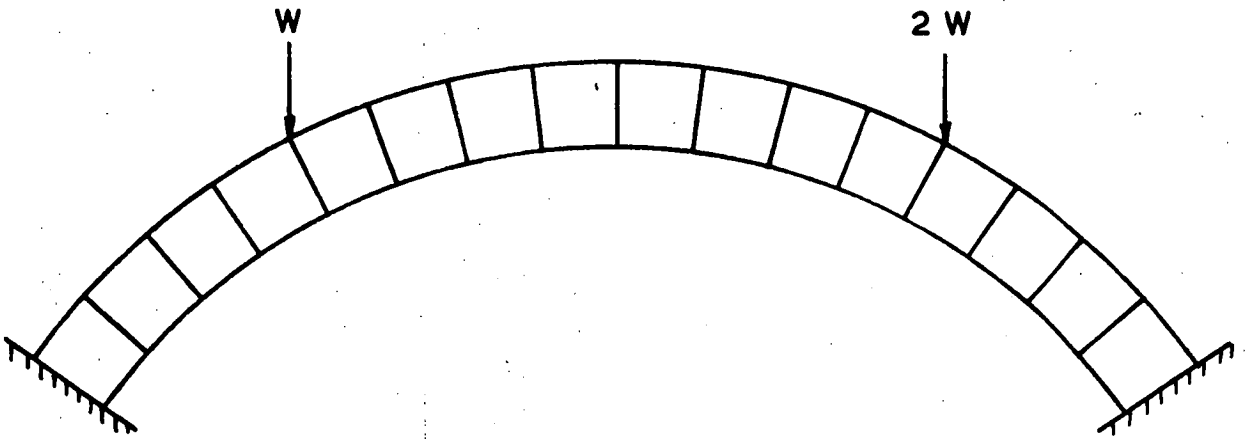


Figure B3.10

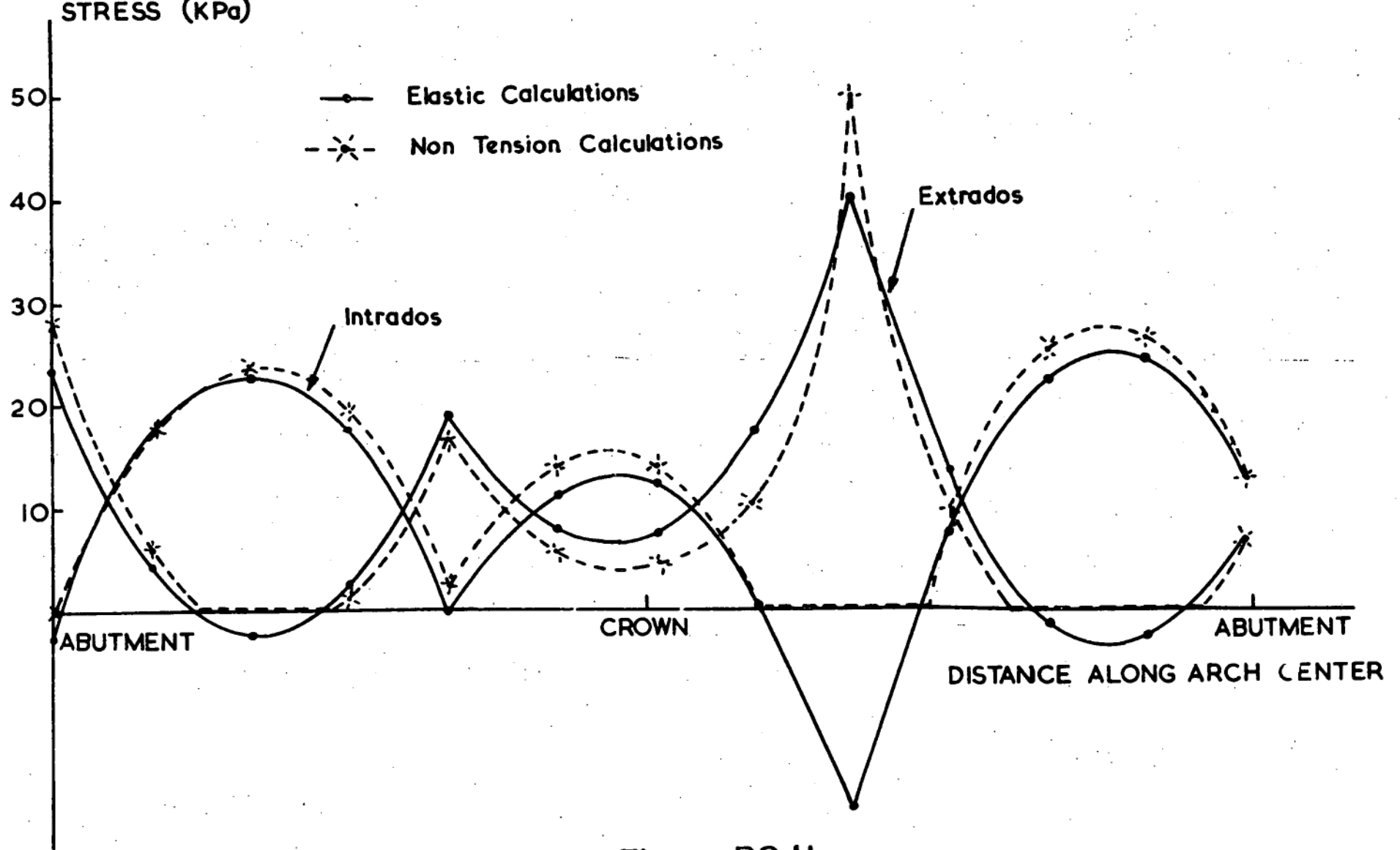


Figure B3.11

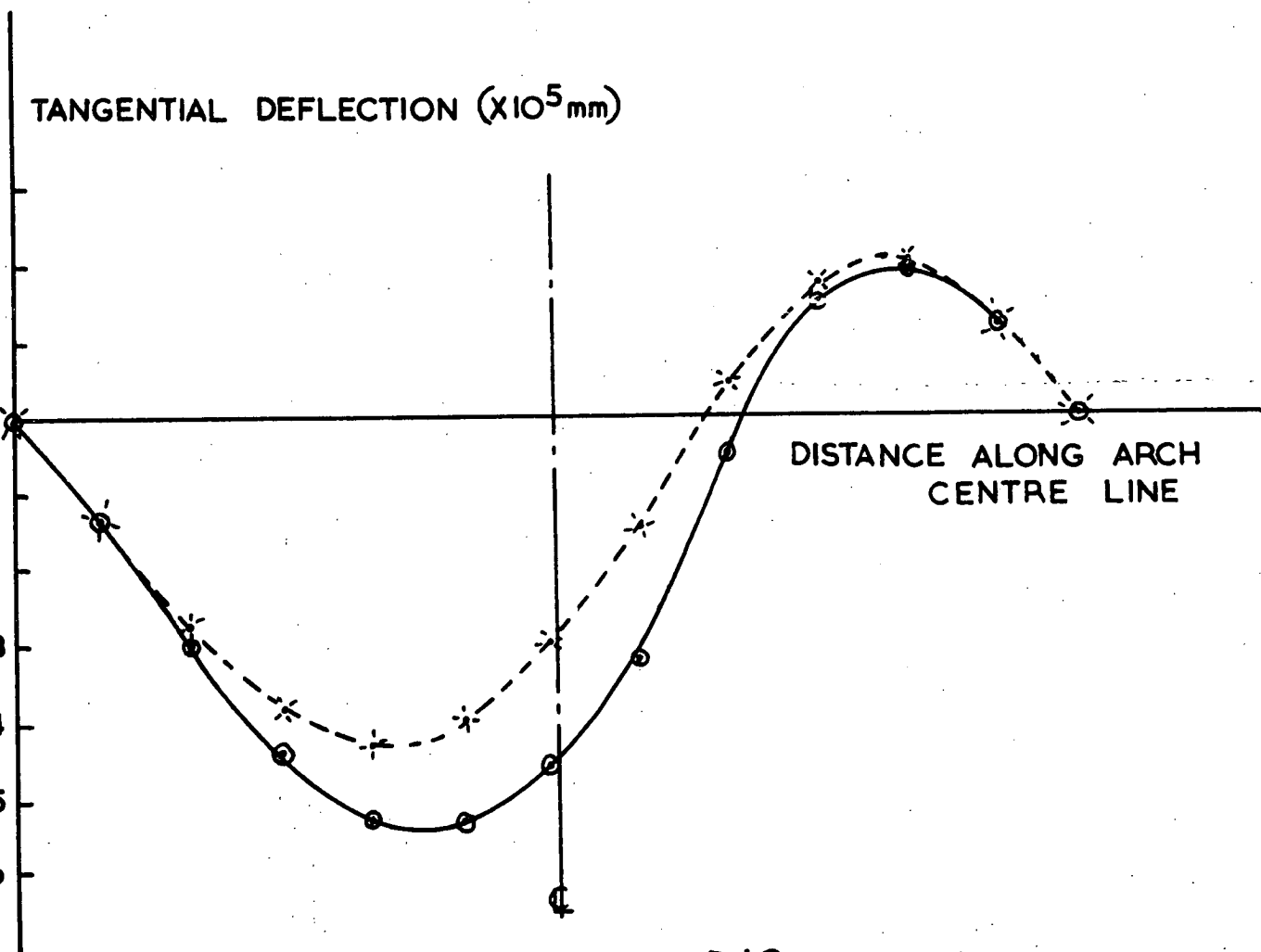
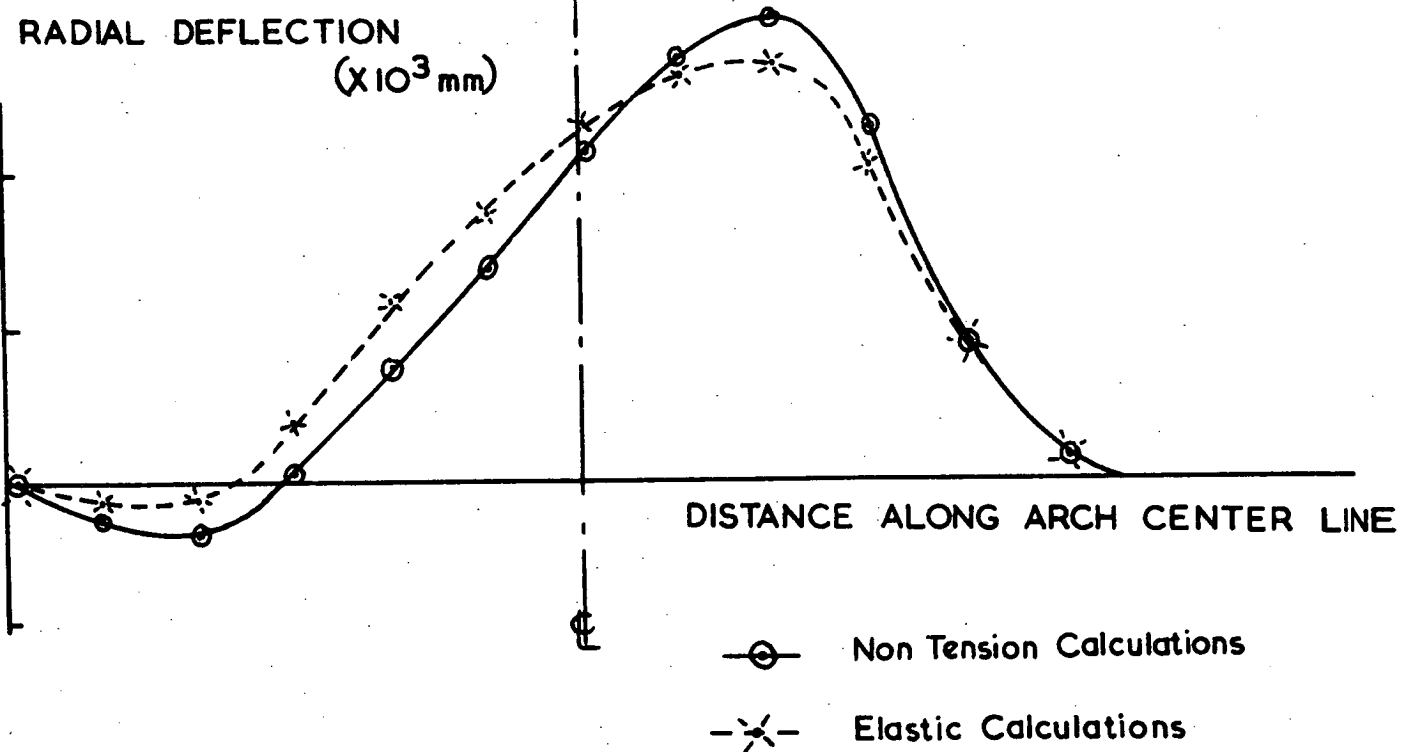


Figure B3.12

REFERENCES

CHAPTER 1

- 1.1 Baker, J.F., Horne, M.R., and Heyman, J.: "The Steel Skeleton, Vol. 2", Cambridge University Press, Cambridge, England, 1956.
- 1.2 Heyman, J.: "Plastic design and limit state design", The Structural Engineer, No. 4, Vol. 51, April, 1973.
- 1.3 CP110: "The Unified Code of Practice for the structural use of concrete", British Standards Institution, 1972.
- 1.4 Baker, J.F., and Heyman, J.: "Plastic design of frames: Vol. 1, Fundamental" Cambridge, 1969.
- 1.5 Heyman, J.: "Plastic design of frames: Vol. 2, Application", Cambridge, 1971.
- 1.6 Timoshenko, S.: "History of Strength of Materials", McGraw-Hill, 1953.
- 1.7 Van Den Broek, J.A.: "Theory of Limit Design", John Wiley and Sons, New York, 1948.
- 1.8 Gregory, M.S.: "Philosophy of Engineering design of Structures", Jnl of Struct. Div. , ASCE, Vol. 89, No. ST6, Dec. 1963.
- 1.9 "Steel Structures Code", AS CA1, Standards Association of Australia.
- 1.10 "SAA Code for Concrete in Building", AS CA2, Standards Association of Australia.
- 1.11 "SAA Loading Code Part I and II", AS CA34, Standards Association of Australia.
- 1.12 "Plastic design in Steel", Manuals and Reports on Engineering Practice-No. 41, American Society of Civil Engineers, 1971.
- 1.13 Hodge, P.G.: "Plastic Analysis of Structures", McGraw-Hill, New York, 1959.
- 1.14 Prager, W.: "Introduction to Plasticity", Addison-Wesley Publishing Co., Reading, Mass., 1959.

REFERENCES

- 1.15 Massonet, C., and Save, M.: "Plastic Analysis and Design, Vol. 1", Blaisdell Publishing Co., New York, 1965.
- 1.16 Heyman, J.: "The Stone Skeleton", Int. J. Solids Struct. Vol. 2, 1966.
- 1.17 Heyman, J.: "On shell solutions for masonry domes", Int. J. Solids Struct. Vol. 3, 1967.

CHAPTER II

- 2.1 "Manual of Steel Construction", American Institute of Steel Construction, New York, 1963.
- 2.2 "Bibliography On Bolted and Riveted Joints", Manuals and Reports on Engineering Practice, No. 48, ASCE, New York, 1967.
- 2.3 Abolitz, A.L.: "Plastic Design of Eccentrically Loaded Fasteners", Engineering Journal, ASCI Vol. 3, No. 3, July, 1966.
- 2.4 Kulak, G.L., and Crawford, S.F.: "Eccentrically Loaded Bolted Connections", Journal of the Structural Division, ASCE, Vol. 97, No. ST3, March, 1971.
- 2.5 Gregory, M.S.: "Riveted Joints, ..." Aust. J. Appl. Sci. 14, 1963.
- 2.6 Higgins, T.F.: "New Formula for Fasteners Loaded Off Center", Engineering News Record, May, 1964.
- 2.7 "SAA High Strength Bolting Code", AS CA45, Standards Association of Australia, 1970.
- 2.8 Lee, J.H., O'Connor, C., and Fisher, J.W.: "Effect of Surface Coatings and Exposure on clip", Journal of the Structural Division, ASCE, No. ST11, November, 1969.
- 2.9 Fisher, J.W., and Wallaert, J.J.: "Shear Strength of High Strength Bolts", Journal of the Structural Division ASCE, Vol. 91, No. ST3, June, 1965.

REFERENCES

CHAPTER III

- 3.1 Baker, J.F., Horne, M.R., and Heyman, J.: "The Steel Skeleton, Vol. 2", Cambridge University Press, Cambridge, England, 1956.
- 3.2 Neal, B.G.: "Plastic Methods of Structural Analysis", Chapman and Hall, 1956.
- 3.3 Heyman, J.: "The Limit design of space frames", J. Appl. Mech., 18, June, 1951.
- 3.4 Makowski, Z.S., and Gogate, M.N.: "Stress Analysis of three-pinned arch-ribbed domes", Proc. Instn. Civ. Engrs, Paper No. 6116, Vol. 5, April, 1956.

CHAPTER IV

- 4.1 Timoshenko, S.: "Theory of plates and shells", McGraw-Hill, 1959.
- 4.2 Kemp, K.O.: "The Yield Criterion for Reinforced Concrete Slabs", International Journal of Mechanical Science, Vol. 7, No. 11, Nov., 1965.
- 4.3 Save, M.: "A Consistent Limit Analysis Theory for Reinforced Concrete Slabs", Magazine of Concrete Research, Vol. 19, No. 58, Mar., 1967.
- 4.4 Lenschow, R., and Sozen, M.A.: "A Yield Criterion for Reinforced Concrete Slabs", Journal of the American Concrete Institute, Proceedings, Vol. 64, May, 1967.
- 4.5 Kemp, K.O.: "A Lower Bound Solution to the Collapse of an Orthotropically Reinforced Slab on Simple Supports", Magazine of Concrete Research, Vol. 14, No.41, July, 1962.
- 4.6 Fox, E.N.: "The existence of exact solutions in limit analysis for homogeneous isotropic plates of rigid perfectly plastic material", Engineering Plasticity, edited by Heyman and Leckie, Cambridge, 1968.

REFERENCES

- 4.7 Hillerborg, A.: "A Plastic Theory for the Design of Reinforced Concrete Slabs", Sixth Congress, International Association for Bridge and Structural Engineering, Stockholm, June, 1960.
- 4.8 Wood, R.H., and Armer, G.S.T.: "The theory of the strip method for design of slabs", Proc. Inst. Civil Engineers, Vol. 41, Oct., 1968.
- 4.9 Holmes, M., and Steel, K.A.: "Upper and Lower Bound Solutions to the Collapse of a Continuous Slab under Uniform Load", Magazine of Concrete Research, Vol. 16, No. 47, June, 1964.
- 4.10 Johansen, K.W.: "Yield Line Theory", Cement and Concrete Association London, 1962.
- 4.11 Johansen, K.W.: "Yield Line Formulae for Slabs", Cement and Concrete Association,
- 4.12 Jones, L.L.: "Ultimate load analysis of reinforced and prestressed concrete structures", Chatto and Windus, London, 1962.
- 4.13 Jones, L.L., and Wood, R.H.: "Yield Line Analysis of Slabs", Thames and Hudson and Chatto and Windus, London, 1967.
- 4.14 Wood, R.H.: "Plastic and Elastic Design of Slabs and Plates", Thames and Hudson, London, 1961.
- 4.15 Ragern, B.V.: "Lower bound Solutions for Continuous Orthotropic Slabs", Journal of the Structural Division, ASCE, March, 1973.

CHAPTER V

- 5.1 Heyman, J.: "The Stone Skeleton", Int. J. Solids Struct. Vol. 2, 1966.
- 5.2 Heyman, J.: "On shell solutions for masonry domes", Int. J. Solids Struct, Vol. 3, 1967.
- 5.3 Heyman, J.: "Spires and fan Vaults", Int. J. Solids Struct, Vol. 3, 1967.

REFERENCES

- 5.4 Heyman, J.: "The Safety of Masonry Arches", Int. J. Mech. Sci., Vol. 11, 1969.
- 5.5 Heyman, J.; et al: "Two Masonry Bridges" Prod. Inst. Civ. Eng., Vol. 52, Part I, November, 1972.
- 5.6 Mainstone, R.J.: Discussion on "Two Masonry Bridges" by Heyman, Inst. Civ. Eng. Vol. 54, pt 1, August, 1973.
- 5.7 Yokel, F.: "Strength of Masonry Walls under Compressive and Transverse Loads", Building Science Series 34, U.S. Dept of Commerce.
- 5.8 Sahlin, S.: "Structural Masonry", Prentice Hall, 1971.
- 5.9 Baxter, J.W., and Gee, A.F.: "Gladesville Bridge", Proc. Inst. Civ. Eng., April, 1965.
- 5.10 Pippard, A.S.: "Discussion on Gladesville Bridge", Proc. Inst. Civ. Eng., April, 1965.
- 5.11 Cowan, H.J.; "Reinforced and Prestressed Concrete in Torsion" E. Arnold, London, 1965.
- 5.12 Zia, P.: "Torsion theories for Concrete Members", Torsion of Structural Concrete, Special Publication No. 18, A.C.I., Detroit, 1968.
- 5.13 Swamy, N.: "The behaviour and ultimate strength of Prestressed Concrete Hollow Beams under Combined Bending and Torsion", Mag. Concr. Res., Vol. 14, No. 40, 1962.
- 5.14 Boulton, N.S., and Boonsukha, B.: "Plastic Collapse Loads for circular arc bow girders", Proc. Inst. Civ. Eng. Vol. 13, June, 1959.
- 5.15 Hill, R.: "A variational principle of maximum plastic work in classical plasticity", Quart. J. Mech., Vol. 1, 1948.

REFERENCES

CHAPTER VI

- 6.1 Rocha, M.: "A Statement of the Physical Problem of the Arch Dam" from "Theory of Arch Dam" ed. J.R. Rydzewski, Pergamon Press, 1965.
- 6.2 Bourgin, A.: "The Design of Dams", Pitmans, London, 1953.
- 6.3 Coyne, A.: "Arch Dams: their philosophy", A.S.C.E. Proceedings, Vol 82, April, 1956.
- 6.4 Fiahlo, F.L.: "Principles of arch dam, new method of designing and dimensioning", Lisbon, 1955.
- 6.5 Bustamente, J.I.; and Rosenblueth, E.: "Ultimate Load Capacity of arch dams", A.S.C.E. Journal Eng. Mech. Div., EM4, August 1966.
- 6.6 Swaminathan, K.V., and Rajaraman, A.: "A method for estimating the ultimate load capacity of arch dams", Water Power, February, 1970.
- 6.7 Flugge, W.: "Stress in Shells", Springer, 1961.
- 6.8 Allen, D.N. de G., Chitly, L., Pippard, A.J.S., and Swern, R.T.: "The experimental and mathematical analysis of arch dams with special reference to Dokan", Proc. I.C.E., Vol 5, pt I, 1956.

CHAPTER VII

- 7.1 Heyman, J.: "On the estimation of deflexions in elastic-plastic framed structures", Proc. I.C.E., Vol 19, May, 1961.
- 7.2 Gregory, M.S.: "Discussion on Ref. 7.1", Proc. I.C.E., Vol 19, May, 1961.
- 7.3 "S.A.A. Code for Concrete in Building", A.S. CA2, Standards Association of Australia.

REFERENCES

- 7.4 Kjar, A.R.: "Southwell plot Extension", Civ. Eng. Trans. I.E. Aust., CE10, 1968.
- 7.5 Van der Woude, F.: "Buckling of Elastic Frames", Ph.D. thesis, University of Tasmania, 1969.
- 7.6 Lam, P.: "Lateral buckling of arches", Hons. thesis, University of Tasmania, 1969.

CHAPTER VIII

- 8.1 Banks, E.: "Notch toughness testing and the Specification of Steel to Avoid Brittle Fracture", AISC Conference on Steel development, Newcastle, Australia, 1973.
- 8.2 Gurney, T.: "Fatigue of Welded Structures", Cambridge U.P., 1968.
- 8.3 "S.A.A. Steel Structures Code", A.S. 1204, Standards Association of Australia.
- 8.4 Wade, J.: "The weldability of Modern Structural Steels", Symposium on Modern Applications of Welding Technology in Steel Structures, Sydney, August, 1972.
- 8.5 "Structural Steels - Ordinary Weldable Grades", A.S. 1204, Standards Association of Australia.
- 8.6 Mann, J.Y.: "Fatigue of Materials", Melbourne U.P., 1967.
- 8.7 Gurney, T.: "A Comparison of Fatigue Design Rules", Conference on Fatigue of Welded Structures, 1970.
- 8.8 McHenry, D.: "A new aspect of creep in concrete and its application to design", A.S.T.M. Proc. 43, 1943.
- 8.9 Fintel, M., and Khan, F.R.: "Effects of column creep and shrinkage in tall structure", A.C.I. Publication, SP.27, 1971.
- 8.10 Forrester, K., and Curtis, T.J.: "Interim Report on Gladesville Bridge Arch Deflexions", Civ. Eng. Trans., I.E. Aust. CE9, 1967.

REFERENCES

- 8.11 Zienkiewicz, O.C.: "The Influence of Creep on the Behaviour of Massive Concrete Structures", Indian Journal of Power and River Valley Development, July, 1973.
- 8.12 Neville, A.M.: "Creep of Concrete: Plain, Reinforced, and Prestressed", North Holland, 1970.
- 8.13 Entrican, G.C.: "Detailing for ductility in Reinforced Concrete Frames Subject to Earthquake forces", The Structural Engineer, August, 1965.

APPENDIX A1

- A1.1 Stevens, L.K.: "Carrying Capacity of Mild Steel Arches", Proc. I.C.E., Vol 6, March, 1957.
- A1.2 Jain, O.P.L "Ultimate Strength of Reinforced Concrete Arches", A.C.I. Journal, Proceedings V.57 No. 6, December, 1960.
- A1.3 Francios, V., Augusti, G., and Sparacio, R.: "Collapse of arches under repeated loadings", Proceeding, ASCE Vol 90, ST1, February, 1964.
- A1.4 Kooharian, A.: "Limit Analysis of Voussoir and Concrete Arches", A.C.I. Journal, Proceedings V.49, 1953.

APPENDIX A2

- A2.1 Johansen, K.W.: "Yield Line Theory", Cement and Concrete Association, London, 1962.

APPENDIX A3

- A3.1 Lam, P.: M.Eng.Sc. thesis, University of Tasmania, 1971.
- A3.2 Tolke, F.: Wasser Kraftanlagen. 2. Halft, 1. Teil - Berlin 1938.
- A3.3 Lombardi, J.: "Les barrages en voute mince", Dun , Paris, 1955.
- A3.4 Bustamente, J.I., and Rosenblueth, E.: "Ultimate Load Capacity of Arch Dams", A.S.C.E. Journ. Eng. Mech. , EM4, August, 1966.

REFERENCES

- A3.5 I.C.E. "Arch Dams - a review of British Research and Development",
The Inst. of Civil Engineers, London, 1968.

APPENDIX B1

- B1.1 Symonds, P.S., and Neal, B.G.: "Recent progress in the plastic methods of structural analysis", J. Franklin Inst. Vol 252, 1951.
- B1.2 Lee, S.L." "The conjugate frame method and its application in the elastic and plastic theories of structures", J. Franklin Inst., Vol 266, 1958.
- B1.3 Stevens, L.K.: "Control of collapse mechanism in triangulated frames", Aust. J. Appl. Sci., Vol 10, 1959.
- B1.4 Heyman, J.: "On the estimation of deflexions in elastic-plastic framed structures", Proc. Inst. Civ. Eng. Vol 19, May, 1961.
- B1.5 Otter, J. et al: "Dynamic Relaxation", Proc. Inst. Civ. Eng., Vol 35, 1966.
- B1.6 Baker, J.F., and Roderick, J.W.: "Tests on Full Scale Portal Frames", Proc. Inst. Civ. Eng, Vol 1, 1952.

APPENDIX B2

- B2.1 Otter, J. et al "Dynamic Relaxation", Proc. Inst. Civ. Eng., Vol 35, 1966.
- B2.2 Van der Woude, F.: Ph.D. thesis, University of Tasmania, 1969.
- B2.3 Guidici, S.: Ph.D. thesis, Oxford University, 1963.

APPENDIX B3

- B3.1 Michalos, J., and Grossfield, B.: "Elastic Plastic Analysis of Arches", Proc. Am. Conc. Inst., Vol 64, May, 1967.

ABSTRACT

The philosophy of design of structures by picturing statically admissible states is outlined and applied to various members and structures. The strength of bolted joints under eccentric loading is investigated. The concept of thrust line is applied to multi story bay frames and space frames, and a graphical method of minimum weight design by guessing points of inflexion is presented. Various solutions for the load-carrying capacity of orthotropic slabs are proposed. The strength and safety of the Gladesville Arch Bridge is investigated; the load factors for the bridge are established for three different loading conditions. An experimental method for directly obtaining a shape for an arch dam under a given loading condition is proposed. Load-carrying capacity of arch dams are also estimated by picturing various statically admissible states. The relation between deflexion, buckling, and strength is discussed. The concept of Non-Euler Buckling is introduced. Various practical design considerations are summarized, including the detailed design of joints. In the appendices, tests on arches, slabs, and a shell are reported, together with related calculations. The numerical method of Dynamic Relaxation is applied to the problem of estimating deflexion in elastic-plastic frames, the elastic stability problem of over-braced frames, and the non-linear analysis of structures made of materials having no tensile strength.